Rectangular Silos; Interaction of Structure and Stored Bulk Solid

A thesis submitted for

the degree of Doctor of Philosophy

by

Richard J. Goodey

Department of Mechanical Engineering

Brunel University

September 2002

Rectangular Silos; Interaction of Structure and Stored Bulk Solid

A thesis submitted for

the degree of Doctor of Philosophy

by

Richard J. Goodey

Department of Mechanical Engineering

Brunel University

September 2002

BRUNEL UNIVERSITY

PUBLICATION OF THESES

Please complete in block capitals

NAME: RICHARD GOODEY

DEPARTMENT: MECHANICAL ENGINEERING

TITLE OF THESIS: RECTANGULAR SILOS; INTERACTION OF STRUCTURE AND STORED BULK SOLID

PLEASE COMPLETE EITHER PART A OR PART B

A. I agree that the abstract of my thesis may be published by the University without further reference to me.

In accordance with the University's Handbook of Procedures, the Head of Library Services may allow my thesis to be copied in whole or in part without further reference to me. Such Authority shall apply only to single copies made for study purposes and shall be subject to normal conditions of acknowledgement.

(See notes overleaf)

Signature: _____

Date: 29/3/03

B. I request that my thesis be held under confidential cover in the Library for a period of _____ years for the following reasons:

_____

_____

_____

_____

Once the period of confidentiality has expired, I agree that the conditions set down in Part A will apply without further reference to me.

Signature: _____

Date: _____

Please pass this form to your supervisor who should sign below indicating his/her agreement to the retention of the thesis under confidential cover.

Signature of Supervisor: _____

Additional comments: _____

_____

_____

Signature _____
(Senior Assistant Registrar)

If you have completed Part A please return this form direct to the Library with evidence of your award.

Part B, when complete, should be returned to the Senior Assistant Registrar (Records & Systems) in the Registry.

For the attention of candidates who have completed Part A

i) Attention is drawn to the fact that the copyright of a thesis rests with its author.

ii) A copy of a candidate's thesis is supplied to the Library on condition that anyone who consults it is understood to recognise that its copyright rests with its author and that no quotation from the thesis and no information derived from it may be published without the prior written consent of the author or the University, as appropriate.

Requests for such permission should be addressed in the first instance to the Head of Library Services.

Abstract

The main aim of this research is directed towards the study of thin-walled rectangular planform silos with a view to maximising their structural efficiency. In thin plates of the type making up the wall, membrane action may increase the load carrying capability and current design guides make no account of this. Designing rectangular silos with this in mind can lead to significant structural savings.

The core of the research involves using the finite element method to study the patterns of pressure exerted by the weight of a granular bulk solid on the walls of the silo structure. The stored granular solid must use an elastic-plastic material law in order to account for large deformations that can occur in a thin-walled structure. The need for this type of constitutive law led to the investigation of bulk solid properties and shows that parameters that have previously been used to categorise bulk solids may not be sufficient to describe all aspects of their behaviour. The finite element model created uses material constitutive laws that can be found in a number of packages. The required granular material parameters can be determined from a number of simple tests. This approach aims to enable engineers to routinely use similar models when designing silos.

The results obtained from the finite element model exhibited some anomalies that had been observed in previous work. These were mainly apparent in the form of localised pressure peaks near the base of the model. These effects were investigated and possible mechanisms that lead to them were proposed.

The results from the finite element model were compared to previous experimental work and existing theories. The model was then used to conduct parametric surveys on square and rectangular planform silos and the distribution of pressure across the wall compared to previous predictive models.

Finally, a scale thin-walled metal silo was constructed and pressure measurements on filling with pea gravel made. These are compared to predictions made by the finite element model.

Acknowledgements

There are of course a number of people to whom I would like to express my gratitude. First and foremost, I would like to thank my supervisor, Mr Chris Brown for providing me with guidance (and funding) throughout the duration of my research. I would also like to thank him for giving me the opportunity of studying for a Ph.D. in the first place.

Secondly, I must thank Professor Michael Rotter of Edinburgh University for his assistance with papers drawn from this work. I must also mention Professor Jørgen Nielsen for his guidance at the onset of this project. Thanks also to my second supervisors, Professor Les Henshall and Professor Luiz Wrobel.

This research would not have been possible without the assistance of the technicians and staff in the department. Many thanks go to Keith Withers, Bob Webb, John Langdon, and Brian Dear.

There has also been a good number of reprobates who I have crossed paths with and have made the whole research experience more enjoyable. My thanks to Dr Richard Torrens, Dr Anthony Morgan, Dr Chang-Jiang Wang and Dave Simpson to mention but a few.

Thanks must go to my parents for their support and hard cash over the large number of years I have managed to stay in full-time education.

Finally, thanks to my girlfriend Lana who has supported me for several years and has only spent a small amount of that time telling me to get a job.

Table of Contents

Abstract i

Acknowledgements ii

Notation ix

List of figures xi

List of tables xvi

1. Introduction 1

1.1 Thesis summary 2

2. Background to the problem 4

2.1 Definitions 5

2.1.1 Planform 6

2.1.2 Height to width ratio 6

2.1.3 Construction materials 6

2.1.4 Flow type 6

2.2 Silos studied 8

3. Stresses and loads in the ensiled material and the silo structure 10

3.1 Silo loads 10

3.2 Stress state in the stored solid 11

3.2.1 Interaction between silo and contents 12

3.3 Calculations for wall pressures 12

3.3.1 Theory of Janssen 13

3.3.2 Theory of Reimbert and Reimbert 16

3.3.3 Theory for squat silos 20

3.4 Assumptions of theories 21

3.5 Evaluation of pressure coefficient – k 22

3.6 Discharge pressures 25

3.7 Other loading considerations 25

3.7.1 Wind loading 26

3.7.2 Seismic loading 26

3.7.3 Thermal loading 26

3.8 Application of theories to rectangular planform silos 27
3.9 Silo response 27
3.9.1 Load supporting actions in silos structures 27
3.10 Membrane actions in rectangular plates 28
3.10.1 General equations for rectangular plates 30
3.10.1.1 Small deflection theory 31
3.10.1.2 Large deflection theory 31
3.10.1.3 Comparison of small and large deflection theory 31
3.10.2 General numerical techniques for plate problems 32
3.11 Structural considerations 32
3.12 Rectangular bin design 34
3.13 Summary 34
4. Numerical methods for the prediction of silo wall pressures 36
4.1 Introduction 36
4.2 Available numerical techniques 36
4.2.1 Finite difference method 37
4.2.2 Finite element method 37
4.2.3 Boundary element method 38
4.2.4 Discrete element method 38
4.3 Choice of numerical technique for use in the current project 39
4.4 Previous application of the finite element method to silo problems 39
4.4.1 Filling pressures 39
4.4.2 Discharge pressures 41
4.5 Summary 42
5. The finite element method applied to silo problems 44
5.1 Analysis type 44
5.1.1 Sources of non-linearity 46
5.1.2 Obtaining a solution in non-linear finite element analysis 46

5.1.3 Non-linearity in silo problems 47
5.1.3.1 Large deformations 47
5.1.3.2 Contact analysis 47
5.2 Constitutive models to describe material behaviour 48
5.2.1 Properties of granular bulk solids 49
5.2.2 Determining granular bulk solids properties for finite element analysis 51
5.3 Material constitutive laws for use in the current work 55
5.3.1 Elastic laws 56
5.3.2 Non-elastic laws 56
5.3.3 Elastic-plastic laws 56
5.4 Constitutive laws available in ABAQUS 57
5.4.1 Linear elastic law 58
5.4.2 Porous elastic law 58
5.4.3 Mohr-Coulomb law 60
5.4.3.1 Plastic potential and flow rule 62
5.4.3.2 Mohr-Coulomb criteria in three-dimensional stress space 64
5.4.4 Drucker-Prager law 64
5.5 Summary 66
6. Calibration and validation of material constitutive laws 67
6.1 Introduction 67
6.2 Axisymmetric model – geometry and boundary conditions 67
6.3 Material models 69
6.4 Elastic material models 70
6.4.1 Linear elastic law 70
6.4.1.1 Poissons ratio as the controlling factor in the linear elastic model 72
6.4.2 Porous elastic model 76
6.5 Elastic/plastic models 83

6.5.1 Application of plasticity criteria to the axisymmetric model 83
6.6 Three-dimensional models 85
6.6.1 Further validation 86
6.6.2 Comparison with Janssen pressure distribution 89
6.6.3 Comparison with experimental sand data 91
6.6.4 Modelling of pea gravel 94
6.6.5 Comparison to Lahlouh et al's (1995) experimental data 95
6.6.6 Best fit of finite element results to experimental data 97
6.7 One-dimensional consolidation tests on the two granular bulk solids 97
6.8 Conclusions and choice of values for PE-DP model for Leighton Buzzard sand and pea gravel 102
7. The effect of the boundary condition at the base of the axisymmetric bin 104
7.1 Flat-bottomed axisymmetric bin 104
7.1.1 Frictionless base condition 105
7.1.2 Frictional base condition 107
7.1.3 Base and wall not connected 109
7.2 Horizontal and vertical stress in the stored solid 111
7.3 Strain in the stored material 114
7.4 Summary of flat-bottomed model 116
7.5 Hopper base condition 117
7.5.1 Pressures in the hopper 122
7.6 Conclusion 125
8. Further investigation of the geometry of Lahlouh et al (1995) 127
8.1 Introduction 127
8.2 Patterns of vertical stress in the stored material 127
8.2.1 Average and local values of k 130
8.3 Predictive law for wall normal pressures 133

8.3.1 Comparison to experimental results in sand 134
8.3.2 Comparison to experimental results in gravel 138
8.4 Comparison with finite element results 142
8.5 Summary 144
8.6 Finite element predictions for an idealised wheat 145
8.6.1 Comparison to Janssen distribution 145
8.6.2 Distribution of pressure across the wall 146
8.6.3 Patterns of vertical stress in the solid 147
8.6.4 Average and local values of k in the solid 147
8.6.5 Comparison with predictive law 149
8.7 Summary 150
9. Parametric study of a square planform silo 152
9.1 Introduction 152
9.2 Type of stored material 153
9.2.1 Relative stiffness between wall and stored solid 155
9.2.2 Deformations in the wall 158
9.3 Planform 159
9.3.1 Square planform silo with 20mm thick wall 159
9.3.2 Stiffness of ensiled material 164
9.4 Wall thickness 166
9.5 Relative stiffness of silo wall and ensiled material 172
9.5.1 Effect of large deformations in the wall 173
9.6 Variation of height of silo 174
9.7 Summary 176
10. Experiment 178
10.1 Silo geometry and construction 178
10.1.1 Adhesive tests 180
10.2 Instrumentation 181
10.2.1 Deflections of the wall 182
10.2.2 Strain in the wall 183
10.2.3 Wall normal pressures 183

10.2.3.1 Wall pressure cells 183
10.2.3.2 Free field cells 184
10.3 Finite element predictions of the experimental rig 185
10.4 Experimental results 187
10.4.1 Pressures across the centreline 188
10.4.2 Comparison with predictive law 188
10.4.3 Strain in the silo wall 190
10.5 Summary 191
11. Rectangular planform silos 192
11.1 Limitations to this study 192
11.2 Current guidance available 193
11.3 Rigid walled silo 196
11.4 Variation of planform ratio 197
11.5 Variation of wall thickness 203
11.6 Summary 205
12. Conclusions and further work 206
12.1 Summary of main conclusions 207
12.2 Further work 209
References 210
Publications 223
Appendix A – Derivation of the Janssen formulae 224
Appendix B – Convergence test on the three-dimensional model 226
Appendix C – Sample finite element input file 228
Appendix D – Example contour plot output from ABAQUS 236
Appendix E - Best fit of finite element predictions to the experimental sand data 238
Appendix F – Investigation of wall pressure cells 240

Notation

(A dot above a symbol indicates a rate (eg. $\dot{\varepsilon}_{ij}$ = directional strain rate))

A	Cross sectional area of silo/Characteristic abscissa
a	Length of long wall
b	Length of short wall
C	Circumference of bin
C_0	Overpressure discharge coefficient
c	cohesion
D	Diameter of bin/Plate flexural rigidity
e	Voids ratio
G	Plastic potential/Shear modulus
H	Height of silo
h_c	Height of surcharge cone
I_1	First invariant of stress tensor
J_2	Second invariant of stress tensor
J_{el}	Elastic volume change
k	Ratio of horizontal to vertical stress in solid
L	Length of silo wall
P_0	Initial stress
P^{el}_t	Elastic tensile limit
P_h	Horizontal wall pressure
P_m	Mean wall pressure
P_n	Normal pressure in hopper
P_t	Tractive force in hopper
P_v	Vertical pressure in solid
P_w	Tractive force down bin wall
p	Average pressure stress
q	Frictional force/Deviator stress
R	Hydraulic radius of bin
r	Radius of bin/Radius of plate

t	Thickness of bin wall
U	Perimeter of rectangular bin
v	Volume of solid
w	Deflection of plate
Y	Yield function
y	Depth from surface of fill
α	Redistribution parameter
α'	Hopper wall angle
β	Drucker-Prager internal angle of friction
γ	Bulk density/Shear strain
E	Young's modulus
E_s	Young's modulus of stored solid
E_w	Young's modulus of silo wall
ε_{ij}	Directional strain
κ	Gradient of reloading lines
λ	Logarithmic bulk modulus/Gradient of initial loading line
μ	Coefficient of friction
ν	Poisson's ratio
σ	Stress
σ_c^0	Initial yield stress
σ_a	Axial stress
σ_r	Radial stress
σ_{ij}	Directional stress
τ	Shear stress
τ_{ij}	Directional shear stress
ϕ	Internal angle of friction
ψ	Dilation angle

List of figures

Figure 2.1 – Comparison of a hydrostatic distribution and a Janssen distribution in a deep silo 4

Figure 2.2 – Figure used to determine the flow type in a silo (from ENV 1991-4 (1995)) 7

Figure 2.3 – Planform shapes of silos 8

Figure 3.1 – Loads exerted on the silo structure from the ensiled material 10

Figure 3.2 – Notation used for silo geometry 13

Figure 3.3 – Equilibrium consideration for Janssen theory 14

Figure 3.4 – A typical Janssen distribution for wall normal pressures 16

Figure 3.5 – Comparison of Janssen and Reimbert theories in a similarly sized circular bin 18

Figure 3.6 – Normal pressures on the long and short wall of a rectangular bin according to Reimbert and Reimbert (1976) 20

Figure 3.7 – Janssen distributions of wall normal pressure using different values of k 24

Figure 3.8 – A rectangular silo with externally applied stiffening 28

Figure 3.9 – Comparison of large and small deflection theory for a circular plate 30

Figure 3.10 – Structural features of cylindrical silos 33

Figure 5.1 – A simple linear elastic load-displacement response 44

Figure 5.2 – A simple non-linear elastic load-displacement response 45

Figure 5.3 – A non-linear system with a non-unique solution 45

Figure 5.4 – Coulomb model for friction 48

Figure 5.5 – A Jenike shear cell 52

Figure 5.6 – Yield loci of granular material determined from the Jenike shear cell 52

Figure 5.7 – Typical results from an oedometer test 53

Figure 5.8 – Apparatus for triaxial test 54

Figure 5.9 – Triaxial test results for wheat material (Ooi, 1990) 55

Figure 5.10 – Volumetric response of a granular solid in compression 59

Figure 5.11 – Distortion of a block of granular material by the application of a force 60

Figure 5.12 – The complete Mohr-Coulomb criterion 61

Figure 5.13 – Variation of a) shear force and b) volumetric strain with shear strain in a granular material (Atkinson and Bransby, 1978) 63

Figure 5.14 – The Mohr-Coulomb criterion in principal stress space 64

Figure 5.15 – The Drucker-Prager criterion in principal stress space 65

Figure 5.16 – The coincidence of the Drucker-Prager and Mohr-Coulomb criteria (Chen, 1994) 66

Figure 6.1 – Restraint at the base of the finite element model of the bin 68

Figure 6.2 – The finite element mesh of an axisymmetric silo 69

Figure 6.3 – Wall normal pressure as calculated from linear elastic constitutive law 72
Figure 6.4 – Comparisons between finite element and Janssen predictions for a range of materials 74
Figure 6.5 – The effect of changing the elastic stiffness in the axisymmetric bin 75
Figure 6.6 – Wall normal pressure as calculated from the porous elastic constitutive law 77
Figure 6.7 – The effect of changing the initial stress in the porous elastic model 78
Figure 6.8 – Simplified figure to show compression of solid in a typical silo 79
Figure 6.9 – Finite element results as determined by the recalibrated porous elastic model 81
Figure 6.10 – The effect of using different initial conditions in the porous elastic model 82
Figure 6.11 – The effect on wall normal pressures of using elasto-plastic constitutive laws in an axisymmetric model 85
Figure 6.12 – Schematic showing the layout of the experimental rig used by Lahlouh *et al* (1995) 87
Figure 6.13 – Finite element model of Lahlouh *et al*'s (1995) geometry 88
Figure 6.14 – Average wall normal pressures as predicted by different constitutive laws 89
Figure 6.15 – Pressures across the wall as predicted by linear elastic law 90
Figure 6.16 – Integrated experimental (Lahlouh *et al*, 1995) and finite element wall normal pressures compared to Janssen distribution for sand 92
Figure 6.17 – Finite element predictions of wall normal pressure across the wall compared to experimental data of Lahlouh *et al* (1995) 93
Figure 6.18 – Comparison between Janssen and FEA results for pea gravel 95
Figure 6.19 – Integrated experimental and finite element wall normal pressures compared to Janssen distribution for gravel 96
Figure 6.20 – Finite element predictions of wall normal pressure across the wall 97
Figure 6.21 – Schematic showing the one-dimensional consolidation test cell 99
Figure 6.22 – One-dimensional consolidation of sand 99
Figure 6.23 – One-dimensional consolidation tests on Leighton Buzzard sand 100
Figure 6.24 – One-dimensional consolidation tests on pea gravel 101
Figure 6.25 – One-dimensional consolidation tests on wheat 102
Figure 7.1 – The effect of Poisson's ratio on the depth over which end effects are present 105
Figure 7.2 – Pressures near the base using different constitutive laws 106
Figure 7.3 – Effect of doubling the mesh density on wall normal pressures 106
Figure 7.4 – The effect of a frictional base in an axisymmetric bin 108
Figure 7.5 – The effect of adopting different values of μ 109
Figure 7.6 – Wall normal pressure predictions in the base and wall disconnected model 110
Figure 7.7 – The distribution of horizontal and vertical stress at two levels in the axisymmetric silo model 111

Figure 7.8 – Effective coefficient of wall friction in the sand model 112
Figure 7.9 – Wall normal pressures from the model with spring-supported base 113
Figure 7.10 – Vertical strain contour plot in axisymmetric model 114
Figure 7.11 – Radial strain contour plot in axisymmetric model 114
Figure 7.12 – Mechanism to account for observed end-effect 115
Figure 7.13 – Effect of small angled hopper on the wall normal pressure prediction 116
Figure 7.14 – The wall normal pressure above the transition with a 45° concentric hopper 118
Figure 7.15 – Wall normal pressure near the base of the model with a hopper 119
Figure 7.16 – Comparison of analysis with LE and PEDP constitutive laws 120
Figure 7.17 – The effect of altering the angle of the hopper on pressures above the transition 121
Figure 7.18 – The effect on wall pressures above the transition of a rigid hopper wall 122
Figure 7.19 – Normal pressure in hoppers of varying angles 123
Figure 7.20 – Deformation of the hopper wall 123
Figure 7.21 – Effect on hopper wall pressure predictions of varying wall stiffness 124
Figure 7.22 – Effective coefficient of friction in hoppers of different angle 125
Figure 8.1 – Proposed arching mechanism of Rotter *et al* (2002) in rectangular silo 128
Figure 8.2 – Patterns of vertical stress at 1m and 2m below the surface of the solid 129
Figure 8.3 – Local and average values of k in sand 131
Figure 8.4 – Local and average values of k in gravel 132
Figure 8.5 – Wall pressure distributions from sand experiments and predictive law 135
Figure 8.6 – Best fit mean pressures in sand 136
Figure 8.7 – The variation of the parameter α with depth in sand in the geometry of Lahlouh *et al* (1995) 137
Figure 8.8 – Predicted distribution resulting from best fit value of α compared to original experimental data for sand (Lahlouh *et al*, 1995) 138
Figure 8.9 – Wall pressure distributions from gravel experiments and predictive law 139
Figure 8.10 – Best fit values of p_m against experimental data and Janssen distribution 140
Figure 8.11 – The variation of the parameter α with depth in gravel in the geometry of Lahlouh *et al* (1995) 140
Figure 8.12 – Predicted distribution resulting from best fit value of α compared to original experimental data for gravel (Lahlouh *et al*, 1995) 141
Figure 8.13 – Comparison of α determined from finite element method and experiment in sand 142
Figure 8.14 – Comparison of α determined from finite element method and experiment in gravel 143
Figure 8.15 – Comparison between FEA results and predictive law of Rotter *et al* (2002) 144

Figure 8.16 – Comparison to Janssen distribution in wheat 145
Figure 8.17 – Wall normal pressure distribution across the wall in wheat 146
Figure 8.18 – Pattern of vertical stress in wheat 1m from the surface of the solid 147
Figure 8.19 – Local and average values of k in wheat 148
Figure 8.20 – α determined from finite element method in wheat 149
Figure 8.21 – Comparison of pressures across the wall from finite element model and predictive law in wheat 150
Figure 9.1 – Wall normal pressures in deep square planform bin 154
Figure 9.2 – Variation of α with depth in different materials 155
Figure 9.3 – Normal deformations (w/t) down the centreline of the bin wall 158
Figure 9.4 – Wall normal pressures for sand in square planform silos 159
Figure 9.5 – Wall normal pressures for gravel in square planform silos 160
Figure 9.6 – Wall normal pressures for wheat in square planform silos 160
Figure 9.7 – Comparison of Janssen and FEA prediction in 3m square planform bin with 100mm thick wall 161
Figure 9.8 – Coefficient α for sand in the square planform bins 162
Figure 9.9 – Coefficient α for gravel in the square planform bins 162
Figure 9.10 – Coefficient α for wheat in the square planform bins 163
Figure 9.11 – Distribution of pressure above the transition 164
Figure 9.12 – Relationship between wall length and elastic stiffness of stored material 165
Figure 9.13 – Relationship between wall length and α 166
Figure 9.14 – Average normal wall pressures down the depth of a 1.5m square planform bin with varying wall thickness (sand fill) 167
Figure 9.15 – Average normal wall pressures down the depth of a 1.5m square planform bin with varying wall thickness (gravel fill) 168
Figure 9.16 – Average normal wall pressures down the depth of a 1.5m square planform bin with varying wall thickness (wheat fill) 168
Figure 9.17 – Variation of α with depth in bins of varying wall thickness (sand) 169
Figure 9.18 – Variation of α with depth in bins of varying wall thickness (gravel) 169
Figure 9.19 – Variation of α with depth in bins of varying wall thickness (wheat) 170
Figure 9.20 – Variation of α at 6m depth with wall thickness 171
Figure 9.21 – Comparison of $E_s L^3/E_w t^3$ with α in sand, gravel and wheat 172
Figure 9.22 – Effect of large deformations on the value of α 173
Figure 9.23 – Comparison of results obtained in a 10m deep bin and 5m deep bin (sand fill) 175
Figure 9.24 – Average wall pressures in a 2m square planform silo of different height (wheat fill) 176

Figure 10.1 – Overall view of the experimental silo structure 179
Figure 10.2 – Internal view of the filler box showing discharge holes 179
Figure 10.3 – The chute and conveyor for emptying the experimental silo rig 180
Figure 10.4 – Wall normal deflections calculated from FEA under different loading conditions 182
Figure 10.5 – Principle of wall pressure cell 184
Figure 10.6 – Free field cell of the type designed by Askegaard (1978) 185
Figure 10.7 – Finite element and Janssen predictions of the mean pressure in the experimental rig 186
Figure 10.8 – Finite element prediction of pressure across the wall in the experimental rig 187
Figure 10.9 – Pressures in the model silo from free field cells and finite element model 188
Figure 10.10 – Predictive law of Rotter *et al* (2002) fitted to experimental results 189
Figure 10.11 – Horizontal and vertical strain down the centreline of the bin wall 190
Figure 11.1 – Notation for rectangular planform silos 192
Figure 11.2 – Ratio of pressures on long side to short side (after Reimbert) 194
Figure 11.3 – Wall normal pressure predictions in a rectangular planform silo 195
Figure 11.4 – Long and short wall pressures in a 2:1 planform ratio bin compared to predictions from ENV 1991-4 (1995) 196
Figure 11.5 – FEA predictions compared to the predictions of Reimbert and Reimbert (1976) 197
Figure 11.6 – Wall normal pressure in a 1.1:1 planform ratio silo (sand fill) 198
Figure 11.7 – Wall normal pressure in a 1.3:1 planform ratio silo (sand fill) 199
Figure 11.8 – Wall normal pressure in a 1.5:1 planform ratio silo (sand fill) 199
Figure 11.9 – Wall normal pressure in a 2:1 planform ratio silo (sand fill) 200
Figure 11.10 – Deformation of the wall at the top of the silo 201
Figure 11.11 – Wall normal pressure in a 1.1:1 planform ratio silo (wheat fill) 201
Figure 11.12 – Wall normal pressure in a 1.3:1 planform ratio silo (wheat fill) 202
Figure 11.13 – Wall normal pressure in a 1.5:1 planform ratio silo (wheat fill) 202
Figure 11.14 – Wall normal pressure in a 2:1 planform ratio silo (wheat fill) 203
Figure 11.15 – Redistribution of wall normal stress in a rectangular bin of planform ratio 1.5:1 204

List of tables

Table 3.1 – Stresses in a rectangular plate as calculated from large and small deflection theories 31

Table 3.2 – Finite element solution to the large and small deflection rectangular plate 32

Table 5.1 – Some properties of granular bulk solids 51

Table 6.1 – Values of bulk density for Leighton Buzzard sand from Lahlouh *et al* (1995) 71

Table 6.2 – Properties of various granular bulk solids as given by Rotter (2001) 73

Table 6.3 – Properties of granular bulk solids for use in the linear elastic model 73

Table 6.4 – Values used to calibrate the porous elastic constitutive law 76

Table 6.5 – Calculation of λ from initial and final densities 80

Table 6.6 – Wall normal pressures (in kPa) in the experimental silo from free field cells in sand (Lahlouh *et al*, 1995) 92

Table 6.7 – Properties of pea gravel measured by Lahlouh *et al* (1995) 94

Table 6.8 – Results from consolidation tests on sand and gravel 101

Table 6.9 – Final properties used for the materials in the finite element model 103

Table 9.1 – Equivalent elastic stiffness of the three materials 157

Table 9.2 – Equivalent elastic stiffness in the square planform bins 164

Table 9.3 – Equivalent elastic stiffness with varying wall thickness 170

Table 10.1 – Results from shear tests of different adhesives 181

Table 10.2 – Values of α and p_m determined from the predictive law of Rotter *et al* (2002) 189

Table 11.1 – Definitions according to EN1991-4 (Note: d_c=b for rectangular silos) 193

Table 11.2 – Length of walls in rectangular planform silo models 198

Chapter 1 - Introduction

In the modern industrial environment there are many situations where granular bulk solids need to be stored. Typical granular bulk solids include corn, plastic pellets for a production line or coal to feed furnaces. The structures used to hold these materials are known as silos, although they are occasionally referred to as bunkers (particularly when referring to the ground supported, squat type typically used to store coal in power stations). Silos are usually constructed from steel or reinforced concrete and it is apparent that much research effort should be directed toward the study of these types of structures as over 1000 structural failures occur in silos in North America alone each year (Jenkyn and Goodwill, 1987).

Silos are most commonly found in circular planform due to the structural efficiency of this type (Trahair, 1985). Circular planform structures support the loads from the ensiled material mainly by membrane actions. They are axisymmetric, potentially simplifying the design process (Rotter, 1985a) but this can lead to a weak structure were any bending actions to arise (Rotter, 1985b). Circular planform silos must be accurately constructed because they are sensitive to any imperfections of the shell surface. One of the alternative silo structural forms is a rectangular planform structure, but this has largely been ignored because it is difficult to assess the response to the loads acting on the structure. In this type of structure the main load carrying action is bending but if the wall deforms sufficiently there may be some membrane action induced. This membrane action will always be dominated by the bending action but can significantly increase the ultimate strength of the plate if it is taken into consideration. Advantageously however, rectangular silos are simply constructed from flat plate which requires little preparatory work and could therefore provide a cost effective alternative to circular planform silos if design codes could be suitably adapted to better predict the behaviour of this type of structure.

Of most importance to structural designers are the (horizontal and vertical) pressures acting on the silo wall. There are several theories that are commonly used to predict pressures (Janssen, 1895; Reimbert and Reimbert, 1976). The resulting pressures are

then usually multiplied by some factor of safety in order to account for any excess pressure that may occur during filling or discharge. Once these are ascertained it is then a matter of using appropriate methodology to design the silo for strength, stiffness and stability. Most of these theories assume the silo (and its contents) has symmetry of rotation but it has been shown that even in a cylindrical silo this is not the case (Nielsen, 1983). It is also obvious that rectangular structures do not have rotational symmetry and therefore the available theories have to be adapted to suit. This adaptation is unsatisfactory because it makes further assumptions which may have a deleterious effect upon the economy of any rectangular silo design. Structures produced in this way tend to have an excess of stiffness; they use thick plates and a large number of external and internal stiffeners. This increases the weight of the silo and hence the cost. These designs could be improved by allowing a certain amount of deformation to occur in the wall of the silo which in turn stiffens the plate by membrane actions.

In previous work (Jarrett, 1991; Lahlouh *et al*, 1995) the emphasis was on experimental determination of the effect of wall flexibility on measured pressures. This project aims to extend the knowledge in the area of rectangular planform steel silos in the following ways:

- By using finite element models to predict wall pressures in flexible walled silos,
- By determining the effect of a very flexible, thin silo wall on wall pressures,
- By comparing experimental results with predictive theories, and
- By assessment and design of instrumentation for use in scale model silos.

1.1 Thesis summary

The work presented in this thesis consists of twelve chapters of which this introduction is the first.

Chapter 2 gives some background into the problem being studied as well as defining some of the terms and concepts used throughout the remainder of the work. Chapter 3 describes some of the methods currently used to assess the loads on, and responses of silo structures. Chapter 4 introduces various numerical methods that can be applied to problems of the type studied in this work. It goes on to describe the choice of the finite element method used for the remainder of the study. Chapter 5 describes the finite element method with respect to silo problems outlining solution techniques and modelling methods used.

Chapter 6 describes the initial investigation and validation of the finite element model. This includes determination of parameters used in various constitutive laws that can describe granular materials of the type stored in silos. This is achieved by a combination of interpretation of experimental data, comparison with current theory and comparison with previous experimental work (Lahlouh *et al*, 1995). Chapter 7 is a study of some of the modelling anomalies experienced in Chapter 6. This is with regard to observed end effects near the base of the bin.

Chapter 8 introduces a two parameter predictive law conceived by Rotter *et al* (2002). This law aims to describe the experimentally observed non-uniform distribution of wall pressure at a given depth in the ensiled material. The law is compared to experimental and finite element results. Chapter 9 describes a parametric survey of a square silo. It is shown that the previously introduced predictive law is a good fit to finite element results for a number of geometrically different bins. Chapter 10 describes an experiment performed on a thin-walled square planform silo and makes comparisons with the predictive law and the finite element model. Chapter 11 presents a parametric study of a rectangular silo and shows that the actions in structures of this type are very different from the actions in a square planform silo.

Finally, Chapter 12 presents conclusions and suggestions for further work.

Chapter 2 - Background to the problem

The structural designer of silos is concerned with the horizontal and vertical pressures acting on the wall of the silo, because these pressures determine the membrane and bending actions that govern design. The response of the silo can be difficult to predict due to the large number of different possible failure modes, interaction between the stored solid and the structure and sensitivity to geometric imperfections.

The wall pressures in silos were originally assumed to be equivalent to hydrostatic (fluid) pressures. Early experiments by Roberts (1882; 1884) showed that this was not the case as some of the weight of the stored material is carried by the wall due to friction at the interface between the materials. Janssen (1895) confirmed this and published his still widely used theory that accounts for this phenomenon. Soon after, Airy (1897) published a second theory to compute wall pressures but this is not in such widespread use as Janssen's. A typical Janssen distribution for normal pressure down the depth of a silo wall is shown in figure 2.1, along with the hydrostatic distribution that was previously assumed to be correct.

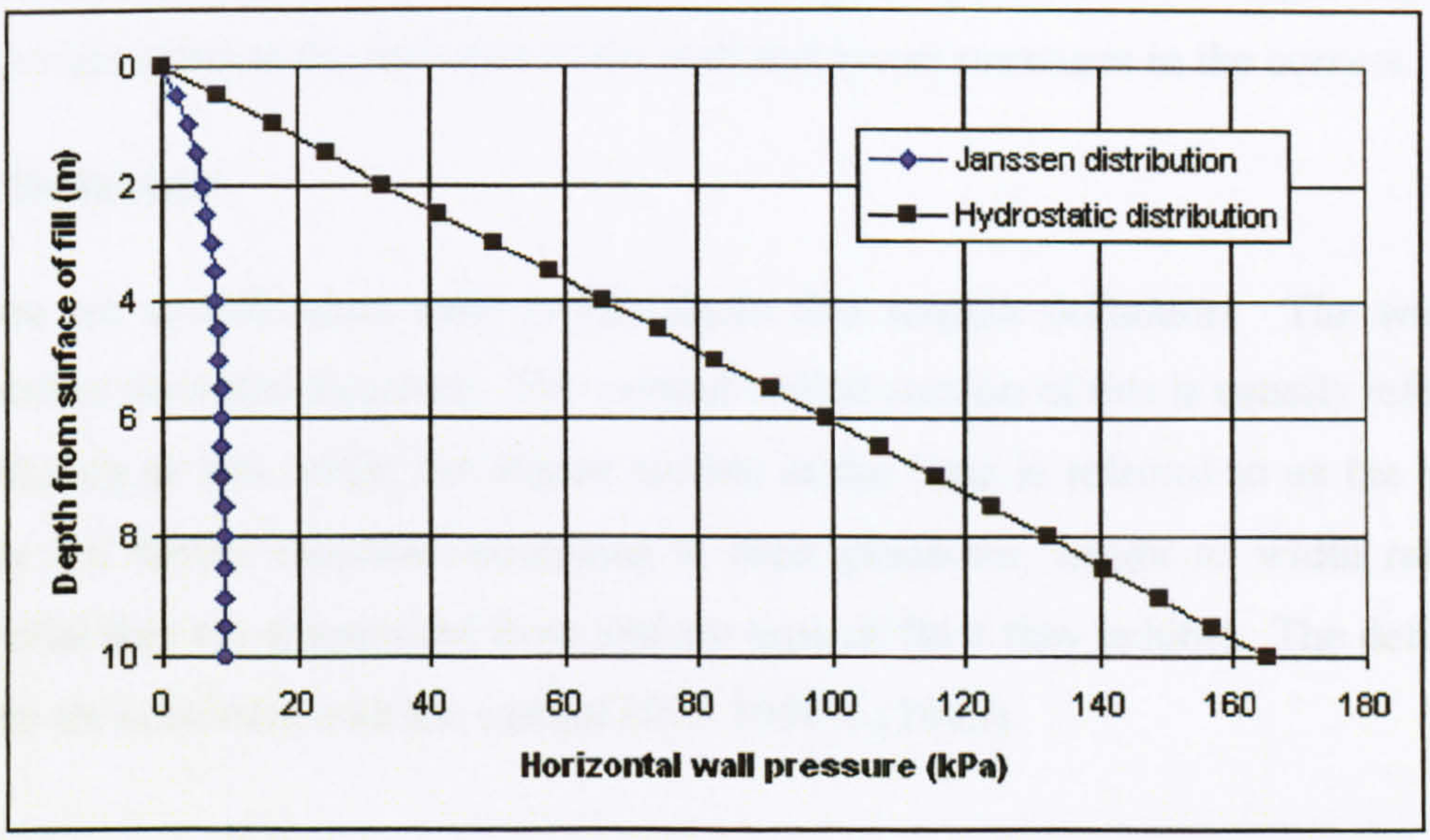

Figure 2.1 - Comparison of a hydrostatic distribution and a Janssen distribution in a deep silo

It is obvious that the pressure predicted by the Janssen theory is substantially lower than the hydrostatic distribution. The reason for this observed phenomenon is that granular materials have shear strength (i.e. they can support some of their own weight) and friction exists at the interface of the wall and the material. This leads to the development of an equilibrium between the weight of the solid and the supporting wall friction. The observation of this property has led to the proposal of many theories in the field of soil mechanics, several of which are specifically for the prediction of pressures in silos. However each of these theories contains assumptions and limitations that may make them unsuitable for particular types of problems.

Theories for silo pressures include the Janssen formula (1895), those developed by Reimbert and Reimbert (1976) from empirical data and earth pressure theories such as Coulomb's (1776). These theories consider the wall to be rigid and the pressure to be invariant at any given depth but it has been shown by Jarrett *et al* (1995) and more recently emphasised by Rotter *et al* (2002), that this is not the case for rectangular planform silos. This research showed that when the wall is flexible an arch can form in the granular solid over the deforming wall leading to lower pressures in the middle of the wall and higher pressures near rigid, supporting boundaries. This is in contrast to Janssen's original postulation that a rectangular planform silo might experience higher pressures at the mid-side of the wall and lower pressures in the corners.

2.1 Definitions

There are several terms used in this thesis that require definition. The word silo describes the entire structure. The vertical walled section of this is usually referred to as the bin or box, while the angled section at the base is referred to as the hopper. Silos are further classified according to their planform, height to width ratio, the material they are constructed from and the type of flow they exhibit. The definitions given are consistent with the current ENV 1991-4 (1995).

2.1.1 Planform

Currently, silos most commonly occur in either circular or rectangular planform. Other planforms are occasionally used and some were investigated by Reimbert and Reimbert (1976). Circular planform silos are efficient structures that carry most of their loads by membrane (hoop) actions. As this form of silo is the most common, the majority of research activity is not unreasonably directed towards their study. Rectangular planform structures may however, need to be used for a number of practical reasons and if the efficiency of this type of structure could be improved then it may provide a viable alternative to circular silos.

2.1.2 Height to width ratio

Silos can also be classified as deep or shallow and an approximate guide to this factor would be that a shallow silo has a height not exceeding one and a half times the diameter (or shortest side length). A deep bin obviously has a ratio greater than this (ENV 1991-4, 1995).

2.1.3 Construction materials

Silos are usually constructed from either steel or reinforced concrete. Concrete structures are more usually used in larger applications such as the storage of cement clinker, coal and grain. Concrete structures are obviously designed with permanency in mind whereas steel structures can be easily constructed, moved, recycled etc. Recently, large concrete designs have been replaced by batches of squat steel silos. The design and testing of concrete structures has been well reported (Eibl, 1998) and will not be covered in this project, although some reference will be made to very stiff structures which could be considered to be like concrete in behaviour.

2.1.4 Flow type

Consideration must be given to the type of flow experienced in a silo. The type of flow leads to different pressure regimes within the silo contents and therefore different pressures on the silo wall (Nielsen, 1998). Flow types can be generally

classified as mass flow and funnel flow (sometimes known as core or internal flow). In mass flow, the ensiled material moves down the silo as one during discharge. In funnel flow, the material tends to flow down a central flow channel while the outer material remains stationary. Whether funnel flow or mass flow occurs in a silo is governed by a number of factors amongst which the material properties and the angle of the hopper walls are most important. A graphical design method for determining which type of flow will occur is employed by most codes and a typical diagram is shown in figure 2.2 (ENV 1991-4, 1995).

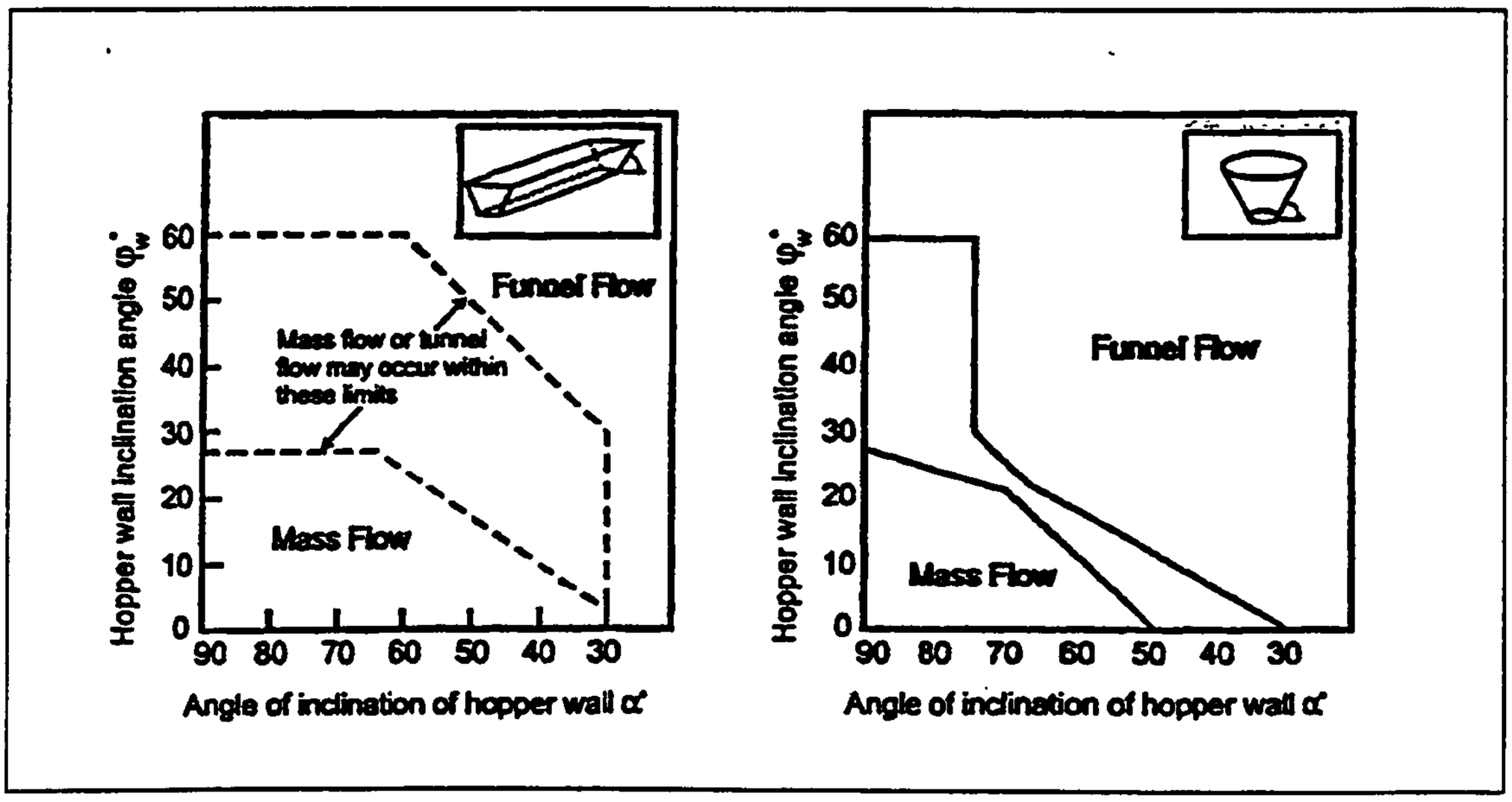

Figure 2.2 - Figure used to determine the flow type in a silo (from ENV 1991-4 (1995))

The figure shows that mass flow will more likely occur in smooth walled silos with steep hoppers and those with rough walls or shallow hoppers will more likely experience funnel flow. The type of flow experienced in the silo is an important starting point in the structural design process. Mass flow may be deemed necessary in food processes because they operate on a first in/first out principle, thus avoiding stagnant zones associated with funnel flow. This stagnant food material could spoil in a low volume production situation. Conversely, space may be limited which precludes the steep hopper angle required for mass flow hoppers and therefore other solutions for assisted discharge would have to be considered such as flow agitators. Another disadvantage is that mass flow silos wear heavily on the wall due to the

abrasive effect of the granular bulk solid sliding down the wall and this must be factored into the design.

2.2 Silos studied

This thesis is concerned with metal, rectangular planform, thin-walled silos. Metal silos appear in many different plan-forms: circular, rectangular, square and hexagonal. They can be tall or squat, ground supported or elevated on columns. Some different forms of silo are shown in figure 2.3.

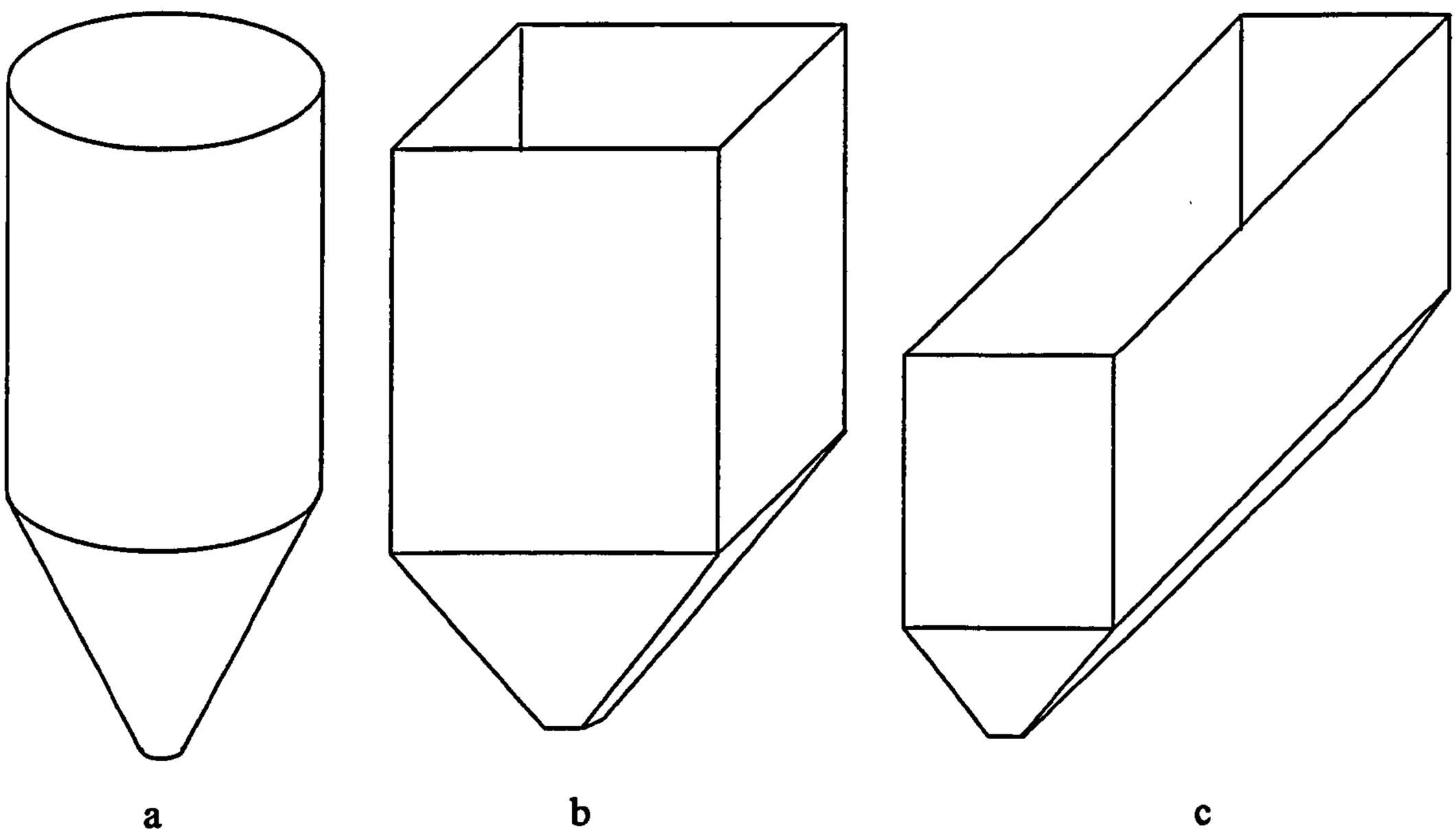

Figure 2.3 – Planform shapes of silos

This variation of form allows the designer to accommodate many different types of loading but the interaction between the stored bulk solid and the silo wall makes the assessment of the wall pressures difficult. Figure 2.3(a) shows a diagram of a typical metal, cylindrical silo. It can be seen that the basic structural form of this type of silo is a thin, axisymmetric shell of revolution making the stress in the structure relatively uniform around the circumference. This makes the analysis of the structure slightly easier for simple, un-stiffened cases. However, silos are regularly stiffened in some

way and when considering a rectangular planform silo their natural shape contains stress raisers such as corners that make the prediction of stress more difficult.

Figure 2.3(b) shows the basic layout of a rectangular plan-form structure of the type that is to be considered in this project. Each form of silo has its own advantages and disadvantages. Rectangular planform silos can be easily constructed from plate material, meaning there is less fabrication work required prior to construction on site. However, rectangular planform silos are not as efficient structures as circular ones because they do not take advantage of membrane stresses (section 3.10). Rectangular structures may also make more use of available ground-space (because they tessellate), which may be important in applications where space is limited.

It is noted that the silos studied in this project are different from the type shown in figure 2.3(c), which is known as a trough bunker. These are usually squat and long (the ratio of long wall to short wall is large and they are often treated as infinitely extending parallel walls) and exhibit plane flow (essentially 2-D flow, the stress state is not a function of the co-ordinate perpendicular to the plane of flow).

Chapter 3 - Stresses and loads in the ensiled material and the silo structure

3.1 Silo loads

Silos are subjected to a number of load cases of various load conditions. Of most importance for design purposes are the loads imposed on the structure by the weight of the granular bulk solid when the silo is filled and emptied. These loads consist of pressure components and frictional tractive forces and are shown in figure 3.1.

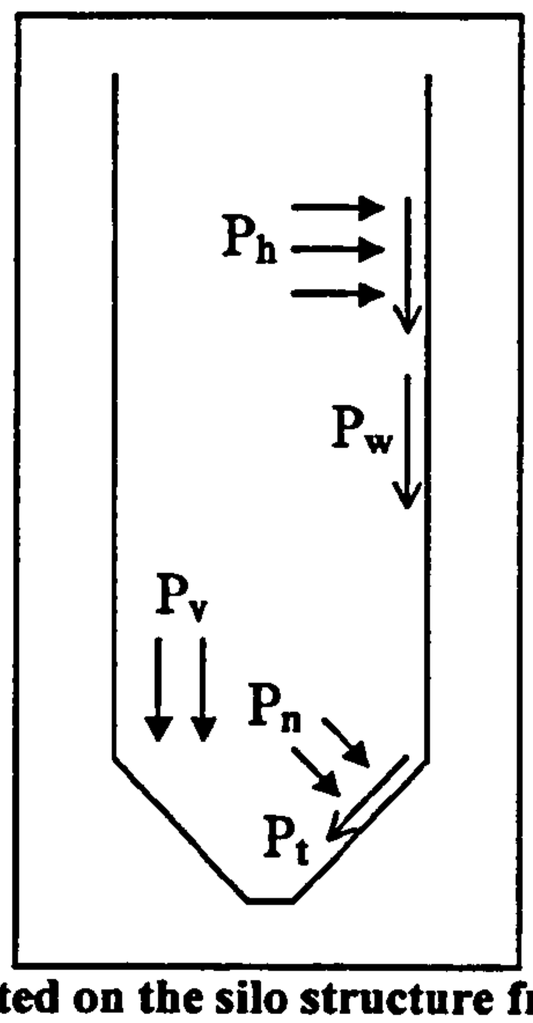

Figure 3.1 – Loads exerted on the silo structure from the ensiled material

Wall pressures can be influenced by a number of factors including the silo geometry, wall friction and type of stored material. There are also a number of other loads that may need to be considered in the design process such as wind loading, thermal loading and other environmental loads.

This thesis is mainly concerned with the determination of the filling pressures in the silo structure and as such most consideration will be given to these loads and the interaction between the ensiled material and the silo structure.

3.2 Stress state in the stored solid

Granular materials at rest in a silo can be said to exist in an elastic state which is limited by the Rankine active and passive pressure coefficients (Gaylord and Gaylord, 1984). These define the point of active failure (caused by expansion of the material) and passive failure (caused by compression of the material). However, throughout the granular material this state can differ which can affect the internal stresses experienced by an ensiled material which in turn affects the pressures experienced on the wall.

This behaviour of stored materials is known to affect the pressures exerted on the walls of a silo structure (Nielsen, 1983). Therefore it follows that the overall stress state that the stored material assumes influences the wall pressures. There are three categories of wall pressure that are usually considered by designers; filling, static and discharge. The assumption that the filling and storage pressures are approximately equal is widely accepted (although some types of granular materials may cause the pressure regimes to alter over a period of time), and so consideration is normally only given to two stress states. The problem is often further simplified by basing the evaluation of discharge pressures on the static/filling pressures which are multiplied by some pre-determined factor that accounts for the apparent excess pressure. This factor is usually determined from codes or design guides (ENV 1991-4, 1995; DIN 1055, 1987). These flow load multipliers are generally derived by consideration of changes in the stress field upon the onset of discharge (Nanninga, 1956; Walters, 1973a,b) and were originally obtained empirically. This process requires the designer to perform only one set of calculations upon which the final design will be based even though there are three different phases of loading. This is before any consideration of any other external loadings. This would appear to be a considerable shortcoming given the variability of experimentally observed static pressures (Nielsen, 1979; Nielsen and Anderson, 1982; Hartlen *et al*, 1984) and discharge pressures (Nielsen, 1998).

The stress state (and hence the wall pressures) is also greatly affected by the eccentricity of the fill and discharge processes. During filling it is unlikely that material will be deposited from directly above the bin in the centre. It is more likely that material will be travelling up a conveyer and will be deposited into the bin towards one side, possibly impacting on the opposite wall in the case of a slender silo. This will have a large effect on the state of stress that exists in the solid at the end of the filling process and this has subsequently been shown to affect the wall pressures (Zhong *et al*, 2001). Similarly, it is possible that the material will be drawn from the silo via an eccentric hopper and this has been shown to produce highly asymmetric pressures in cylindrical bins (Rotter, 1986).

3.2.1 Interaction between silo and contents

The pressure exerted on the silo wall is dependent on the interaction between the wall and the stored bulk solid. This is especially so when the wall is flexible in a systematic way, as in a rectangular planform silo. Little work is currently available, although several research groups have shown that the flexibility of the wall of a cylindrical silo can have an effect on the wall pressures (Ooi and Rotter, 1990; Mahmoud and Abdel-Sayed, 1981). Others have performed studies of the silo-material interaction (Emanuel *et al*, 1983; Ibrahim and Dickenson, 1983). Most of these studies have used a two-dimensional finite element model. In order to improve the study of this phenomenon a three-dimensional model would be the most suitable but until recently this would have been impractical due to the constraints of computer systems.

Jarrett *et al* (1995), Lahlouh *et al* (1995) and Rotter *et al* (2002) have presented experimental results for square planform steel silos showing that the flexibility of the wall and the type of granular material used affects the measured pressures.

3.3 Calculations for wall pressures

There are a number of theories available for the prediction of the wall pressures and these have been reviewed extensively elsewhere (Arnold *et al*, 1980; Gaylord and

Gaylord, 1984). Most of these theories are applicable to cylindrical silos because these structures can be reduced to two dimensions by the assumption of axisymmetry. As it is known that the wall deformation and hence the wall pressure in a rectangular silo varies at constant depth then a three dimensional analysis is required (Ibrahim and Dickenson, 1983). However, as there are not any specific formulae for this type of calculation, the cylindrical theories are usually applied to rectangular planform structures, although these are sometimes modified slightly to take account of parameters such as the ratio of the length of the side walls. Only the most commonly used theories will be assessed here, along with their assumptions and suitability towards the current problem. Figure 3.2 shows the notation used for the geometry of the silo in the forthcoming sections.

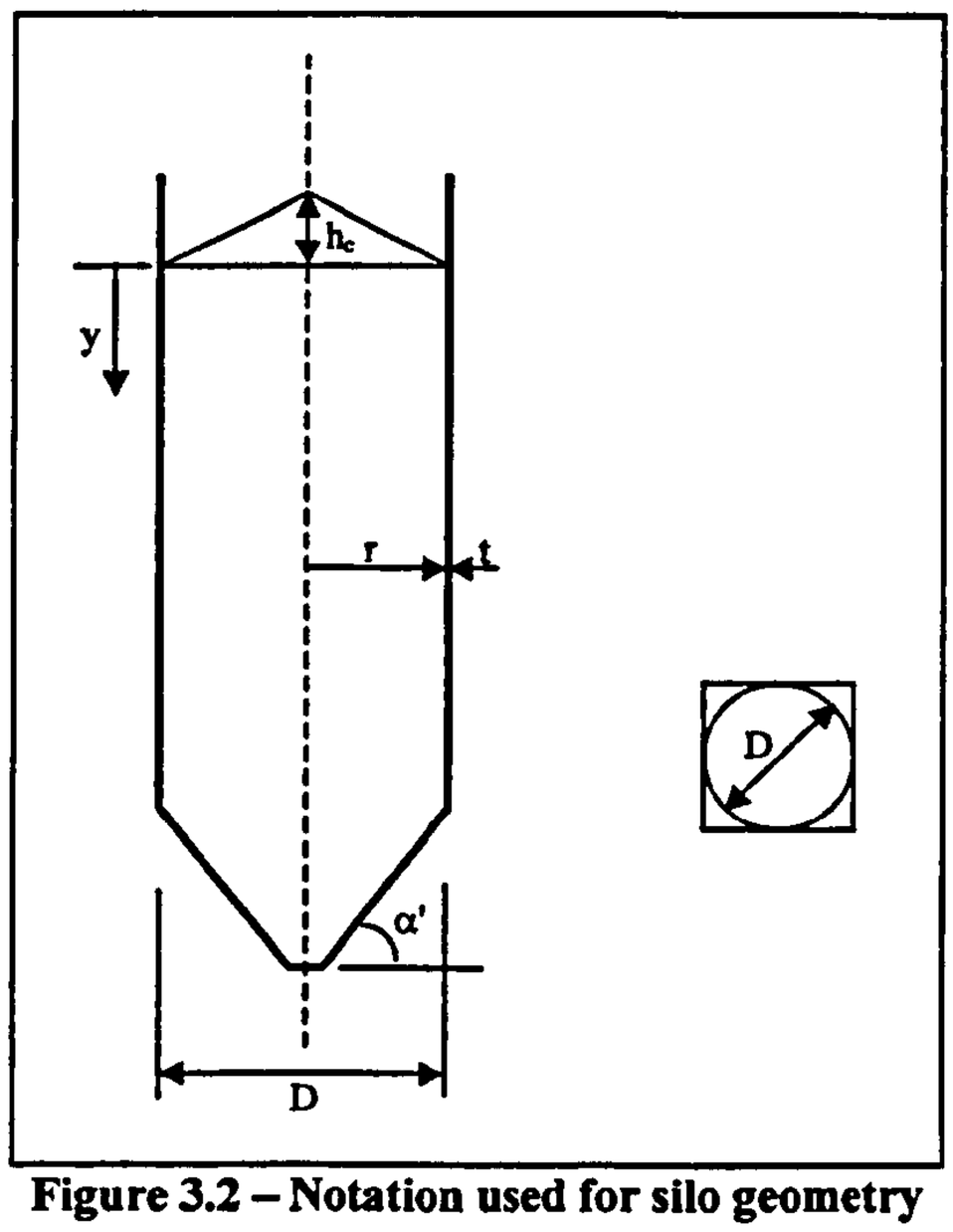

Figure 3.2 – Notation used for silo geometry

3.3.1 Theory of Janssen

Pressures in deep silos of circular planform are usually calculated by the theory of Janssen (1895). This is derived by considering the equilibrium of a horizontal slice of material in the silo as shown in figure 3.3.

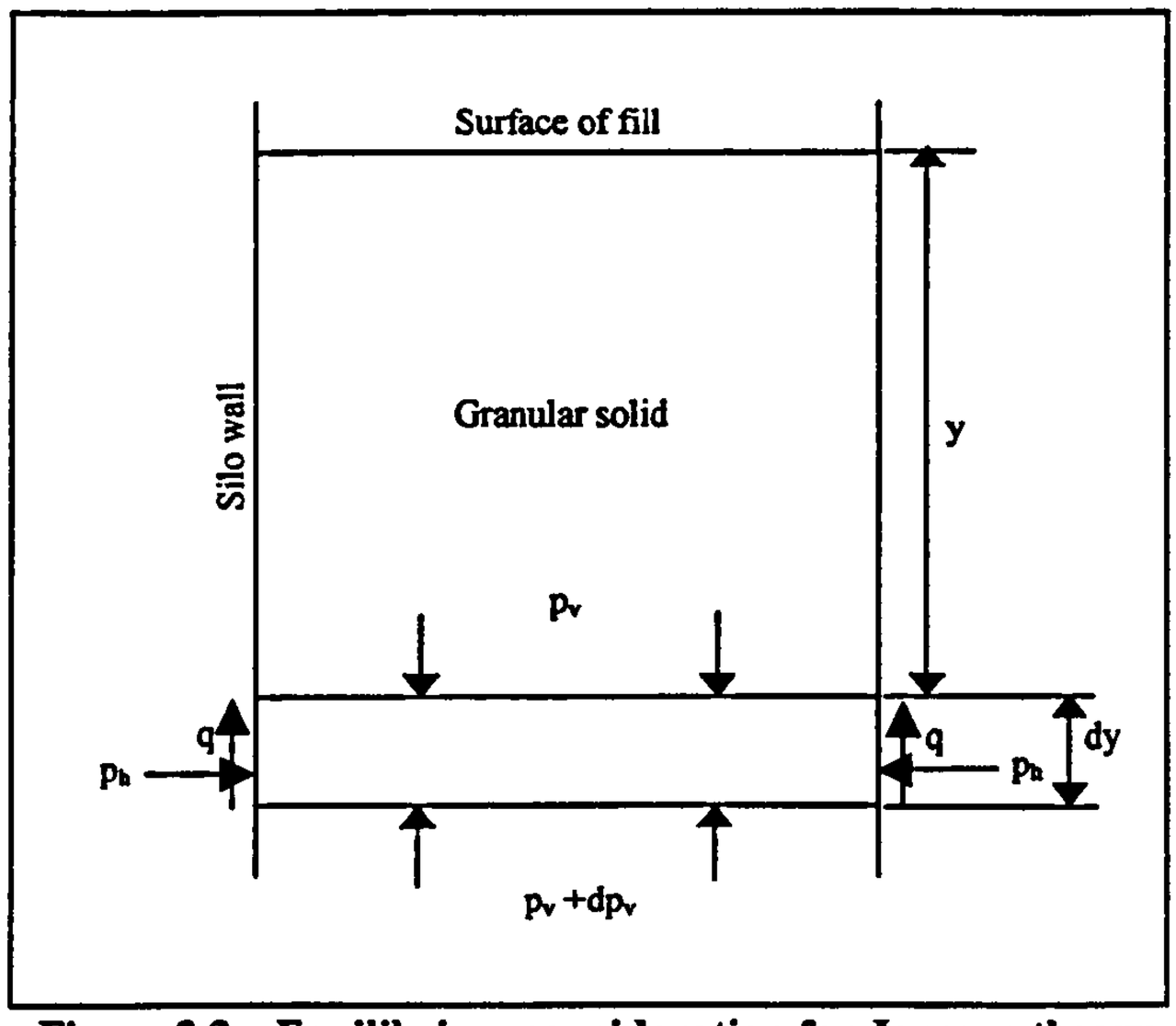

Figure 3.3 – Equilibrium consideration for Janssen theory

Summation and integration of these forces yields the following equation for the vertical pressure in the solid:

$$P_v = \frac{\gamma R}{\mu k}\left(1 - e^{-\mu k\, y/R}\right) \tag{3.1}$$

Where γ = bulk density of the stored material, R = A/C = hydraulic radius of the silo, μ = the coefficient of wall friction, k = the ratio of horizontal to vertical stress and y = the depth of the solid above the section, which is assumed to be level. The outline derivation of this formula can be seen in Appendix A.

The Janssen formula makes a number of assumptions that have an effect on the usefulness of the model.

- The vertical stresses are zero at the free surface
- The coefficient of friction between the material and the wall is constant and friction is mobilised throughout
- The average ratio of horizontal to vertical stress is constant
- The stored material is isotropic and uniform in weight

These assumptions limit the cases to which the Janssen formula should be applied but it is still used as the basis for a large number of design codes (ENV 1991-4, 1995; DIN 1055, 1987).

The pressure coefficient, k, relates the horizontal to vertical stress in the solid:

$$k = \frac{P_h}{P_v} \tag{3.2}$$

And hence the horizontal wall pressure is given by the formula:

$$P_h = \frac{\gamma R}{\mu}\left(1 - e^{-\mu k\, y/R}\right) \tag{3.3}$$

The usefulness of the Janssen theory is therefore dependant on the method used to assess this coefficient, k, and this is discussed further in section 3.5. The use of the hydraulic radius of a bin (rather than the circumference or the diameter) allows the designer to account for non-circular cross-sections, but the resulting solution is still two dimensional and therefore gives no indication about the pressure distribution across a non-circular bin at any given depth. It is therefore commonly assumed to be uniform. A typical Janssen distribution for wall normal pressures (P_h) is shown in figure 3.4.

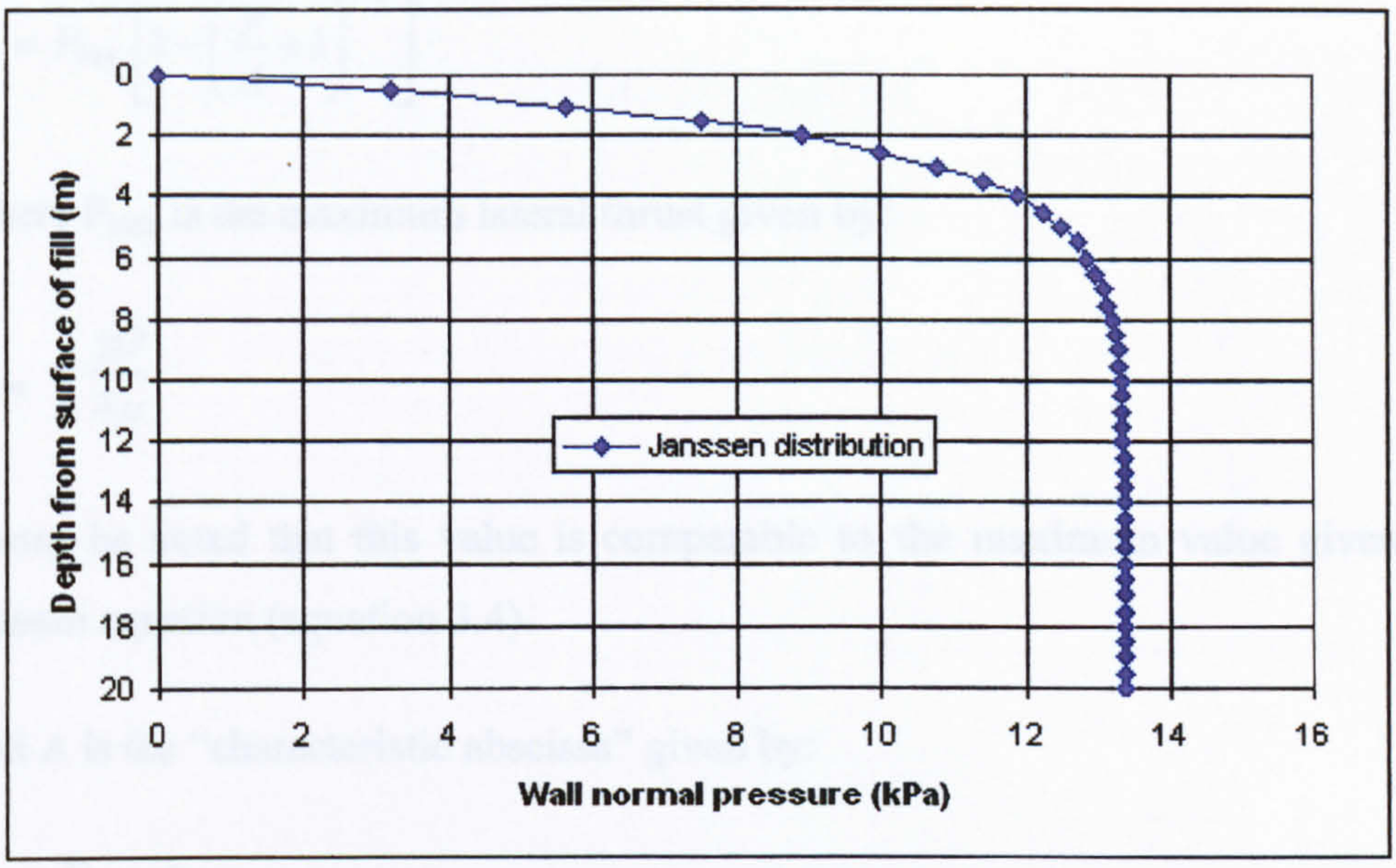

Figure 3.4 – A typical Janssen distribution for wall normal pressures

It can be seen that at great depth the pressures tend to an asymptotic value. This asymptotic value can be calculated by reducing the exponential component of equation 3.1 to zero making the maximum horizontal and vertical pressures equal to equations 3.4 and 3.5 respectively.

$$P_h = \frac{\gamma R}{\mu} \tag{3.4}$$

$$P_v = \frac{\gamma R}{\mu k} \tag{3.5}$$

3.3.2 Theory of Reimbert and Reimbert

Another method of prediction of wall pressure is that of Reimbert and Reimbert (1976) which is an empirically derived method resulting from a large number of experiments. This theory allows for the differences in planform that can occur in silos and also the value of k to change with respect to the depth below the surface of fill. It is based on the calculation of what is termed the "characteristic abscissa". For a cylindrical silo the horizontal pressure at a given depth is:

$$P_h = P_{\max}\left[1-\left(\frac{y}{A}+1\right)^{-2}\right] \tag{3.6}$$

Where P_{max} is the maximum lateral thrust given by:

$$P_{\max} = \frac{\gamma D}{4\mu} \tag{3.7}$$

It may be noted that this value is comparable to the maximum value given by the Janssen equation (equation 3.4).

And A is the "characteristic abscissa" given by:

$$A = \frac{D}{4\mu k} - \frac{h_c}{3} \tag{3.8}$$

D = diameter of silo and h_c = height of cone of surcharge.

The value of k taken in the original formulae was the Rankine active ratio (see below, equation 3.17). It may also be noted that this theory takes account of any surcharge on the material's surface which the Janssen equations do not (they are modified to accommodate an equivalent surface). This is a major deficiency in the Janssen theory as the surface boundary condition is clearly incorrect. A conical surcharge must lead to a finite value of vertical stress where the solid first makes contact with the wall. However, the wall normal pressure at this point must be zero and therefore the value of k must also be zero. This discrepancy has no real effect in a deep silo because the surcharge is small relative to the overall depth but in a squat silo the surcharge can have a large effect and different methods of treating this problem are shown in section 3.3.3.

The following graph shows the horizontal pressure distribution down the wall of a cylindrical deep silo as calculated by the Janssen and the Reimbert and Reimbert formulae assuming a horizontal surface (figure 3.5).

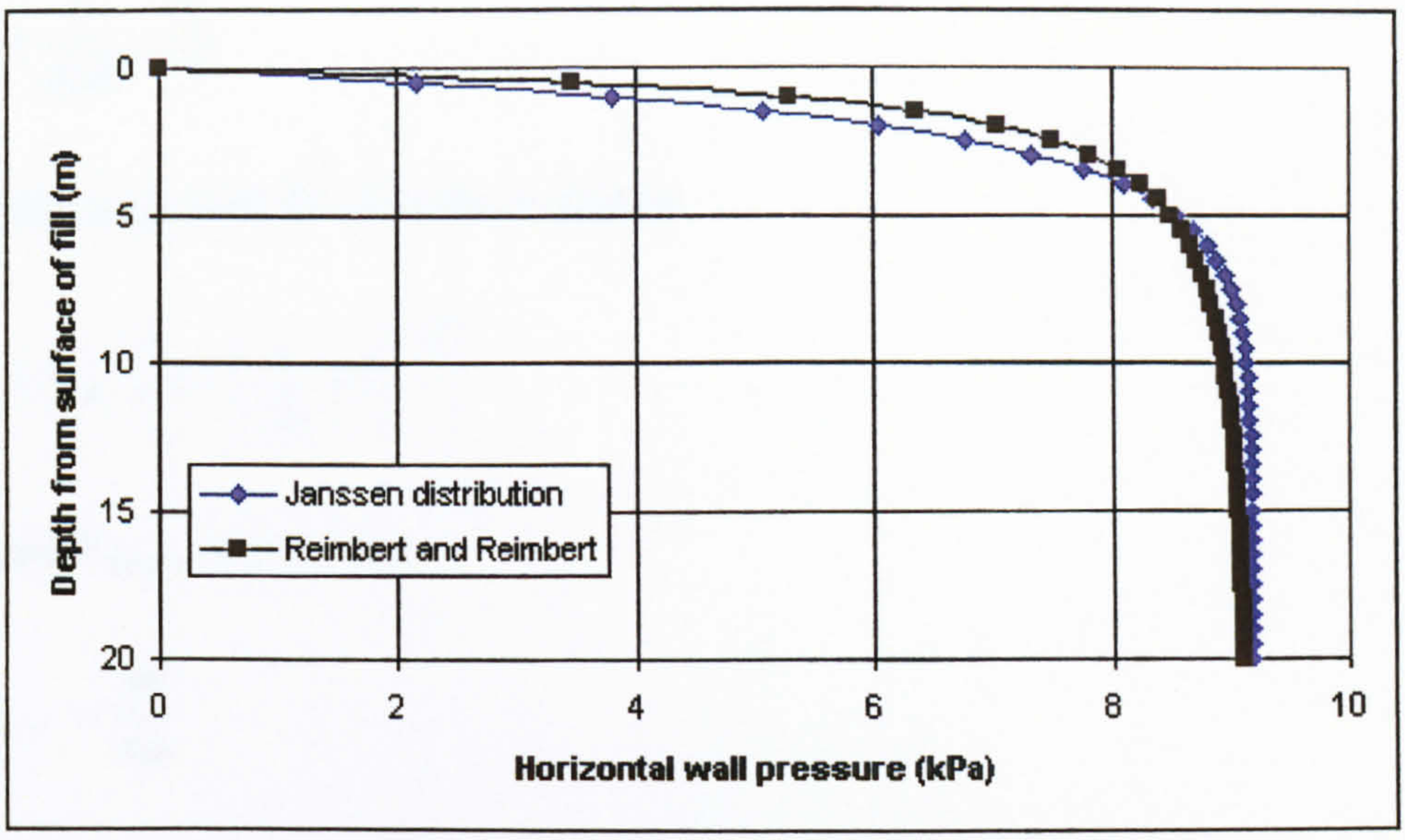

Figure 3.5 – Comparison of Janssen and Reimbert theories in a similarly sized circular bin

The value of k taken here was that of the Rankine active ratio. The choice of this ratio is discussed in further detail in section 3.5. The graph clearly shows that both methods tend towards an asymptote at a great depth and the maximum value is identical.

The Reimbert and Reimbert method also gives specific formulae for the calculation of the pressure in a rectangular bin. This is based on the calculation of the relevant P_{max} and A for the long and the short walls using the same basis as for the cylindrical silo (i.e. the equilibrium requirement is maintained).

If the width of the short wall is denoted as *b* and the long wall as *a* then the pressure on the short wall can be calculated from:

$$P_h = P_{\max.b}\left[1-\left(\frac{y}{A_1}+1\right)^{-2}\right] \tag{3.9}$$

Where $P_{max.b}$ is given by:

$$P_{\max.b} = \frac{\gamma b}{4\mu} \tag{3.10}$$

And A_1 given by:

$$A_1 = \frac{b}{\pi\mu k} - \frac{h_c}{3} \tag{3.11}$$

For the long wall the formula is similar:

$$P_h = P_{\max.a}\left[1-\left(\frac{y}{A_2}+1\right)^{-2}\right] \tag{3.12}$$

Where $P_{max.a}$ is given by:

$$P_{\max.a} = \frac{\gamma b'}{4\mu} \tag{3.13}$$

With:

$$b' = \frac{2ba - b^2}{a} \tag{3.14}$$

And A_2 given by:

$$A_1 = \frac{b'}{\pi\mu k} - \frac{h_c}{3} \tag{3.15}$$

Figure 3.6 shows the horizontal pressures on the walls of a deep rectangular bin where the ratio of long wall to short wall is 2:1.

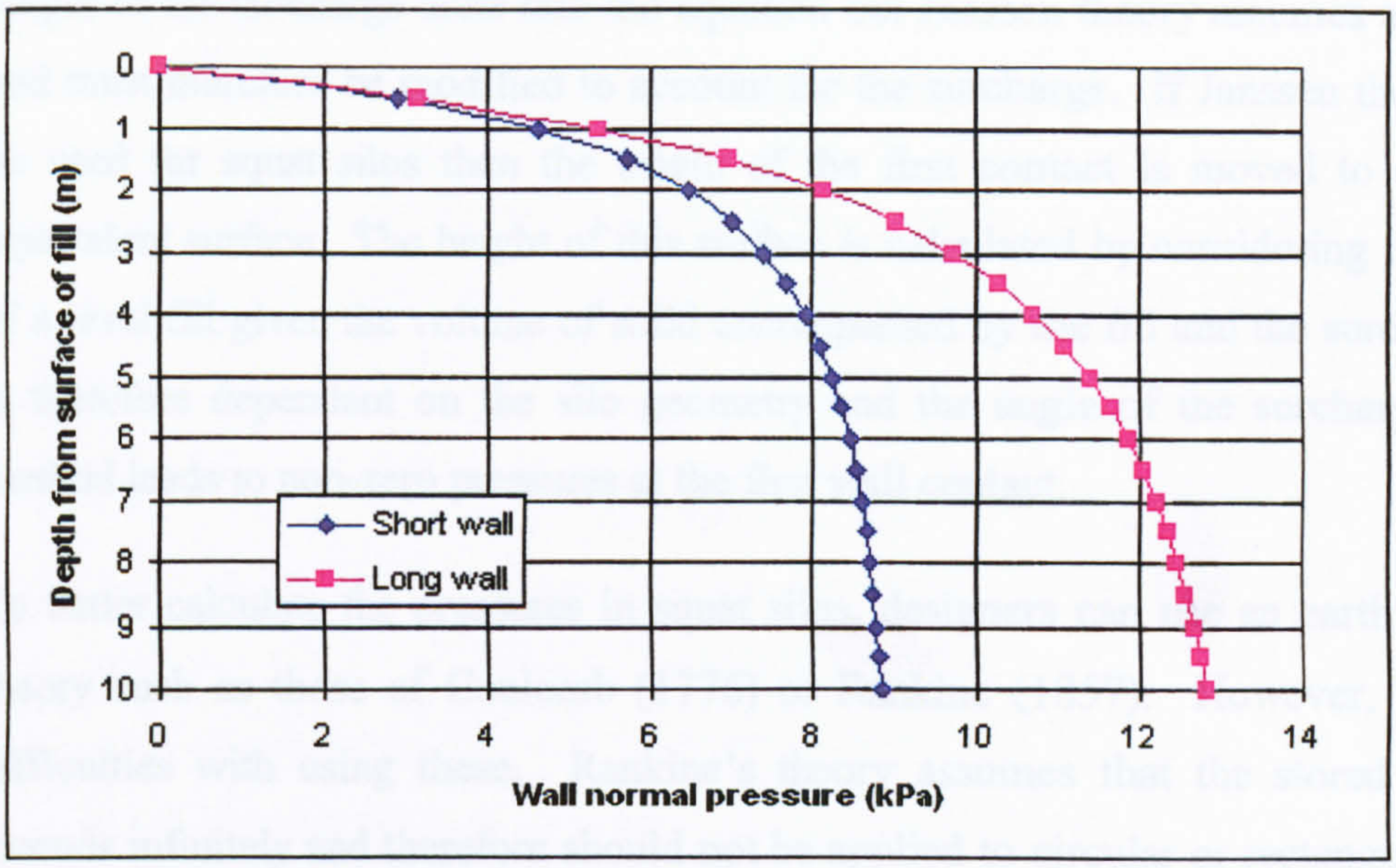

Figure 3.6 – Normal pressures on the long and short wall of a rectangular bin according to Reimbert and Reimbert (1976)

It is clear that this theory predicts that the shorter wall will experience a much lower pressure than the longer one. This arises from the granular bulk solid spanning across the shorter distance between the long walls and hence more load is transferred to the long walls.

3.3.3 Theories for squat silos

The above theories are most suited to deep bins but when the height to diameter ratio of a silo becomes less than about 1.5 then the silo can be referred to as squat although H/D values of between 1 and 1.5 are defined as intermediate by the Eurocode (ENV 1991-4, 1995). There is even some debate about this definition with other limiting values being proposed (Fischer, 1966), for example:

$$H \leq 1.5\sqrt{A} \tag{3.16}$$

Where H is the height of the silo and A the cross-sectional area.

Janssen, and Reimbert and Reimbert theories do not predict the pressures in these type of bins very well because of the influence of any conical surcharge. The Reimbert and Reimbert theory makes an allowance for this by incorporating the

height of the surcharge cone into the equation but Janssen theory assumes a level fill and must therefore be modified to account for the surcharge. If Janssen theory is to be used for squat silos then the origin of the first contact is moved to create an equivalent surface. The height of this surface is calculated by considering the height of a level fill given the volume of solid encompassed by the fill and the surcharge. It is therefore dependant on the silo geometry and the angle of the surcharge. This method leads to non-zero pressures at the first wall contact.

To better calculate the pressures in squat silos, designers can use an earth pressure theory such as those of Coulomb (1776) or Rankine (1857). However, there are difficulties with using these. Rankine's theory assumes that the stored material extends infinitely and therefore should not be applied to circular or rectangular silos. Neither does it take account of the wall friction and thus tends to underestimate the wall pressures. The Coulomb theory also fails to take account of the wall friction and assumes a horizontal fill surface which can lead to errors in silos of this type. The Coulomb method has therefore been adapted by some researchers in order to take account of these factors (Mayniel, 1808; Muller-Breslau, 1906). Muller-Breslau (1906) modified the Coulomb theory to account for wall friction and a sloping backfill (this theory is essentially for earth pressure behind a retaining wall but the sloping backfill can be equated to the surcharge in a silo). However, the volume of surcharge on the silo is limited by its size and hence incorporation of the sloping backfill tends to over-estimate the pressures on the wall and a more accurate answer may be obtained from this theory by assuming the surface is a level fill.

It is apparent that more work needs to be directed towards squat structures in order to provide designers with satisfactory guidelines for the assessment of loads. This is especially important as batteries of squat silos are becoming more common in place of larger concrete structures.

3.4 Assumptions of theories

The above described theories make a number of assumptions of which some have been mentioned. There are a great number of implied assumptions that can affect the

accuracy and usefulness of the theories and the most important of these are now set out.

1. Wall friction is assumed to be constant down the depth of the bin. This may not always be the case as relative movement between the wall and solid can affect the value of μ.

2. The stored material is incompressible, homogeneous and isotropic. Granular materials exhibit very complicated behaviour which is discussed further in section 5.2.1. Granular materials contain voids which make them compressible and they are sensitive to the method of filling in the silo which can affect the stress state producing a very anisotropic fill (Zhong *et al*, 2001). However, Munch-Anderson *et al* (1992) and Ooi *et al* (1990) have shown that the average pressure on a level in a circular silo is well represented by the Janssen distribution.

3. Discharge pressures are simplified by using an over pressure factor dependent on the type of flow exhibited in the silo. This is a gross over-simplification of the mechanisms that are occurring in a discharging silo; these have been shown to be very complex and produce wall normal pressures that are above the estimations made from over-pressure factors, and in most cases are not constant at a given depth in a cylindrical silo (Nielsen, 1983). The onset of discharge also has a large effect on the behaviour of the stored material which further emphasises the limitations described in Point 2 above. The modelling of discharge is outside the scope of this thesis.

3.5 Evaluation of the average pressure coefficient – k

As mentioned, the evaluation of k affects the predictions of the above theories for the wall pressures in a silo. This thesis will discuss the average value of k (the ratio determined by consideration of the silo contents as a whole) and the local value of k (the ratio determined at a point of inspection). It is usually assumed that the average ratio is constant throughout the contents of the silo but local values of k can differ

from the assumed value due to the influence of factors such as wall deformation and wall friction. Methods that allow for the variation of the average value of k have been developed (Reimbert and Reimbert, 1976) but the overall result is often one that does not differ too greatly from using a single value of k. Using the single value of k has been considered sufficiently accurate for most researchers (Jaky, 1948; Pieper and Wenzel, 1965; Walker, 1966) but there has been much discussion of what value k should be. Rankine (1857) shows that there are theoretical boundaries for the value of k known as the active and passive pressure ratios. These two extremes can be demonstrated by the consideration of a mass of cohesionless soil behind a retaining wall and are:

- The active pressure ratio that results from the movement of the wall away from the granular material, and
- The passive pressure ratio that results from the movement of the wall towards the granular material.

The active pressure is the minimum value and occurs just before failure of the granular material as the wall moves away. The passive pressure is the maximum value and occurs just before the granular material compressively fails. As calculated by Rankine these two coefficients are given by equations 3.17 and 3.18.

Active:
$$k = \frac{1-\sin\phi}{1+\sin\phi} \tag{3.17}$$

Passive:
$$k = \frac{1+\sin\phi}{1-\sin\phi} \tag{3.18}$$

Where ϕ is the internal angle of friction of the granular material.

The active pressure ratio could be experienced in a flexible walled silo as there is scope for the material to fail if the wall deforms. This ratio has been used by some designers. It is unlikely that the passive pressure ratio would be reached in a silo problem.

Values of k for use in silo problems have been suggested including Jenike *et al*'s (1973) suggestion of 0.4 (no matter what the material is) and Jaky's (1948) ratio for earth pressure at rest:

$$k = 1 - \sin\phi \tag{3.19}$$

This is used mainly for silos with rough walls and has been adopted (with slight modification) by the modern ENV 1991-4 (1995) which gives the value of k as:

$$k = 1.1(1 - \sin\phi) \tag{3.20}$$

Figure 3.7 shows the effect of using the different values of k on the normal wall pressure distribution in a deep cylindrical silo when using the Janssen formula.

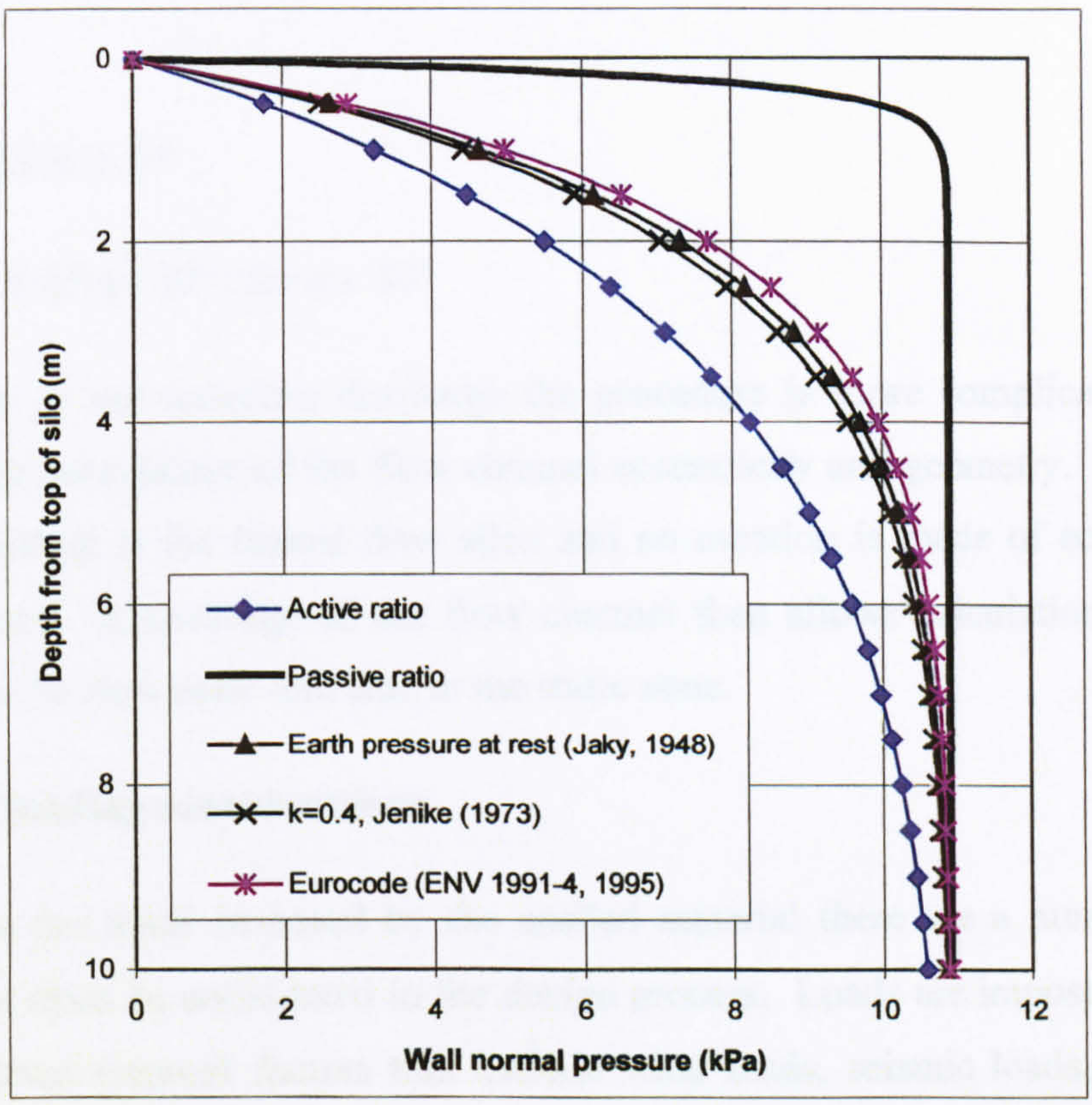

Figure 3.7 – Janssen distributions of wall normal pressure using different values of k

The two limiting cases can clearly be seen and are quite different from the majority of the predictions which tend to have similar values of k.

3.6 Discharge pressures

This thesis is concerned with the prediction of the filling pressures but it is necessary to have some understanding of the methods currently used to predict discharge pressures in design codes. Most current codes (ENV 1991-4, 1995; DIN 1055, 1987) handle the prediction of the discharge pressures in a silo by calculation of a flow load multiplier and then applying this to the filling pressures. This method would appear simplistic given the number of variables that have been identified that can affect the symmetry of wall pressures even in a cylindrical bin.

The Eurocode (ENV 1991-4, 1995) gives guidelines for discharge from concentric and eccentric hoppers. In the case of the concentric hopper the normal wall pressure multiplier is based upon the characteristics of the material.

$$P_{hd} = C_o P_h \tag{3.21}$$

$$C_o = 1.35 \text{ for } \phi \leq 30° \tag{3.22}$$

$$C_o = 1.35+0.02(\phi - 30°) \text{ for } \phi \geq 30° \tag{3.23}$$

In the case of the eccentric discharge the procedure is more complicated and first involves the calculation of the flow channel eccentricity and geometry. This implies that the method is for funnel flow silos and no mention is made of eccentric mass flow hoppers. Knowledge of the flow channel then allows calculation of the wall pressure in the flow zone and also in the static zone.

3.7 Other loading considerations

As well as the loads imposed by the ensiled material there are a number of other factors that must be considered in the design process. Loads are imposed on the silo structure from external factors that include wind loads, seismic loads, and thermal loads caused by expansion and contraction of either the structure or the stored material.

3.7.1 Wind loading

Any immovable structure experiences actions from the wind. Many statistical tools are available for the prediction of possible wind speeds in a given geographical area and these can be used to assess wind loads. The shape of the silo and the material it is constructed from affect this loading, a tall, rough square silo will experience a higher wind load than a squat, smooth cylindrical bin. Consideration must also be given to the location of the silo with respect to other structures. This can include other silos if a multi-cellular installation is being considered. The design of the roof can also have considerable effect on the passage of wind round the silo and if the design does not call for a roof at all then the possible effect of the wind acting on the internal surfaces of the bin must be examined. Wind loading can be critical for empty silos so consideration must be given to whether the filling/emptying cycle will involve periods where the silo may remain empty for some time.

3.7.2 Seismic loading

This type of load is not really applicable to designs intended for use in the UK or other areas of the world where seismic activity is low. However, there are a large number of regions where seismic activity is an important factor and some codes give guidance on designing for this type of load (ENV 1998-4, 1999). The response of the structure will be a function of the material it is constructed from, the type of foundation and the structure's natural periods of vibration.

3.7.3 Thermal loading

If the overall temperature of the silo's immediate environment increases then the structure will expand. If the relative magnitude of the expansion of the structure compared to the ensiled material is large enough then the material stored inside may assume a new position. However, on contraction the material will experience a large passive pressure which in turn leads to compaction and stiffening of the stored material. As well as the high stresses in the wall of the structure there may be discharge problems associated with this compaction. Some researchers have

investigated this effect (Zhang *et al*, 1986; 1989). This phenomenon could have a significant effect in areas where extreme temperature cycles are apparent.

3.8 Application of theories to rectangular planform silos

All of the previously described theories are most applicable to circular planform silos. Some codes recommend ways in which the theory can be adjusted to take account of the different shape (ENV 1991-4, 1995; DIN 1055) and some have been adapted to make them more applicable (Reimbert and Reimbert, 1976). Janssen's original paper (1895) postulated that the pressure at the mid-side of a rectangular silo would be higher than that at the corner. For a flexible walled silo this has been shown experimentally to be incorrect and the pressure at the mid-side can be considerably lower than the pressure at the corner (Jarrett *et al*, 1995). The Reimbert and Reimbert (1976) formulae would appear to be most useful as they give values for the wall pressure on the long and the short wall. None of the theories however give any sort of information about the variation of the pressure across the wall at any given depth. This is where structural savings can be made because if the pressure is shown to be lower in the middle of the wall then the bending moment is lower and hence the required strength is reduced. There is also the strengthening effect of taking into consideration the membrane stiffness of the plate.

3.9 Silo response

3.9.1 Load supporting actions in silo structures

This section of the thesis discusses how the alternative forms of silo carry their loads and how this can have an effect on silo design. Cylindrical silos support most of their loads using in-plane (membrane) forces although some bending may occur in order to maintain compatibility of the boundary (Rotter, 1985a). Therefore, in most cases membrane theory is used for the design of cylindrical shells. Rotter (1985b) discusses several cases where the effects of bending stress may be of importance, such as under repeated cyclic loadings, where large bending stresses could cause a fatigue failure.

Rectangular structures however are usually designed so that the primary load supporting action is that of bending stresses (Brown, 1998). Structures are often designed with externally applied stiffening which divides the more flexible plate material into a number of panels which are treated and analysed separately. This tends to lead to an inefficient structure being designed with an excess of strength. Figure 3.8 shows a typical rectangular silo with a large amount of external stiffening.

Figure 3.8 – A rectangular silo with externally applied stiffening

However, as will be shown later, in an unstiffened structure using thin plates, membrane stress can be induced when the plate undergoes large deflections. Therefore, if a design could be formulated that permitted large deflections then some of the load would be carried by this membrane stress, creating a more efficient structure. This would have particular benefit for smaller, unstiffened rectangular structures.

3.10 Membrane actions in rectangular plates

When considering plates of the sort that a rectangular planform silo may be constructed from, the main supporting action is that of bending actions. However, with thin plates, when the deflection at the midpoint is large compared to the thickness of the plate, the middle surface becomes strained, resulting in in-plane

tensile stress levels that stiffen the plate by a considerable amount. This stress is called diaphragm, direct or membrane stress. Ugural (1981) defines a large deflection in a plate as one where the deflection is greater than the thickness of the plate but goes on to show that significant differences between large and small deflection solution methods occur when the deflection exceeds half of the thickness.

A plate undergoing large deflections has non-linear elastic load-deflection and load-stress relationships which are not accounted for by small-deflection bending theory (the usual approach to plate bending problems). Therefore a modified theory must be employed which accounts for the large deflections. This is usually achieved by determining the bending stress as per the original theory and then adding to this the membrane stress. As an example consideration is given to a circular plate that is fully fixed about its edge (Ugural, 1981). The bending (small deflection) solution of this problem is given by equation 3.24.

$$w_{max} = \frac{p_1 r^4}{64D} \qquad \text{or} \qquad p_1 = \frac{64D}{r^4} w_{max} \tag{3.24}$$

The bending and membrane (large deflection) solution is given by equation 3.25 (for derivation see Ugural (1981)).

$$p_1 = \frac{64D}{r^3}\left(\frac{w_{max}}{r}\right) + \frac{8}{3}\frac{E}{(1-\nu)}\frac{t}{r}\left(\frac{w_{max}}{r}\right)^3 \tag{3.25}$$

Figure 3.9 shows deflections in the range $0<(w_{max}/t)<1.5$ and the corresponding load. It can be seen that the small deflection theory is suitable for midpoint deflections up to half the thickness of the plate but large errors occur after that point. At the point w = t there is a 65% error in the load predicted according to the small deflection theory.

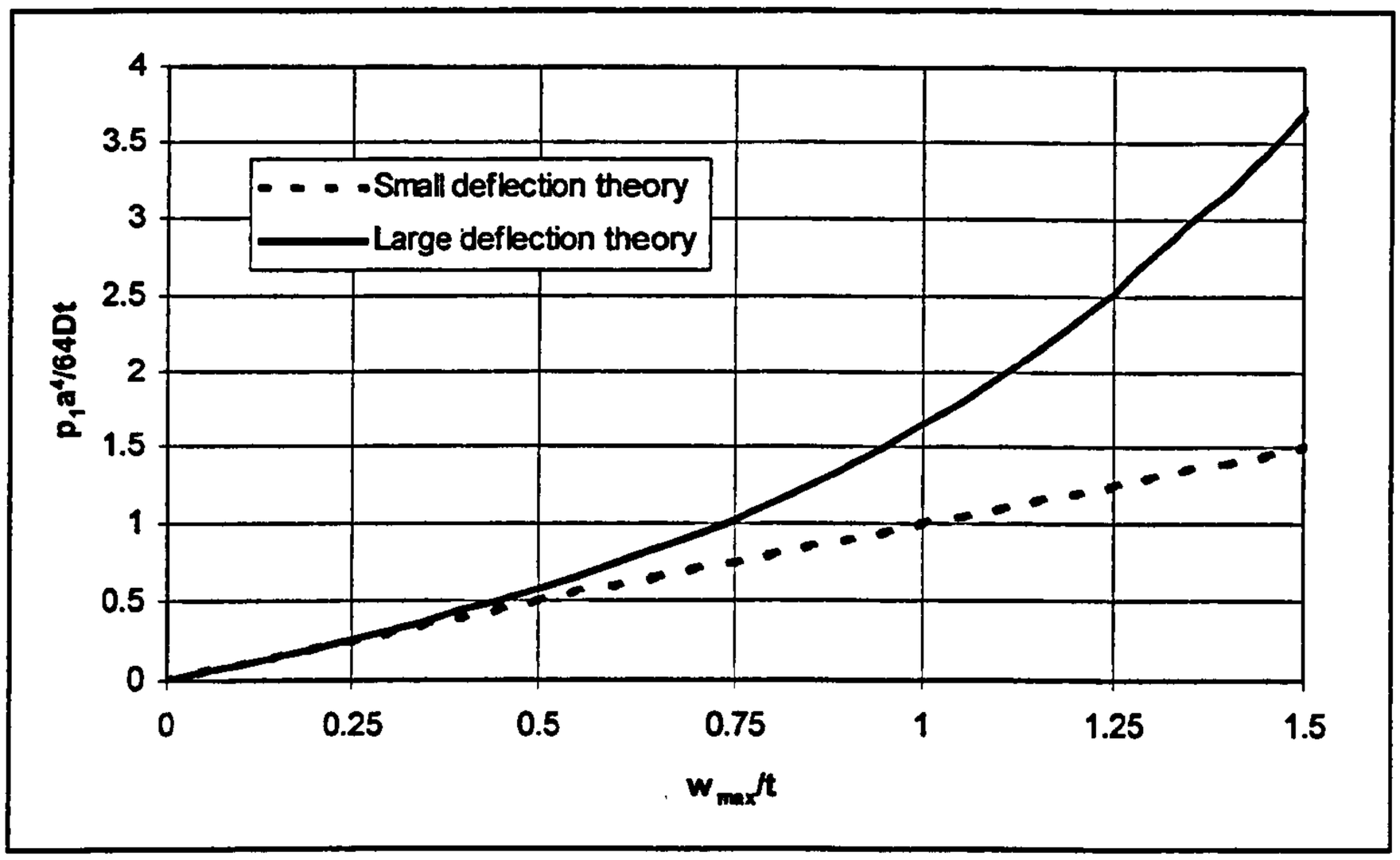

Figure 3.9 - Comparison of large and small deflection theory for a circular plate

3.10.1 General equations for rectangular plates

Von Kármán (1910) introduced governing differential equations for large deflections of thin plates. These take the form of coupled, non-linear partial differential equations and where realistic problems are concerned obtaining a solution is a complex and time-consuming task. Some approximate solutions of simple shapes under uniform loading have been determined (Timoshenko and Woinowsky-Krieger, 1959; Roark and Young, 1975) but it is only since the advent of numerical techniques that the general problem has been treated satisfactorily (Zienkiewicz and Taylor, 1989).

Solutions for rectangular plates are therefore normally obtained by experimental or numerical techniques. However, some examples are available from literature (e.g. Barés (1979) for small deflections and Levy (1942) for large deflections) and these have been collated by Roark and Young (1975) for engineering design purposes.

The effect of calculating the stresses in rectangular plates using the two different theories can be easily shown using an example. Consider a square plate, fully fixed and loaded with a uniform load of 2 kPa. It is made from steel with E=210 GPa and ν=0.3 and has dimensions of 1m square and thickness 3mm.

3.10.1.1 Small deflection theory

From Roark and Young (1975) the formulas for the bending stress and deflection at the mid-point of a fully fixed square plate under uniform load are given as:

$$\sigma = \frac{0.1386qb^2}{t^2} \tag{3.26}$$

$$\max w = \frac{0.0138qb^4}{Et^3} \tag{3.27}$$

where q = load per unit area, b = width of plate, t = thickness, σ = bending stress, w = deflection and E = Young's modulus.

3.10.1.2 Large deflection theory

In Roark and Young (1975) analytical results from various sources are tabulated. This table is given for $\nu = 0.316$ so results would be slightly different from those given by the small deflection theory. Large deflection solutions are expressed in terms of the coefficients w/t, qb^4/Et^4 and $\sigma b^2/Et^2$. Once the value of qb^4/Et^4 is determined then the table can be used to obtain values for the other coefficients. Interpolation between the values in the table may be necessary to provide values of stress and deflection for a particular problem.

3.10.1.3 Comparison of large and small deflection theory

Table 3.1 shows the maximum stress in the plate and the deflection at the middle point as calculated from the two theories.

	Mid-point stress (MPa)	**Mid-point deflection (mm)**
Small deflection theory	30.8	4.87
Large deflection theory	23.8	3.12

Table 3.1 - Stresses in a rectangular plate as calculated from large and small deflection theories

It can be seen that by accounting for the membrane stress of a plate undergoing large deflections, lower values for stress and displacement are obtained. If membrane

stress is accounted for it can lead to more efficient use of the strength of a plate when designing structures. Designing the structure so that large deflections occur may prove difficult and therefore accounting for membrane stiffness may have other benefits. More realistically, this method may make it possible to evaluate the true factor of safety in the structure.

3.10.2 General numerical techniques for plate problems

As previously mentioned since the advent of computer based numerical techniques problems in large deflection plate bending have become easier to assess. The above rectangular example can be repeated using a simple finite element model and the results for this are shown in table 3.2.

Element behaviour	σ (MPa)	y (mm)
Bending only	31.98	4.94
Bending and membrane	24.64	3.16

Table 3.2 - Finite element solution to the large and small deflection rectangular plate

It is clear that the finite element method agrees well with both theories but of course it is not limited to the small number of geometries and load cases that are available from literature, and it can be used for many plate sizes or geometries.

3.11 Structural considerations

There are a large number of other structural components in a silo other than the main shell (or plate) structure. All of these can have an effect on the structural response of the silo. Figure 3.8 showed a rectangular silo and figure 3.10 shows an elevated cylindrical silo with a number of commonly used structural features.

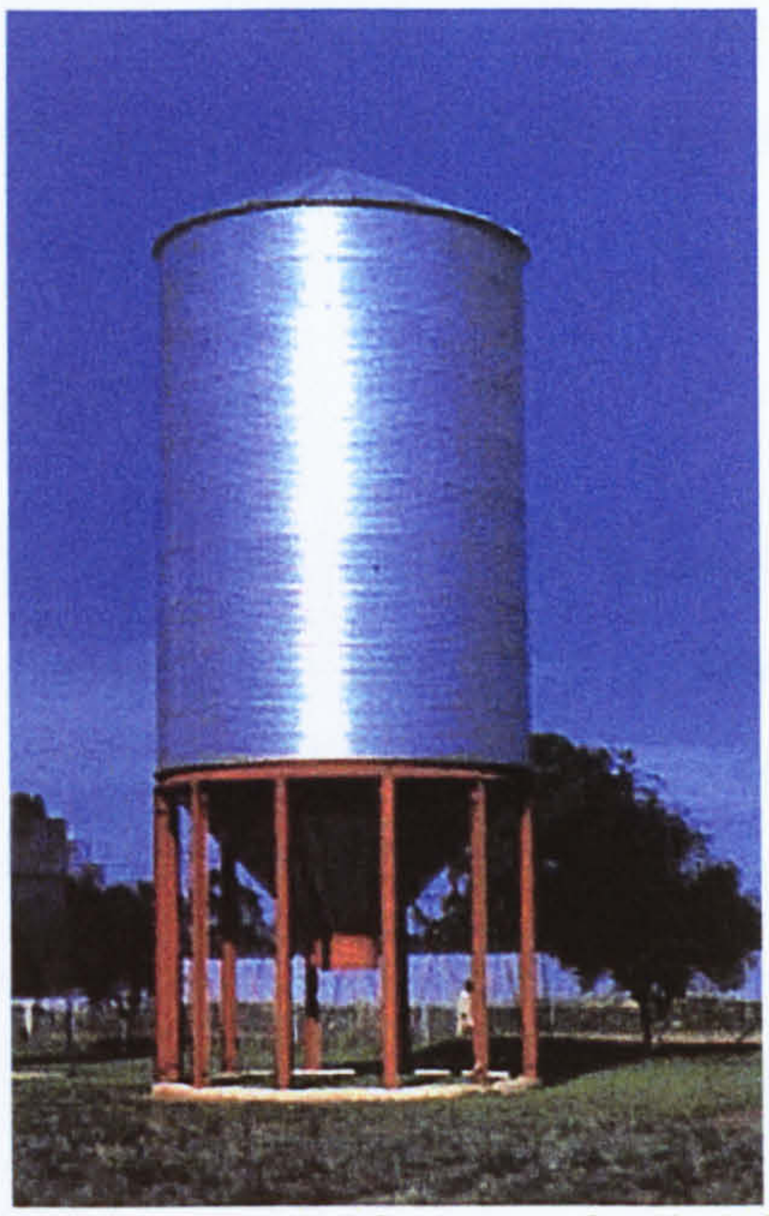

Figure 3.10 – Structural features of cylindrical silos

These features include a ring beam which provides a junction between the parallel section of the silo and the hopper. The overall support of the silo is by columns which are also attached to the ring beam. This ring beam is therefore subjected to a complex loading from the weight of the bin structure and the membrane tension caused by the hopper. The ring beam also acts as a stiffener at this point of the silo. Comparable in this sense to the ring beam is the roof which as well as protecting the contents from exposure to the elements also provides stiffening at the top of the bin.

Figure 3.8 shows a rectangular silo that features externally applied stiffening. The use of this type of stiffener results in a structure that can be considered to act like a series of flexible panels supported between the stiffeners and there are a number of methods given for the analysis of this type of structure (Troitsky, 1980). This method of design usually leads to an overly stiffened structure which does not take advantage of its full load carrying capability. This is obviously wasteful of construction material but also underlines the lack of knowledge concerning rectangular structures. Although not shown in figure 3.8 another occasionally used feature of rectangular silos are internal ties across the corners. These are used to prevent spreading of the corners in the silo but must be carefully considered before use as they can affect the flow of the material. There is little openly available

material concerning the use of internal corner ties because it is commercially sensitive but Khelil (1998) discusses some of the effects that internal ties can have on wall pressures and flow patterns.

3.12 Rectangular bin design

As this thesis is concerned only with design of rectangular silos a full description of the design process for circular planform silos is unnecessary. There are a large number of codes, references and design guides that are devoted to this topic (DIN 1055, 1987; ENV 1991-4, 1995; Rotter, 2001). It is worthwhile though to discuss some of the aspects of structural design specific to rectangular planform silos. Troitsky (1980) has produced a design guide specifically for rectangular steel silo structures.

Most silos of this type would be expected to contain a ring beam at the junction between the hopper and the wall. The ring beam is subjected to a variety of loads especially if the structure is supported on discrete columns. It must distribute the weight of the silo to the supporting columns. At the onset of filling the ring beam will be subjected to inward forces from the weight of the hopper. As filling continues this force is offset by the horizontal pressure exerted on the walls of the silo.

The columns that support a circular silo usually terminate at the ring beam. In rectangular bin design they often are extended to the top of the bin in order to provide more stiffness. There is often another ring beam at the very top of the silo to prevent excessive deflections at the free edge although this could be incorporated into the roof design.

3.13 Summary

The basis of silo design is knowledge of the internal pressures caused by the weight of the material that is to be stored. A number of theories and methods for determining these pressures have been developed. Some are specific to a certain silo form (e.g. Muller-Breslau (1906) for squat silos) but generally most codes use one

method no matter what the shape. The Eurocode (ENV 1991-5, 1994) attempts to address this problem by classifying silos according to their shape, height etc.

The correct determination of the wall pressures is also hindered by the assumptions made by the theories. Chiefly, the adoption of a constant value of k is a major simplification especially when considering rectangular planform silos which have been shown experimentally to exhibit large variations in the value of k throughout the stored bulk solid (Rotter *et al*, 2002).

When considering rectangular silo design, bending moments are usually the basis. It has been shown that by accounting for membrane actions that may arise in the plate structure, lower stresses and deflections for a given load are predicted. Membrane stress arises as a result of wall deformation but this deformation does not need to be too large (compared to the thickness of the plate) for structural savings to be made. Rectangular planform steel silo designs are often produced that use a large amount of external stiffening. This limits the plate deformation which in turn limits any membrane actions and removal of a large amount of this stiffening may result in a structure with the same load carrying capability but using a reduced amount of raw material.

Chapter 4 - Numerical methods for the prediction of silo wall pressures

4.1 Introduction

Due to the many limitations of the analytical methods for determining silo wall pressures that arise from the assumptions described in section 3.4, researchers have turned to numerical methods. The current work aims to investigate the interaction between the ensiled material and the silo structure when the wall is flexible and large deflections occur using a numerical model. There are a number of numerical methods available to the structural designer, some of which may be suitable for analysing silo problems. Initially, the use of these numerical methods and their potential applicability to the current problem is assessed before results are presented for analysis performed using a finite element method.

4.2 Available numerical techniques

With the advent of affordable yet powerful computers, numerical techniques have been developed that take advantage of this increased computational power. Systems of difficult and time-consuming equations can now routinely be solved in a matter of minutes. There are three main techniques used for structural analysis; the finite difference method, finite element method and boundary element method. These methods rely on some form of discretization (dividing the problem into units that have known geometry and properties) of the problem (this could be a fluid flow domain, structural component etc.) and the resulting mesh (combined with knowledge of the boundary conditions) is used to construct a system of equations to describe the problem mathematically. These equations can then either be solved implicitly or explicitly (depending on the type of problem) to produce the required results (stresses, pressures etc.). There also exists a fourth method, the discrete element method, that can be used for the simulation of granular bulk solids problems. This method models individual particles and the interaction between them, and would

appear to be ideally suited for problems of the type studied here. There are however limitations to each method, described below.

4.2.1 Finite difference method

This method is most commonly applied to problems that can be described as two-dimensional, such as the temperature distribution across a thin plate or the velocity profile of a fluid at a cross-section of a duct. The system is divided into a regularly spaced grid and a function to describe the required variable is derived at each of the points on the grid. Assuming knowledge of the function's value at the boundaries, then solution of the system of equations can be performed manually or by using a simple computer program. This method is not commonly used in commercial structural analysis and design because the equations to be solved must be determined for each separate problem which would be extremely time-consuming for a large analysis. The finite difference method is the most established numerical method discussed here but is considered unsuitable for the complex problem that is posed by the three dimensional simulation of silo filling.

4.2.2 Finite element method

This technique is currently one of the most commonly used numerical techniques for mechanical engineering design. It can be applied to many different types of problem, with the result that one package can be used to solve problems in a wide range of fields (structural, magnetic flux, fluids, electrical). As in the finite difference method the problem is divided into a series of smaller elements connected by nodes. These nodes can be compared to the grid points in the finite difference method but they do not have to be regularly spaced and thus, much more geometrically complex problems can be modelled using the finite element technique.

There are a large number of commercial finite element packages available; which generally include a GUI (Graphical User Interface). This makes it possible for the engineer to create complex models that may contain many thousands of degrees of freedom without having to have specialist programming knowledge. In the past,

computer based implementation of numerical methods has generally involved coding as required, making programs application specific and more time-consuming to use. Modern software packages almost entirely eliminate the need for knowledge of programming languages etc., as they are driven by sophisticated graphical interfaces. The commercial need for this type of software has led to extremely robust code that is ideal for the solution of problems of the current type.

4.2.3 Boundary element method

As the name implies, the form of discretization used in this method involves meshing the boundaries of a structure. This technique is relatively new but has already been applied to silo problems by at least one research group (Wu and Schmidt, 1991). In their published work a two dimensional silo was examined and the results obtained gave good agreement with the predictions of Janssen (1895). Because this technique only meshes the boundaries of a problem it has the advantage of reducing a two dimensional problem to one dimension and likewise a three dimensional problem to two dimensions. This has advantages in that the level of computational power is reduced for a given problem especially when compared to the finite element method (which is very similar). However, there are comparatively few commercial boundary element packages available which, in part, is due to the established nature of the finite element method which has been used successfully for a number of years.

4.2.4 Discrete element method

This method would appear to be the most suitable for this project as it is specifically aimed at problems involving granular materials. It has been used on a number of occasions for the solution of silo problems and a comprehensive review of both this technique and the finite element method is given by Rotter *et al* (1998). The material is represented by a number of particles and the interaction between these particles is modelled numerically. This should appear to give the most accurate representation of the behaviour of bulk solids. However there are a number of disadvantages to using this method. Because each particle of granular bulk solid and the interaction between adjacent particles is modelled, an enormous computing resource is required to

perform even a simple two dimensional analysis. Rotter *et al* (1998) specified 10,000 particles for a small two dimensional problem. This is currently considered to be approaching the practical machine limit in terms of computation for this method. However in a real three dimensional silo of the type considered here the actual number of particles could be in the region of 10^{13} (Chen *et al*, 1999).

4.3 Choice of numerical technique for use in the current project

Because of the widespread adoption of the finite element method by design engineers, a large number of proven and robust packages are available. Several of these commercial packages have been shown to be suitable for modelling silo problems (Guines *et al*, 2000; Ooi and She, 1997). Therefore this method is adopted for the remainder of the work presented here. Although there are several specialist codes available for prediction of silo wall pressure (Ragneau *et al*, 1998), these are not generally available and therefore a commercial package is utilised. The package ABAQUS is chosen for its superior handling of the material and model non-linearities which are important features of a thin-walled rectangular silo.

4.4 Previous application of the finite element method to silo problems

Since the finite element method is one of the most commonly used computational methods in the study of the mechanics of solids there is extensive silo research that has utilised it. There are two distinct phases that have been explored, filling (and static) pressures, and pressures upon discharge. These are often studied separately as the numerical techniques for the two cases can differ significantly.

4.4.1 Filling pressures

Many researchers have used the finite element method to predict the wall pressures upon filling a silo. They include Jofriet *et al* (1977), Mahmoud and Abdel-Sayed (1981), Ooi and Rotter (1990), Ragneau and Aribert (1993), Ooi *et al* (1996), Ooi and She (1997), and Chen *et al* (2000). This work is, in the main, aimed towards axisymmetric modelling of cylindrical silos as it allows easy comparison with the Janssen method.

For an axisymmetric silo, Jofriet *et al* (1977) showed that a finite element model could produce good agreement between the predictions and the Janssen model. Mahmoud and Abdel-Sayed (1981) further showed that the finite element method could produce results that agreed reasonably well with experimental measurements. Both of these pieces of work used custom written finite element code which is outside of the scope of this thesis.

All of analyses described above have adopted a constitutive law to describe the ensiled material. Most of the laws used in silo problems involve plasticity to take account of large deformations of the material. The assumption that highly complicated material models are required for axisymmetric analyses is one that was disproved by Ooi and Rotter (1990) who showed that in analysis of this type an elastic model could describe the ensiled material and provide results that still compared favourably with the Janssen predictions. This is because circular silos have a high radial stiffness which means that strain developed in the stored material is quite small. The key parameters to matching the Janssen theory to the finite element model in this type of problem are shown to be the wall friction and the Poisson's ratio of the material. This is because the wall friction appears explicitly in the Janssen theory and the Poisson's ratio is implicit due to its relationship with k (the ratio of lateral to vertical pressure). Further discussion of this relationship is given in section 6.4.1.

Analysis in three-dimensions is less common as the two-dimensional representation of the Janssen equations and an axisymmetric finite element model has been considered sufficiently accurate for the design of the more commonly occurring circular planform silo. Some three-dimensional analysis has been performed and has been applied to rectangular planform silos. Results have been presented by Ragneau *et al* (1994) and Guines *et al* (2000). Both of these works have characterised the ensiled material as an elastic/plastic material. Ragneau *et al* (1994) used the non-linear elastic model of Boyce (1980) coupled with both the Drucker-Prager (1952) and the Wilde (1979) plasticity criteria. Guines *et al* (2000) also used a non-linear elastic model (Hujeux, 1979) and coupled it with a Cam-Clay (Roscoe *et al*, 1965)

plasticity model. This work has demonstrated the complex patterns of wall pressure that occur in this type of silo but has not extended the work to give guidelines for the design of these types of structure.

It is known that the interaction between the stored solid and the structure can have an effect on the wall pressures. Axisymmetric analysis of this interaction has been carried out by both Mahmoud and Abdel-Sayed (1981) and Emanuel *et al* (1983). The latter modelled a horizontal slice through a silo in order to show that the bending moments that arise in the wall at a given level can be non-uniform. Ooi and Rotter (1990) showed that the ratio of the stiffness of the solid to the stiffness of the wall could have a large effect on the predicted pressures and that an overall parameter of $(E_s r)/(E_w t)$ could best represent this behaviour for cylindrical silo shells. Chen *et al* (2000) explored the effect of ring stiffeners in an axisymmetric silo. A previously studied experimental silo (Rotter *et al*, 1995) was modelled with the finite element method and similar peaks in wall pressure were observed in the vicinity of the stiffening rings.

Rotter *et al* (1998) conducted a large international study into the use of the finite element and discrete element methods for filling pressures. A well defined problem was analysed by a number of research groups and the results obtained vary significantly. The conclusions of this study were that the finite element method can be very sensitive to assumptions made when constructing the model. The filling method modelled has an effect but the main differences arise from the researcher's choice of material properties. It was concluded that these choices need to made with extreme care as the effect on the predicted pressure can be very large for only a small change in a parameter's value.

4.4.2 Discharge pressures

Although the current study is concerned with prediction of the filling pressures only it is important to consider the modelling of discharge pressures. There is often a large pressure peak at the onset of discharge which is referred to as a switch pressure. Several researchers (Jenike and Johanson, 1968; Walters, 1973a) explain this switch

pressure as a change in the stress field in the solid. However, it is often the case that only part of the material is moving (funnel flow) and therefore there is no overall change but rather, localised changes resulting in asymmetry of the discharge pressures.

As well as this switch pressure, the pressures exerted on the wall by a discharging solid are often locally higher during the discharge process than during filling and most codes consider the discharge pressure to be a factor of the filling pressure (ENV 1991-4, 1995; DIN 1055, 1987). It may therefore be argued that modelling of the filling stage is sufficient for design purposes because these predictions can then be treated in a similar way to arrive at discharge pressures (which are usually over predicted, resulting in silos with a high factor of safety). This appears to be the accepted trend since research groups (Runesson and Nilsson, 1986) who have specifically modelled the discharge stage have done so in order to study other phenomena such as the discharge patterns.

Modelling of discharge is often carried out separately to the modelling of the filling. This is because different techniques must be employed for this type of problem. Some groups (Feise and Daiß, 2001) have used a fluid dynamics method to model the flow of the solid whereas others have used a dynamic finite element model (Runesson and Nilsson, 1986). Those groups (e.g. Link and Elwi, 1987) that have examined the wall pressures resulting from discharge seem to have confirmed the existence of a switch pressure and found agreement between the finite element results and theories of Jenike (1964) and Walker (1966).

4.5 Summary

The finite element method has been chosen because of it proven ability to model complex structural problems. A large number of silo problems have been modelled using this technique but have, in the main, been restricted to axisymmetric analysis of cylindrical silos. Little work has been directed towards three-dimensional modelling and of the work available only preliminary investigations of rectangular planform silos have been carried out. This may be due to the difficulty in determining a

suitable method for characterising the behaviour of the granular bulk solid. This is investigated in Chapter 5.

Chapter 5 - The finite element method applied to silo problems

The finite element method has been used extensively by researchers to model silo problems. Analysis has been carried out by using a mixture of custom code and commercial packages. The work presented below intends to use a commercial package. An excellent description of the general techniques of the finite element method is given by Zienkiewicz and Taylor (1989), but there are a number of aspects that must be considered when modelling silo problems.

5.1 Analysis type

There are two basic types of analysis that the finite element method uses for problems in structural mechanics; linear and non-linear. The deformation of a beam under a point load can be described as linear elastic as long as the load does not reach a level where the beam experiences large deformations or the stress and strain in the material do not exceed the yield point. Figure 5.1 shows the load-deflection of a simple elastic system.

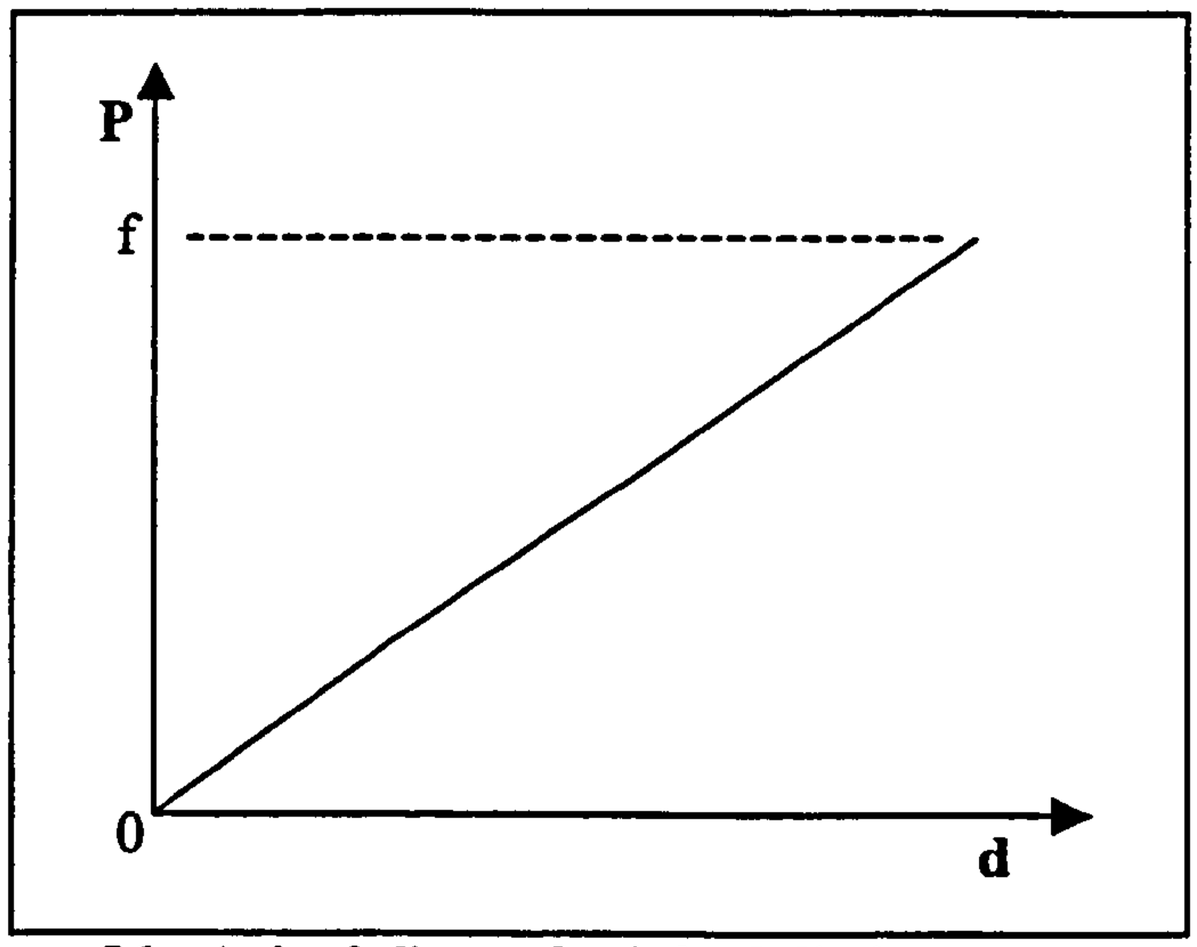

Figure 5.1 – A simple linear elastic load-displacement response

If this system is modelled using the finite element method then the response of the system to the load P = f can be described uniquely by a system of equations derived from knowledge of the stiffness of the structure, the loads applied and the boundary conditions. The resulting set of equations can be solved directly.

Non-linear analysis, as the name implies, deals with systems that exhibit a non-linear response to the applied load. Figure 5.2 shows the non-linear response of a system.

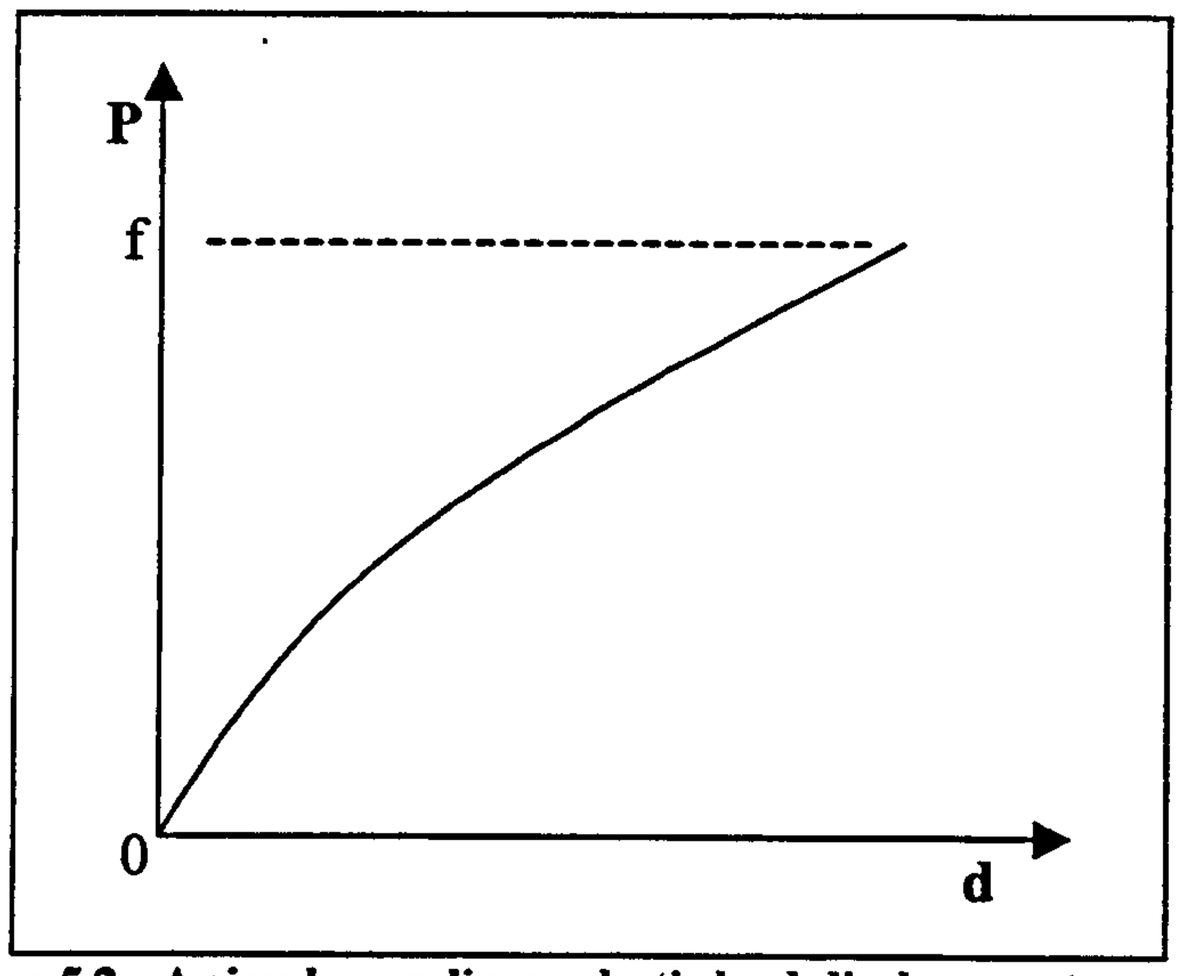

Figure 5.2 - A simple non-linear elastic load-displacement response

This system can no longer be described by a single set of uniquely defined equations but the required solution must be determined implicitly by using an iterative procedure which applies the load incrementally. Solutions to non-linear problems may also not be unique making their solution more difficult. This situation is shown in figure 5.3.

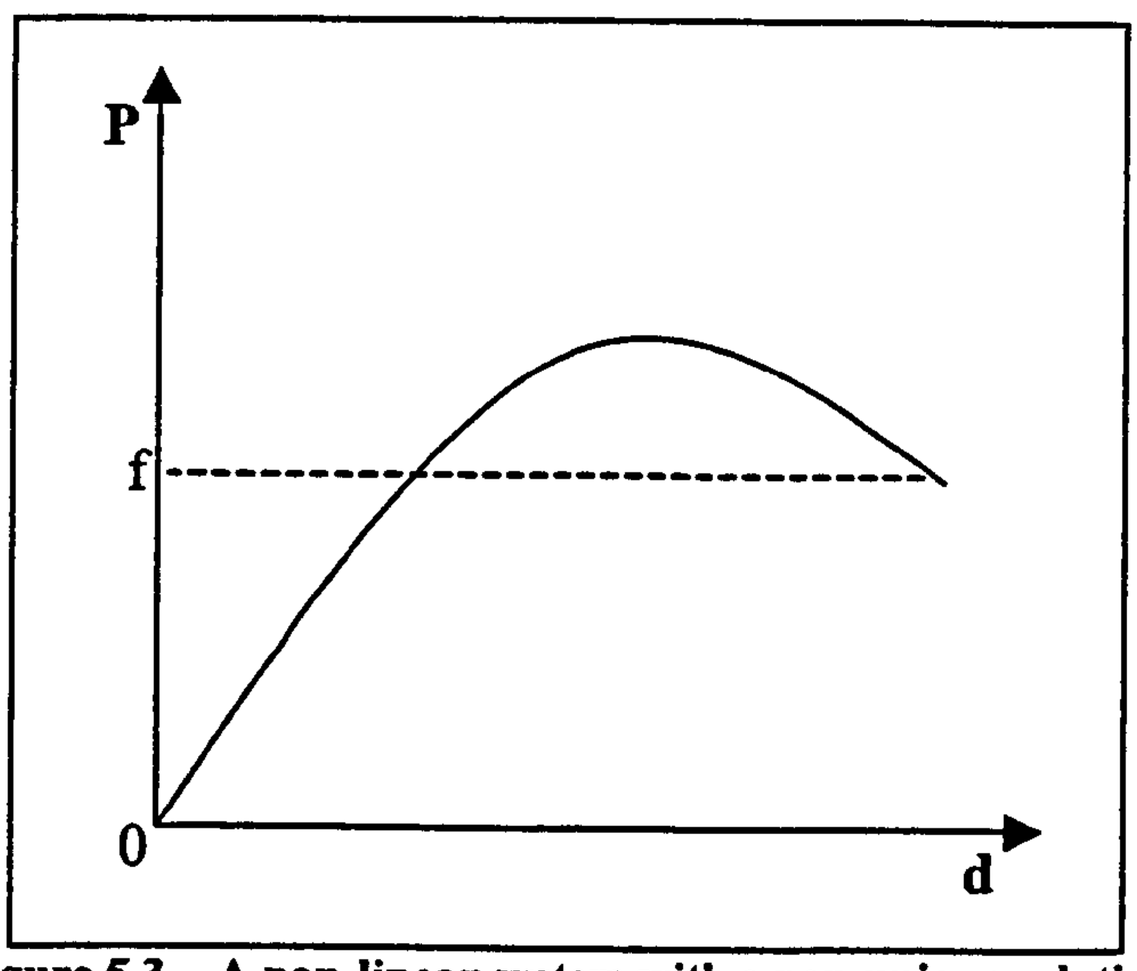

Figure 5.3 – A non-linear system with a non-unique solution

The figure shows that there are two values of displacement for the given load. In order to solve a system like this the load must be incremented very slowly so that the true response of the system is followed. If this type of behaviour is expected then engineering judgement and other calculations may also be required to determine which is the correct (required) solution.

5.1.1 Sources of non-linearity

There may be several features of a problem that can give rise to non-linearity. Non-linearities can arise from geometric non-linearity (large strains and deflections), material non-linearity (creep, plasticity etc) and contact interface conditions between separate areas of the model. A large number of problems contain non-linearity and different solution techniques must be adopted for non-linear and linear (small displacement) analyses.

5.1.2 Obtaining a solution in non-linear finite element analysis

Most commercial finite element packages use a Newton–Raphson method in order to solve non-linear problems. This is an iterative process that divides the problem into a number of increments often called time steps. This does not imply that the problem is mechanically dynamic; the time step is not measured in real units and it may be easier to consider the increments as a percentage of load (i.e. it ranges from 0 (no load) to 1 (full load)).

This technique involves taking the tangential stiffness matrix at the starting conditions and incrementing (for example) the load. A solution is obtained and the iterative correction (which is calculated as the difference between the applied external loads and the internal forces) can be determined. If this value were zero then the structure would be in equilibrium but that is rarely the case. This correction value is compared to a set criterion and if this is satisfied the increment is said to have converged. If not, the tangential stiffness matrix is reformulated using the new configuration and the process repeated until convergence is obtained. Using this method it may take several iterations for each time increment to obtain the solution.

Since the software reforms the model stiffness matrix and solves the system of equations for each iteration the computational time required for non-linear analysis is much greater than that required for linear analysis.

5.1.3 Non-linearity in silo problems

A three-dimensional finite element model of a silo will contain all the sources of non-linearity mentioned above. As the current work deals with silo walls that may exhibit large deflections there is a geometric non-linearity implicit in the problem. There must also exist contact between the silo walls and the contents of the silo, and finally the stored material will exhibit non-linear properties (mostly plastic deformations).

5.1.3.1 Large deformations

Linear elastic small strain analysis assumes that the higher order terms in the elastic equations can be ignored and therefore the solution can be obtained by consideration of a single set of explicit equations. It is also assumed that displacements and strains are small in the model and that the geometry remains unchanged under loading. However this is rarely the case and the example of a large deformation analysis that was given in section 3.10 showed that a plate could support more load if large deformations were accounted for and membrane action was enabled. In the finite element method this type of situation is dealt with by a geometrically non-linear analysis. The strains are now related to the displacements by a non-linear function and solution techniques described in section 5.1.2 must be adopted.

5.1.3.2 Contact analysis

In order to model the interaction between the stored material and the silo structure, there should be a mechanism to transfer the force exerted by the weight of the stored material to the walls of the silo. This is achieved by using contact elements. These are elements that are meshed over the surface of the underlying structural elements (representing the bulk solid and the steel silo structure) at points where contact may occur. They effectively couple together the degrees of freedom of the discontinuous portions of the model and allow the transfer of loads across the interface. In a

structural problem these loads take the form of pressure across or relative sliding between the contact surfaces. The interaction can be modelled as frictional, smooth or tied. These elements can give rise to large displacements and non-linear solution techniques must be employed. This work uses a Coulomb model for friction which relates the shear stress at slip to the normal stress by a simple coefficient, μ (figure 5.4). The contact is not tied to the wall and therefore it is possible for the stored material to move away from the wall and lose contact. There is also a small amount of allowable "elastic" movement between the contact surfaces. This implies that the stored material must move a small amount in order for friction to become fully mobilised. Chen *et al* (2000) investigated the parameter controlling this movement in a silo model and concluded that the standard value in the ABAQUS package gave satisfactory results.

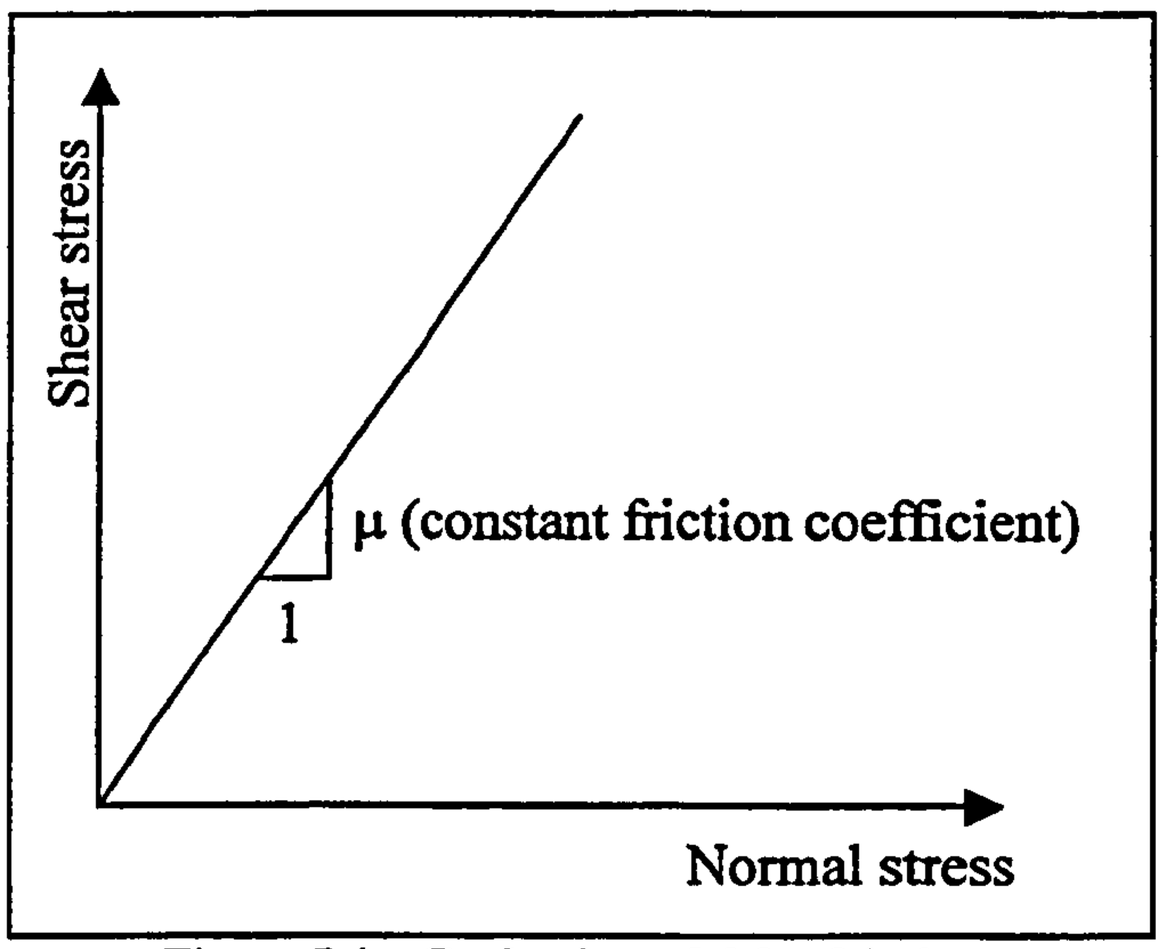

Figure 5.4 – Coulomb model for friction

5.2 Constitutive models to describe material behaviour

In order to define material behaviour in finite element analysis a constitutive material model must be used. A constitutive model defines the relationship between the stress and the strain in a material. This is required by the finite element method in order that the displacements of the model may be calculated from the forces applied.

Material constitutive laws can be simple (such as a linear elastic law defined using only two parameters) or extremely complex such as the Karlsruhe law developed by Kolymbas (1988) for granular solids that uses upwards of thirteen parameters to define the material behaviour.

In the current work a constitutive law is required for steel (for the structure) and the granular solid (for the ensiled material). The steel used in the silo structure will be considered to be a linear elastic material with no yield criteria specified. This is considered suitable because the steel will not be strained to yield levels and therefore it is not necessary to accommodate its post-elastic behaviour. However, it may not be appropriate to treat granular materials in the same way as they are capable of large plastic strains when unconfined and therefore an appropriate constitutive law for the granular solid must be formulated. In order to do this the main properties that affect the granular materials behaviour must be identified and quantified.

5.2.1 Properties of granular bulk solids

The materials that are stored in structures of the type being studied in this report are classed as granular bulk solids. This puts them into the same category as soils, and hence references will be made to soil mechanics as this field has much relevance to the work presented here.

The complex behaviour of granular bulk solids has already been mentioned. The fact that they exhibit highly non-linear behaviour makes the determination of their material properties more complicated than, for example, those of a steel sample.

Material properties are required for a number of reasons which might include, design, calculation or, in this case, numerical modelling. Considering steel as an example, this material's elastic behaviour can be simply described by two variables; the elastic modulus and the Poisson's ratio. This would give no indication of the yield stress or post-yield behaviour (although this could be incorporated) but is sufficient information for a simple, small-strain problem. Values for these variables would be determined from tensile tests, which are relatively easy to perform.

The aforementioned variables alone are not enough to adequately describe the full range of behaviour of a granular bulk solid. Even the determination of values for these parameters would pose difficulties as a bulk solid does not assume a form that would make performing a tensile or compressive test practical.

Kolymbas (1988) has identified many characteristics for defining the behaviour of bulk solids and of these the most important are:

- Plasticity: Irreversible deformations.
- Dilatancy: When bulk solids shear the material changes density even if the hydrostatic stress remains the same.
- Barotropy: The material behaviour depends in the stress level.
- Pyknotropy: The behaviour of the material depends on the bulk density even if the particle density remains the same.
- Cohesion: Most materials are cohesionless (have no strength in tension) but some can carry a small load and are known as cohesive materials.

In order to assess these characteristics geotechnical engineers have developed alternative tests to determine the properties of granular bulk solids. These tests include, the shear box, biaxial tester and the triaxial tester. A list of some of the parameters that are used to describe bulk solids properties is shown in table 5.1.

Angle of internal friction, ϕ	The angle between a tangent to the yield locus of the material and the normal stress axis. Determined from shear box tests.
Bulk density, γ	The mass of a quantity of bulk solid divided by its total volume.
Cohesion, c	The shear stress at yield under zero normal stress. Gives an indication of whether the material can support any load.
Dilation, ψ	The increase in volume due to shear.
Voids ratio, e	The ratio of volume of voids between the particles to volume of solid particles.

Table 5.1 - Some properties of granular bulk solids

5.2.2 Determining granular bulk solids properties for finite element analysis

As already mentioned there are a large number of tests that can be performed on bulk solids in order to determine values for the parameters shown in table 5.1. It would be impractical to discuss all of these tests so attention will be paid only to some of the tests that are most relevant to finite element modelling. As this work is interested in filling pressures the measured properties need to be those that give information about the static behaviour of the material such as the compressibility, the shear strength and the density.

Some of the more commonly performed tests are the shear cell test, an oedometer (one-dimensional consolidation) test and the triaxial test and the methodology and example results are presented below.

The shear cell test enables the engineer to determine the internal angle of friction. A shear test cell is shown in figure 5.5 and is often referred to as a Jenike shear cell (1964).

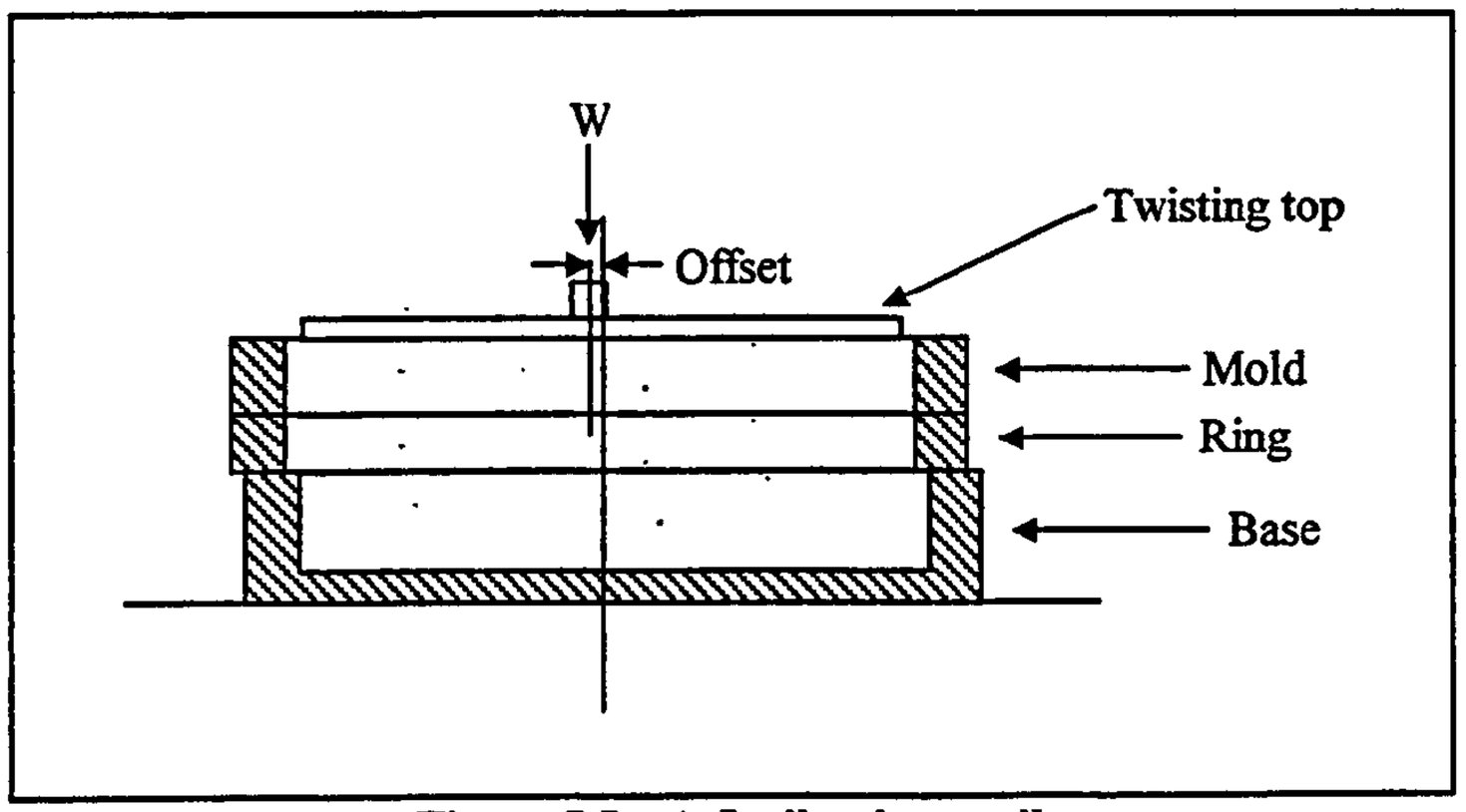

Figure 5.5 – A Jenike shear cell

The basic principle of operation is that the top of the cell is loaded with a force W and then a shear force is applied to the side of the cell until the specimen shears at a value S. This procedure is then repeated with lower values of W in order to determine the yield locus shown in figure 5.6. A Mohr circle tangent to this line is then drawn through the origin which determines the unconfined yield strength (f_c). A second Mohr circle is drawn tangent to the first point on the yield locus (W,S) which determines the consolidating pressures of the material, p_1 and p_2. The effective angle of internal friction is shown as δ in the figure and is the angle between the x-axis and a line drawn through the origin and at a tangent to the Mohr circle determined from the experiments. For a cohesionless material this angle is the same as ϕ.

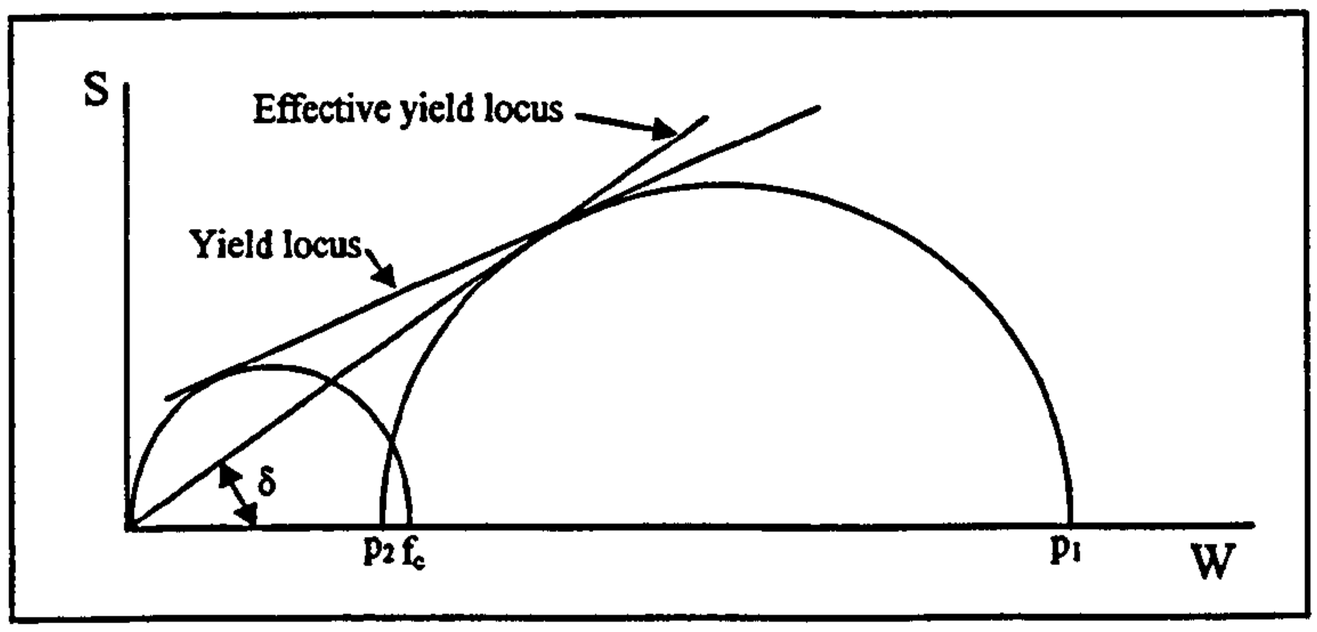

Figure 5.6 – Yield loci of granular material determined from the Jenike shear cell

This diagram can also determine the cohesion of the material. A large number of granular bulk solids are cohesionless (have no shear strength) but some can support a

small load. In the case of a cohesional material the yield locus would cross the S axis on the above figure at a non-zero value.

This test gives basic information about the granular bulk solid that may be used for certain calculations or in conjunction with other parameters determined from other tests for more complex calculations.

The oedometer can be used to give simple information about a granular solid's one-dimensional compression response. This may be comparable to a tensile or compressive test on a material such as steel. A sample of granular material is loaded into a test cell and is then simply compressed via a platen on the surface. The results of this form of test are usually plotted as the direct stress applied via the platen against the height of the sample or some derived volumetric parameter. Figure 5.7 shows a typical plot of the results from an oedometer test.

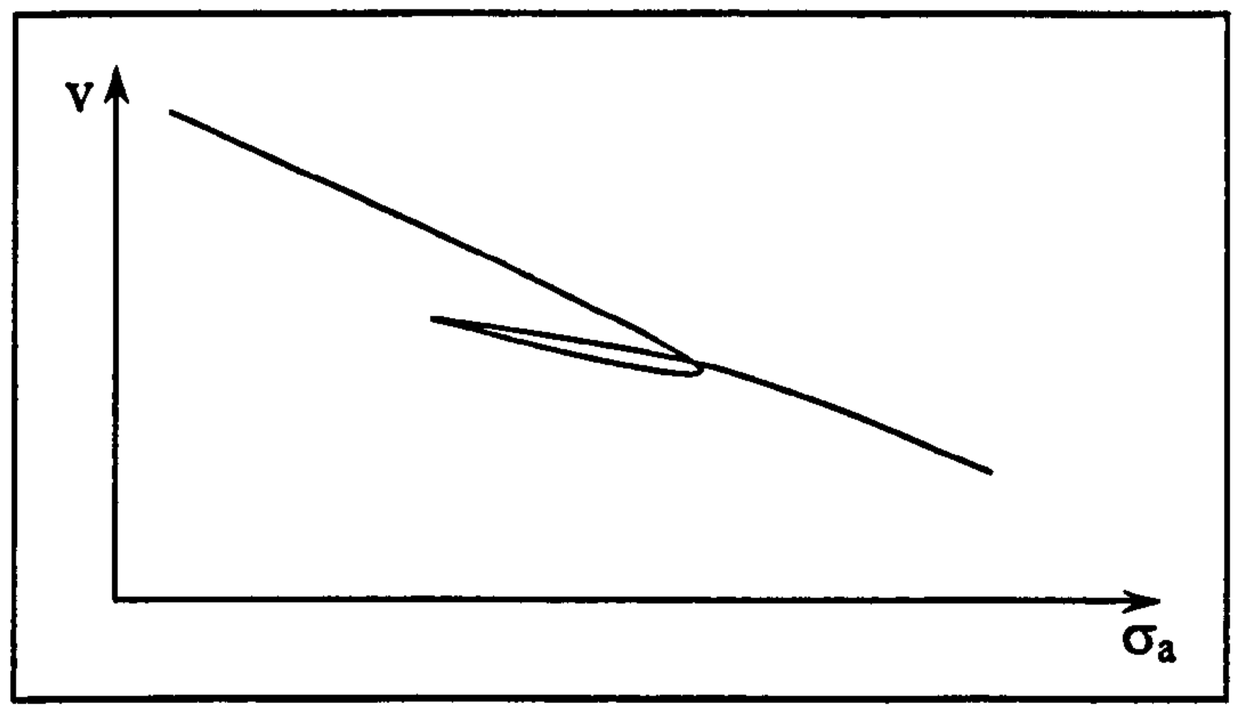

Figure 5.7 – Typical results from an oedometer test

These results give simple ideas about the stress-strain relationship in a soil. They may be interpreted to give an equivalent elastic stiffness for a simple constitutive law or to calibrate a more complex constitutive law that accurately models volumetric response. If more detailed knowledge is required of the stress-strain curve of the material then a triaxial test is regularly used. The apparatus is shown in figure 5.8 and the procedure is outlined fully by Bishop and Henkell (1957).

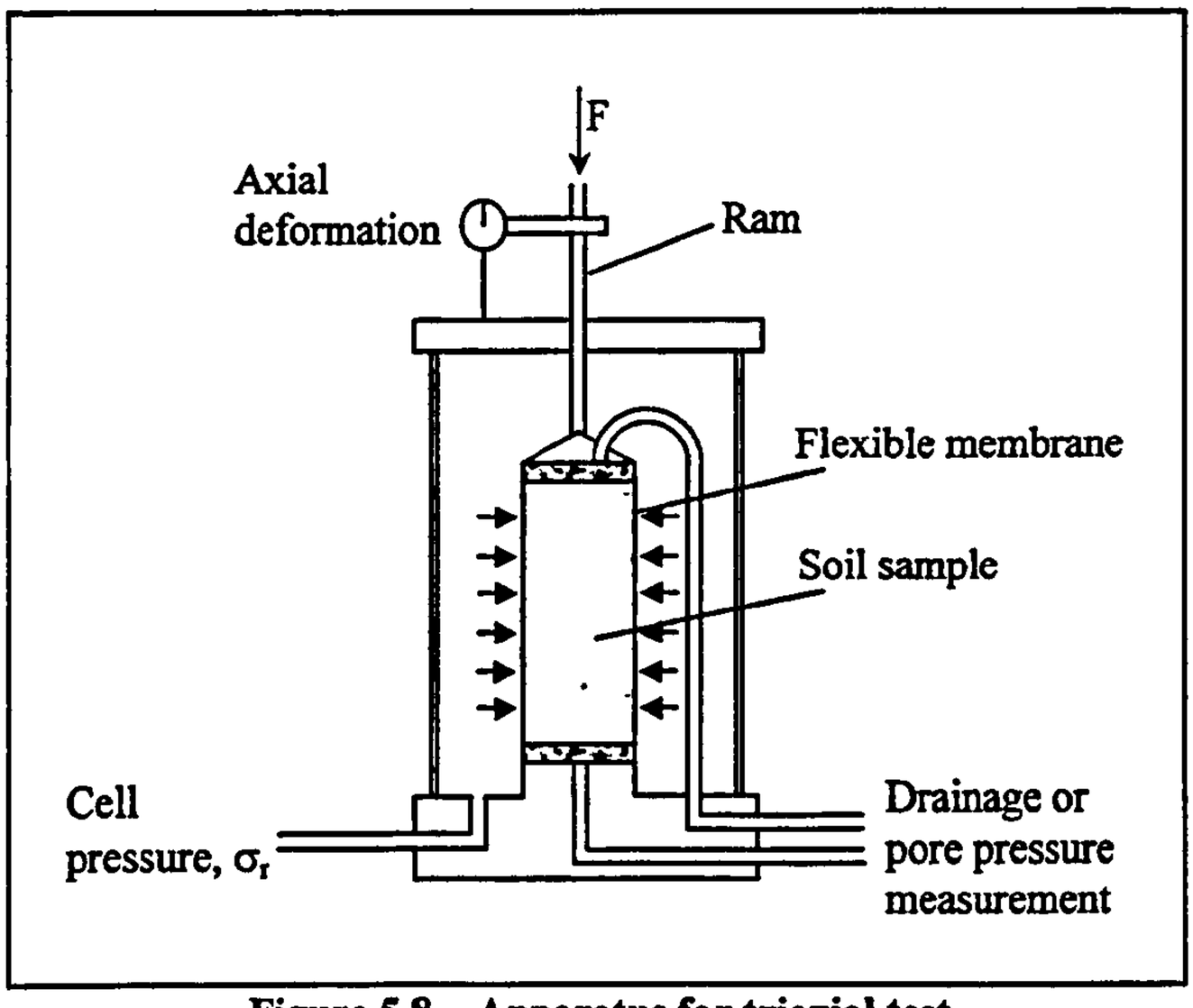

Figure 5.8 – Apparatus for triaxial test

The sample is prepared and sealed in a rubber membrane. It is then placed in the apparatus and brought into contact with the top and bottom platens. The radial stress (σ_r) is kept constant (usually by applying fluid pressure) and upon loading in the axial (σ_a) direction the volumetric strain is measured by observation of the radial expansion and the axial compression of the sample. The results can then be plotted in many ways although most common is as a function of deviator stress against axial strain as these are controlled from outside the test cell and are therefore easily measured. The deviator stress is given as the difference between the axial and the radial stress.

$$q = \sigma_a - \sigma_r \tag{5.1}$$

This test is repeated a number of times with different confining pressures (σ_r) in order to produce different stress-strain curves and a typical example can be seen in figure 5.9 (taken from Ooi (1990))

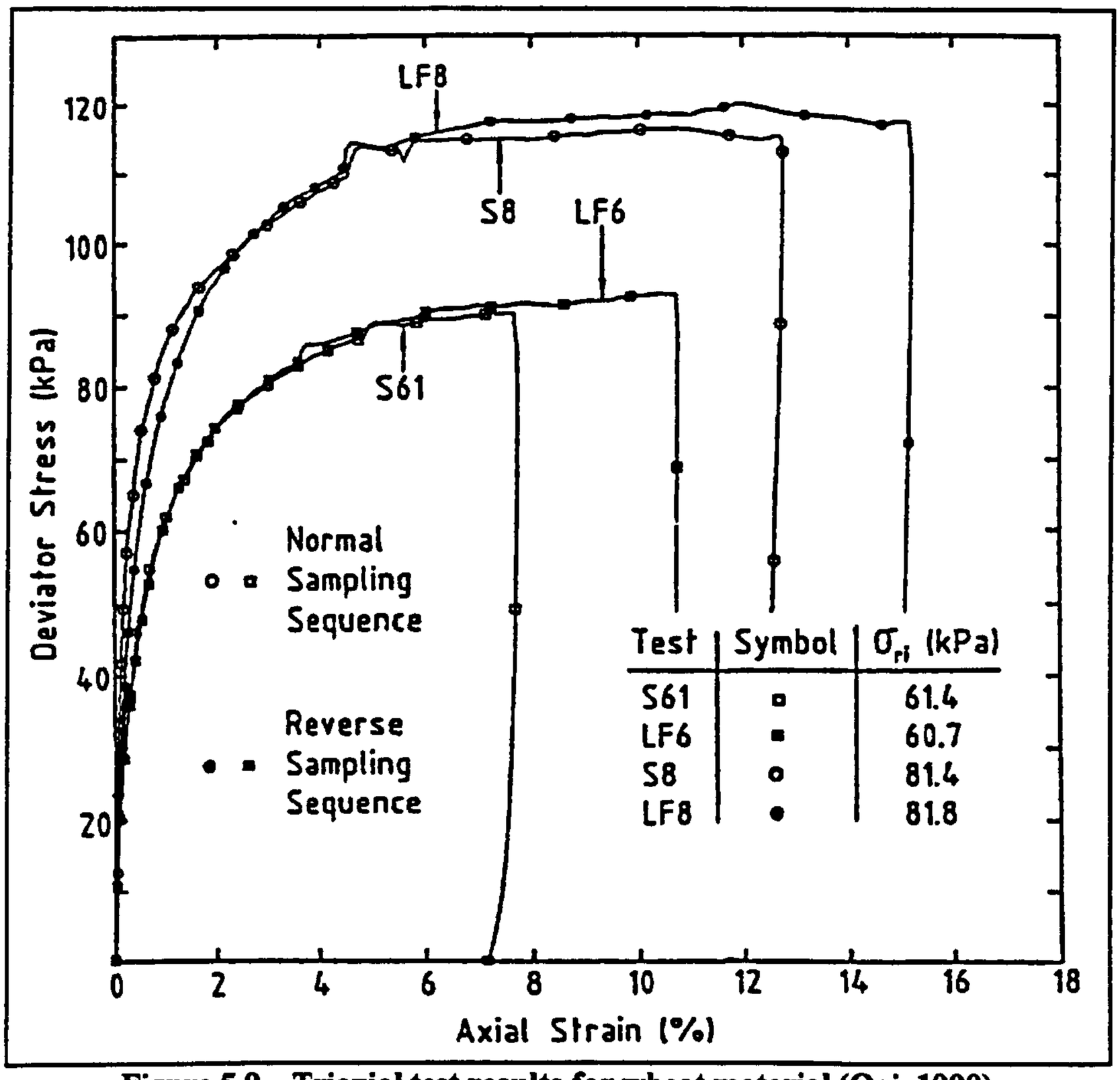

Figure 5.9 – Triaxial test results for wheat material (Ooi, 1990)

These curves illustrate one of the characteristics of granular bulk solids mentioned above which is barotropy (the material behaviour depends on the stress level).

5.3 Material constitutive laws for use in the current work

Once the relevant properties have been identified and values determined from appropriate testing, a numerical constitutive law can be formulated to describe the behaviour of the solid in the finite element software. This law is a set of relationships that defines the elastic or the plastic behaviour of a material (or both). Nielsen and Weidner (1998) state that the constitutive law must be chosen with respect to the ability to describe stress-strain paths that are relevant to silo problems.

There are a large number of these laws, proposed mainly by civil engineers in the field of soil mechanics. Not all of them are applicable to the field of silo research because of the differences in loading, water flow etc. Hence only those that are

suitable will be discussed. Not all of these models represent all of the properties above so care must be taken to choose an appropriate constitutive model for any particular application.

5.3.1 Elastic laws

This type of constitutive law is one of the simpler laws for the description of a material. Elastic laws have been used in a small number of axisymmetric silo analyses because they are simple to implement and make the solution of the problem much easier (Ooi and Rotter, 1990). In this case the law was linear but non-linear laws are available such as the model proposed by Boyce (1980) specifically for granular materials. However, by definition these models cannot describe irreversible deformations and are thus not suitable for use in silo models where plasticity of the solid may occur.

5.3.2 Non-Elastic laws

These can describe irreversible deformations and include metal plasticity and creep laws. A study of creep is beyond the scope of this project and so model laws incorporating creep specifically will not be reported here. Laws for use with soils are generally derived from metal plasticity laws such as Von Mises. They divide the strain rate into a reversible and irreversible part and use a yield surface to distinguish between elastic and plastic deformations. A yield surface is a surface set in stress space which divides the elastic and plastic regions of the model. Anything inside the yield surface is considered reversible and outside, irreversible.

5.3.3 Elastic-Plastic laws

An elastic-plastic law can be used to more accurately describe the behaviour of bulk solids. This type of model also makes use of a yield surface and one of the more commonly used is the Mohr-Coulomb law. This law has been implemented extensively in the field of soils research with useful results. It proposes that a material loaded by some normal stress can only support some maximum shear stress and if this loading becomes bigger then the material will start to plastically strain.

This sustainable shear stress depends on the angle of internal friction (ϕ) and the cohesion (c) of the solid. A further law of this type is the Drucker-Prager law which has been used by some research groups for silo problems (Aribert and Ragneau, 1990). The Drucker-Prager failure criterion has the advantage over the Mohr-Coulomb in that it is described by simple formulae, and is thus numerically easier to handle. Both of these laws are capable of describing a number of the properties mentioned above (plasticity, dilatancy, barotropy etc) but they are still rate-independent and isotropic (Feise and Schwedes, 1998). Again these constitutive laws may be considered to be extensions of metal plasticity laws.

As well as the yield surface, the elastic behaviour and the flow rule (which determines the direction and rate of plastic flow) must also be defined. The elastic behaviour can be modelled by any one of the linear or non-linear elastic laws mentioned in section 5.3.1. A more detailed description of the Mohr-Coulomb and Drucker-Prager yield criteria can be found in sections 5.4.3 and 5.4.4.

This is not a comprehensive list of the types of constitutive models that are applicable to geotechnical problems but most others are little used and will not be investigated in this work. Other models include rate-type, polar, creep and microscopic and discussion of these can be found in Feise and Schwedes (1998).

5.4 Constitutive laws available in ABAQUS

In this project several bulk solids will be modelled in order that the validity of the constitutive laws may be tested against Janssen theory and experimental data. Experimental data is available from several sources (Lahlouh *et al*, 1995; Rotter *et al*, 2002) and the materials used in those studies were Leighton Buzzard sand and pea gravel. A suitable constitutive law must therefore be chosen to model the behaviour of these materials as accurately as possible. Several constitutive laws of the types described above were implemented in this study. These are:

- Linear elastic (will be referred to as LE).
- Porous elastic (PE).

- Linear elastic with Mohr-Coulomb plasticity (LE-MC).
- Linear elastic with Drucker-Prager plasticity (LE-DP).
- Porous elastic with Drucker-Prager plasticity (PE-DP).

These laws have been chosen because the ABAQUS finite element software (as well as other commercially available packages) provides support for them. It is possible to code different constitutive laws in ABAQUS but the performance of the pre-defined models was investigated first with a view to using one of them. If one of these laws provides a realistic representation of the granular material then models can be created for design purposes using a wide range of finite element packages. It is accepted that these laws may not provide results that cover all aspects of granular material behaviour in silos when compared to silo specific material laws (e.g. Kolymbas, 1988) but their availability in other finite element packages would make the design problem more tractable for practising designers.

5.4.1 Linear elastic law

The linear elastic law is based on Hooke's (1678) observation that up to a certain limit the extension of a bar under tension was proportional to the load applied. The linear elastic law is described completely by two parameters (Young's modulus and Poisson's ratio).

5.4.2 Porous elastic law

This constitutive law is provided specifically for the modelling of granular materials or materials containing voids. It is a non-linear law relating the elastic strain to the change (decrease) in volume caused by increasing pressure levels and is based on critical state soil mechanics as originally proposed by Schofield and Wroth (1968). Critical state soil mechanics (CSM) aims to mathematically describe the response of granular materials by using the results obtained from triaxial tests. Consideration is given to the stress history of the material, as this will affect the behaviour of the material upon subsequent loading. Of principal concern in this method are the

relationships between the effective stress and the volume of the bulk solid. These relationships are typically determined from triaxial tests as described in section 5.2.2. This work is mainly related to soil mechanics and hence the pressure and loading regimes may be different to those experienced in silos, but this type of constitutive model has been successfully utilised by other researchers (Chen *et al*, 2000).

A typical volumetric response of a granular solid as it is compressed is shown in figure 5.10(a) and for the purposes of critical state soil mechanics this data is re-plotted on a semi-logarithmic scale shown in figure 5.10(b). This produces a series of straight lines which represents a simplified characterisation of the materials behaviour but is however readily described mathematically.

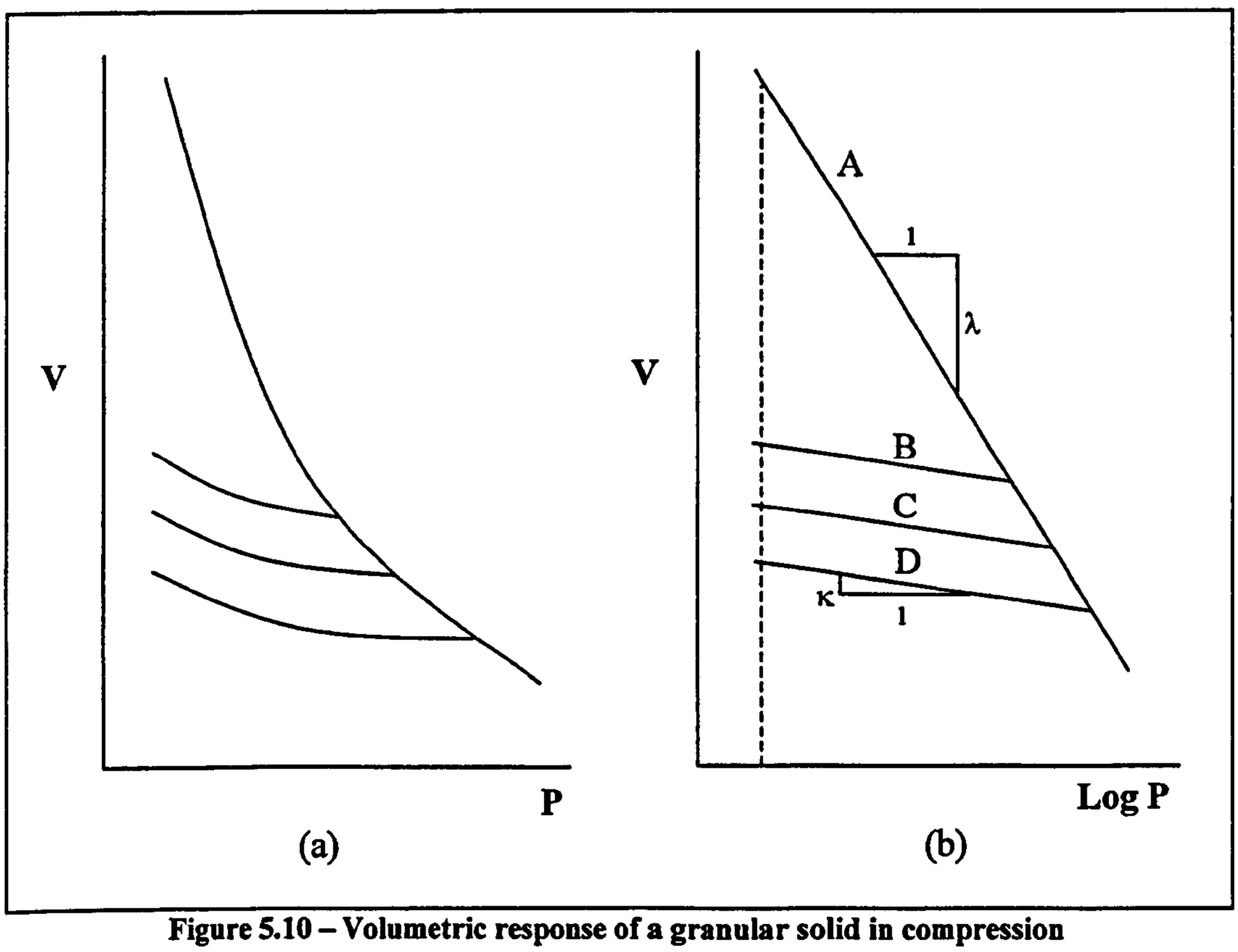

Figure 5.10 – Volumetric response of a granular solid in compression

The line A represents the initial compression of an unstressed sample and has the gradient λ. The lines B, C and D represent subsequent unloading and reloading of the specimen and these have the same gradient κ which is generally assumed to be the same for each line. It is the initial compression that this project is concerned with

as it is assumed the material will be unstressed when it is placed in the silo and that there will be no unloading or reloading after gravity is applied.

5.4.3 Mohr-Coulomb law

The Mohr-Coulomb criterion is one of the simplest models for granular materials and may be considered an extension of the Tresca criterion for metal plasticity (1864). Figure 5.11 shows the distortion of a block of granular material, supported on a rigid base, due to the application of a force.

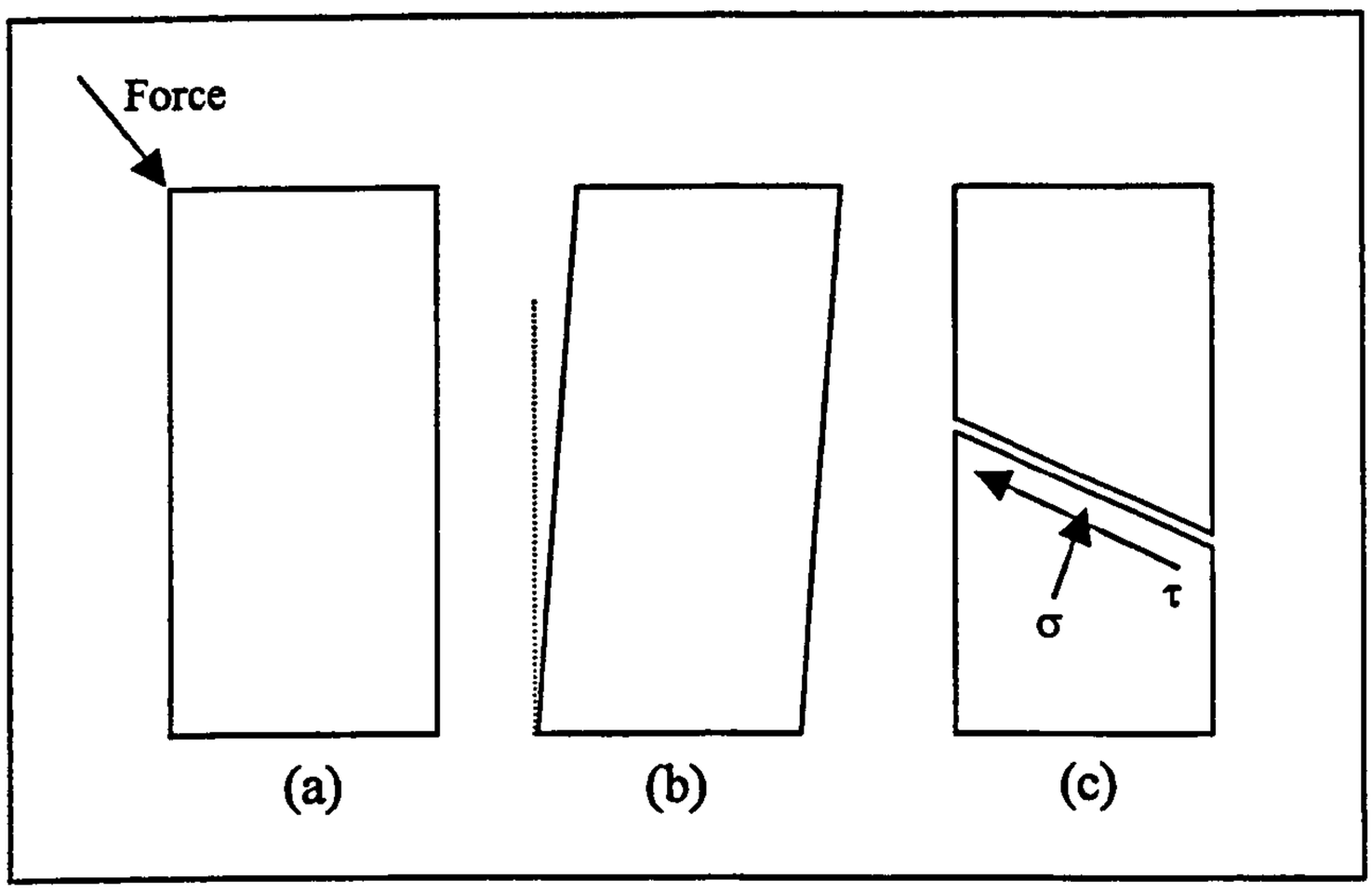

Figure 5.11 - Distortion of a block of granular material by the application of a force

If this experiment were conducted it can be shown that for small values of force there is a small elastic deformation of the granular material represented by figure 5.11(b). When the force reaches some critical value, the material divides itself into two blocks which slide past each other as shown in figure 5.11(c). The shear stress is not related to the rate or the extent of the deformation and if the elastic deformations are ignored then this behaviour can be classified as a rigid-plastic failure mode. That is to say that the material divides into two rigid blocks that are separated by a localised plastic zone. This is the basis of an ideal Coulomb material which defines the value of shear stress at which slip will occur with respect to the normal stress. The failure criteria can be written as:

$$\tau = \sigma \tan\phi + c \tag{5.2}$$

Where c is the cohesion of the material. It may be noted that many coarse materials have a very low or zero value of c. It is also noted that for the special case of $\phi = 0°$ then this reduces to the Tresca criterion.

There are three states to consider in an ideal Coulomb material,

1. $\tau < \sigma\tan\phi + c$, this implies that no slip can occur.

2. $\tau = \sigma\tan\phi + c$, this implies a slip plane will form but the extent of this slip is unknown and governed by the boundary conditions of the material.

3. $\tau > \sigma\tan\phi + c$, these values cannot occur because if values of τ greater than those given by equation 5.2 imply that the material is not in static equilibrium and one of the "blocks" would accelerate away from the other.

Figure 5.12 shows the complete Mohr-Coulomb failure criteria.

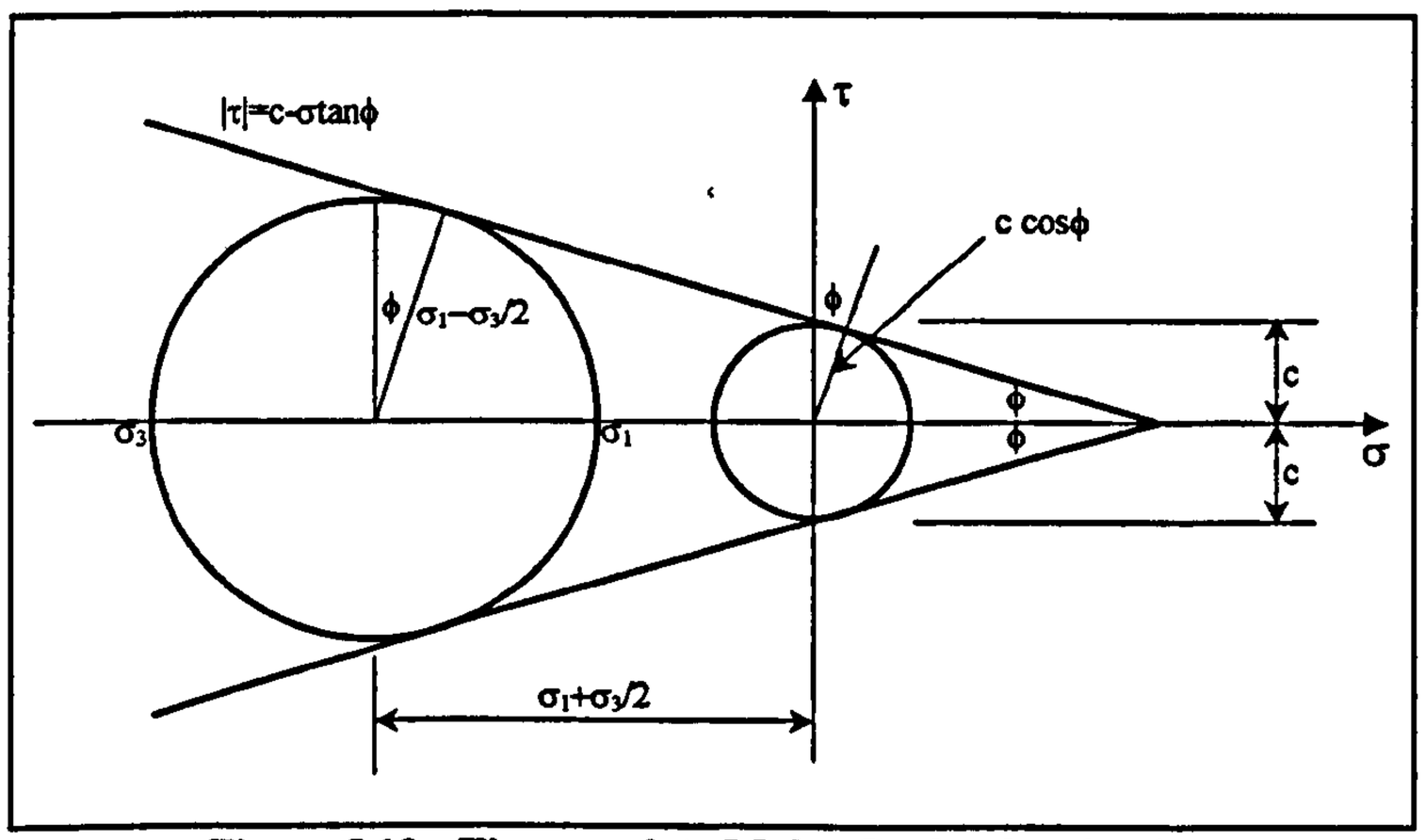

Figure 5.12 - The complete Mohr-Coulomb criterion

The three states above can be shown on the diagram. If the Mohr's circle is below the line then the material is in a state given by condition 1 above. If the Mohr's circle touches the line then condition 2 above is said to exist. From condition 3 it can be deduced that the line may not intersect the circle.

The yield function, Y, is the formalised way of expressing the failure criteria. By definition the yield function must satisfy the function:

$$Y=0 \tag{5.3}$$

And thus if the Coulomb function is re-written in terms of co-ordinates *n* and *s* which are normal to and along the slip plane respectively, the yield function can be written as:

$$Y = |\tau_{ns}| - \sigma_{nn} \tan \phi \tag{5.4}$$

5.4.3.1 Plastic potential and flow rule

The above equations determine the level of stress at which the material will yield but do not describe the direction or rate of yield. In order to determine these unknowns the concept of a plastic potential function (G) is introduced which is analogous to ideal fluid flow conditions. Once the plastic potential surface is defined, the strain rates in any direction are related to the derivatives of the plastic potential with respect to the corresponding stress.

$$\dot{\varepsilon}_{ij} = \xi \frac{\delta G}{\delta \sigma_{ij}} \tag{5.5}$$

Where *i* and *j* are any combination of the co-ordinate variables (polar, Cartesian) and ξ is a scalar constant.

The relationship between the yield function and the plastic potential is known as the flow rule. One special case is the associated flow rule. This postulates that the plastic potential is identical to the yield function and for the Coulomb material results in the mathematical prediction that shear causes an increase in the volume of the material (dilation).

$$\dot{\varepsilon}_v = -|\dot{\gamma}_{ns}| \tan \phi \tag{5.6}$$

Experimental observation of consolidated materials show that the actual level of dilation is less than that predicted by equation 5.6 (Nedderman, 1992) and it is therefore usual to define an angle of dilation (ψ) such that:

$$\dot{\varepsilon}_v = -|\dot{\gamma}_{ns}| \tan\psi \tag{5.7}$$

Materials that obey the associated flow rule therefore have:

$$\psi = \phi \tag{5.8}$$

Most real materials however must use a non-associated flow rule where:

$$\psi < \phi \tag{5.9}$$

Figure 5.13 shows idealised results from a shear box test adapted from Atkinson and Bransby (1978).

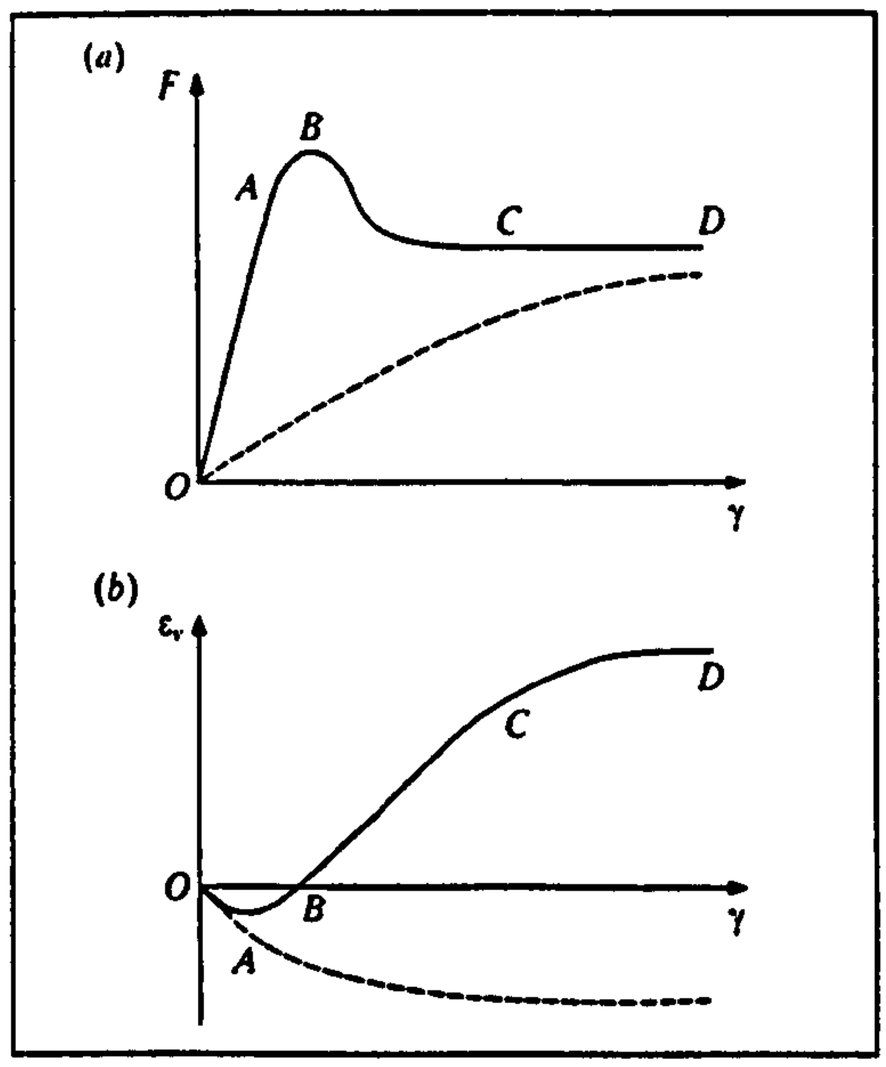

Figure 5.13 - Variation of a) shear force and b) volumetric strain with shear strain in a granular material (Atkinson and Bransby, 1978)

The figure shows the volumetric strain rate with respect to the shear strain. It may be observed that the volumetric strain reaches a maximum at about point C. This corresponds to a shear strain of about 2% after which no more dilation occurs. It is

not possible using the ABAQUS constitutive laws to model this exact behaviour and therefore a value of 0° is adopted for the angle of dilation in all the analyses.

5.4.3.2 Mohr-Coulomb criterion in three-dimensional stress space

When the Mohr-Coulomb criterion is projected into three-dimensional stress space it forms a yield surface. This is simply an extension of the above figure 5.12 where stresses under the line were treated as elastic and stress above the line resulted in plastic deformation. Figure 5.14 shows the three-dimensional representation of the Mohr-Coulomb criterion which appears as an irregular hexagon. It follows from the above that stresses inside the surface are treated as elastic and those outside (or more specifically on the surface) are treated as inelastic.

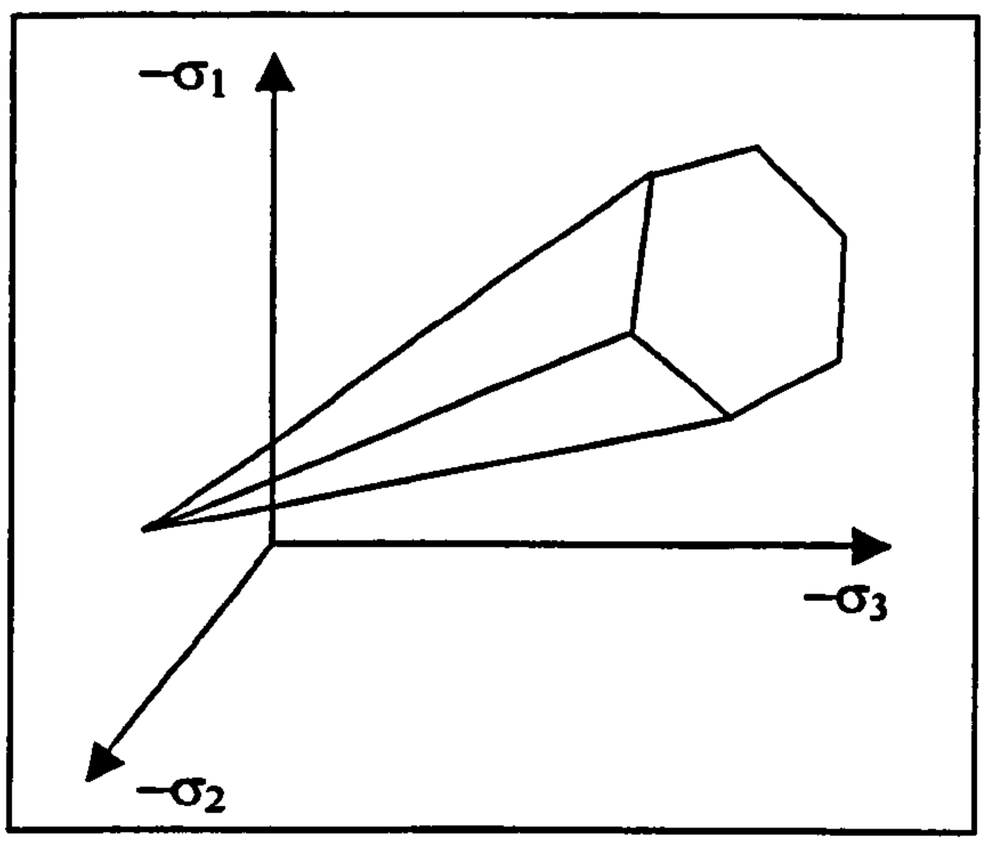

Figure 5.14 - The Mohr-Coulomb criterion in principal stress space

5.4.4 Drucker-Prager law

If the Mohr-Coulomb criterion is considered to be an extension of the Tresca (1864) criterion based on maximum shear stress then the Drucker-Prager criterion is an extension of the von Mises (1913) criterion for elastic breakdown. This is based on shear strain energy.

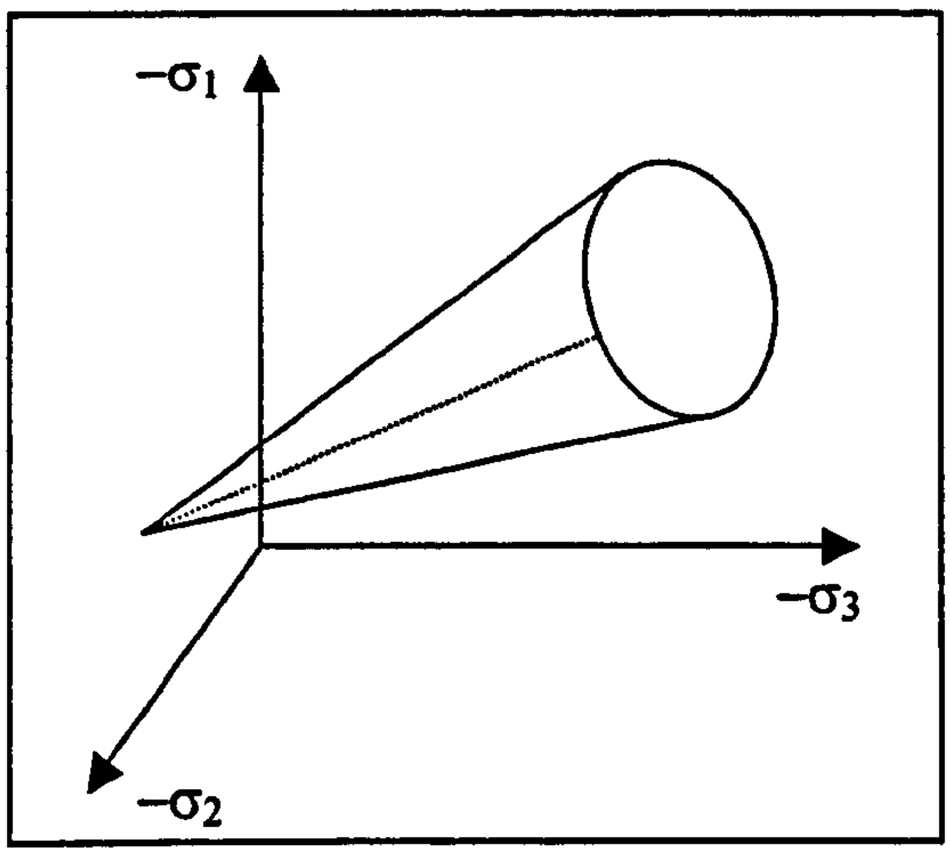

Figure 5.15 - The Drucker-Prager criterion in principal stress space

In principal stress space the Drucker-Prager yield surface appears as a cone (figure 5.15) which has numerical advantages over the Mohr-Coulomb criteria shown in figure 5.14. Numerical problems with the Mohr-Coulomb criterion can occur when calculating the direction of yield which is normal to the surface. If yield in the Mohr-Coulomb model occurs on a vertex of the cone then the normal direction is hard to calculate. The Drucker-Prager criterion eliminates this problem as the normal to the yield surface will always be uniquely defined.

In terms of the stress invariants the Drucker-Prager criterion is expressed as:

$$f(I_1, J_2) = \alpha I_1 + \sqrt{J_2} - \beta \tag{5.10}$$

Where I_1 is the first invariant of the stress tensor:

$$I_1 = \sigma_1 + \sigma_2 + \sigma_3 \tag{5.11}$$

J_2 is the second invariant of the stress deviator tensor:

$$J_2 = \frac{1}{6}\left[(\sigma_x - \sigma_y)^2 + (\sigma_y - \sigma_z)^2 + (\sigma_z - \sigma_x)^2\right] + \tau_{xy}^2 + \tau_{yz}^2 + \tau_{zx}^2 \tag{5.12}$$

α and β are material constants.

The Drucker-Prager criterion can be calibrated in such a way that it approximates the Mohr-Coulomb criterion. This is achieved by adjusting the size of the cone so that

the outer apices of the Mohr-Coulomb coincide with the Drucker-Prager cone. This situation is shown in figure 5.16.

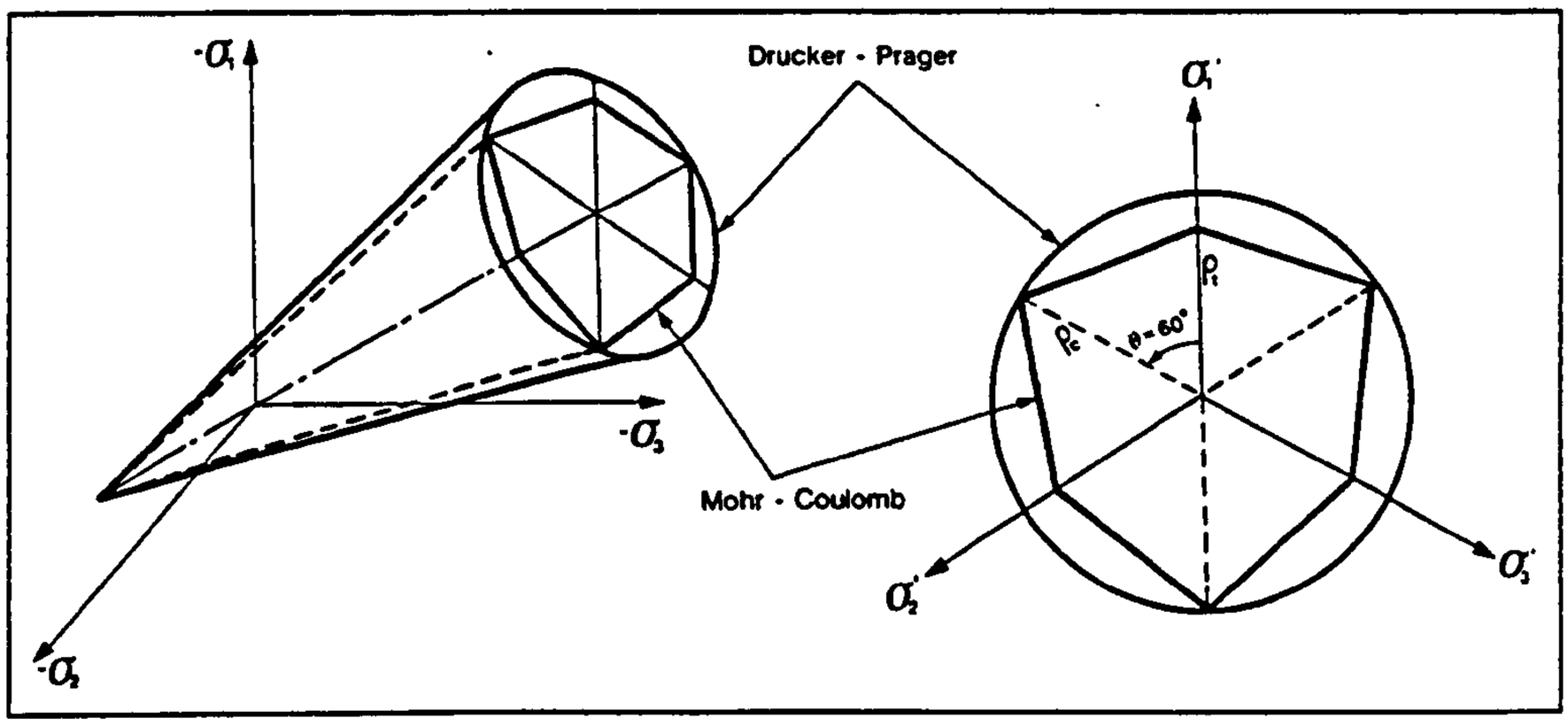

Figure 5.16 - The coincidence of the Drucker-Prager and Mohr-Coulomb criteria (Chen, 1994)

The two criteria will not give the exact same results as they do not coincide at all points.

As in the Mohr-Coulomb example, once the yield criterion has been defined then the plastic potential and flow rule can be expressed in a similar form to that expressed in section 5.4.3.1.

5.5 Summary

The aspects of the finite element analysis that need to be considered with respect to silo problems have been discussed. Non-linear solution techniques must be used to accommodate the non-linear behaviour of the structure and the stored solid.

A constitutive law must be used in order to model the finite element continuum as a granular bulk solid. There are a large number of such laws available and those provided by the finite element package being used here were discussed. It now remains to investigate the chosen laws by the methods outlined in Chapter 6.

Chapter 6 - Investigation and validation of material constitutive laws

6.1 Introduction

When using the finite element method it is important to validate the model in some way. This is achieved by comparing results obtained against known conditions. These conditions may include results from experiments or from reliable theoretical models.

For validation of the chosen material constitutive laws and hence the finite element model, results are initially compared to a Janssen pressure distribution. In Janssen's original work, there is only one boundary condition (the stress at the surface is zero) but the accuracy of the predictions compared to real silo pressure measurements is found to be much improved given the following:

- The bin is deep.
- The bin has a rigid wall.
- The surface has a level fill.

The finite element model with which to compare the Janssen distribution is therefore one that takes account of these assumptions rather than starting with a more complex three-dimensional model of a rectangular bin.

6.2 Axisymmetric model - geometry and boundary conditions

An axisymmetric bin, 10m deep with a flat bottom and with diameter 1.5m is modelled. This size is chosen as h/d = 6.66 which classifies this silo as slender (ENV 1991-4, 1995). It is also deep enough to potentially enable pressures in the stored material to reach the Janssen asymptotic values. The walls are taken as 5mm thick steel. This is rather thicker than would be expected in a real silo of this size where the shell thickness would be less, but using this thickness ensures that the wall in the finite element model is very stiff and thus satisfies the Janssen requirement. Steel is modelled as a linear elastic material with elastic modulus (E) = 210GPa and

Poisson's ratio (ν) = 0.3. All of the nodes making up the base of the silo are restrained against movement in the y-direction (vertical) but are unrestrained in the x-direction (radial), allowing the walls and base of the model to expand radially (if need be) but preventing any rigid body motions. This is shown in figure 6.1. This figure shows schematically three supports on the base but in the finite element mesh each node would be restrained in the y-direction.

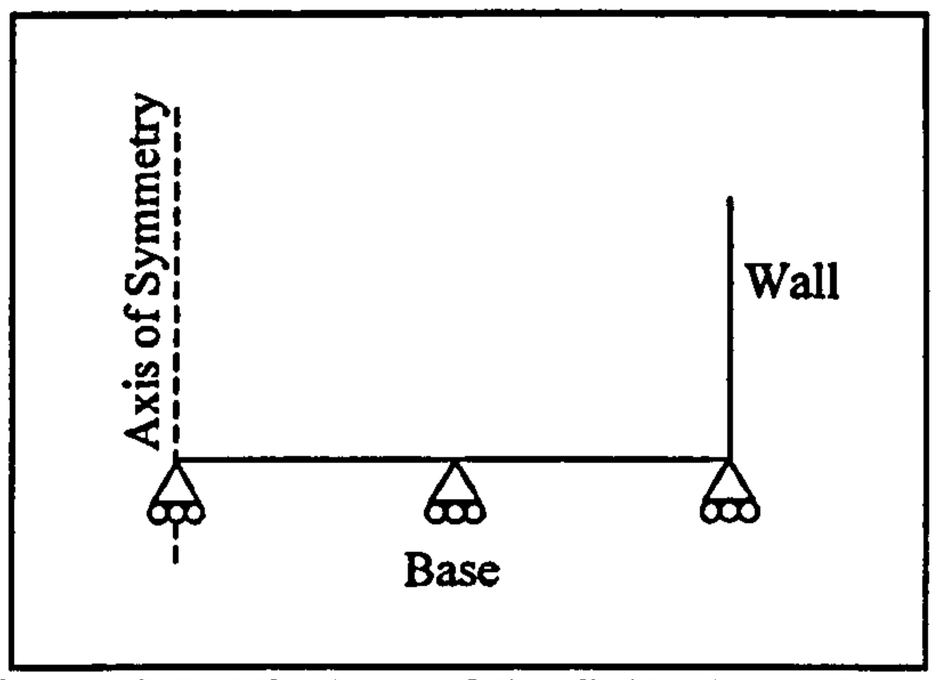

Figure 6.1 – Restraint at the base of the finite element model of the bin

This boundary condition could be likened to having the silo ground-supported although the base is initially modelled as smooth (i.e. there is no friction between the base of the bin and the material inside). A more detailed study of the effects of the boundary condition at the base is presented later (Chapter 7). The walls are modelled as frictional with a simple Coulomb friction model.

When predicting filling (static) pressures using the finite element method, two methods of loading have been reported (Rotter *et al*, 1998). The first is a progressive fill method whereby layers of unstressed material are placed into the silo under gravity. Numerical iteration occurs in order to produce an equilibrium solution and then further layers of material are placed into the silo until it is filled. This method has been used successfully by Ragneau *et al* (1994). The second method is incremental gravitational loading. The silo is initially filled with unstressed material and gravity is "switched on" in small increments until the full self-weight of the ensiled material is acting upon the structure. This second method is the one adopted in this study. Previous research has shown that different results might be obtained by

these methods but aside from Rotter *et al*'s assessment (1998) there is currently little comparative work in this area.

Figure 6.2 shows a schematic representation of the finite element model of the axisymmetric silo. The mesh shown is for illustrative purposes only.

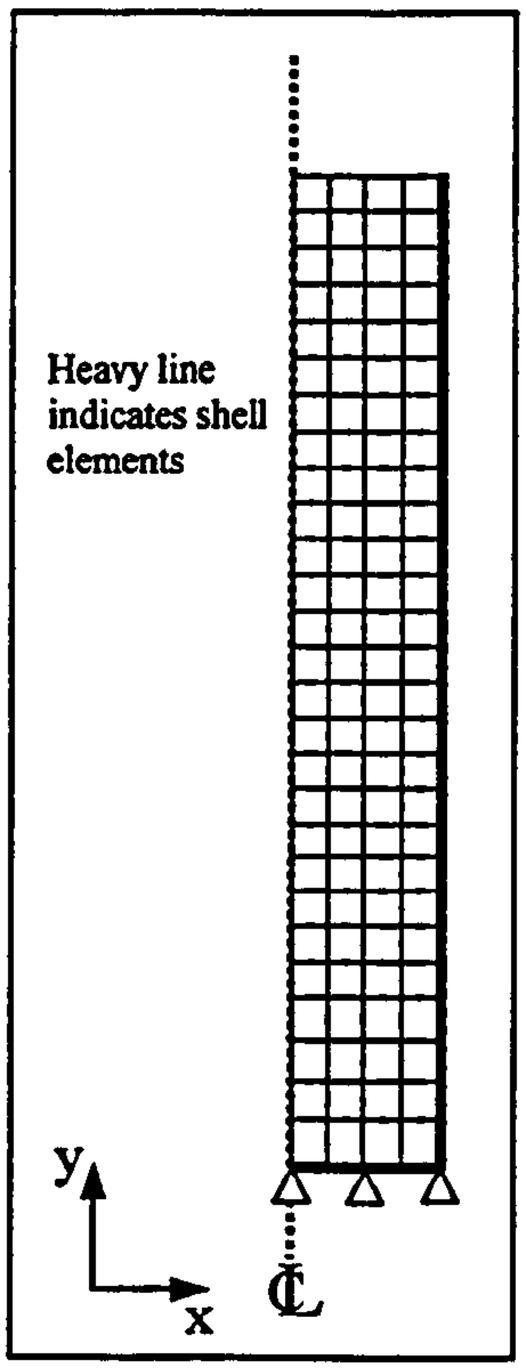

Figure 6.2 - The finite element mesh of an axisymmetric silo

6.3 Material models

To describe the ensiled material, five alternative material constitutive models are considered. Literature (Ooi and Rotter, 1990) shows that the expected response in an axisymmetric bin of this type will be mainly elastic (small strains) and hence plasticity conditions may not be required for this type of analysis and the type of failure criterion chosen may be less important at this stage. The five material models are as presented in Chapter 5:

- Linear elastic (LE)
- Porous elastic (PE)

- Linear elastic with Mohr-Coulomb plasticity (LE-MC)
- Linear elastic with Drucker-Prager plasticity (LE-DP)
- Porous elastic with Drucker-Prager plasticity (PE-DP)

It may be noticed that the porous elastic model is not combined with the Mohr-Coulomb criterion. This is because the ABAQUS software does not allow this combination although no reason for this is given.

Parameters for each of these constitutive laws are determined by performing suitable tests upon the granular material and translating the results into the finite element model. Examples of the types of tests performed on geotechnical materials were given in section 5.2.2.

6.4 Elastic material models

6.4.1 Linear elastic law

Values are required for the elastic modulus (E) and either the Poisson's ratio (ν) or the lateral pressure ratio (k) used in the Janssen equation. Values of ν and k are inter-dependant for elastic solids. k is the ratio of horizontal to vertical stress in the solid and the value used in this report is as defined by ENV 1991-4 (1995), and is assumed to be constant:

$$k = 1.1(1 - \sin\phi) \tag{6.1}$$

where ϕ is the angle of internal friction of the material.

The angle of internal friction can be related to the Poisson's ratio of the material by equation 6.2 (Rotter, 2001).

$$\nu = \frac{k}{1+k} \tag{6.2}$$

For the Leighton Buzzard Sand in question, $\phi = 35.4°$ (Lahlouh *et al*, 1995) and therefore $k = 0.463$ and hence, $\nu = 0.3164$. E is taken as 10MPa after Chen *et al* (2000).

The bulk density of the material must be determined. Several values are given for the bulk density by Lahlouh *et al* (1995), relating to various stress states within the material. These are loose density, density after a 200mm fall and vibrated (compacted) bulk density. Table 6.1 shows these values:

Mean loose bulk density (kg/m^3)	1,576
Mean bulk density from a 200mm fall (kg/m^3)	1,610
Mean vibrated bulk density (kg/m^3)	1,672

Table 6.1 - Values of bulk density for Leighton Buzzard sand from Lahlouh *et al* (1995)

Initially the bulk density is taken as the mean of these three values ($1,619kg/m^3$) in an attempt to estimate the density that would be observed at the relatively low pressure levels experienced in silos. This value must also be used in the Janssen calculations for comparison purposes.

Figure 6.3 shows the wall normal pressures in the deep bin filled with Leighton Buzzard sand as calculated by the linear elastic law. The appropriate Janssen distribution is also shown. To determine the Janssen distribution consistent values of parameters must be used. The pressures shown in this and all subsequent figures are taken from the individual nodes in the model as opposed to being an average across the face of each element.

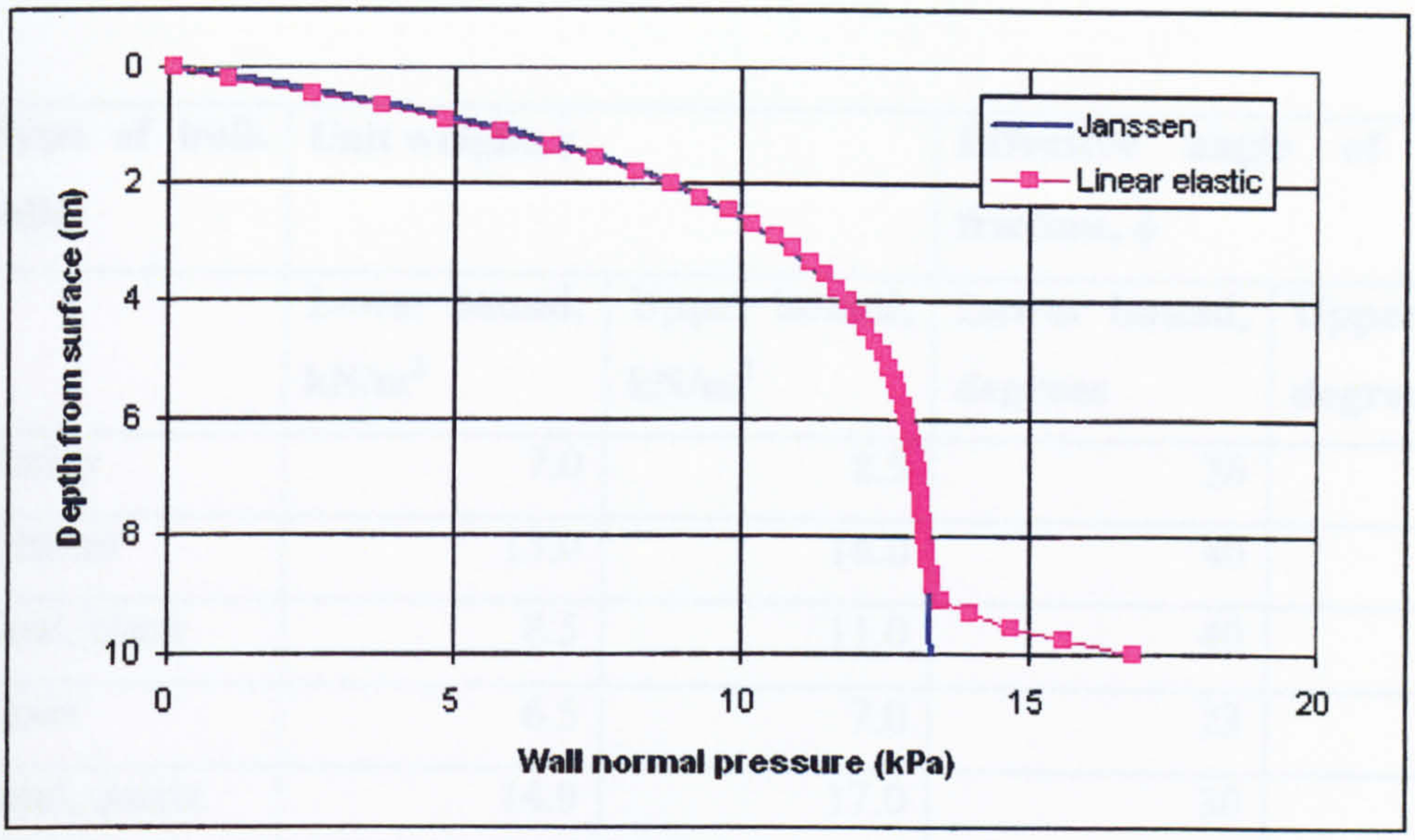

Figure 6.3 - Wall normal pressure as calculated from linear elastic constitutive law

With the exception of the results near the base, agreement between the finite element results and the Janssen distribution is within 1%. The lack of agreement at the bottom of the bin is attributed to the effect of the boundary condition of the base. Effects of this type have been noticed by previous authors (Rotter *et al*, 1998) and are attributed to the proximity of the base. The effect on the pressures of the base boundary condition is discussed in Chapter 7 below.

6.4.1.1 Poisson's ratio as the controlling factor in the linear elastic model

From equation 6.2 Poisson's ratio can be determined for any value of k. In the axisymmetric case this allows the modelling of almost any granular solid given its density and angle of internal friction. Table 6.2 shows values for the properties of several materials that may be stored in silos from Rotter (2001).

Type of bulk solid	Unit weight, γ		Effective angle of internal friction, ϕ	
	Lower bound, kN/m^3	Upper bound, kN/m^3	Lower bound, degrees	Upper bound, degrees
Barley	7.0	8.5	26	33
Cement	13.0	16.0	40	50
Coal, black	8.5	11.0	40	60
Flour	6.5	7.0	23	30
Sand, quartz	14.0	17.0	30	40
Sugar	9.0	9.5	33	38
Wheat	7.5	9.0	20	26

Table 6.2 – Properties of various granular bulk solids as given by Rotter (2001)

The following table shows representative values of k (from the above table) converted to values of Poisson's ratio. An appropriate mean density is also shown for each material.

Type of bulk solid	Mean unit weight, γ	Effective angle of internal friction, ϕ	k value from Eq. 6.1	Effective Poisson's ratio (Eq. 6.2)
Barley	7.75	29.5	0.558	0.358
Cement	14.5	45	0.322	0.244
Coal, black	9.75	50	0.257	0.204
Flour	6.75	26.5	0.609	0.378
Sand, quartz	15.5	35	0.469	0.319
Sugar	9.25	35.5	0.461	0.316
Wheat	8.25	23	0.670	0.401

Table 6.3 – Properties of granular bulk solids for use in the linear elastic model

Figure 6.4 shows finite element results for some of these materials along with the corresponding Janssen distributions.

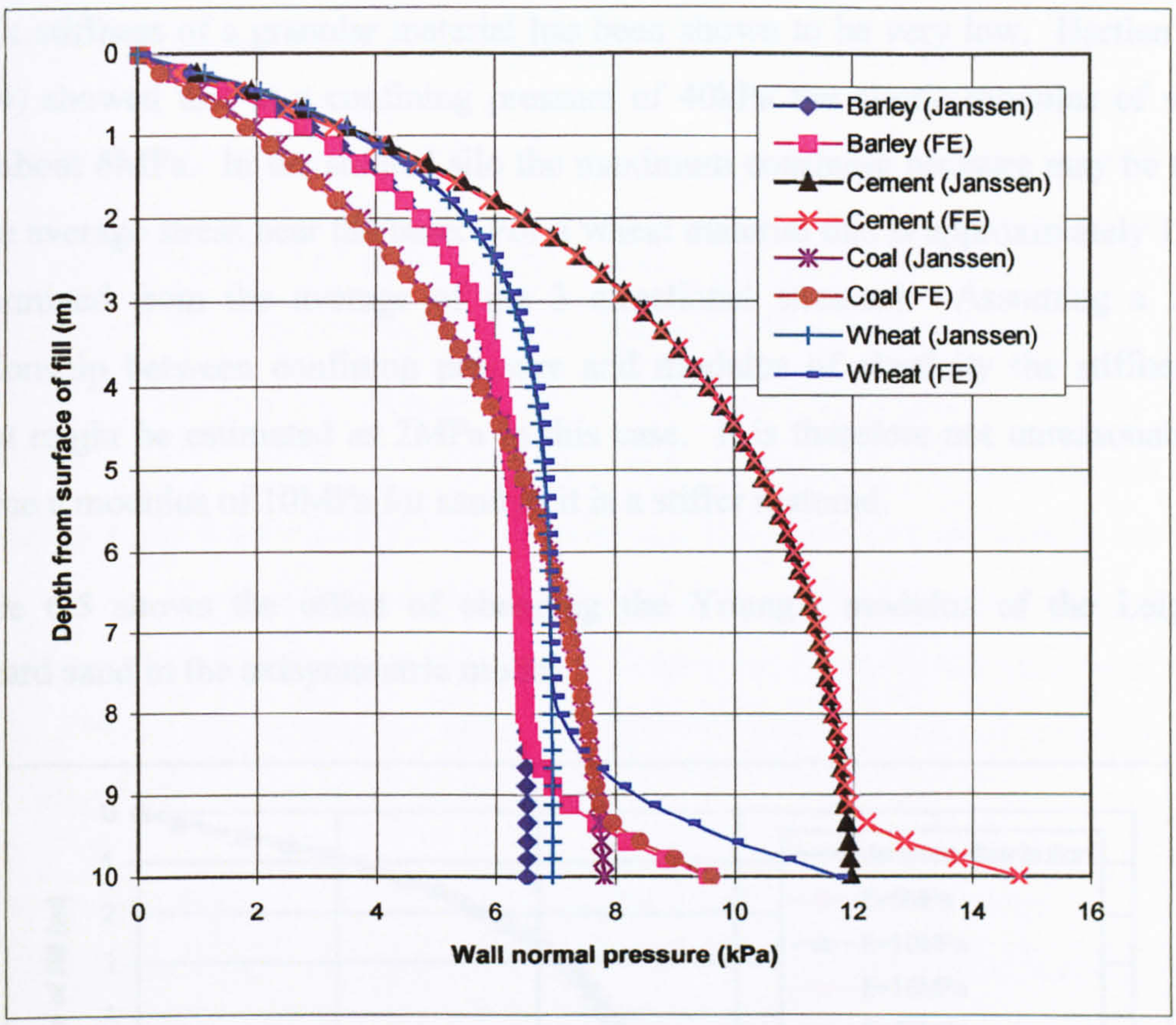

Figure 6.4 – Comparisons between finite element and Janssen predictions for a range of materials

Again, the agreement between the finite element results and the Janssen distributions is in the order of 1% over the majority of the bin. The materials that have lower values of ϕ and γ show more pronounced end effects. These effects are discussed in more detail in Chapter 7.

The linear elastic model gives good agreement over the majority of the bin for a large range of materials compared to the Janssen distribution in axisymmetric type problems. The above analyses were carried out using the assumed low value of initial elastic stiffness from Chen *et al* (2000) of 10MPa. This value of elastic stiffness has been adopted by other researchers to represent granular materials (Ooi and She, 1997) but would appear to be chosen arbitrarily. Data for the elastic

stiffness of granular materials is difficult to obtain for reasons discussed in section 5.2.1 but some information is available. Granular material behaviour is known to be dependent on the overall stress level and at low confining pressures the equivalent elastic stiffness of a granular material has been shown to be very low. Hartlen *et al* (1984) showed that at a confining pressure of 40kPa the elastic modulus of wheat was about 6MPa. In the studied silo the maximum confining pressure may be taken as the average stress near the base. For a wheat material this is approximately 12kPa (determined from the average of the 3 directional stresses). Assuming a linear relationship between confining pressure and modulus of elasticity the stiffness of wheat might be estimated as 2MPa in this case. It is therefore not unreasonable to assume a modulus of 10MPa for sand as it is a stiffer material.

Figure 6.5 shows the effect of changing the Young's modulus of the Leighton Buzzard sand in the axisymmetric model.

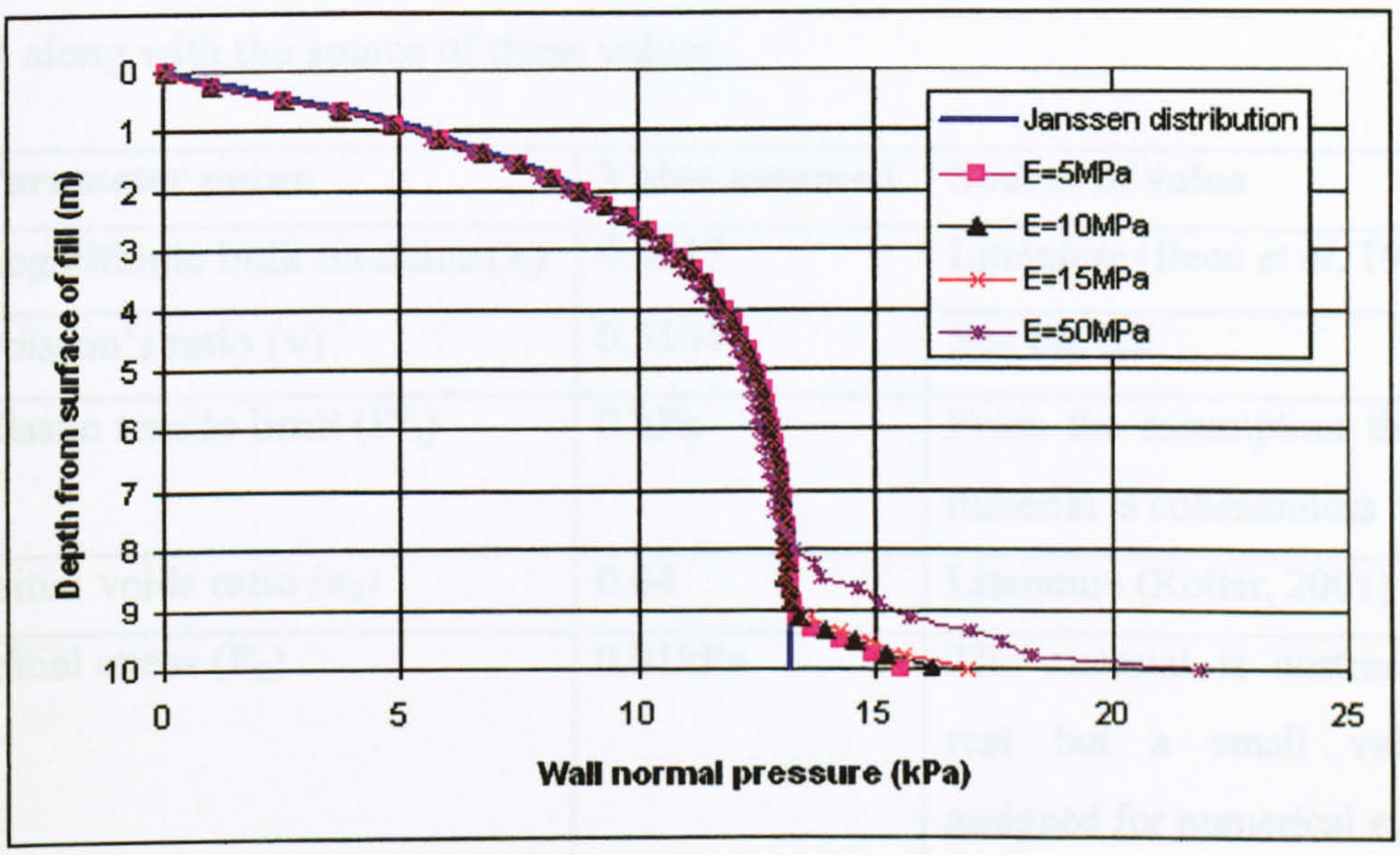

Figure 6.5 – The effect of changing the elastic stiffness in the axisymmetric bin

Figure 6.5 shows that for low values of Young's modulus the predicted pressures do not vary significantly. However, when E = 50MPa, the end effect in the bin is more pronounced although pressures further up the bin are relatively unaffected. These results probably indicate that this value of elastic modulus is too high to represent a

granular material but it appears that as long as the value taken is small then the actual value of Young's modulus is not critical to the performance of the model.

The value of 10MPa is therefore accepted as a good approximation of the stiffness of the Leighton Buzzard sand and is used for the remainder of the analyses.

6.4.2 Porous elastic model

The porous elastic law uses several specific parameters for which values must be determined. The most suitable way to determine these values would be to perform a triaxial test (Bishop and Henkel, 1957). This would give a more complete overview of the behaviour of the granular bulk solid. Performing this type of test however requires significant specialist equipment and expertise that are outside the scope of this work. It was therefore decided to initially calibrate the porous elastic model from a variety of literature sources and subsequently check this data with materials tests. Values for the porous elastic law that were initially adopted are shown in table 6.4 along with the source of these values.

Parameter name	**Value assumed**	**Source of value**
Logarithmic bulk modulus (λ)	0.0217	Literature (Been *et al*, 1991)
Poisson's ratio (ν)	0.3164	See Eq. 6.2
Elastic tensile limit (P^{el}_t)	0 kPa	From the assumption that this material is cohesionless
Initial voids ratio (e_0)	0.64	Literature (Rotter, 2001)
Initial stress (P_0)	0.01kPa	The material is unstressed at rest but a small value is assigned for numerical stability

Table 6.4 - Values used to calibrate the porous elastic constitutive law

The results using these parameters when compared to an equivalent Janssen distribution are shown below (figure 6.6).

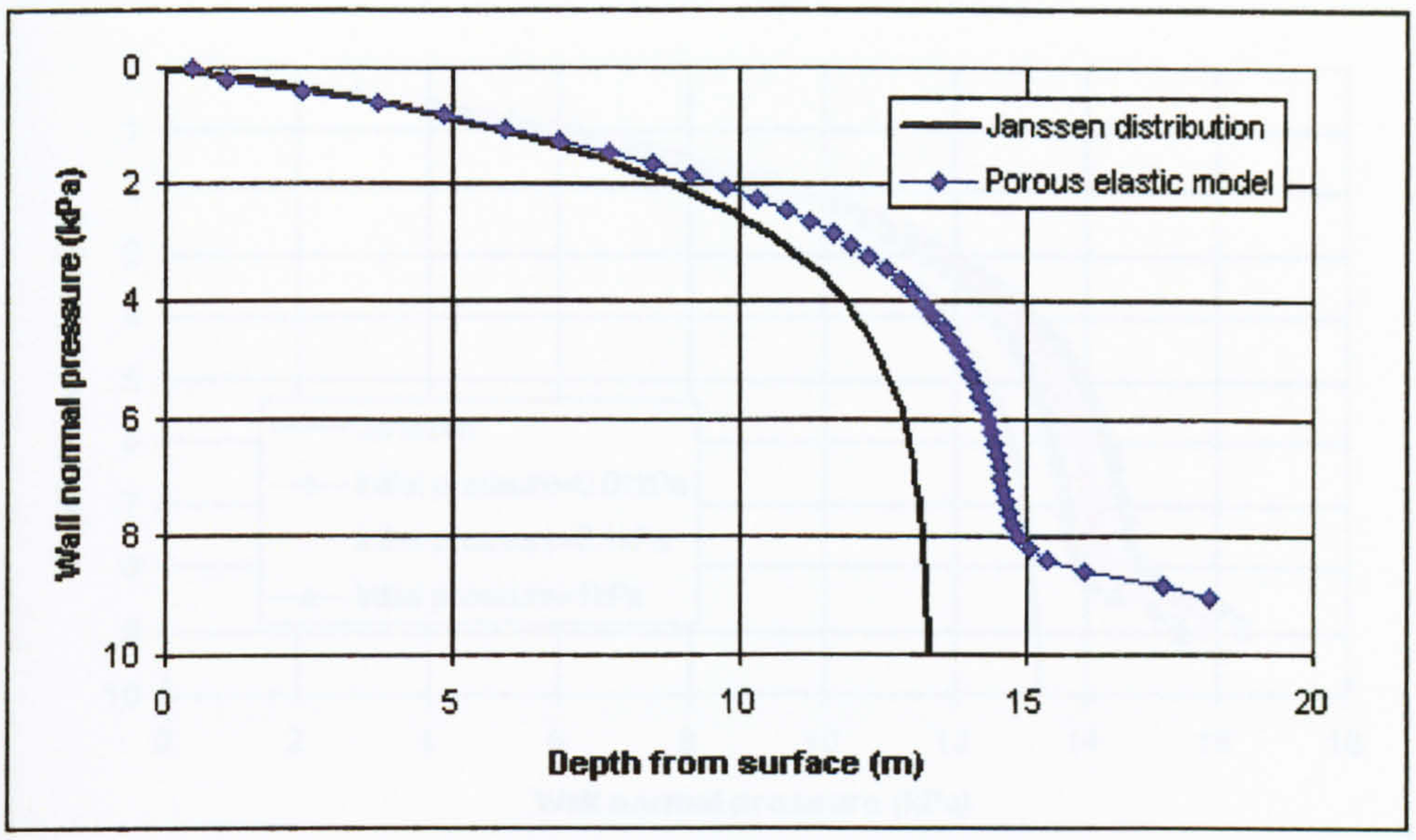

Figure 6.6 - Wall normal pressure as calculated from the porous elastic constitutive law

The figure shows that this material model does not predict the pressure as well as the previous linear elastic law when compared to the Janssen distribution. Both of these constitutive laws should produce results that agree with the Janssen distribution in this silo. The behaviour of the material should be entirely elastic as small deformations in the wall and solid are predicted/expected and equilibrium (implicit in Janssen's theory) should be maintained. Therefore it is assumed that one or more of the values in the porous elastic model has been incorrectly adopted. Poisson's ratio and the elastic tensile limit are assumed to be correctly chosen because of the previous study on Poisson's ratio and the fact that the material is cohesionless. Therefore investigation was carried out to determine whether one or more of the values adopted for λ, e_0 or P_0 was poorly chosen. Figure 6.7 shows the effect of changing the values of P_0.

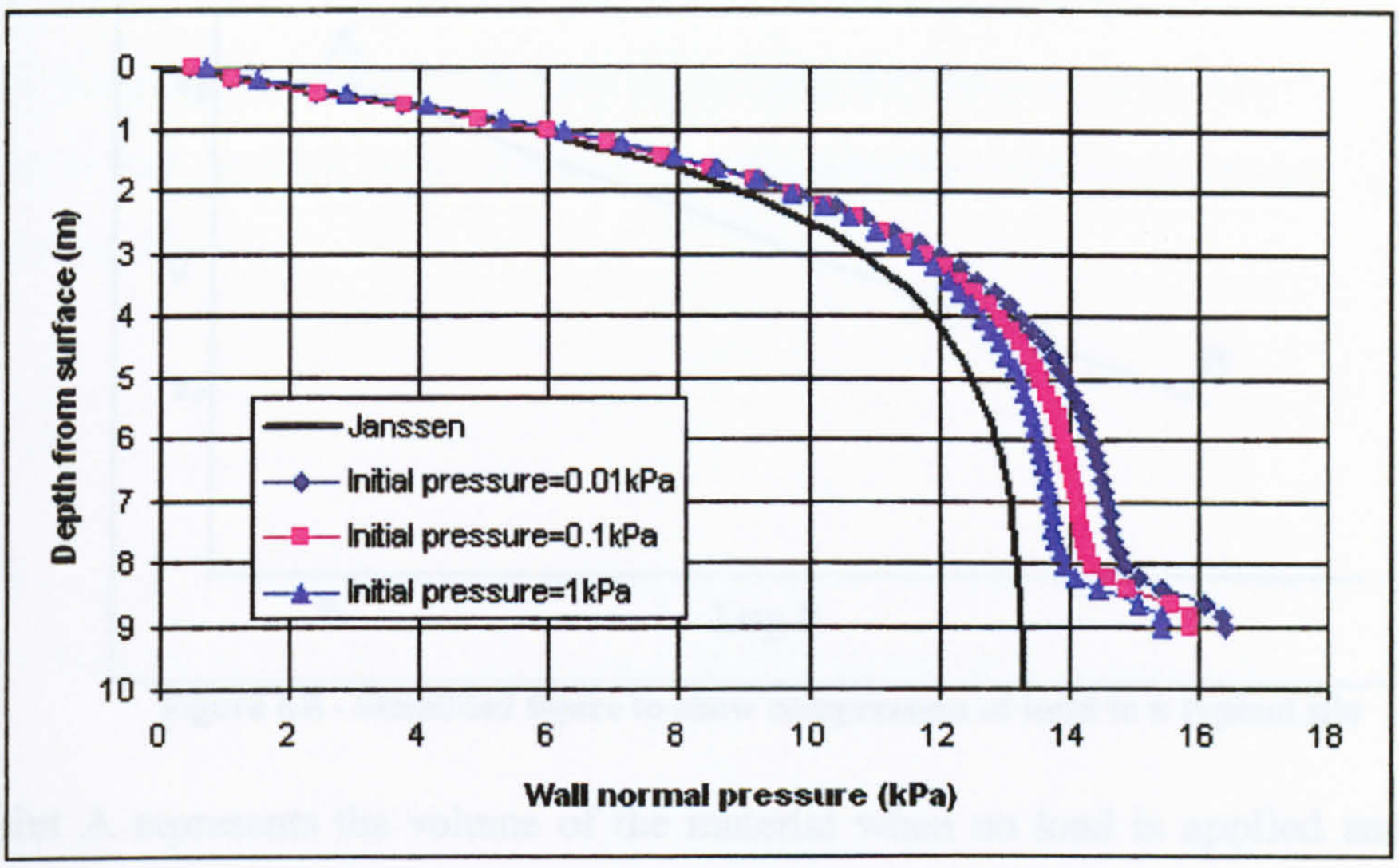

Figure 6.7 - The effect of changing the initial stress in the porous elastic model

Changing this value has a noticeable effect on the predicted pressures in the bin but this change is not sufficient to match the results to the Janssen distribution. Using a value of P_0 = 1kPa gives results closest to the Janssen prediction but it is questionable as to whether an initial stress of 1kPa is acceptable in this case as the material is initially modelled as weightless and would therefore be experiencing no load. 1kPa is also not an insignificant stress with respect to the maximum normal stress that is expected to occur in this bin (13.3kPa) and in future models it may be difficult to predict what effect this relatively large initial stress may have. It is therefore assumed that the value of e_0 or λ requires investigation. From inspection of figure 5.11 it can be seen that these two parameters, as well as the bulk density, are intrinsically linked. If the value of one of these parameters is changed then the others must be re-calculated to reflect that change. Figure 6.8 shows a simplified version of figure 5.11 that represents the volumetric behaviour of the solid in the silo as described by the porous elastic law.

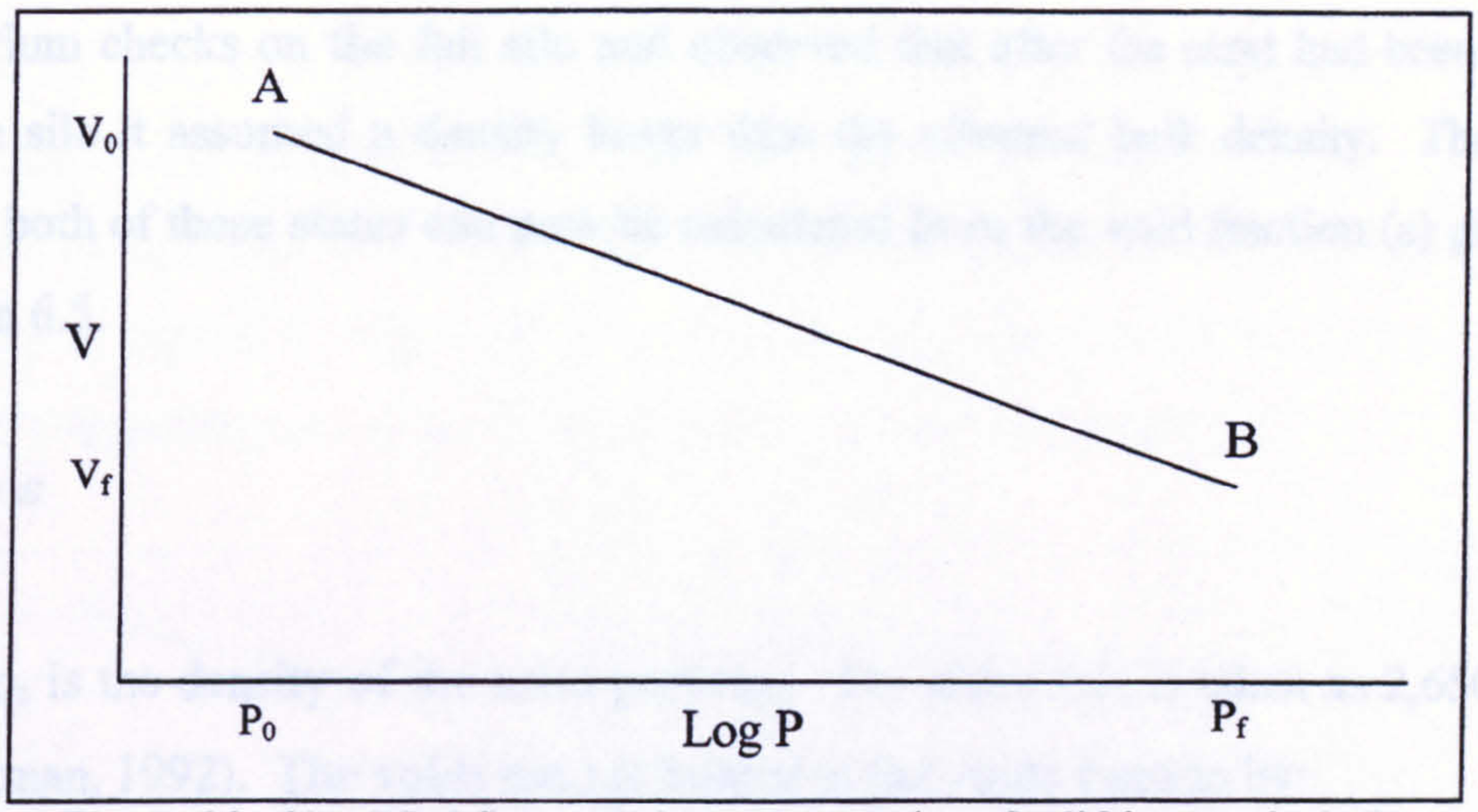

Figure 6.8 - Simplified figure to show compression of solid in a typical silo

Point A represents the volume of the material when no load is applied and can be calculated from the initial values of pressure, bulk density, voids ratio and particle density. Point B represents the material at rest in the filled silo and can be calculated from knowledge of the final Janssen condition (assuming that Janssen is a good representation). It is known that for any given silo and material there is a Janssen distribution and that at an infinite depth the normal vertical pressure reaches an asymptote which is given by equation 6.3.

$$P_v \max = \frac{\gamma R}{\mu k} \tag{6.3}$$

Given this value, the final bulk density and the value of the density of the solid particles in the granular material, it is possible to calculate the final voids ratio that corresponds to the Janssen asymptotic condition. Point B can then be plotted since:

$$v = 1 + e \tag{6.4}$$

By following a similar calculation and taking an initial (unstressed) bulk density and pressure, point A can be calculated. Referring back to table 6.1 Lahlouh *et al* (1995) give bulk densities that can be used to perform these calculations. The initial bulk density is taken as the loosest form (i.e. it is unstressed) and the final bulk density is taken as the value measured after a 200mm fall. This value is chosen over the vibrated (denser) value due to the fact that Lahlouh *et al* (1995) performed

equilibrium checks on the full silo and observed that after the sand had been placed into the silo it assumed a density lower then the vibrated bulk density. The voids ratio in both of these states can now be calculated from the void fraction (ε) given by equation 6.5.

$$1-\frac{\gamma}{\rho_s}=\varepsilon \tag{6.5}$$

Where ρ_s is the density of the solid particles. For silica this is taken as 2,650kg/m^3 (Nedderman, 1992). The voids ratio is related to the voids fraction by:

$$e=\frac{\varepsilon}{1+\varepsilon} \tag{6.6}$$

These two states of the material are assumed to exist at some pressure. The initial pressure corresponding to e_0 and the initial value of γ is taken as the same as that used in the porous elastic model (0.01kPa). The final pressure is taken as the asymptotic value calculated from equation 6.3 which for this material is 27.8kPa. Given this information and the assumption that in the semi-logarithmic diagram the points are joined by a straight line, the diagram can be drawn. The gradient of the line between the two points gives the value of logarithmic bulk modulus. Table 6.5 shows the information used in the above figure and the calculated value of λ.

	Bulk density (kg/m3)	**Voids ratio (e)**	**Pressure (kPa)**	**λ**
Initial state	1,576	0.681	0.01	0.0044
Final (Janssen) state	1,610	0.646	27.8	

Table 6.5 - Calculation of λ from initial and final densities

It can now be seen that any comparison between the finite element results and a Janssen distribution must use the final value of bulk density in the Janssen calculations as opposed to the original value which was an average of the three values given in table 6.1. Figure 6.9 shows the finite element results using the newly determined properties, as well as the appropriate Janssen calculation.

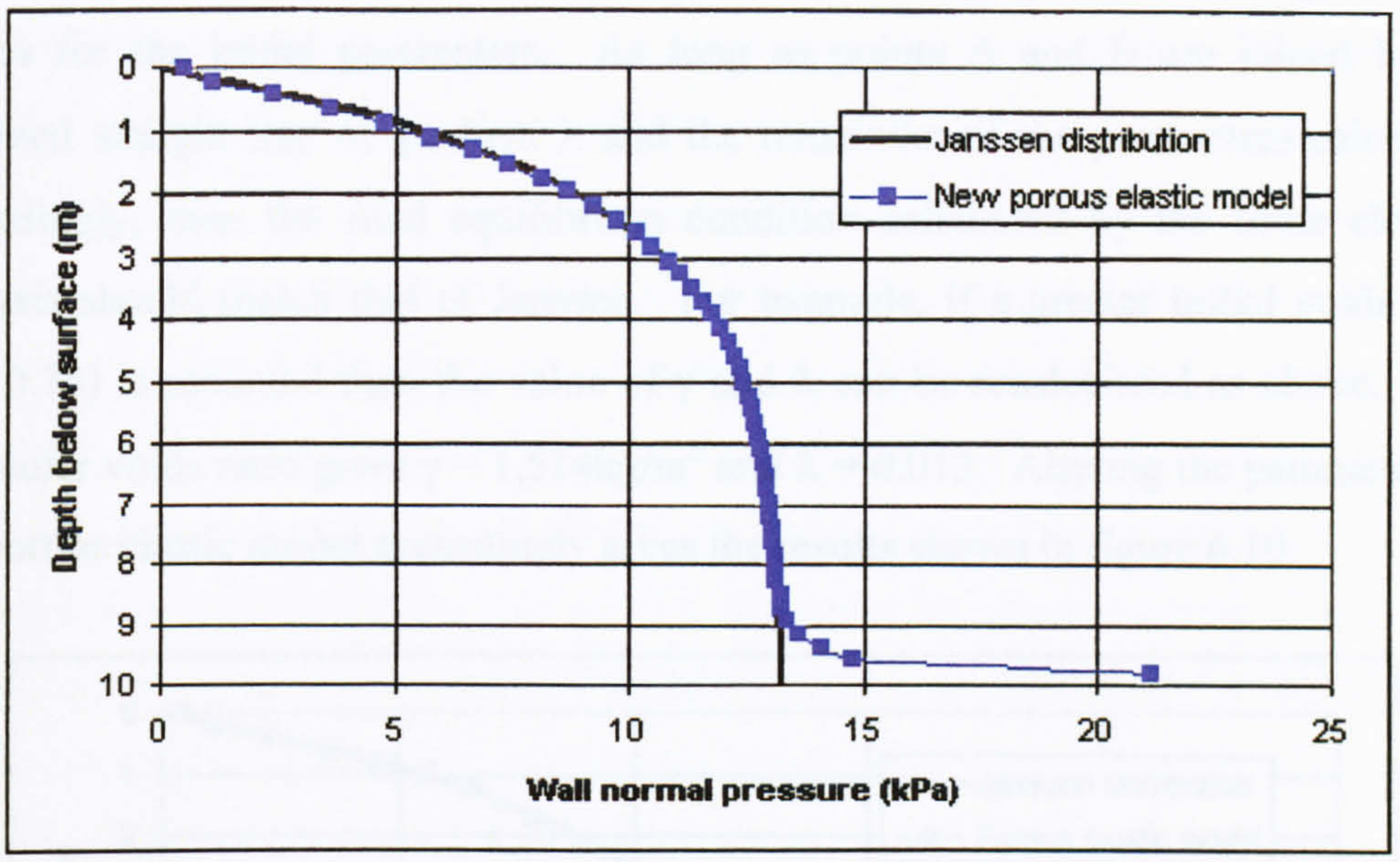

Figure 6.9 - Finite element results as determined by the recalibrated porous elastic model

This model now shows agreement between the results and the Janssen model comparable to the agreement between the linear elastic model and Janssen. Again there are noticeable end effects and the finite element results do not extend to a full depth of 10m. This effect is due to compression of the stored material as the gravity load is applied. This highlights a disadvantage in the gravity method of loading in that if this occurs no more material can be added to the silo model (if required). This would be possible in a progressive fill model. This phenomenon would only be a significant problem if the granular material modelled was very compressible, in which case after gravity was applied the silo may end up not completely full. The materials modelled here are not in that order of compressibility so the small change in volume is not cause for concern but should be taken as a limitation of this simple model.

In figure 6.8 only point B is fixed by the equilibrium conditions imposed by calibration against the Janssen equation. This is because the Janssen theory assumes a single value of bulk density and therefore for a given silo, equation 6.3 gives the value of the maximum vertical pressure. This pressure along with equations 6.5 and 6.6, which gives the voids ratio at that density, fixes point B on the graph by utilising equation 6.4. Point A however, can be moved on the graph by assuming different values for the initial parameters. As long as points A and B are joined by the assumed straight line of gradient λ and the remainder of the parameters calculated accordingly, then the final equilibrium condition calculated by the finite element analysis should match that of Janssen. For example, if a greater initial voids ratio (say 0.75) is assumed then the value of γ and λ can be recalculated as above. This particular voids ratio gives $\gamma = 1{,}514 kg/m^3$ and $\lambda = 0.013$. Altering the parameters of the porous elastic model accordingly gives the results shown in figure 6.10.

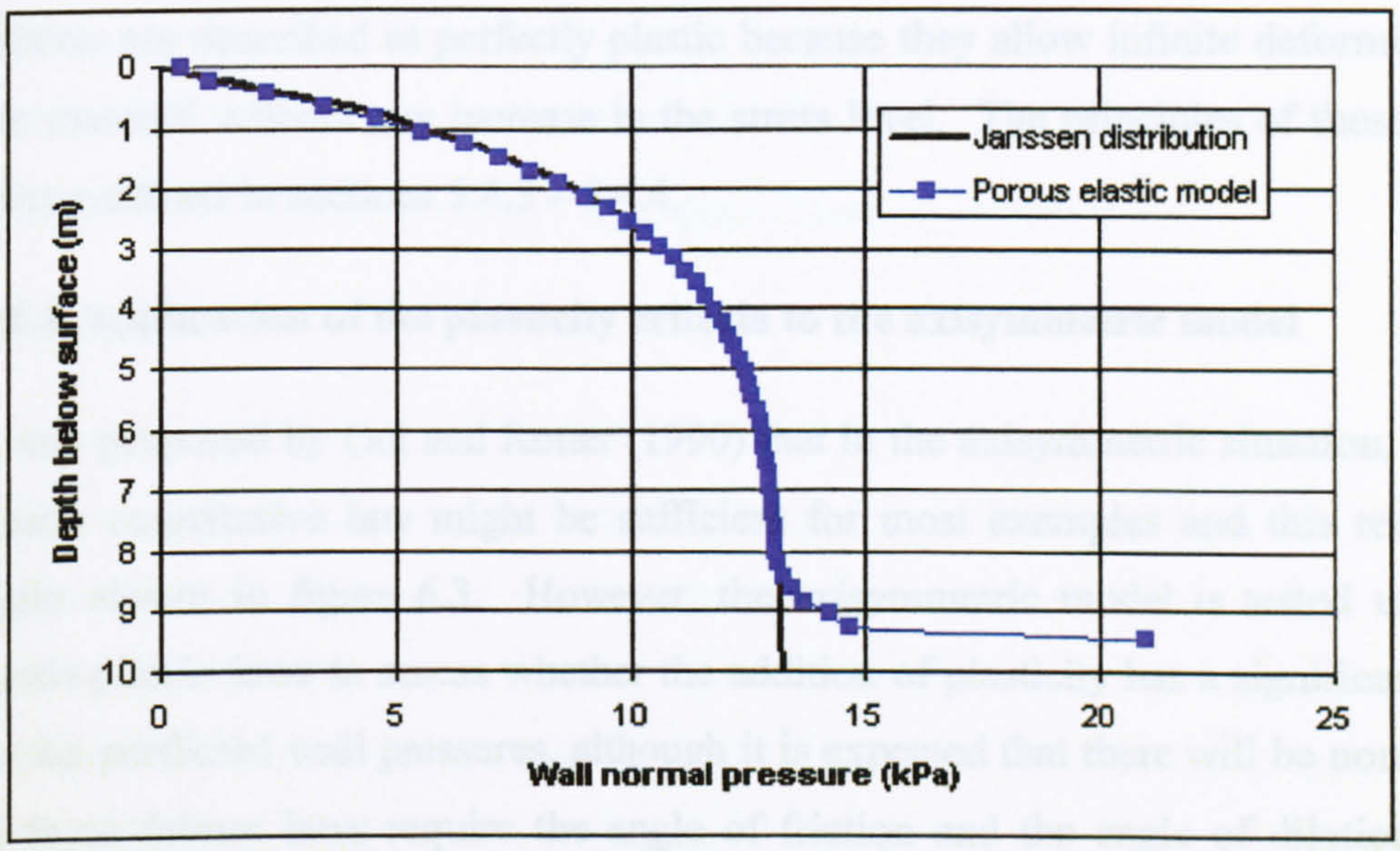

Figure 6.10 - The effect of using different initial conditions in the porous elastic model

Again the agreement between the results is good but the overall compressibility, exhibited by volume change, has been altered. These results have been calculated using an entirely different set of material parameters. It may therefore be argued that the value of λ that was initially calculated may be incorrect. The value of λ was determined from values of density taken from Lahlouh *et al* (1995) but there is no

way of confirming these results or ascertaining how the values where calculated or derived. However, those values give results that compare very well with the theoretical Janssen distribution and are accepted as a representation of the material for future constitutive models of sand.

6.5 Elastic-plastic models

In examining constitutive laws suitable for use in a three-dimensional model where large strains may occur, the ensiled material is very likely to undergo inelastic deformations. Therefore a failure criterion is required. A failure criterion defines the level of stress at which the material's behaviour changes from elastic to inelastic. The Mohr-Coulomb and the Drucker-Prager (1952) criteria are two commonly used plasticity criteria. These may be combined with elastic laws to provide a full elasto-plastic model that will be capable of modelling the granular material's behaviour in large strain situations (as well as still incorporating small strains). Both of these criteria are described as perfectly plastic because they allow infinite deformations of the material without any increase in the stress level. The principles of these criteria were outlined in sections 5.4.3 – 5.4.4.

6.5.1 Application of the plasticity criteria to the axisymmetric model

It was proposed by Ooi and Rotter (1990) that in the axisymmetric situation, a solely elastic constitutive law might be sufficient for most examples and this result was again shown in figure 6.3. However, the axisymmetric model is tested using the elasto-plastic laws to assess whether the addition of plasticity has a significant effect on the predicted wall pressures, although it is expected that there will be none. Both of these failure laws require the angle of friction and the angle of dilation of the material to be defined. The dilation angle is assumed to be 0° as set out in section 5.4.3.1 and the angle of friction is taken to be 35.4°. However this value only relates to the angle of friction used by the Mohr-Coulomb model as it was determined from a shear box test. In order to use the Drucker-Prager model the Mohr-Coulomb data must be reinterpreted so that the response of both models is matched. There are two options for performing this conversion. One is to match the failure definition in

triaxial compression and tension. However the ABAQUS manual (2001) only recommends this approach for materials with low values of internal friction.

The second approach is to match the plane strain response of the two models. It may be argued that for any subsequent three-dimensional analysis this plane strain assumption could be invalid but this matching procedure has been used before for similar problems (Holst *et al*, 1996) and produced results comparable to theoretical methods. In the case of non-dilatant flow (ψ=0°) the Drucker-Prager angle of internal friction is given by:

$$\tan\beta = \sqrt{3}\sin\phi \tag{6.7}$$

Where β is the Drucker-Prager angle of internal friction. The initial yield stress of the material is given by:

$$\sigma_c^0 = \frac{1}{1-\frac{1}{3}\tan\beta} d \tag{6.8}$$

Where d is a parameter related to the Mohr-Coulomb cohesion c by:

$$\frac{d}{c} = \sqrt{3}\cos\phi \tag{6.9}$$

For the sand this gives values of 46.1° for the internal angle and 0 for the initial yield stress (because it is assumed that c = 0, the material is cohesionless). In practice a small value (0.25kPa) is assumed for the value of σ^0_c in order to maintain numerical stability. This value is not critical in the axisymmetric analysis due to the very small amount of plastic strain in these models. Later testing in three-dimensional models further shows that for small values of σ^0_c, the effect on wall pressures is negligible.

Figure 6.11 shows the results in the axisymmetric bin of the three elasto-plastic constitutive laws (LE-MC, LE-DP and PE-DP) for sand.

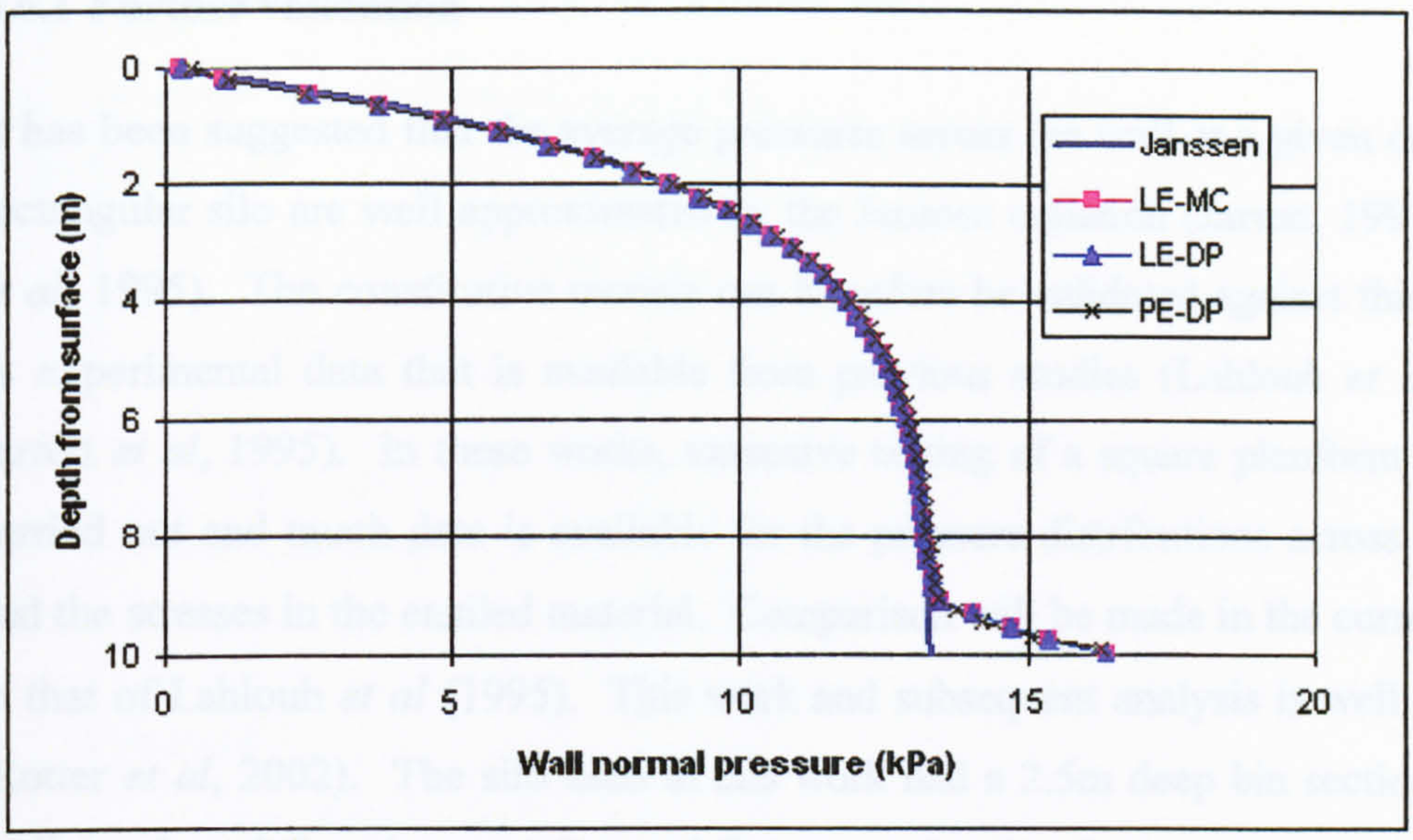

Figure 6.11 - The effect on wall normal pressures of using elasto-plastic constitutive laws in an axisymmetric model

As predicted the results show that the use of a failure model in this type of problem is unnecessary, as pressures predicted are identical to those predicted by the simpler elastic models. This however does not mean that a failure model will not be required for other types of simulation (notably three-dimensional simulation).

6.6 Three Dimensional models

In order to predict the wall pressures in rectangular or square silos a three-dimensional model is required. A two-dimensional model could be used to make simple predictions about the pressures down the wall, as with the axisymmetric cases described above, but it is known that in rectangular silos there is a non-uniform pressure distribution across the wall at any constant depth (Jarrett *et al*, 1995). It is important to be able to predict this phenomenon for design use and consequently only a three-dimensional model will suffice. Three-dimensional modelling of this problem is rare because of the need for silo research towards more commonly used circular plan-form structures where (as shown above) the assumption of axisymmetry is valid. Methods used by codes in the treatment of three-dimensional problems were given in section 3.3.2.

6.6.1 Further validation

It has been suggested that the average pressures across the wall at a given depth in a rectangular silo are well approximated by the Janssen equation (Jarrett, 1991; Jarrett *et al*, 1995). The constitutive models can therefore be validated against this as well as experimental data that is available from previous studies (Lahlouh *et al*, 1995; Jarrett *et al*, 1995). In these works, extensive testing of a square planform silo was carried out and much data is available for the pressure distributions across the wall and the stresses in the ensiled material. Comparison will be made in the current work to that of Lahlouh *et al* (1995). This work and subsequent analysis is well reported (Rotter *et al*, 2002). The silo used in this work had a 2.5m deep bin section with a shallow, funnel flow hopper. It was 1.5m square in plan-form and is constructed of 6mm thick steel plate. At this size the silo could almost be classified as squat (h/d = 1.667). Figure 6.12 shows the layout of this rig.

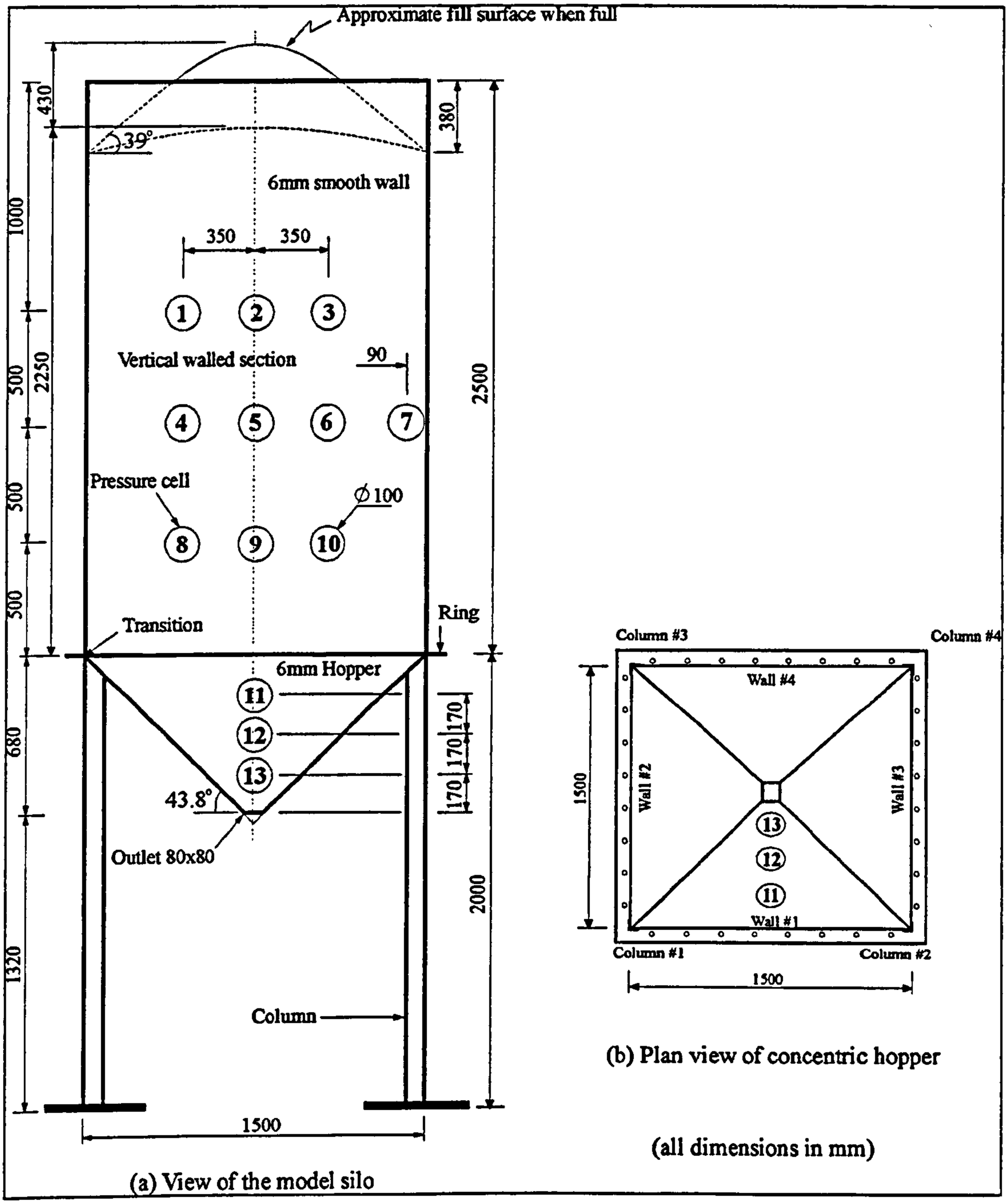

Figure 6.12 - Schematic showing the layout of the experimental rig used by Lahlouh *et al* (1995)

The finite element model of the experimental rig uses 4-noded quadrilateral shell elements to model the bin, and 8-noded brick solid elements to model the ensiled material. Higher order elements could have been selected but it was anticipated that the final model could become very large and hence computational resources may have become strained. Advantage is taken of the symmetry of the bin and hence only

one quarter of the silo is modelled. It is supported at the corner to simulate the columns but they are not themselves modelled. The corners of the wall were welded in the original experiment with no additional support and this condition is reproduced in the finite element model. The experimental rig featured a ring beam that, for simplicity, is not modelled here. As in the axisymmetric case the walls are modelled as frictional with the Coulomb friction model. Figure 6.13 shows the finite element mesh. Appendix B shows the method used to determine the number of elements used in this mesh.

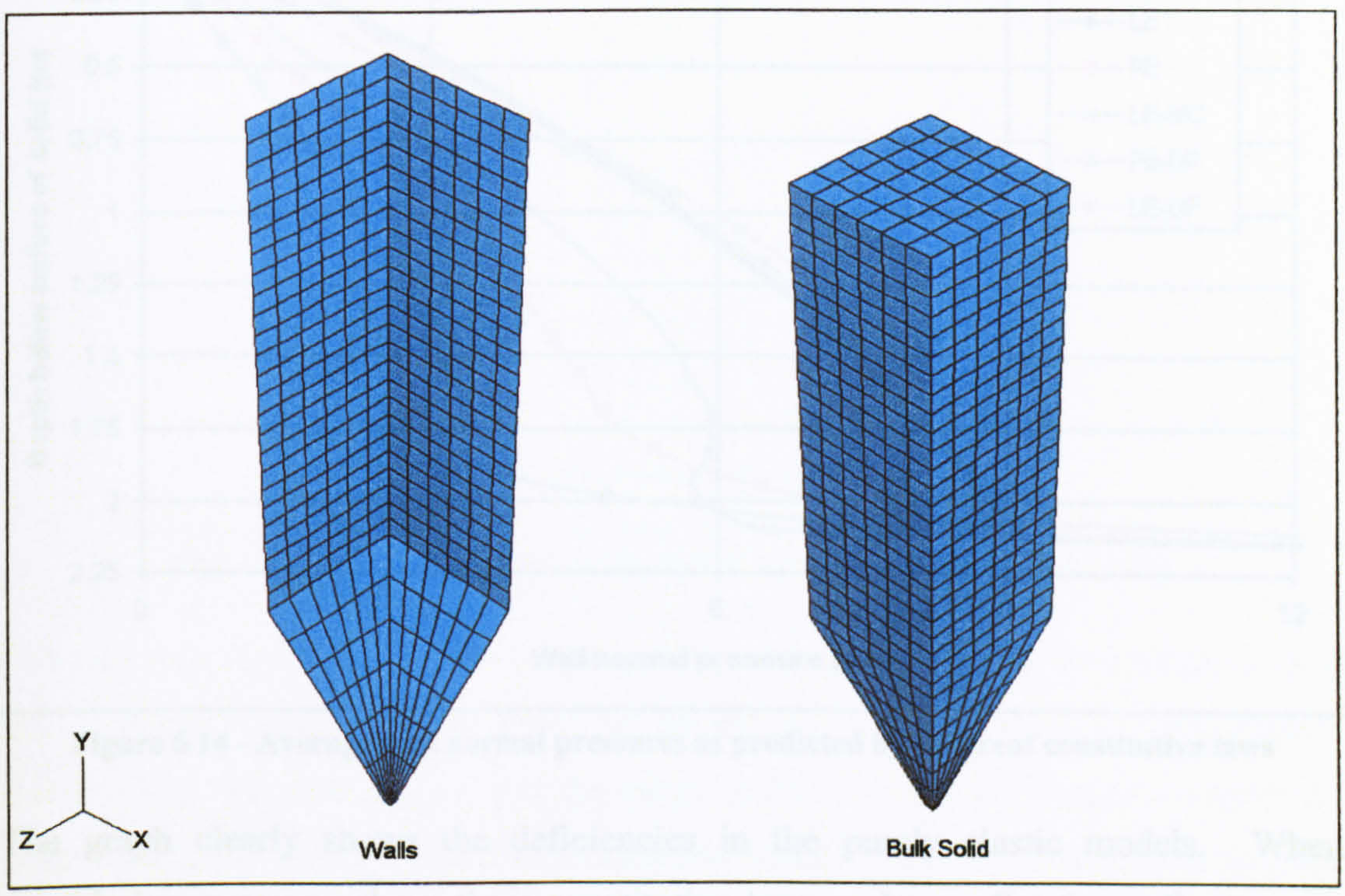

Figure 6.13 - Finite element model of Lahlouh *et al*'s (1995) geometry

The finite element model does not initially take account of any conical surcharge upon the surface of the fill that may have been evident in the experiment. Appendix C shows a typical input dataset for this model and Appendix D shows some sample output in the form of contour plots.

6.6.2 Comparison with Janssen pressure distribution

Figure 6.14 shows the average (integrated) wall normal pressure as determined from each of the five constitutive models. The appropriate Janssen curve is also shown. Integration of the finite element results was carried out using Simpson's rule at each level in the silo to produce the average pressure acting at that level.

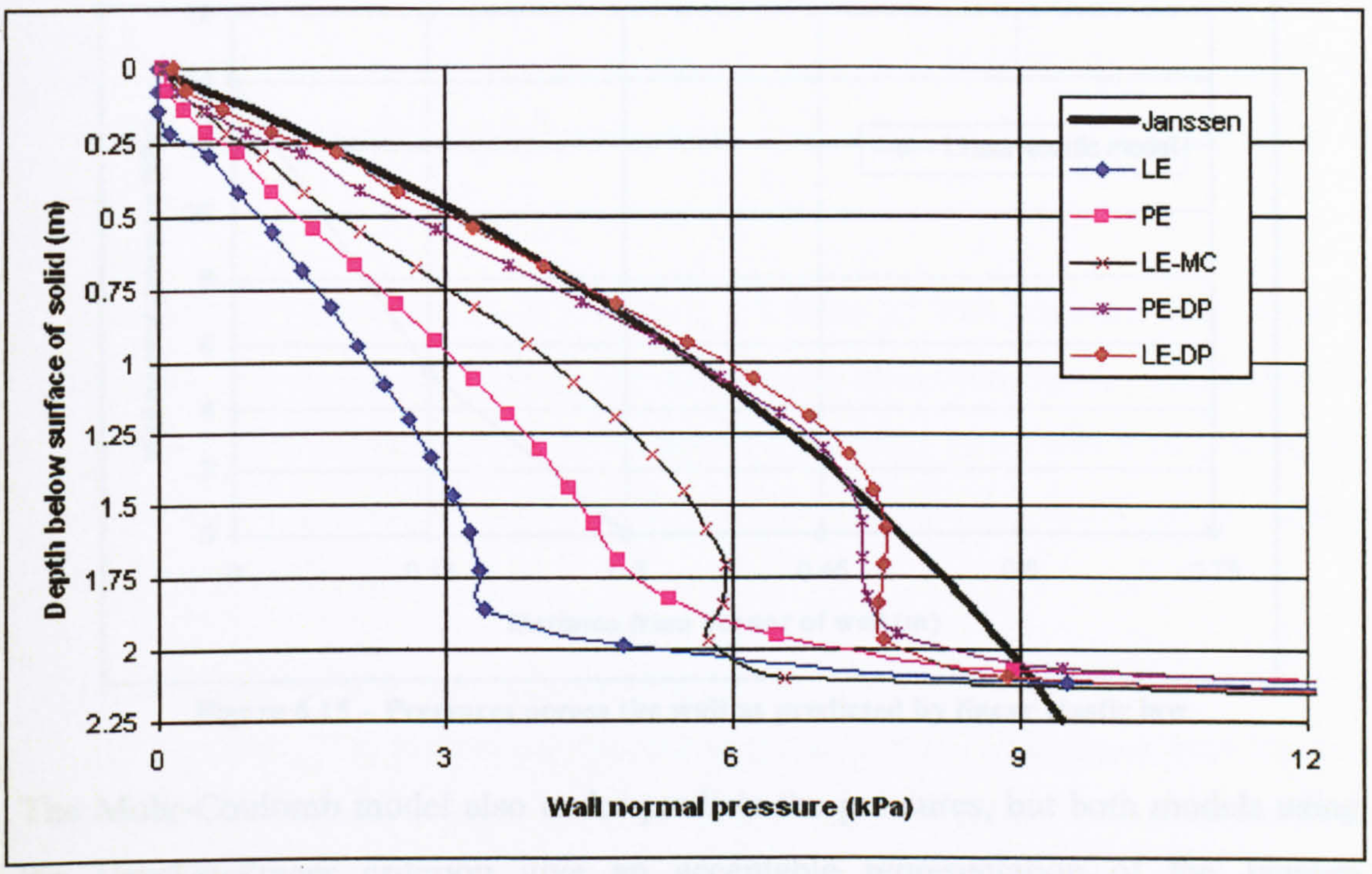

Figure 6.14 - Average wall normal pressures as predicted by different constitutive laws

The graph clearly shows the deficiencies in the purely elastic models. When considering average values, these constitutive laws under-predict the wall pressures in the three-dimensional model when compared to the Janssen distribution. This inaccuracy is caused by the large deformations that occur in the modelled granular bulk solid. These give rise to large strains in the ensiled material which simple elastic laws are not capable of modelling correctly. Inspection of the wall pressures and deformations shows that both of the elastic models support most of the lateral load near the corners of the walls. The high lateral load causes the flexible wall to deform outwards but the shear strength of the ensiled material means it is incapable of following this deformation. The final situation is that the stored material loses

contact with the silo wall at the centre and hence pressures are zero across a large percentage of the wall. This is obviously a poor representation of the actions occurring in a real silo. Figure 6.15 shows the pressure across the wall at mid-height as calculated by the linear elastic law. It is clear that the load is entirely supported near the corner of the silo walls.

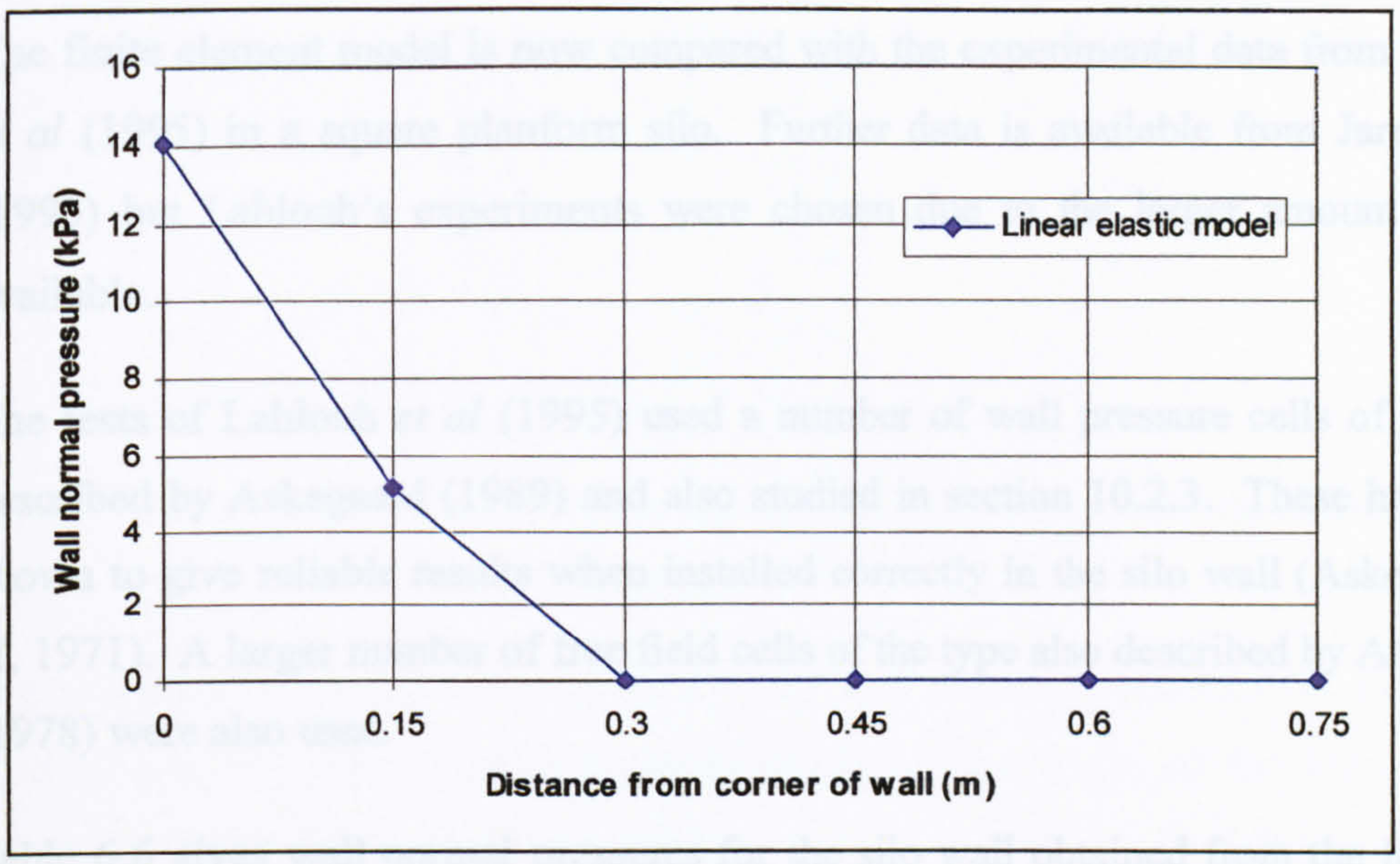

Figure 6.15 – Pressures across the wall as predicted by linear elastic law

The Mohr-Coulomb model also under-predicts the pressures, but both models using the Drucker-Prager criterion give an acceptable representation of the Janssen distribution. The assumption may therefore be that the Drucker-Prager criterion is a better model for use in silo problems than the Mohr-Coulomb. This may be because the Mohr-Coulomb criterion does not take into account the intermediate principal stress whereas the Drucker-Prager model does. Experiments have shown that the intermediate principal stress does have an effect on the failure of a soil (Lee, 1970).

For the remainder of the project the suitable choice of constitutive law would appear to be restricted to either the LE-DP model or the PE-DP model. The porous elastic based model was chosen because it uses input parameters that can be obtained from tests routinely performed on granular bulk solids. If the LE-DP law were chosen then it would be necessary to determine a suitable value of Young's modulus. This value is difficult to determine directly from the material and would inevitably be an

extrapolation from other test data. Using the PE-DP law allows the modelling of a wide range of materials, that if treated as linear elastic, may appear almost identical whereas in fact there are small differences in (for example) voids ratio that could have a large effect on the final material behaviour.

6.6.3 Comparison with experimental sand data

The finite element model is now compared with the experimental data from Lahlouh *et al* (1995) in a square planform silo. Further data is available from Jarrett *et al* (1995) but Lahlouh's experiments were chosen due to the larger amount of data available.

The tests of Lahlouh *et al* (1995) used a number of wall pressure cells of the type described by Askegaard (1989) and also studied in section 10.2.3. These have been shown to give reliable results when installed correctly in the silo wall (Askegaard *et al*, 1971). A larger number of free field cells of the type also described by Askegaard (1978) were also used.

Table 6.6 gives wall normal pressures for the silo wall obtained from the free field cells in sand. The vertical component is given in terms of distance from the top of the silo and it is noted that the point of first contact on the wall is approximately 0.3m below the top of the silo and therefore the actual depth below the surface of the sand is approximately 0.3m less than the values given.

Depth below top of silo (m)	Distance from corner of bin (m)			
	0.05	0.20	0.40	0.75
0.50	2.0	2.9	3.3	2.8
0.75	8.1	5.9	4.6	2.8
1.00	11.5	6.0	4.6	4.0
1.25	16.1	7.2	5.2	4.0
1.50	18.0	7.7	4.7	5.4
1.75	23.0	10.2	6.5	6.2
2.00	20.0	8.4	6.3	6.3
2.25	24.7	14.4	7.4	5.1
2.50	19.3	21.8	16.1	13.0

Table 6.6 - Wall normal pressures (in kPa) in the experimental silo from free field cells in sand (Lahlouh *et al*, 1995)

Figure 6.16 shows the comparison of the average wall normal pressures from the free field cells and from the finite element model down the depth of the bin. The appropriate Janssen distribution is also shown.

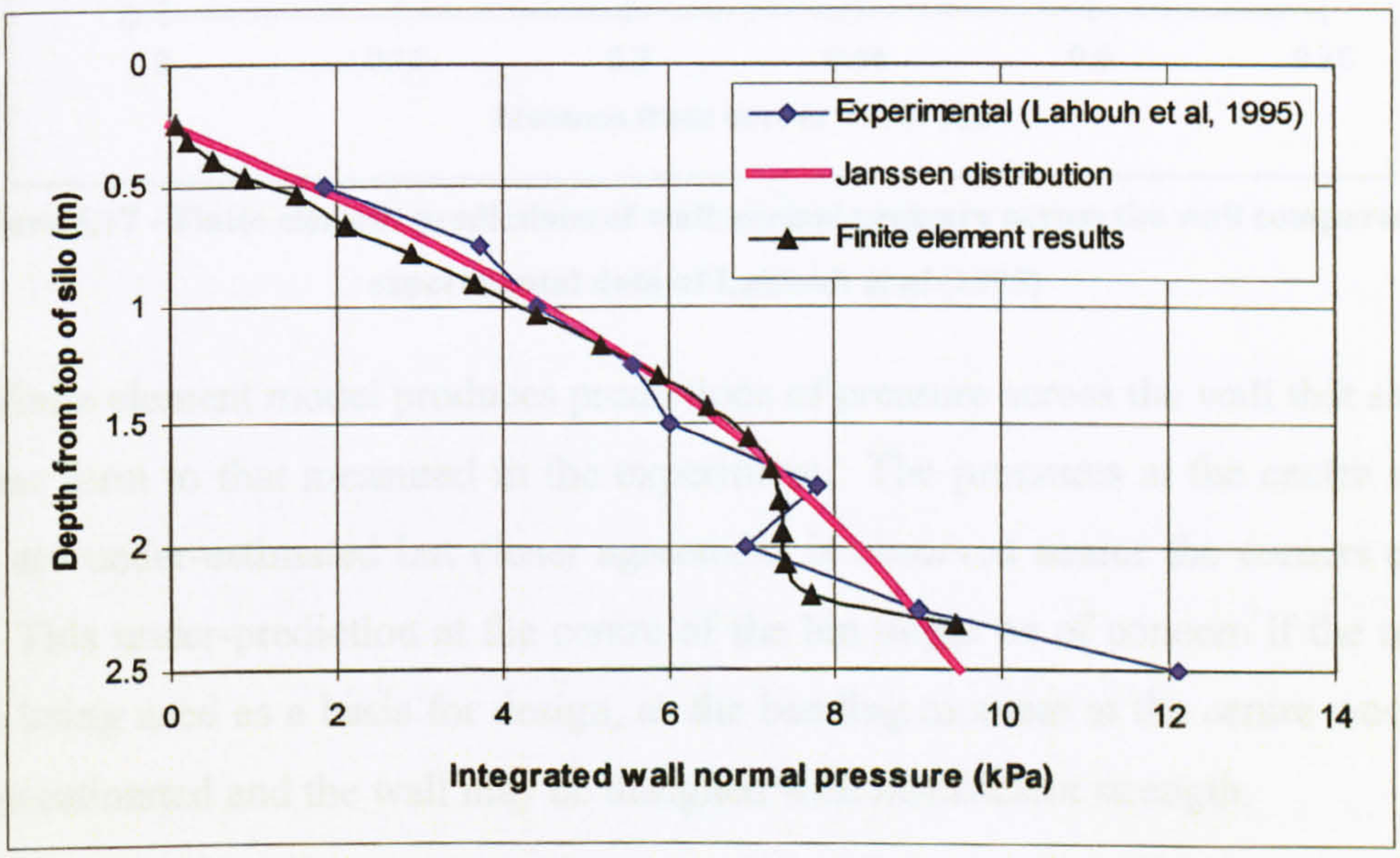

Figure 6.16 - Integrated experimental (Lahlouh *et al*, 1995) and finite element wall normal pressures compared to Janssen distribution for sand

The experimental and finite element results closely follow the Janssen distribution, but this however gives no information about the distribution of the normal pressures across the wall.

The measured wall normal pressures were of a non-uniform distribution. The experimental distribution is therefore compared with data obtained from the finite element model. Figure 6.17 shows the pressure distribution across the wall in the experiment at two levels and the corresponding predictions from the finite element model using a PE-DP constitutive law.

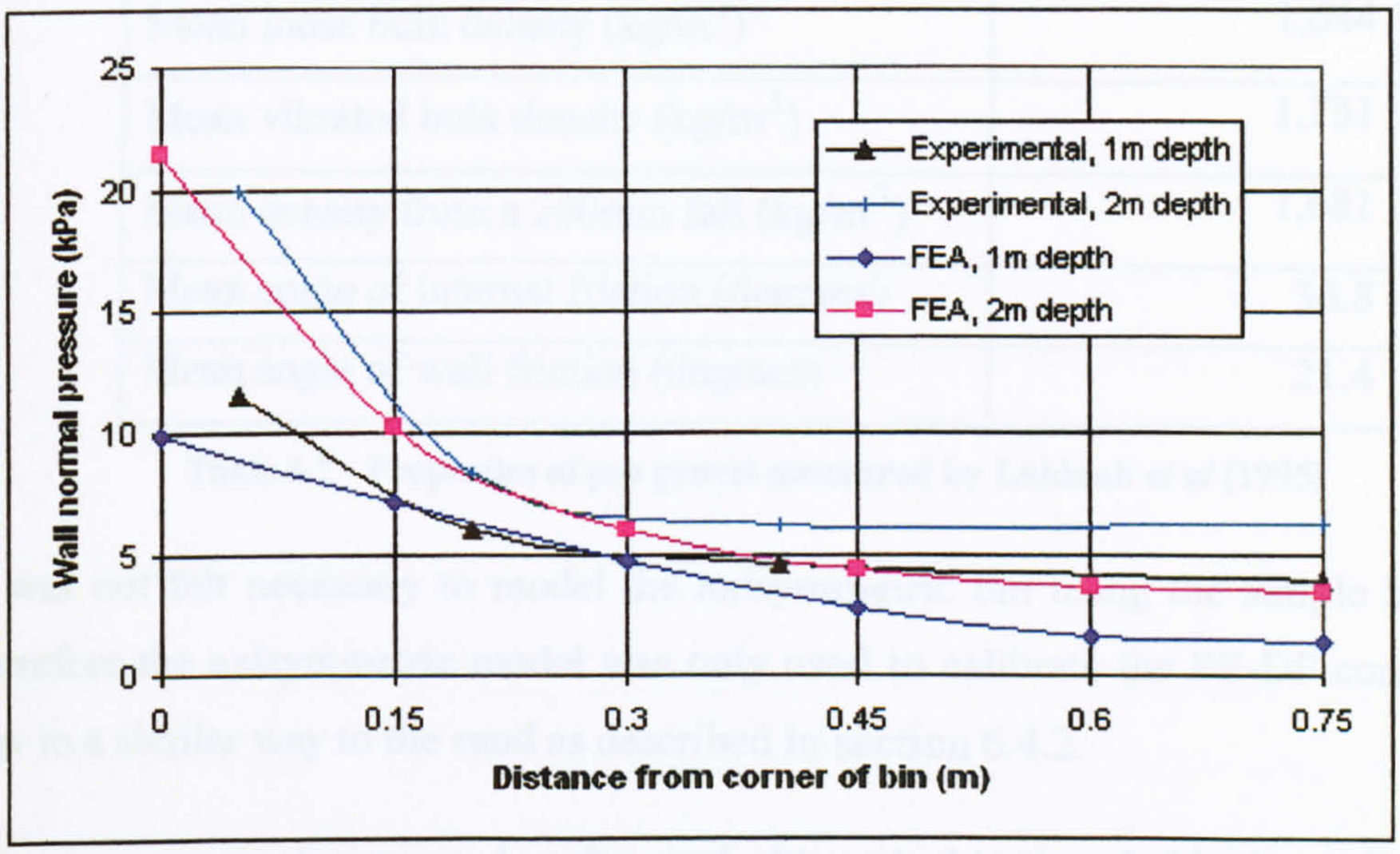

Figure 6.17 - Finite element predictions of wall normal pressure across the wall compared to experimental data of Lahlouh *et al* (1995)

The finite element model produces predictions of pressure across the wall that show a similar form to that measured in the experiment. The pressures at the centre of the wall are under-estimated but closer agreement is observed nearer the corners of the bin. This under-prediction at the centre of the bin might be of concern if the results were being used as a basis for design, as the bending moment at the centre would be under-estimated and the wall may be designed with insufficient strength.

6.6.4 Modelling of pea gravel

As well as using Leighton Buzzard sand, Lahlouh *et al* (1995) performed tests using a pea gravel. This was chosen as it had many similar measured properties to the sand but the particle size of the material was larger. Leighton Buzzard sand has a mean particle size of 0.53mm and the pea gravel has a mean particle size of 2.55mm. Other properties as measured by Lahlouh *et al* (1995) are shown in table 6.7.

Property	
Mean particle diameter (mm)	2.55
Mean loose bulk density (kg/m^3)	1,644
Mean vibrated bulk density (kg/m^3)	1,731
Mean density from a 200mm fall (kg/m^3)	1,681
Mean angle of internal friction (degrees)	36.8
Mean angle of wall friction (degrees)	21.4

Table 6.7 - Properties of pea gravel measured by Lahlouh *et al* (1995)

It was not felt necessary to model the axisymmetric bin using the simple laws and therefore the axisymmetric model was only used to calibrate the PE-DP constitutive law in a similar way to the sand as described in section 6.4.2.

The same approach was used as for sand although this time Lahlouh *et al*'s (1995) equilibrium checks showed that the gravel assumes a more dense state when placed into the bin. Therefore in this case the starting and final bulk densities are taken as the loose and vibrated values respectively. Equations 6.3 – 6.6 are again used and give an initial voids ratio of 0.61 and a logarithmic bulk modulus of 0.0098. This implies that the gravel is more compressible over the small pressure range that is being assumed here. Later testing showed this to be correct (section 6.7)

This data is again used in the axisymmetric model to validate against the Janssen distribution and the results are shown in figure 6.18.

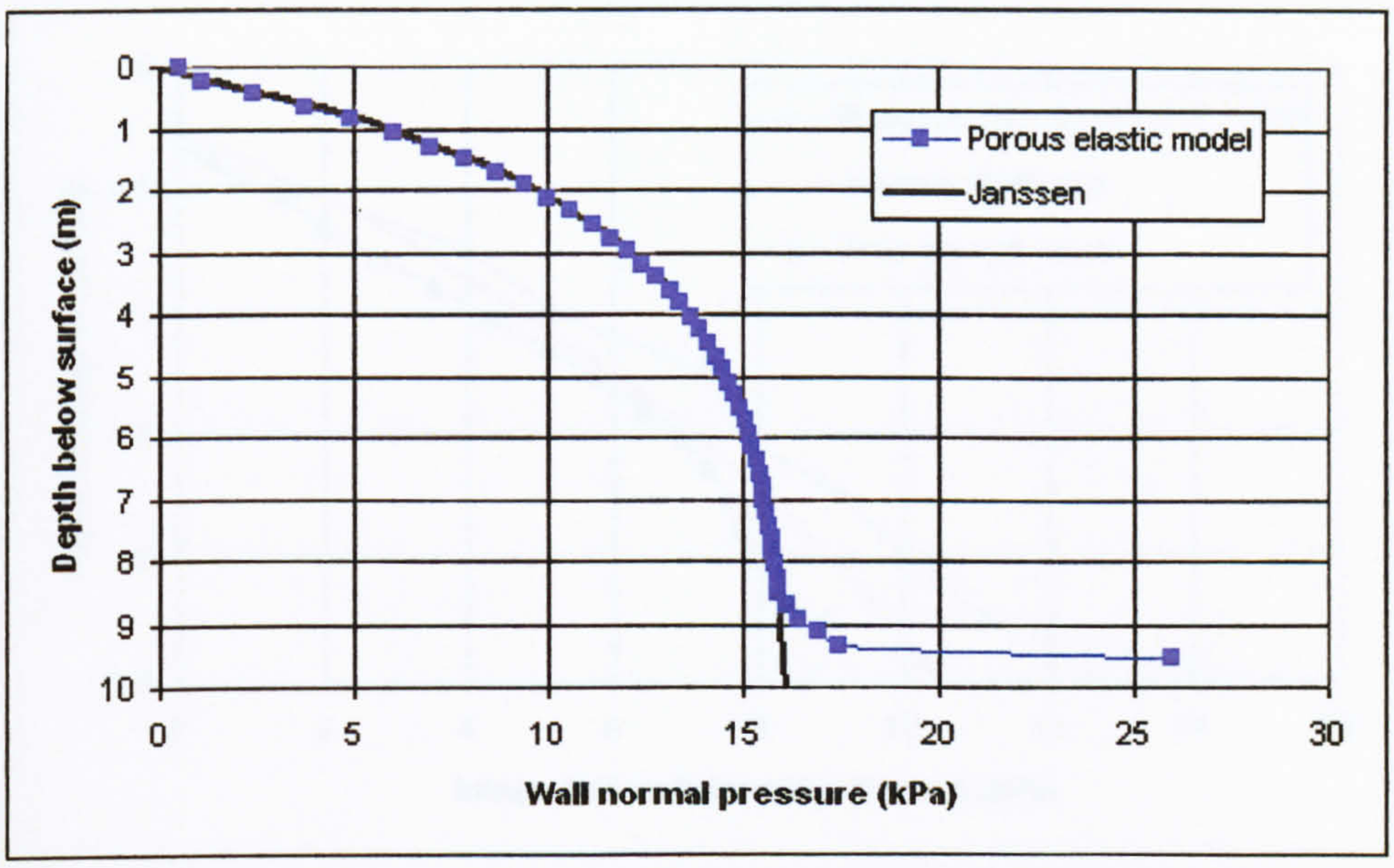

Figure 6.18 - Comparison between Janssen and FEA results for pea gravel

Again, the results show the same high level of corroboration across the majority of the bin as the sand model. A higher level of compression is observed as a result of the higher value for λ.

6.6.5 Comparison to Lahlouh *et al*'s (1995) experimental data

The values for the gravel model obtained above are used in the geometry of Lahlouh *et al*'s (1995) work. As with the Leighton Buzzard sand experimental data is available from wall pressure cells and free field cells. The results from the finite element analysis compared to the average experimental data taken from free field cells and the Janssen distribution are shown in figure 6.19.

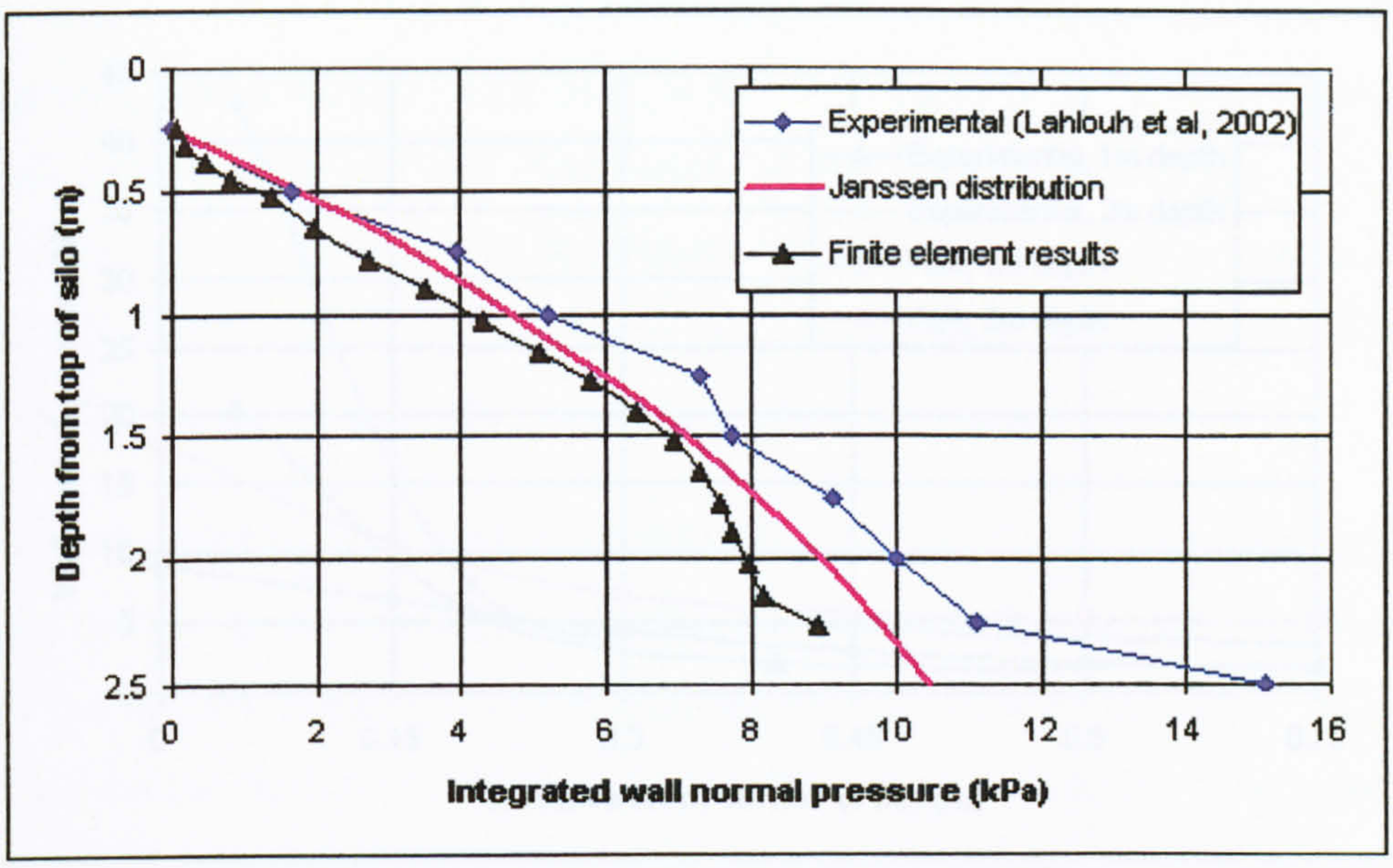

Figure 6.19 - Integrated experimental and finite element wall normal pressures compared to Janssen distribution for gravel

Again, the results from the experiment and the finite element model are of the form of the Janssen distribution although the values obtained from the experiment are systematically higher than those given by the Janssen distribution and the finite element method. This may be due to the fact that a smaller number of tests were performed by Lahlouh *et al* (1995) with the pea gravel and thus there were less data for this material. There is also the possibility that due to the larger grain size present in the pea gravel, the results obtained from the free field cells could be adversely affected. For the free field cells to operate correctly there must be good contact between the cell and the medium. In the case of the pea gravel the relative cell face to particle size between the medium and the cell is quite large and it is possible that this could lead to irregular contact which in turn might affect the observed pressure on the cell. However, $d_{agg}/d_{cell} < 1/30$ which should minimise any possible effects of this type.

There is data available for the distribution of pressure across the wall and this can again be compared with the finite element analysis as shown in figure 6.20.

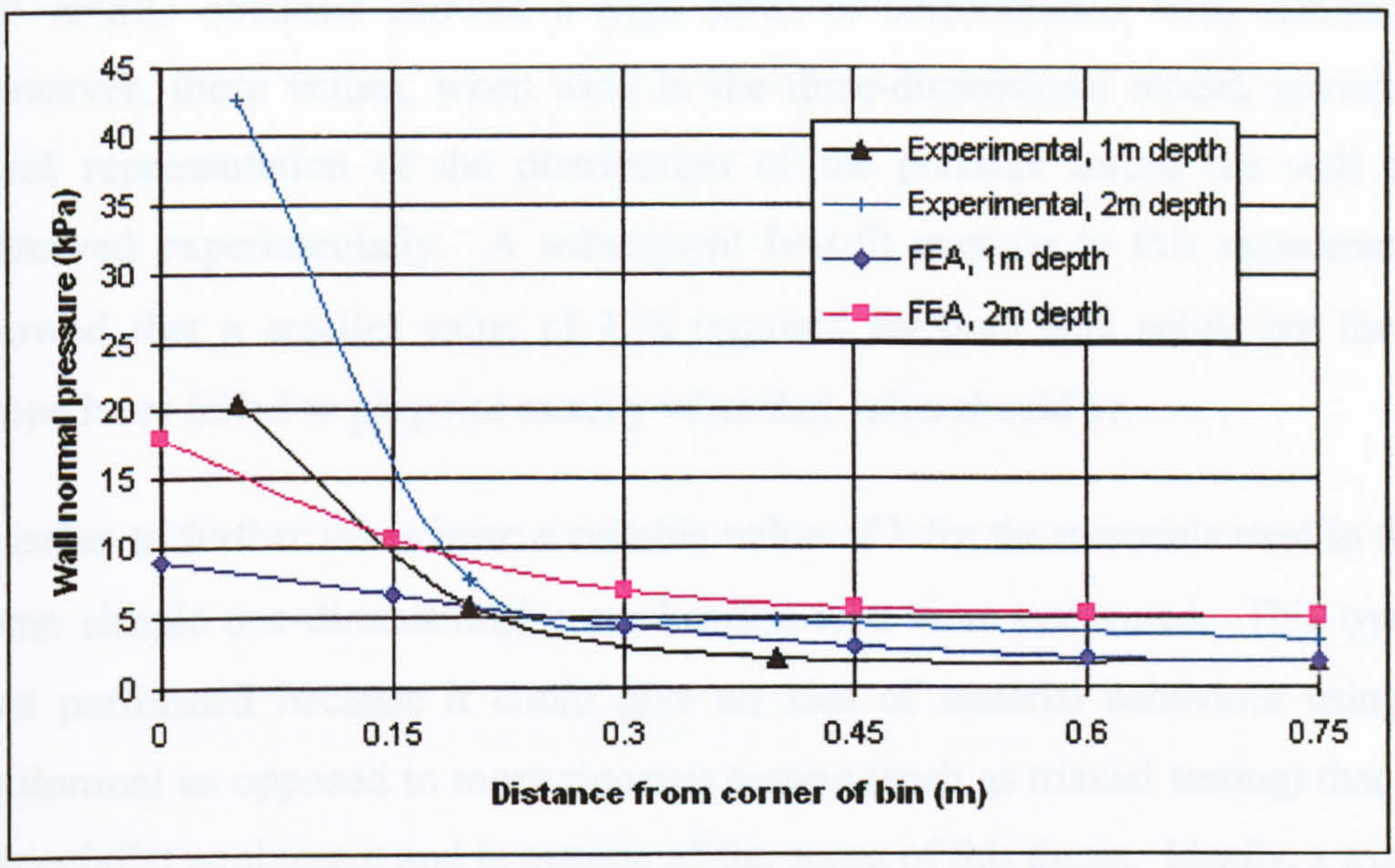

Figure 6.20 - Finite element predictions of wall normal pressure across the wall

In this material the prediction of the pressure across the wall compared to the experimental data is relatively poor. However, the corroboration would appear better towards the centre of the bin.

6.6.6 Best fit of finite element results to experimental data

In order to further investigate the effect of the value of λ on the wall pressure predictions a best fit exercise was carried out. λ was varied in the sand and the gravel models and a least-squares fit between the finite element results and the experimentally obtained values performed. This data can be found in Appendix E. It was only possible to conclude from this exercise that the value of λ required to best fit the experimentally observed distributions of wall pressure needs to be a small value.

6.7 One-dimensional consolidation tests on the two granular bulk solids

The finite element analysis has shown that the selection of the value of logarithmic bulk modulus is critical to the output from the finite element model. Initially, values were derived from literature and these gave predictions that did not agree well with the Janssen theory. Secondly, values were calculated from density measurements and

the results obtained showed a high level of corroboration with Janssen theory. However, these values, when used in the three-dimensional model, provided a not ideal representation of the distribution of the pressure across the wall that was observed experimentally. A subsequent best-fit exercise to this experimental data showed that a smaller value of λ is required for both bulk solids but the various procedures failed to pinpoint exactly what that value should be.

In order to further investigate a suitable value of λ for the materials used in this work some simple one-dimensional consolidation tests were performed. This type of test was performed because it could give an idea of material behaviour using simple equipment as opposed to more rigorous testing (such as triaxial testing) that requires a specialist equipment and is outside of the scope of this thesis. Ideally, a triaxial test would have been performed. This would give a more complete picture of the materials behaviour and could have been performed at the low pressure levels that this work deals with (conventional triaxial tests usually subject the specimen to very high pressures).

The one-dimensional tests are performed by placing the granular bulk solid in a cylindrical cell and then using a stiff platen to apply a pressure. By monitoring the displacement of the platen the axial strain can be related to the pressure level in the solid. Care must be taken when placing the solid in the cell in order to avoid consolidation before the test is started This also includes knocking the cell in any way as this will cause the sample to settle. Figure 6.21 shows the arrangement. The size of the cell was chosen to be long enough to ensure that end-effects were not significant and the diameter large enough to ensure that the wall friction had as little effect as possible. The overall height of the cell was 300mm and the internal diameter, 140mm.

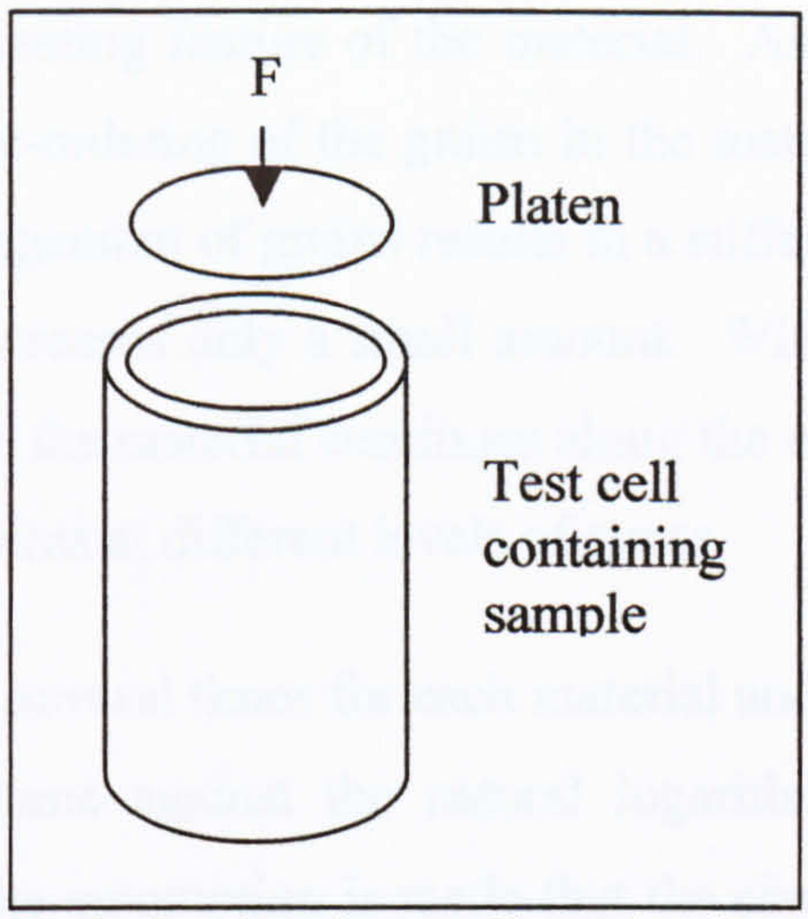

Figure 6.21 – Schematic showing the one-dimensional consolidation test cell

The tests were performed in a Series 8500 Instron. The maximum force applied to the platen was 200N which equates to a pressure level of approximately 15kPa. This was chosen as representative of the pressure level that would be experienced in a small rectangular silo.

Figure 6.22 shows the raw data for one of the tests with Leighton Buzzard sand. The displacement of the platen has been converted to axial strain (given knowledge of the fill level in the cell) and is plotted against the direct pressure applied.

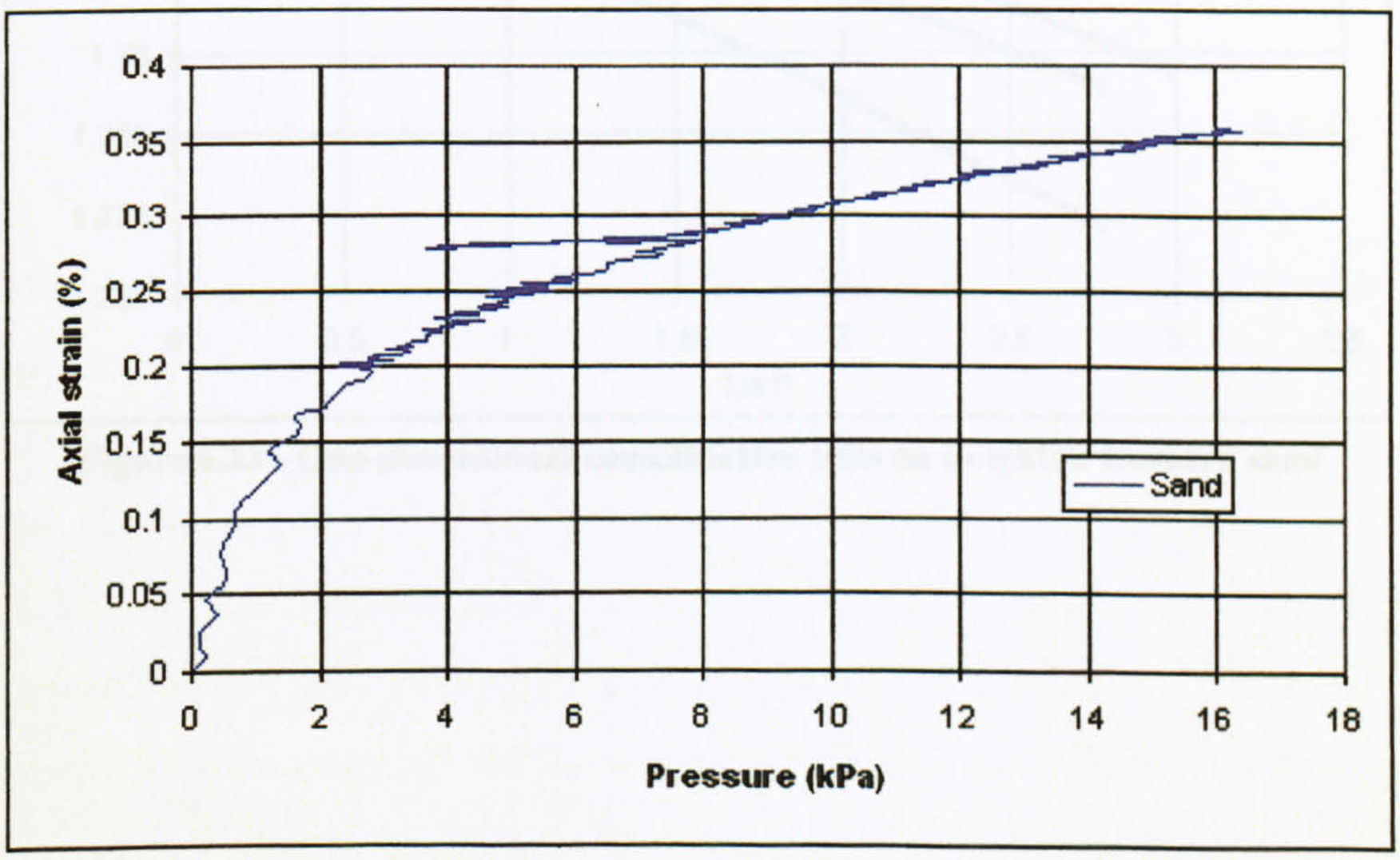

Figure 6.22 - One-dimensional consolidation of sand

The graph shows an interesting feature of the material. As the pressure approaches 8kPa there is a possible re-ordering of the grains in the material causing the pressure to reduce. This new arrangement of grains results in a stiffer material and as the load is re-applied the strain increases only a small amount. When 8kPa is again reached and exceeded the strain in the material continues along the original path. Subsequent tests revealed similar patterns at different levels of stress.

The tests were performed several times for each material and the results interpreted to show the change in volume against the natural logarithm of the pressure using equations 6.4 to 6.6. If the assumption is made that the change in volume is entirely due to change in voids ratio then these results can be used to determine the value of λ relevant to each material. Figure 6.23 shows the plots for the sand while figure 6.24 shows the plots for the gravel.

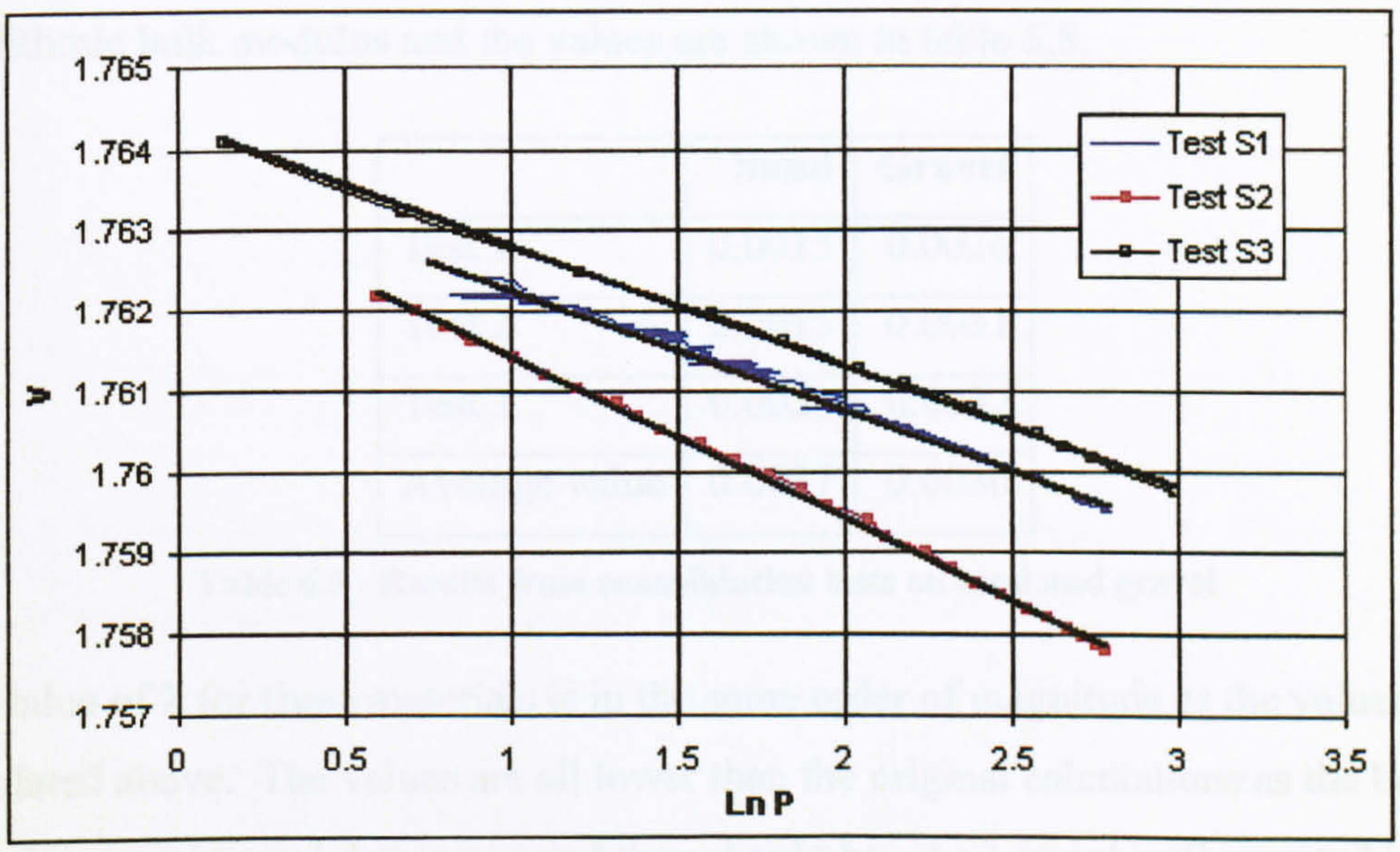

Figure 6.23 - One-dimensional consolidation tests on Leighton Buzzard sand

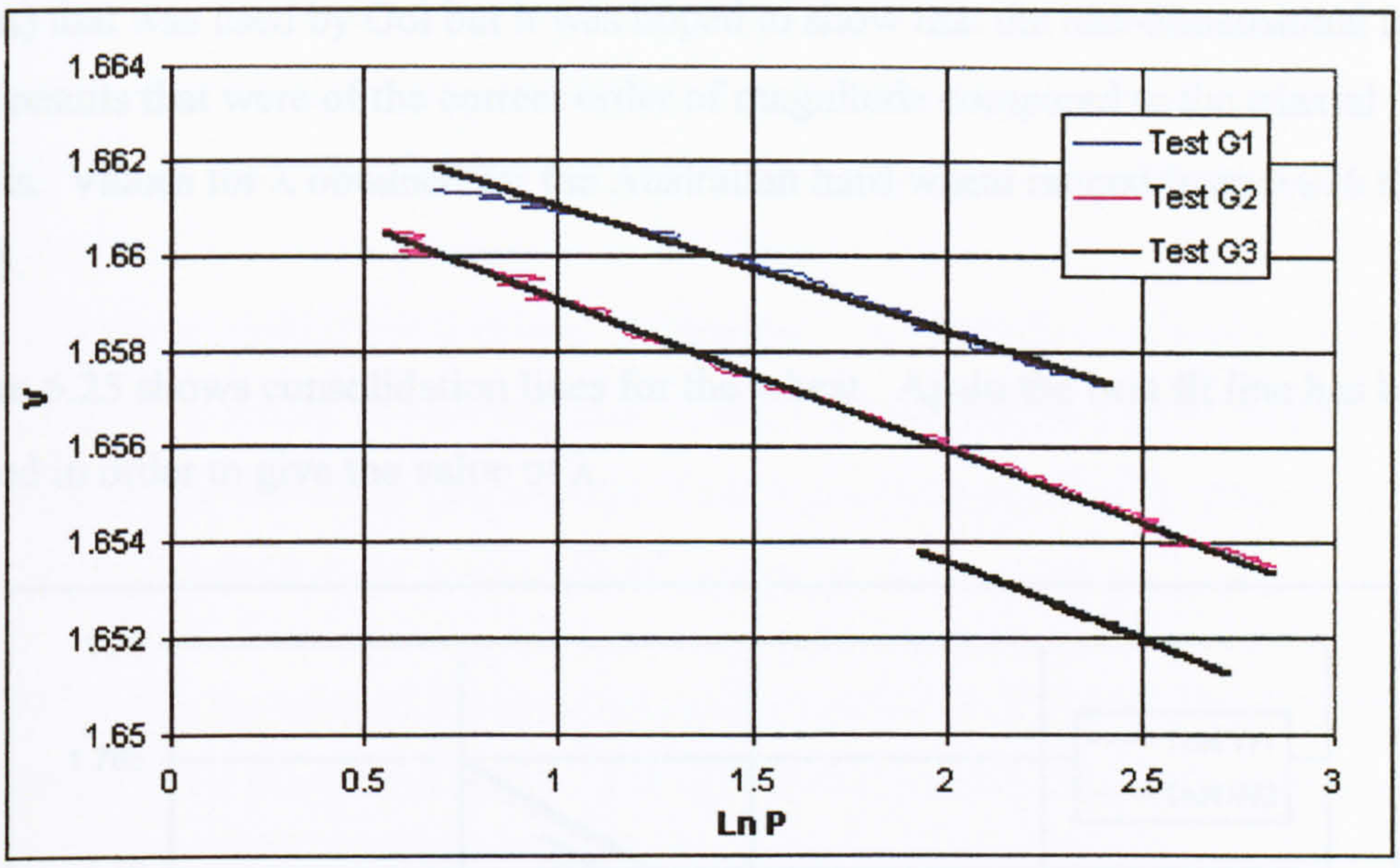

Figure 6.24 - One-dimensional consolidation tests on pea gravel

The best fit straight line has been added to each set of results to determine the logarithmic bulk modulus and the values are shown in table 6.8.

	Sand	Gravel
Test 1	0.0015	0.0026
Test 2	0.0015	0.0031
Test 3	0.0020	0.0032
Average value	0.0017	0.0030

Table 6.8 - Results from consolidation tests on sand and gravel

The value of λ for these materials is in the same order of magnitude as the values calculated above. The values are all lower than the original calculations as the best fit to the experimental data suggested they should be. As λ is not well reported in the literature for these materials there is no other data to compare these values with. This makes it difficult to assess whether these values provide a good representation of the material. However, Ooi (1990) performed a series of rigorous triaxial tests on wheat and interpreted this data to give values of λ for his own finite element models. In order to attempt to corroborate the method employed above the tests were repeated on wheat. It was not possible to obtain the exact same type of wheat (Australian hard

wheat) that was used by Ooi but it was hoped to show that the one-dimensional tests gave results that were of the correct order of magnitude compared to the triaxial results. Values for λ obtained for the Australian hard wheat ranged from 0.016 to 0.021.

Figure 6.25 shows consolidation lines for the wheat. Again the best fit line has been plotted in order to give the value of λ.

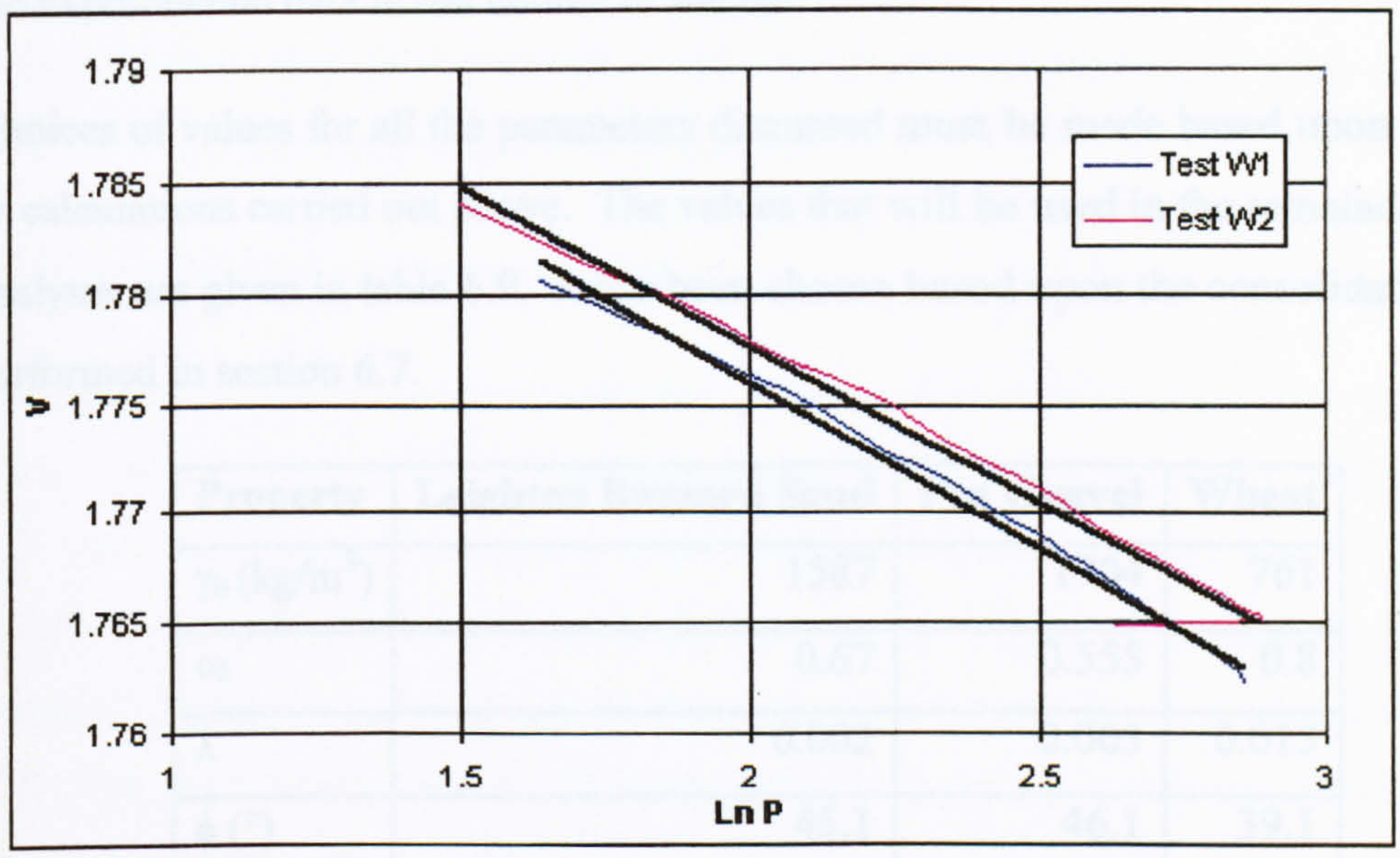

Figure 6.25 - One-dimensional consolidation tests on wheat

The average value of λ obtained for the type of wheat tested is 0.015. This compares well with the values obtained by Ooi (1990) and shows that this simple test may suitable for determining values of λ for preliminary calculations, without having to perform the more rigorous triaxial test.

6.8 Conclusions and choice of values for PE-DP model for Leighton Buzzard sand and pea gravel

After performing initial tests and comparison with theoretical models in an axisymmetric finite element model the porous elastic/Drucker-Prager constitutive law was chosen for use in this project. It was determined that the value of λ in the porous elastic portion of the law was critical to the overall performance of the model and a

number of tests were performed to determine values for the materials. These tests showed that the value of λ needs to be small in order to best match the Janssen distribution given the density data available. Simple consolidation tests have also shown that the order of magnitude determined from density based calculations is correct but the actual value is hard to pinpoint. The best fit exercise performed on the experimental results of Lahlouh *et al* (1995) has shown that a very small value of λ would predict the corner pressures well but higher values may be required to better fit the experimental data in the middle of the bin.

Choices of values for all the parameters discussed must be made based upon the tests or calculations carried out above. The values that will be used in the remainder of the analyses are given in table 6.9. λ has been chosen based upon the consolidation tests performed in section 6.7.

Property	Leighton Buzzard Sand	Pea Gravel	Wheat
γ_0 (kg/m^3)	1587	1704	761
e_0	0.67	0.555	0.8
λ	0.002	0.003	0.015
ϕ (°)	45.1	46.1	39.1
ψ (°)	0	0	0
σ^0_c (kPa)	0.25	0.25	0.25
ν	0.3164	0.306	0.3685
P^{el}_t (kPa)	0	0	0
μ	0.445	0.392	0.44

Table 6.9 - Final properties used for the materials in the finite element model

Chapter 7 - The effect of the boundary condition at the base of the bin

In Chapter 6 it was noted that there were end effects present in the results for the wall normal pressures in the axisymmetric bin. These take the form of a local pressure increase near the base when compared to the Janssen distribution. This is attributed to the influence of the base condition but it is not clear whether this a function of the modelling process or reflects some real phenomenon in silos. The results presented in this chapter show an investigation into this phenomenon using a variety of models with differing boundary conditions at the base.

7.1 Flat-bottomed axisymmetric bin

The axisymmetric examples presented in the previous chapter showed that given sound representation of the stored bulk solid the finite element results compare very well with the Janssen prediction apart from in regions near the base. All of the models so far analysed have been flat-bottomed and the base of the structure has been restrained along its entire length in the y-direction but not in the x-direction (figure 6.1). The interaction between the base and the stored solid has been idealised and modelled as frictionless.

In section 6.4.3 a range of materials was modelled in the flat-bottomed silo. This showed that materials with a lower value of internal friction (and hence a higher value of ν) exhibited end-effects over a larger proportion of the bin (figure 6.4). This effect is assumed to be due to the larger Poisson's ratio giving a larger Poisson effect near the base where the vertical stress is high, leading in turn to more load being transferred to the wall. Figure 7.1 shows a plot of Poisson's ratio versus the depth at which the finite element prediction in the bin starts to deviate from the Janssen prediction.

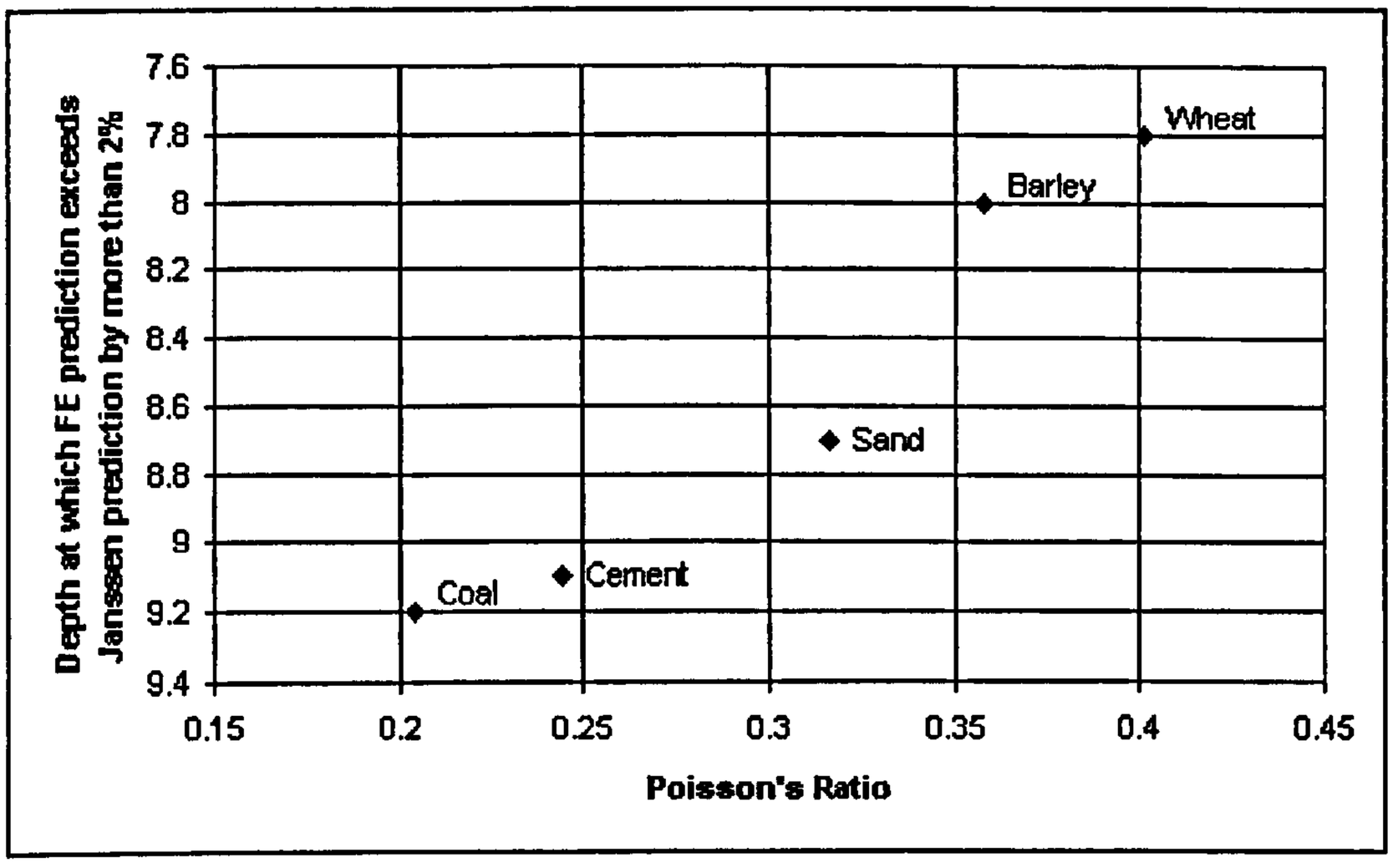

Figure 7.1 – The effect of Poisson's ratio on the depth over which end effects are present

Clearly the higher the Poisson's ratio the greater the distance over which the end-effect occurs.

In order to investigate whether the observed end-effects are a function of the finite element model or represent a real phenomenon in silos, a number of models were created. These models have different boundary conditions at the base of the silo. Initially a flat-bottomed axisymmetric silo is modelled and investigated and then a concentric hopper is added with varying wall angles.

7.1.1 Frictionless base condition

Results for the model that was studied in the previous chapter are again presented here. Figure 7.2 shows the distribution of wall normal pressure at the bottom of the wall using the linear elastic law and the porous elastic/Drucker-Prager law to describe the ensiled material's behaviour. Only the area of the bin near the base is shown as the results away from this area in the parallel section of the bin are very close to the Janssen distribution.

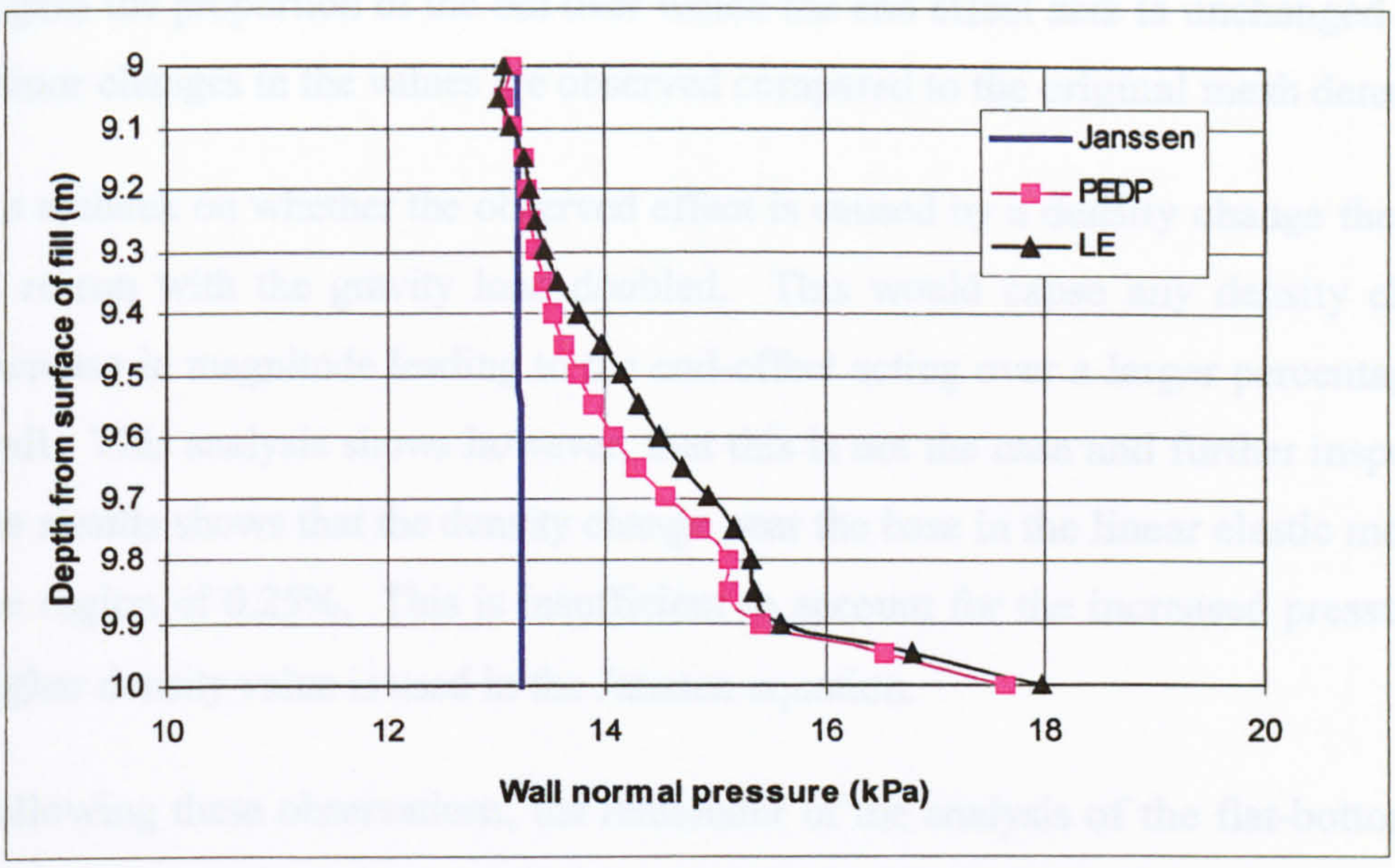

Figure 7.2 – Pressures near the base using different constitutive laws

Only a small difference in the wall pressures predicted near the base is observed, attributable to the way the materials are modelled. The portion of the bin over which the end-effect is apparent is the same for both material laws.

The linear elastic model was repeated with the mesh density doubled to check that the effect is not a function of the mesh density. Figure 7.3 shows the results for this.

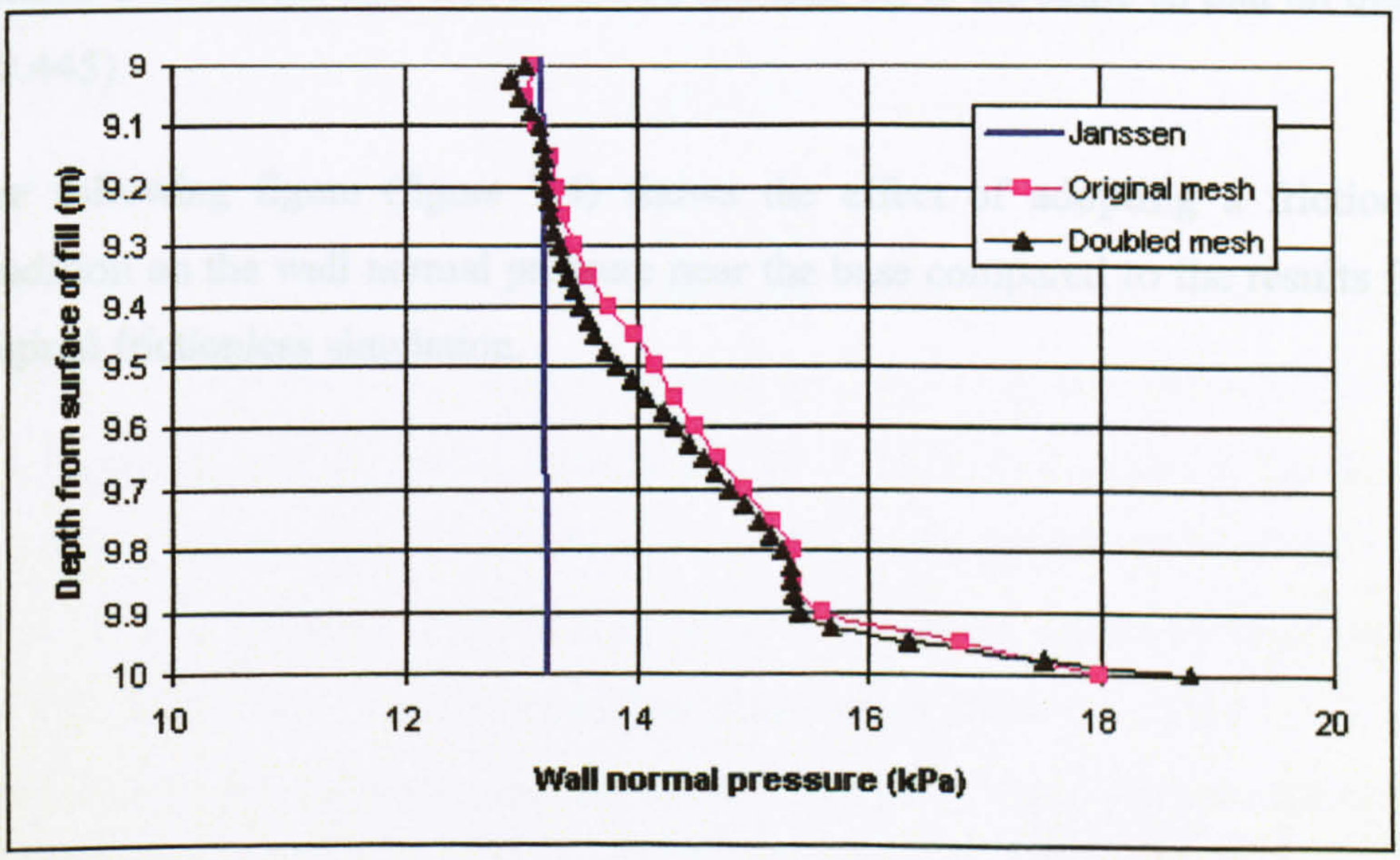

Figure 7.3 – Effect of doubling the mesh density on wall normal pressures

Again the proportion of the bin over which the end effect acts is unchanged and only minor changes in the values are observed compared to the original mesh density.

As a check on whether the observed effect is caused by a density change the analysis is re-run with the gravity load doubled. This would cause any density change to increase in magnitude leading to the end-effect acting over a larger percentage of the wall. This analysis shows however, that this is not the case and further inspection of the results shows that the density change near the base in the linear elastic model is in the region of 0.25%. This is insufficient to account for the increased pressure if the higher density value is used in the Janssen equation.

Following these observations, the remainder of the analysis of the flat-bottomed silo is carried out using the linear elastic material constitutive law.

7.1.2 Frictional base condition

In a real silo of this type the interaction between the base and the stored material is not frictionless as was assumed in the previous analysis. The coefficient of friction would be the same as that seen on the wall (assuming the base is constructed from the same material). Therefore the above analysis is repeated with the coefficient of friction between the base and the stored material set to the same as that on the wall ($\mu = 0.445$).

The following figure (figure 7.4) shows the effect of adopting a frictional base condition on the wall normal pressure near the base compared to the results from the original frictionless simulation.

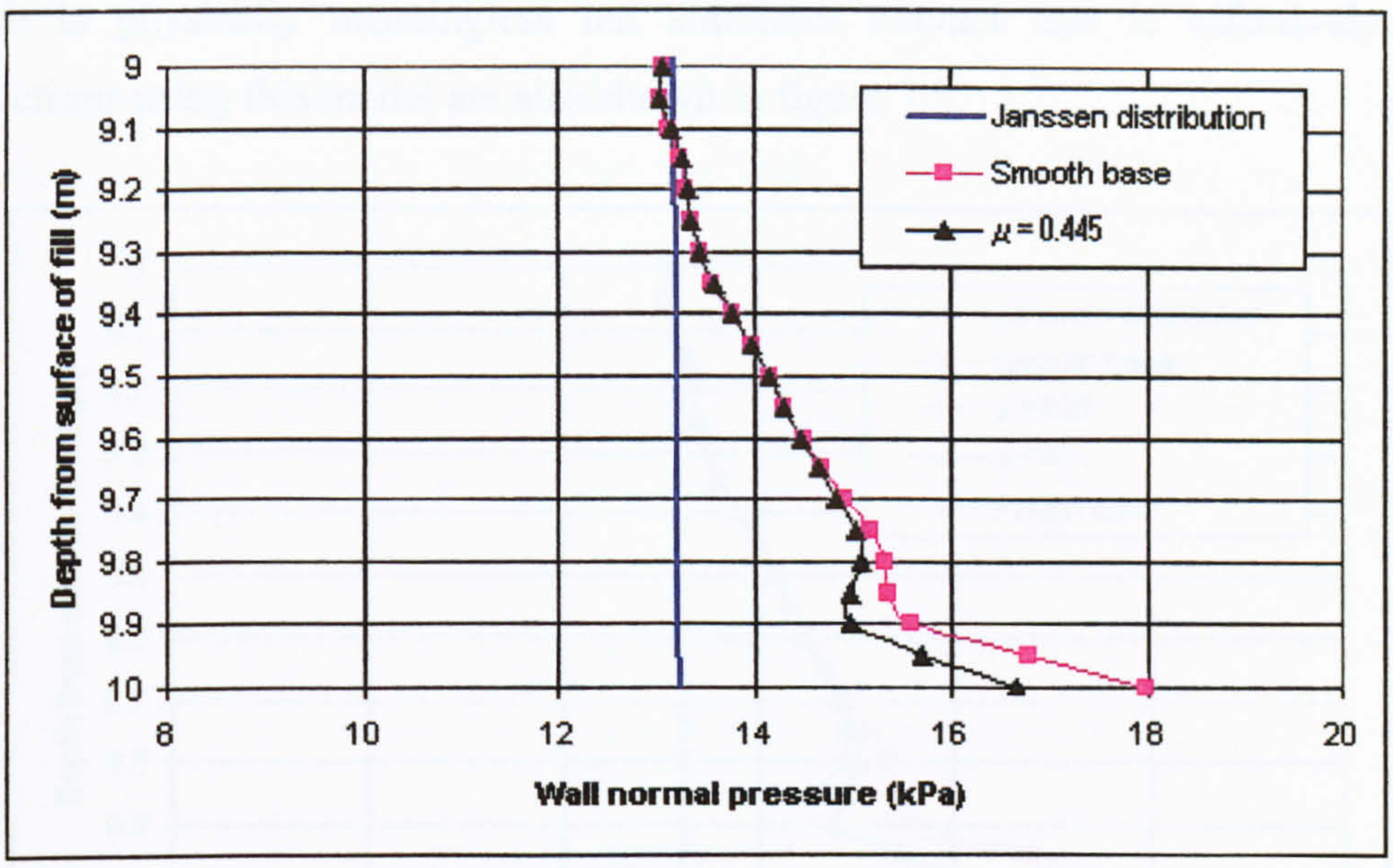

Figure 7.4 - The effect of a frictional base in an axisymmetric bin

A difference in wall pressure can be seen in the final 0.3m of the bin wall. The final node experiences a pressure reduction of 7.5% compared to the original frictionless model. The frictional nature of the base prevents the material being forced outwards by the weight of the material above, this leads to the observed reduction in pressure in this area. This figure also shows that there are two end-effects in operation. In the final 0.3m of the bin there is an effect that can be attributed to the frictional nature of the base but this is superimposed on another phenomena that appears unchanged by any change in friction. This effect also extends over the final 1m of the bin (10% of the total depth).

In order to further investigate this mechanism other artificial values of μ were adopted ($\mu = 0.09$ and 0.71). The value of $\mu = 0.71$ is chosen to represent the value of the materials internal friction coefficient ($\phi = 35.4°$ and therefore $\tan \phi = \mu = 0.71$). Using this coefficient of friction causes the stored material to "see" the base as another layer of material. The value of $\mu = 0.09$ is chosen arbitrarily to observe the effect of a small value. Results from these analyses are shown in figure 7.5. Also, as an extension of the different frictional coefficients the Abaqus software package has a "rough" frictional option. This option implies that the friction coefficient $\mu \Rightarrow \infty$

which is physically meaningless but simulates contact that is effectively tied. Predictions using this model are also shown in figure 7.5.

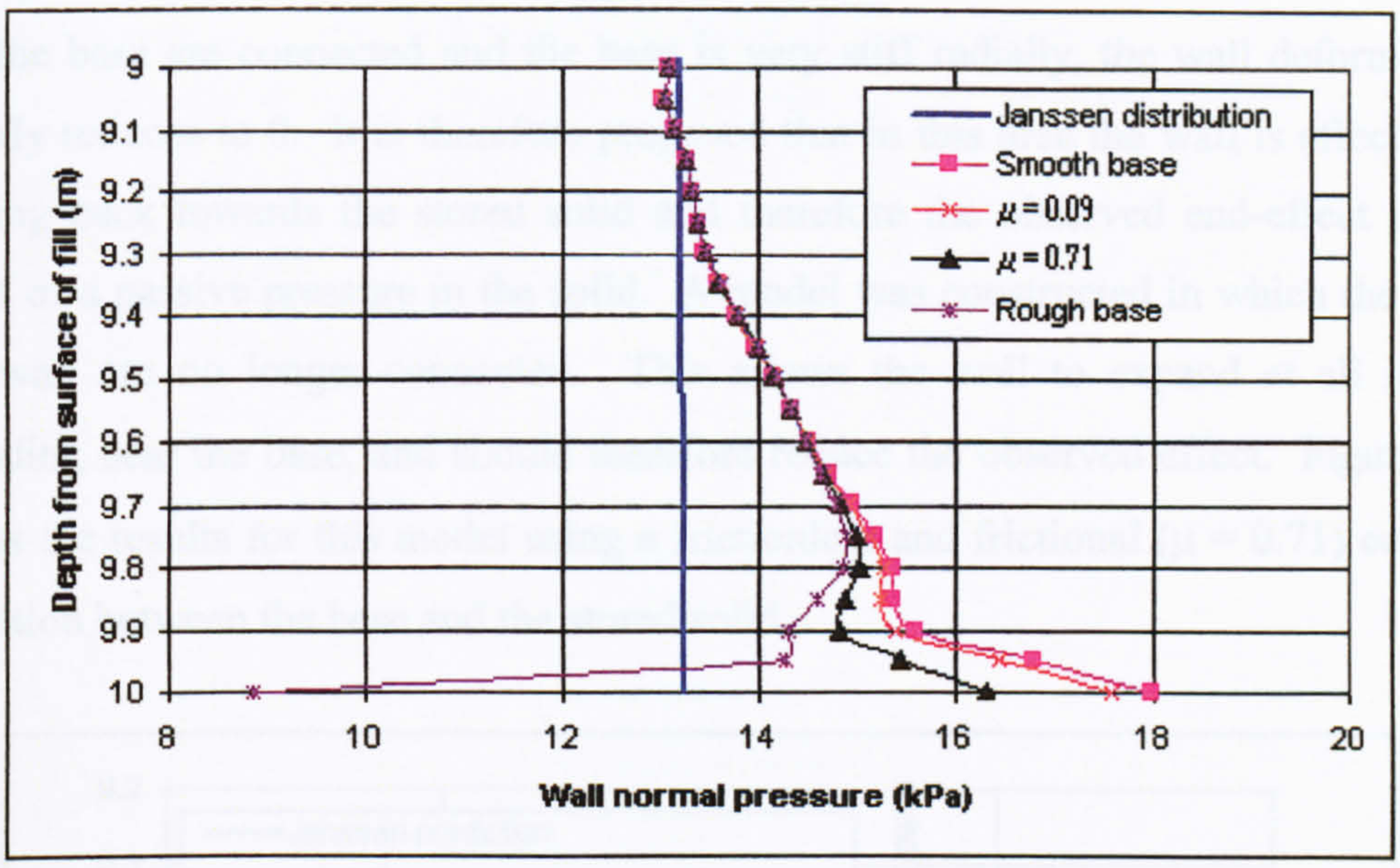

Figure 7.5 - The effect of adopting different values of μ

The results obtained using $\mu = 0.09$ are slightly lower in magnitude than the frictionless results while those obtained from $\mu = 0.71$ are lower than those obtained from $\mu = 0.445$. In general there is a trend of pressure reduction near the base as the value of μ increases.

In the case of the rough base condition, it can be seen that the effect is similar to the previous frictional models but due to the fully rough nature of the base the final node that is in the corner, and therefore in contact with the base, experiences a much reduced lateral pressure. This is due to the high coefficient of friction effectively restraining the node against movement in the radial direction.

7.1.3 Base and wall not connected

The results presented above showed that adoption of a number of base conditions had some effect on the predicted pressure near the base, however, even assuming the rough base condition does not eliminate the end-effect entirely, it merely reduces it. Therefore another mechanism to account for the increased pressure must be in

operation. Inspection of the radial deformation in the shell shows that there is little deflection near the top of the silo. Moving down the wall this deflection increases to a maximum approximately 0.5m above the base. By virtue of the fact that the wall and the base are connected and the base is very stiff radially, the wall deformation quickly reduces to 0. It is therefore proposed that in this area the wall is effectively moving back towards the stored solid and therefore the observed end-effect is the result of a passive pressure in the solid. A model was constructed in which the base and wall are no longer connected. This allows the wall to expand at all levels including near the base, and should therefore reduce the observed effect. Figure 7.6 shows the results for this model using a frictionless and frictional ($\mu = 0.71$) contact condition between the base and the stored solid.

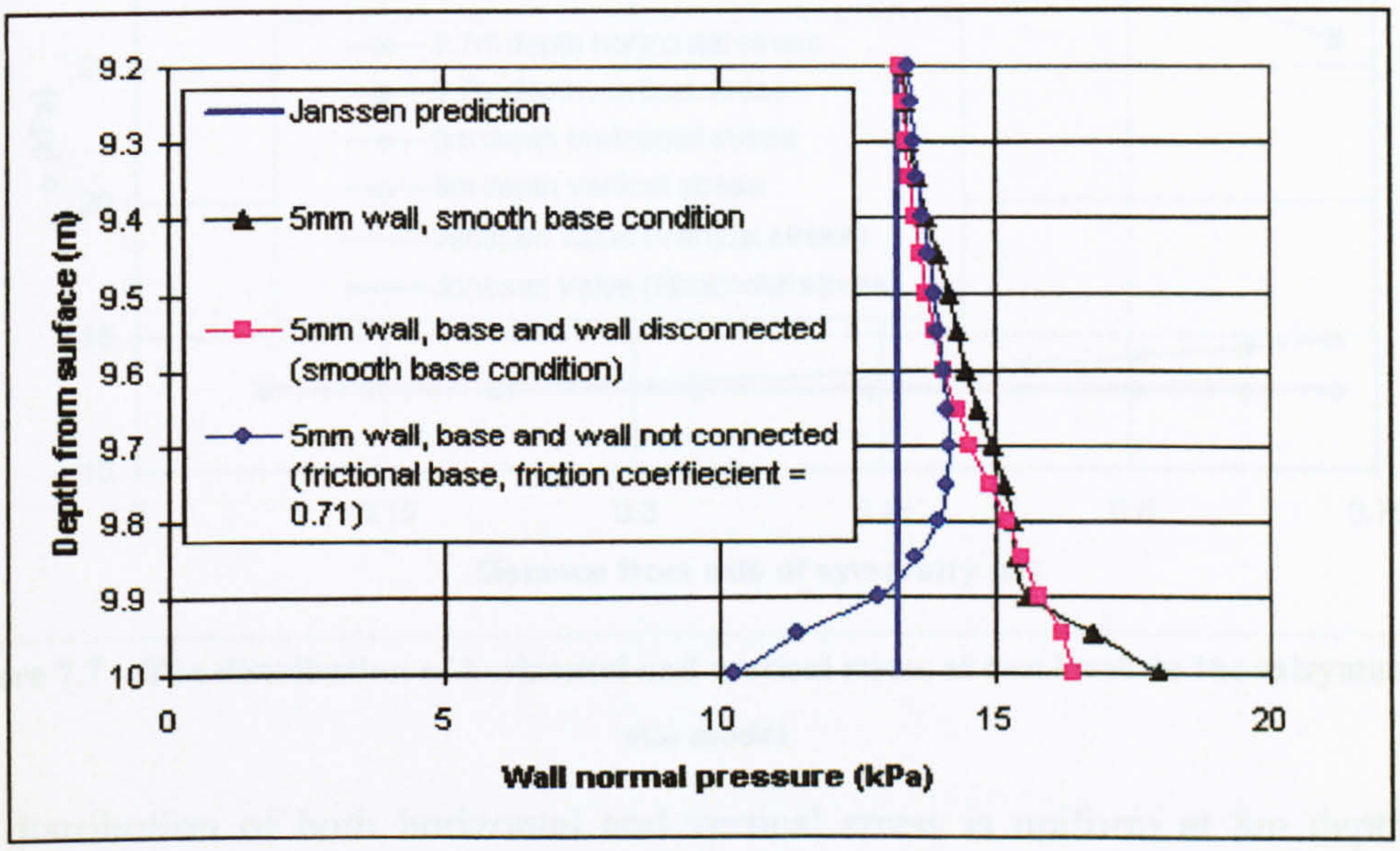

Figure 7.6 – Wall normal pressure predictions in the base and wall disconnected model

A marked increase in pressure near the bottom of the wall is still apparent. In the model with the frictional contact at the base there is a reduction in pressure below the Janssen value. This is due to stored material being restrained from radial movement along the base by friction. However, an increase in pressure above this region near the base is still observed. In general the end-effect is not eliminated.

7.2 Horizontal and vertical stress in the stored solid

In order for the observed wall pressure to change from that predicted by Janssen there must be a change in the distribution of stress in the material. The Janssen theory assumes that the stress is invariant across the bin at any given level and in a cylindrical silo this is generally found to be true. Figure 7.7 shows the distribution of horizontal and vertical stress through the stored material at a depth of 8m and 9.7m in the frictionless base model.

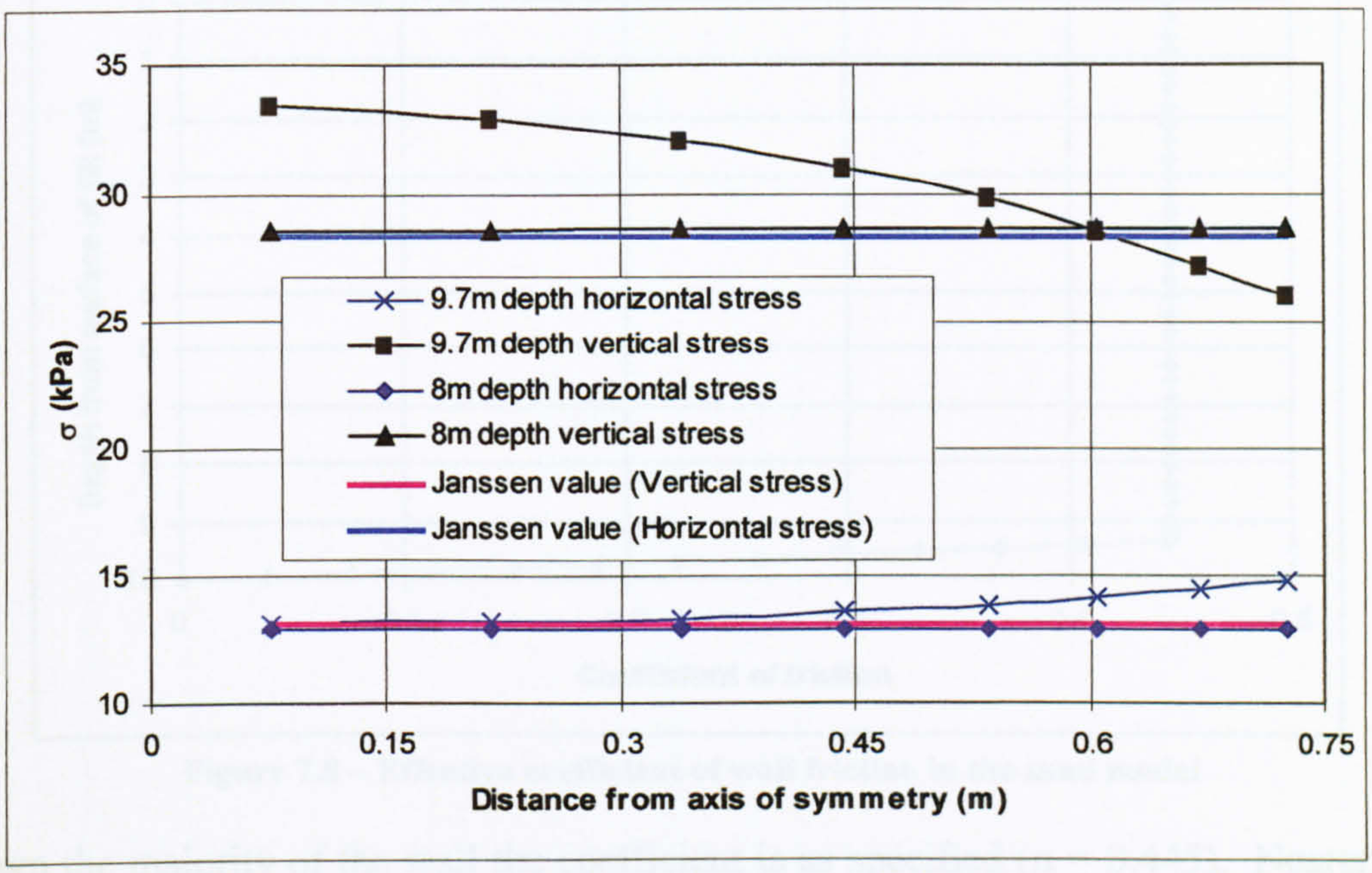

Figure 7.7 – The distribution of horizontal and vertical stress at two levels in the axisymmetric silo model

The distribution of both horizontal and vertical stress is uniform at 8m depth and agrees well with the Janssen values. The average ratio k is calculated as 0.452 which is consistent with the material being modelled.

The distribution of horizontal and vertical stress at a depth of 9.7m (which is inside the area that is experiencing a deviation from the Janssen distribution) is no longer uniform. There is a large increase in vertical stress and a decrease in horizontal stress at the centre of the bin. This leads to large variations in the value of k in the finite element model with $k = 0.39$ at the centre on the solid and $k = 0.57$ near the wall. These results reflect those of Ooi and Rotter (1990).

Inspection of the results shows that the maximum shear within the material occurs near the wall due to its frictional nature. This shear increases with depth up to a maximum. The shear reduces closer to the base because of the support the material receives from the vertically rigid base. It therefore follows that as there is little movement of the solid in this area the frictional nature of the wall may not be fully mobilised. Figure 7.8 shows the effective coefficient of friction determined from the finite element results.

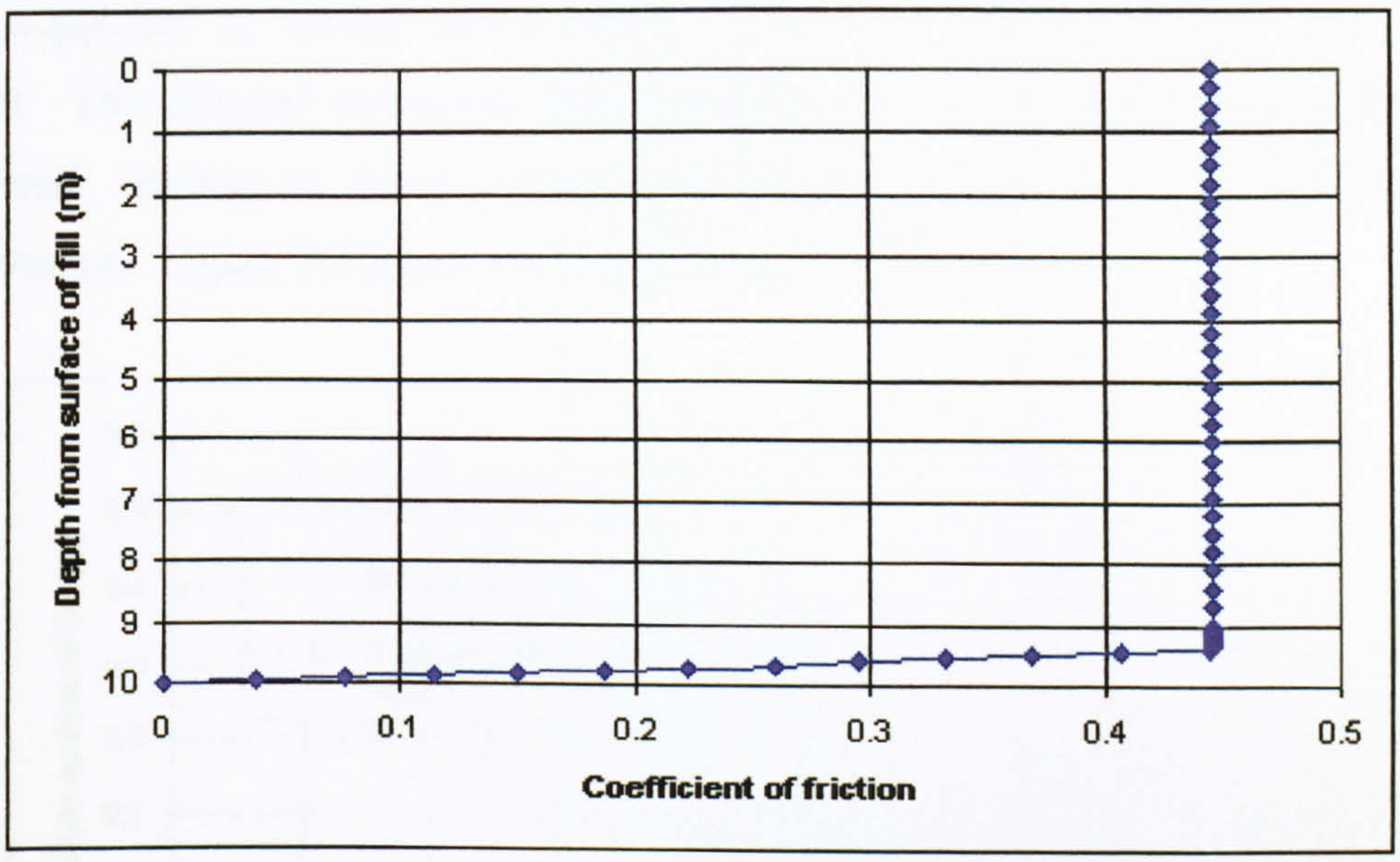

Figure 7.8 – Effective coefficient of wall friction in the sand model

Down the majority of the wall the coefficient is as specified ($\mu = 0.445$). Nearer the base however, the effective coefficient of friction reduces, eventually diminishing to zero at the very base. This reduction in the effective value of μ is a possible cause of the observed internal stress distributions in the solid as wall friction is no longer supporting all of the vertical stress. Vertical stress is therefore transferred to the centre of the bin leading to higher lateral stress at the wall in order to maintain equilibrium.

The reason the friction is not mobilised near the base is due to the movement of the contact surfaces relative to one another. Although the coefficient of friction is specified in the model it is not mobilised if there is no movement between the contact surfaces. This movement gives rise to shear and normal stresses which can be used

to calculated the effective coefficient of friction. Near the bottom of the bin the rigid base (which is fully supported in the vertical direction) stops the stored solid moving down the wall. This leads to reduced shear stresses and hence the reduced value of wall friction. If the base condition could be modelled in such a way as to allow the wall friction to support the full weight of the stored material then the end effect seen should be much reduced.

The silo is again modelled as having the wall and base disconnected. The base is then supported by springs which allow a reasonably large movement of the solid above. This allowed movement should mobilise the friction at all points down the bin wall, leading to finite element predictions that are closer to the Janssen distribution. Figure 7.9 shows the results from this model.

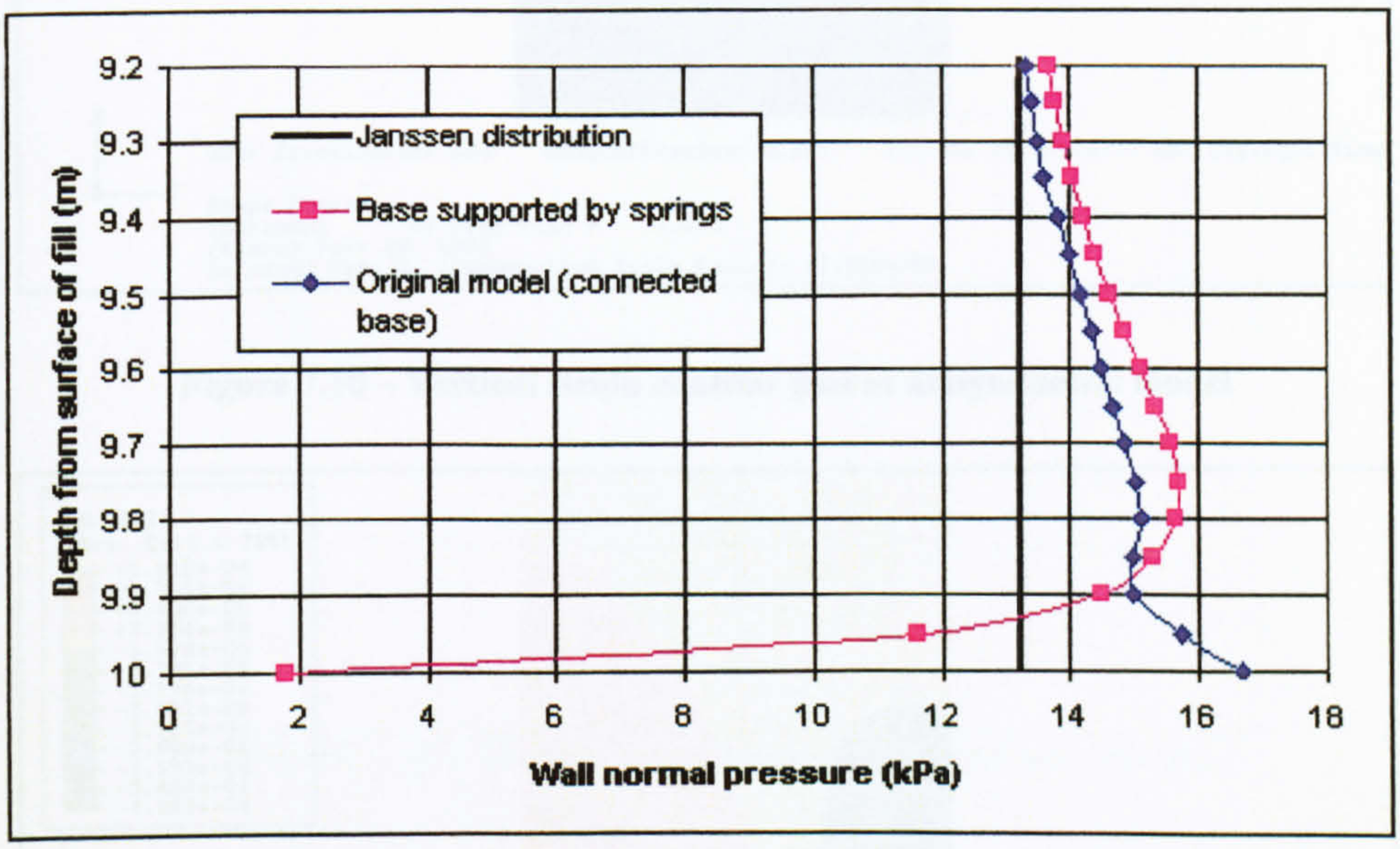

Figure 7.9 – Wall normal pressures from the model with spring-supported base

The initial observation is that this representation of the boundary condition increases the magnitude of the end effect. Changing the value of stiffness of the supporting springs in order to alter the amount of movement in the solid has little effect on the pressure predictions. Inspection of the normal and shear stress at the wall however, shows that because of the allowed movement, friction is fully mobilised all the way down the bin wall with the prescribed value of $\mu = 0.445$.

7.3 Strain in the stored material

Figures 7.10 and 7.11 show contour plots of the vertical and radial strain in the stored material taken from the original frictionless base condition model.

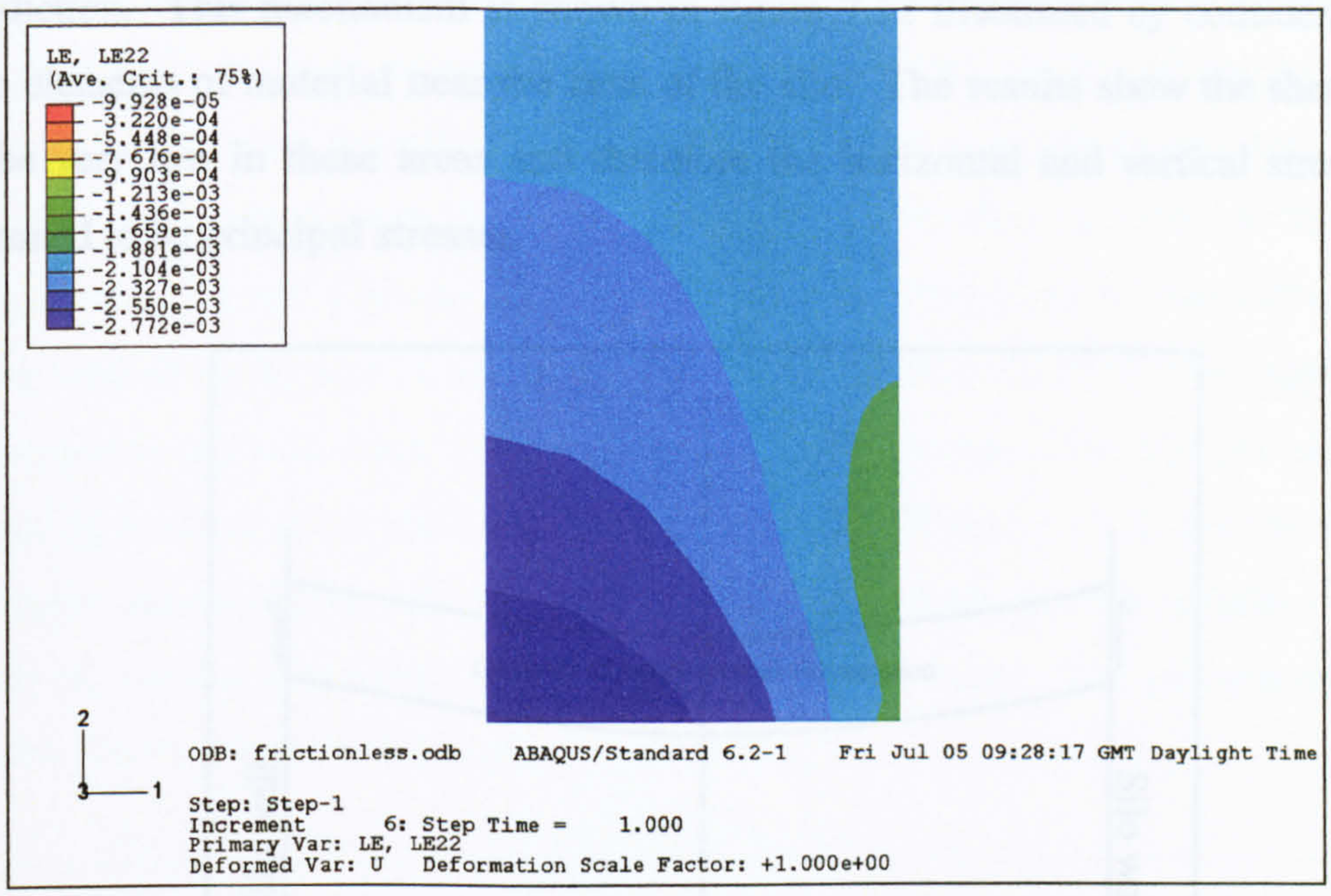

Figure 7.10 – Vertical strain contour plot in axisymmetric model

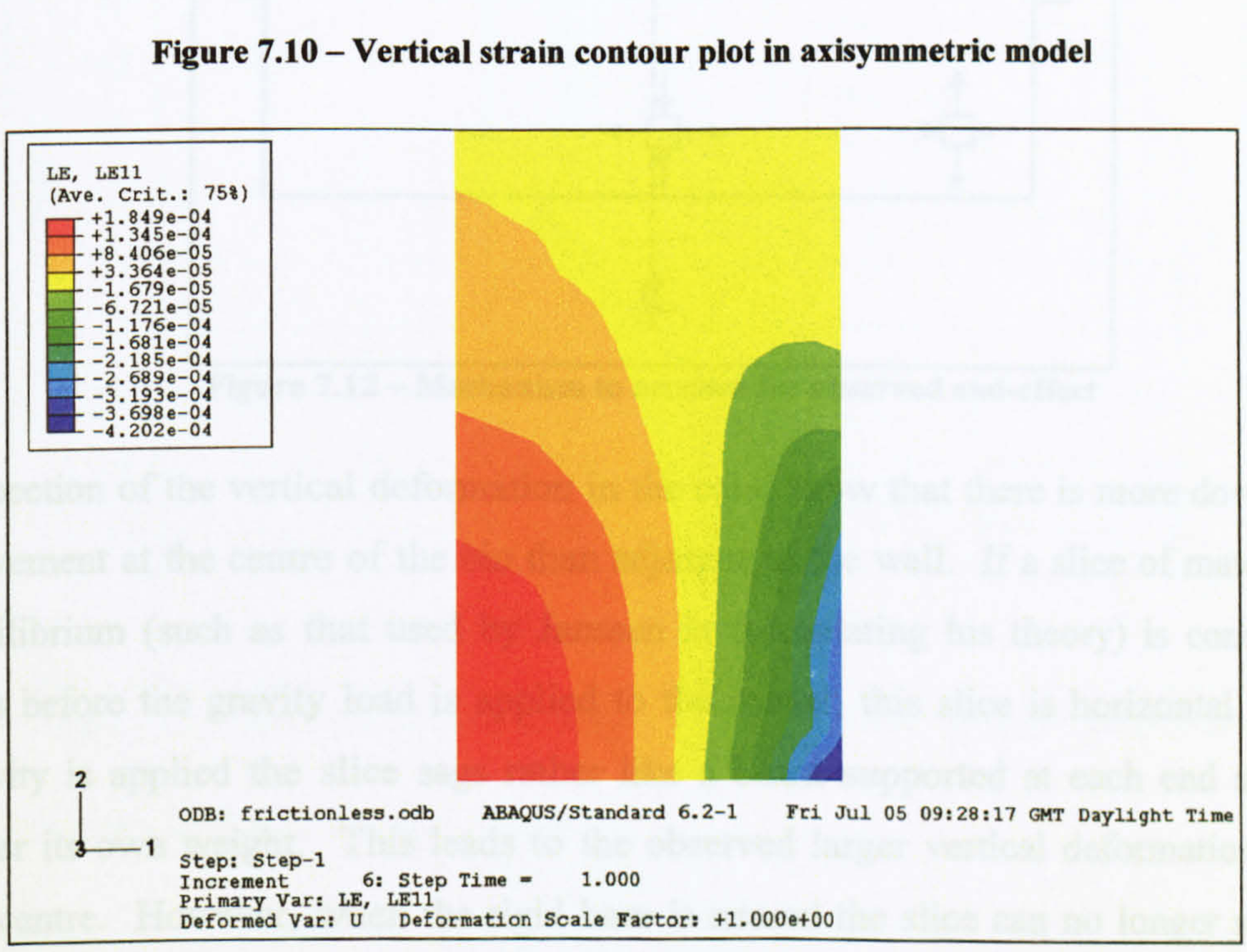

Figure 7.11 – Radial strain contour plot in axisymmetric model

Figure 7.10 shows that there is a high compressive vertical strain at the centre of the bin near the base. The resulting Poisson effect leads to high tensile lateral strain at this point (figure 7.11) which in turn leads to high compressive lateral strain adjacent to the wall. This leads to the observed pressures that are higher than the Janssen prediction. This mechanism is shown in figure 7.12 illustrated by consideration of two elements of material near the base of the silo. The results show the shear stress to be very low in these areas and therefore the horizontal and vertical stresses are assumed to be principal stresses.

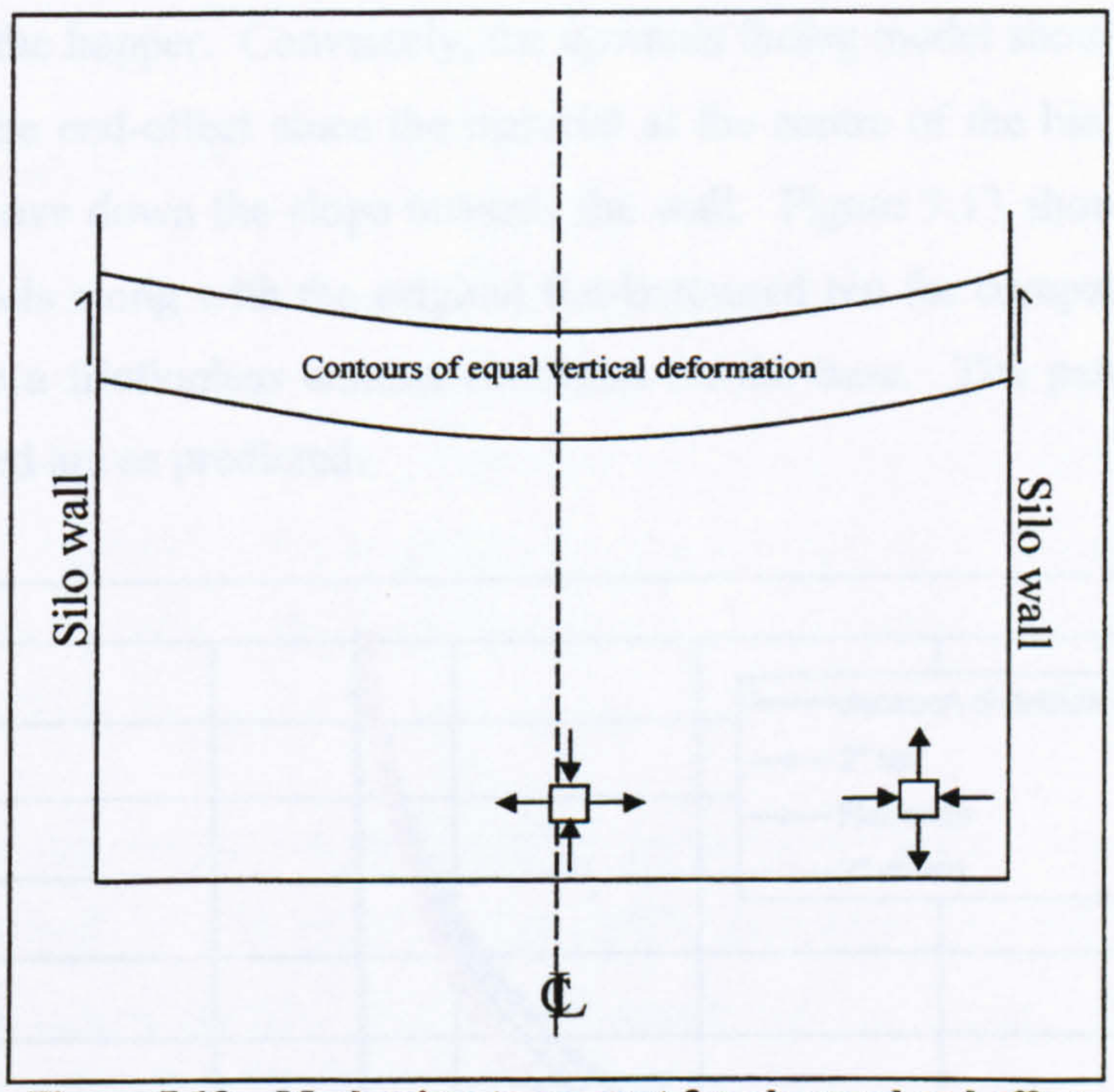

Figure 7.12 – Mechanism to account for observed end-effect

Inspection of the vertical deformation in the solid show that there is more downward movement at the centre of the bin than adjacent to the wall. If a slice of material in equilibrium (such as that used by Janssen in formulating his theory) is considered then before the gravity load is applied to the model, this slice is horizontal. Once gravity is applied the slice sags rather like a beam supported at each end sagging under its own weight. This leads to the observed larger vertical deformations near the centre. However, when the rigid base is neared the slice can no longer sag and

therefore the material at the centre experiences the observed increase in vertical strain.

In order to test this theory two more models are created, one with a 2° upward sloping base (sloping upwards from the transition) and one with a downward sloping base, also of 2° (sloping downwards from the transition). If the above proposed mechanism holds true then the end-effect should decrease in the model that slopes downwards. This is because the high lateral compressive strain adjacent to the wall will be relieved slightly by the action of the material attempting to move down the sloping wall of the hopper. Conversely, the upwards facing model should experience an increase in the end-effect since the material at the centre of the bin will now be attempting to move down the slope towards the wall. Figure 7.13 shows the results from these models along with the original flat-bottomed bin for comparison. These models all have a frictionless contact condition on the base. The patterns of wall pressure observed are as predicted.

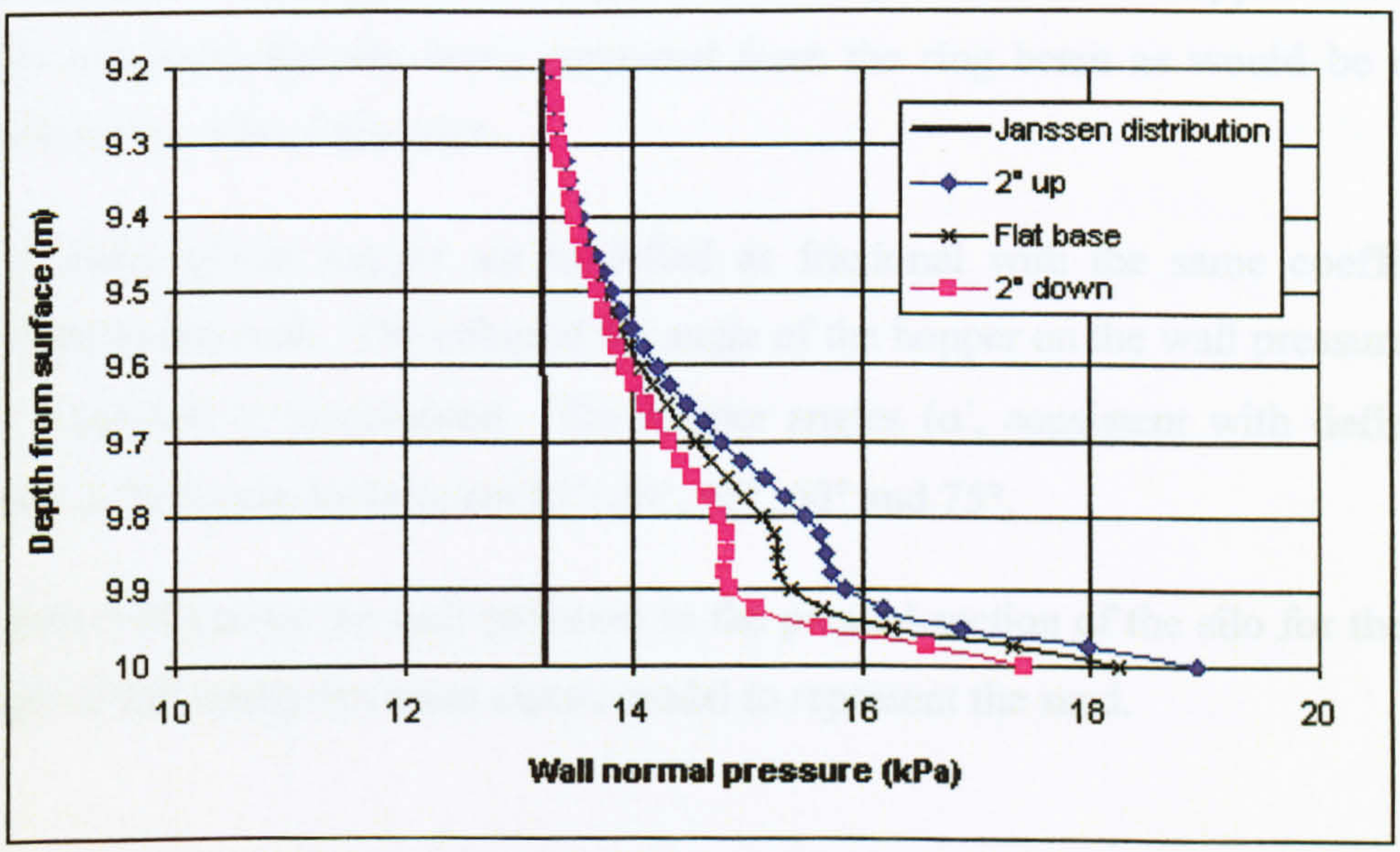

Figure 7.13 – Effect of small angled hopper on the wall normal pressure prediction

7.4 Summary of flat-bottomed model

A number of finite element models with differing boundary conditions have been investigated. The results obtained have shown that the choice of boundary condition

made can have a considerable effect on the accuracy of the pressures predicted when compared to the Janssen distribution. A mechanism to account for the increased pressures observed near the base has been identified and further investigation supports the proposed theory.

The mechanism identified above accounts for the initial observations concerning the end effect occurring over larger portions of the bin for materials with a higher value of Poisson's ratio. As the Poisson's ratio increases the end effect will increase due to larger Poisson effects near the base where the vertical strain near the centre is increasing.

7.5 Hopper base condition

The work is now extended by considering a similar model but with a concentric hopper at the base rather than the flat bottom. It is not realistic to represent this type of model as ground supported and therefore the supporting boundary condition must be changed. The model is now supported at the junction of the hopper and the wall. This simulates the silo being supported from the ring beam as would be common practice in a silo of this type.

The walls of the hopper are modelled as frictional with the same coefficient of friction as the wall. The effect of the angle of the hopper on the wall pressures above the transition is investigated. The hopper angles (α', consistent with definition in figure 3.2) chosen initially are 15°, 30°, 45°, 60° and 75°.

Figure 7.14 shows the wall pressures in the parallel section of the silo for the hopper angle of 45° using the linear elastic model to represent the sand.

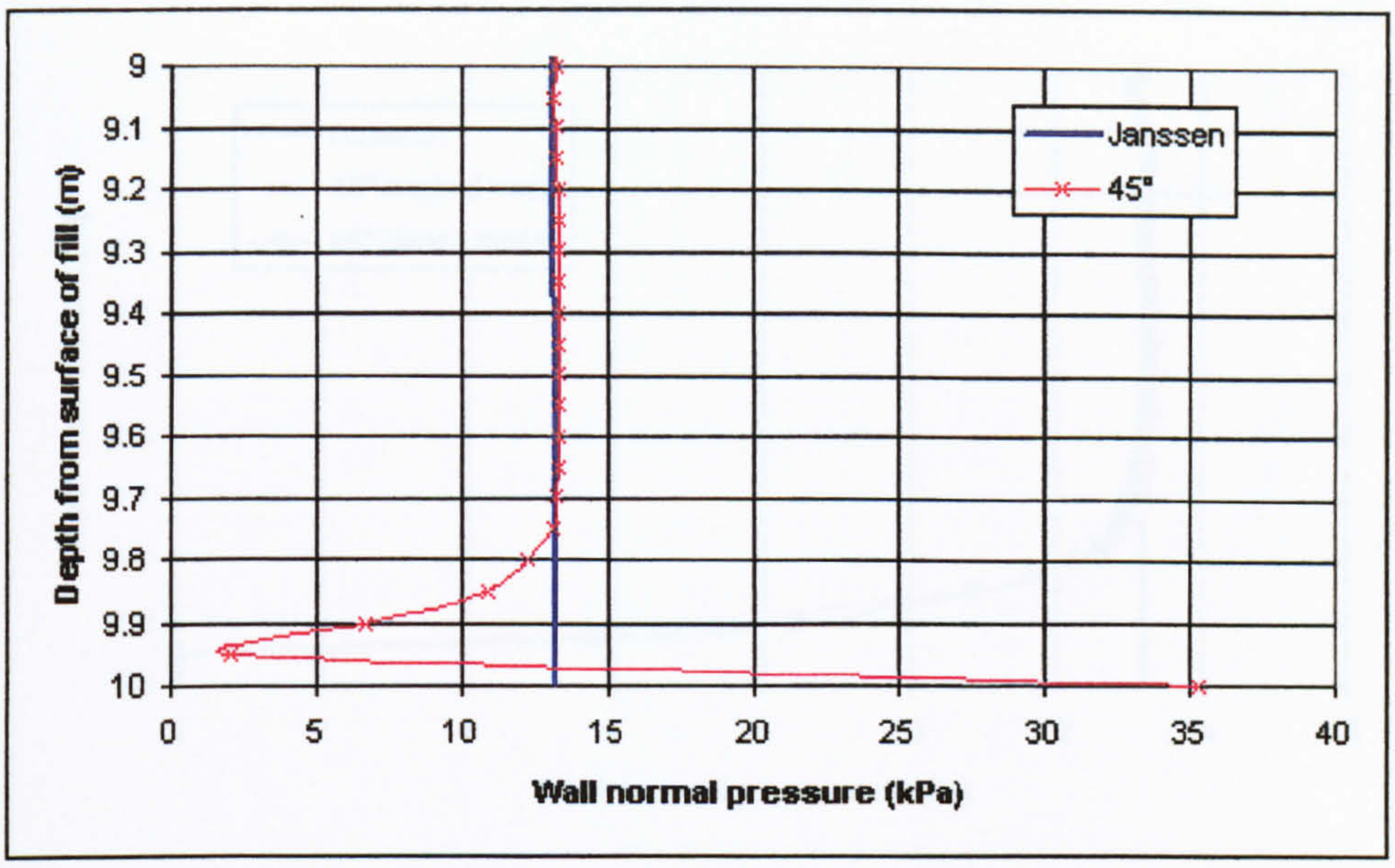

Figure 7.14 – The wall normal pressure above the transition with a 45° concentric hopper

Again only the bottom of the wall is plotted as results above this point compare well with the Janssen distribution. The end effect in this case does not extend over such a large portion of the bin as was observed in the flat-bottomed case. The final node exhibits a very large pressure and inspection of the results shows that this node has slid down the wall into the hopper, accounting for this large normal pressure value. The pressures from this distorted element are therefore disregarded. Other researchers (Martínez *et al*, 2002) have also observed distortion of the mesh at the transition in problems of this type and concluded that this distortion can lead to unreliable pressure predictions. Above the level of this final element there is a decrease of pressure when compared to the Janssen distribution.

As in the previous investigation the mesh was doubled to check whether the effects seen are a function of the mesh density. Figure 7.15 shows these results.

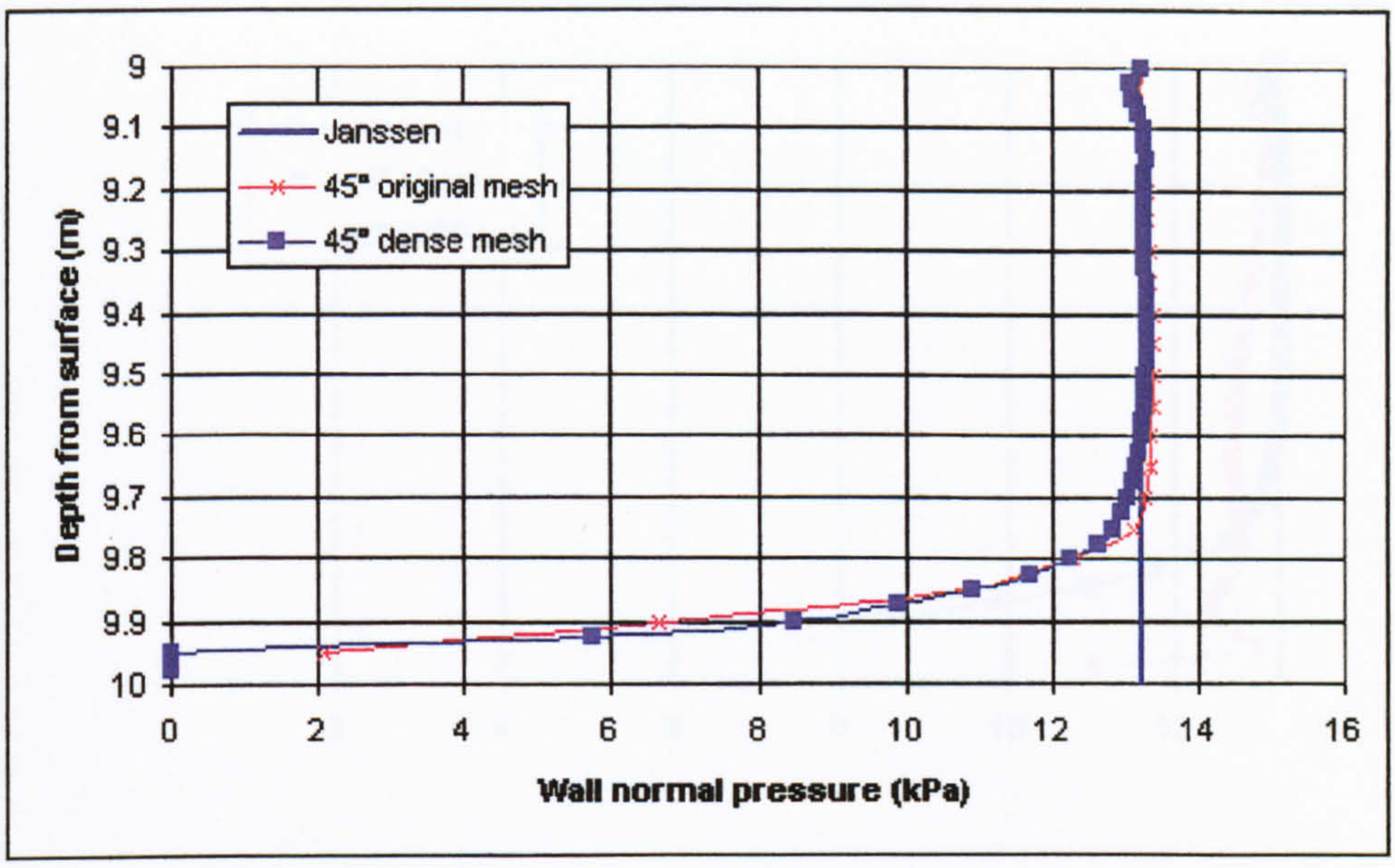

Figure 7.15 - Wall normal pressure near the base of the model with a hopper

The final node that has moved into the hopper (and therefore shows a very large pressure) is considered to give unreliable results and has therefore been removed from this plot to improve clarity.

It is apparent that in this model the doubling of the mesh has an effect on the observed pressures. With the more dense mesh several of the nodes just above the transition have zero pressures implying that there is a loss of contact between the stored material and the wall at this point. Even in this simple case the use of the linear elastic model may not be sufficient to accurately model the behaviour around changes in geometry such as the transition.

The analysis is therefore repeated using the linear elastic/Drucker-Prager model outlined in Chapter 6. The denser mesh is again used and figure 7.16 shows the results compared to those obtained from the linear elastic law.

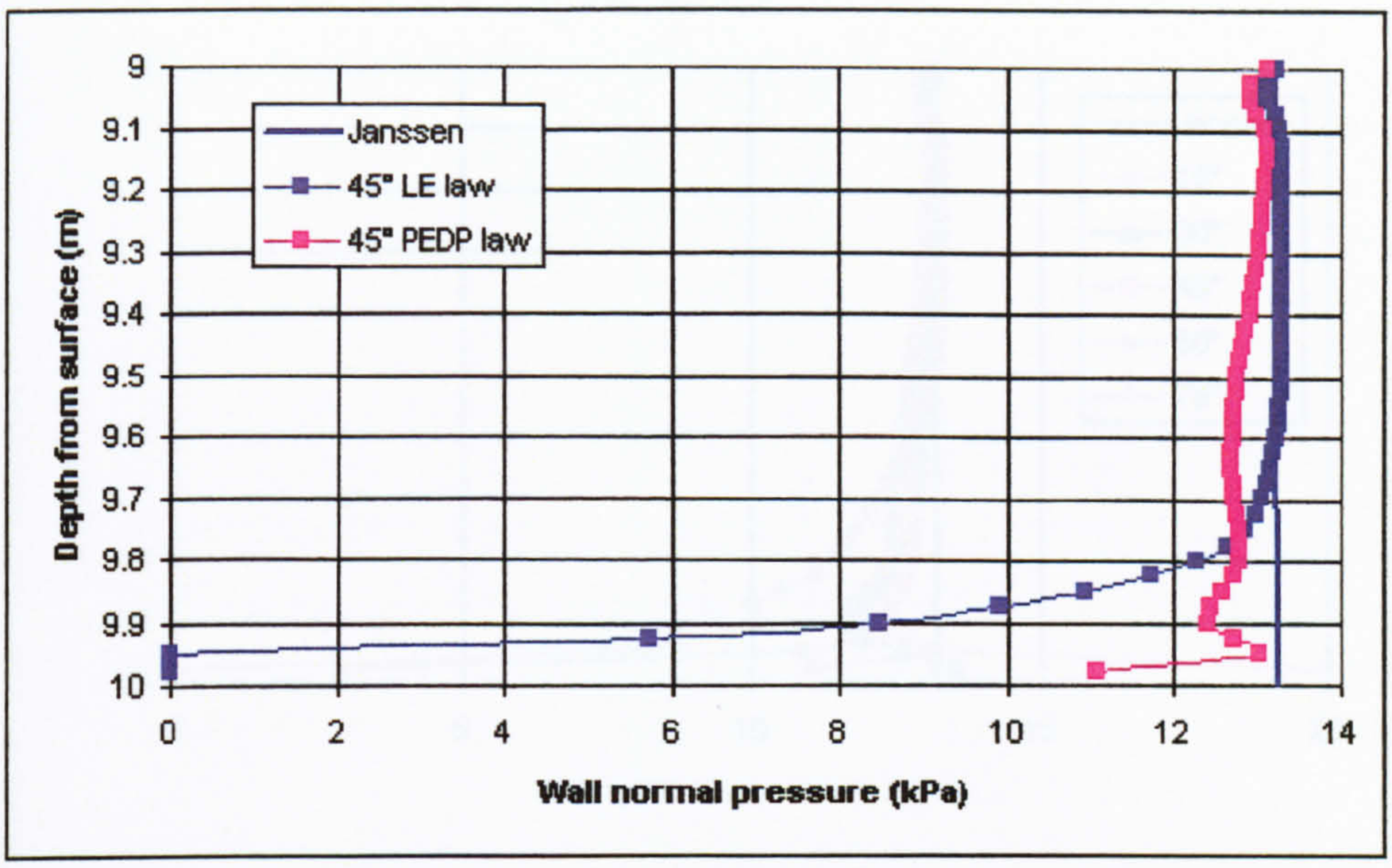

Figure 7.16 – Comparison of analysis with LE and PEDP constitutive laws

There is a very large difference in the predicted form of the pressure distribution. inspection of the results shows plastic strains forming near the transition which would affect the resulting stress distribution. It is therefore accepted that the linear elastic law is not suitable to model this type of geometry and the remainder of the investigation is continued using the PEDP constitutive law for the ensiled material.

Figure 7.17 shows the effect of changing the hopper angle on the wall normal pressure above the transition.

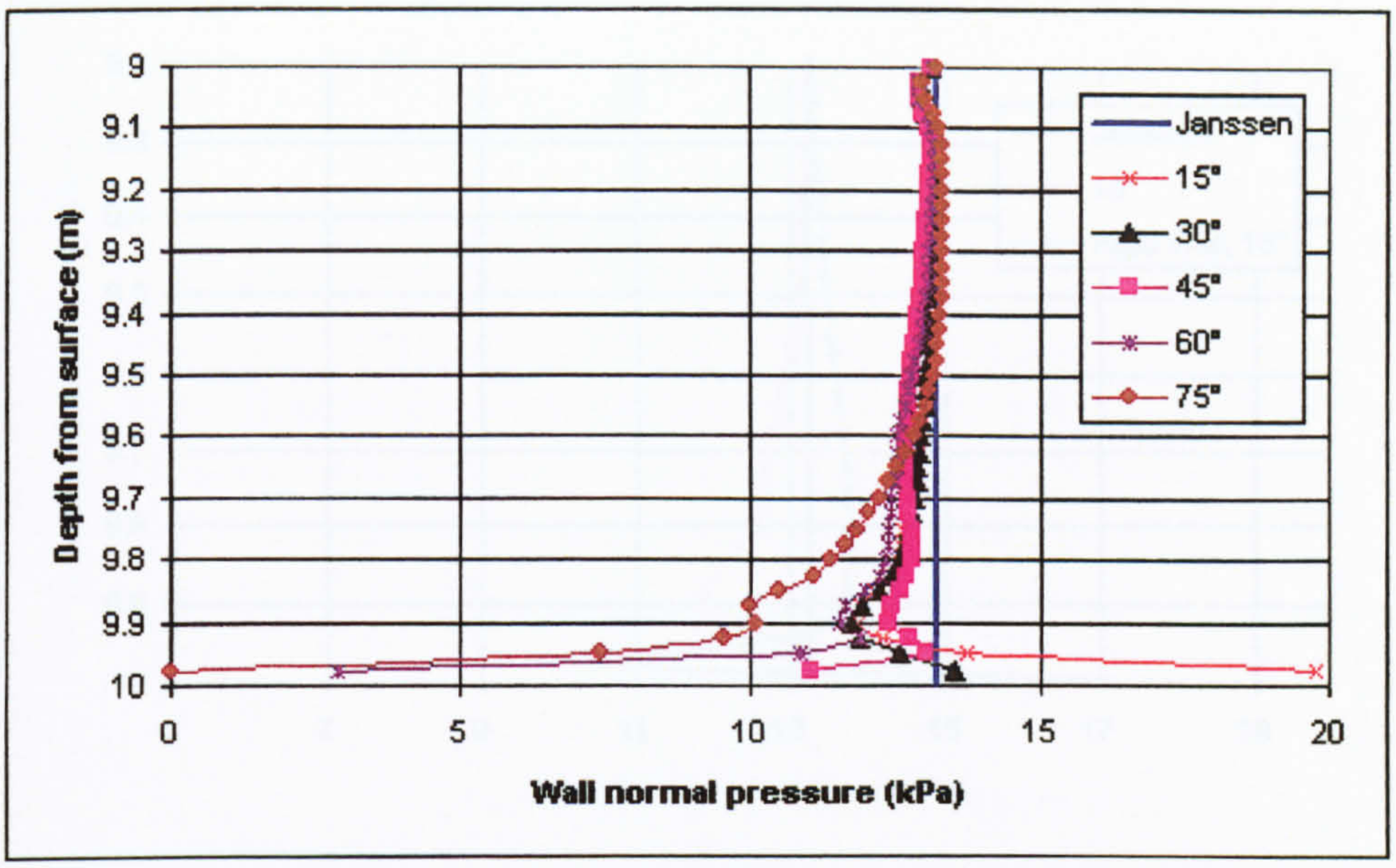

Figure 7.17 – The effect of altering the angle of the hopper on pressures above the transition

As the hopper angle increases there is a systematic reduction of wall pressure above the transition. Inspection of the vertical and radial strains in the model shows that outward deformation of the hopper leads to tensile vertical strain adjacent to the wall above the transition. A Poisson effect in this area leads to the reduced lateral pressures. If this mechanism is a correct representation of the actions occurring then a fully rigid hopper wall should lead to a situation where the vertical strain is compressive (since the hopper wall is no longer deforming) and an end-effect above the value of the Janssen prediction will be observed similar to the flat-bottomed model. The 15° hopper is therefore re-run with a fully rigid hopper wall and the results for the pressures above the transition are shown in figure 7.18.

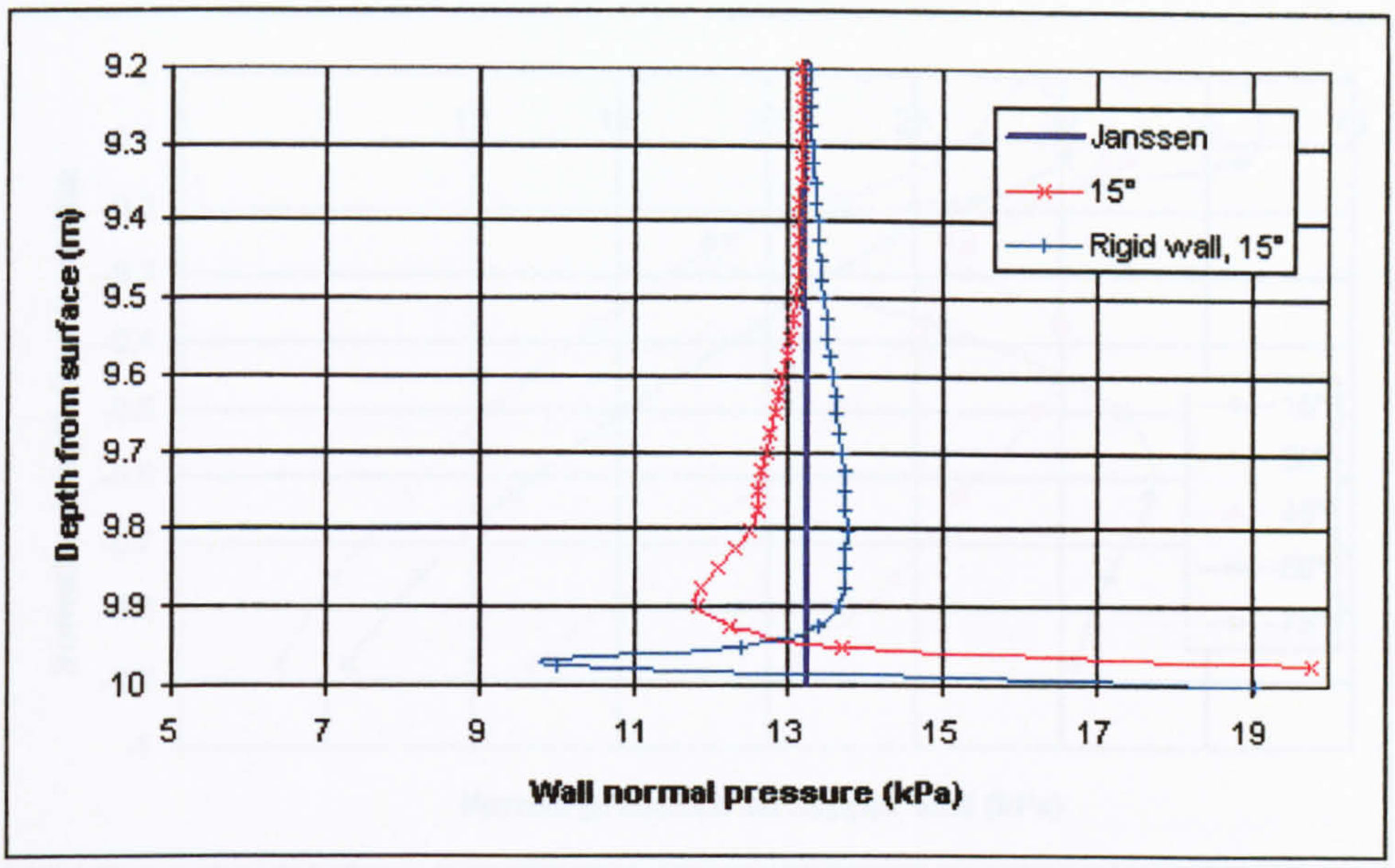

Figure 7.18 – The effect on wall pressures above the transition of a rigid hopper wall

As expected there is now an increase in lateral wall pressure and inspection of the strains in the material show that the mechanism proposed above is a good representation of the actions occurring.

7.5.1 Pressures in the hopper

In the previous section it was observed that even though the cylindrical hopper walls were modelled as 5mm thick there was still an effect on the pressures above the transition resulting from deformations in the hopper wall. It therefore follows that the deformations of the hopper wall will have an effect on the pressures in the hopper itself. Figure 7.19 shows the normal pressures in the hopper for the 5 angles chosen for the analysis. The results are presented in a plot of normalised depth below the transition level against the pressures. The pressure shown on the final node is disregarded as inspection of the results show this to be anomalous due to the way the contact surfaces are modelled in this area.

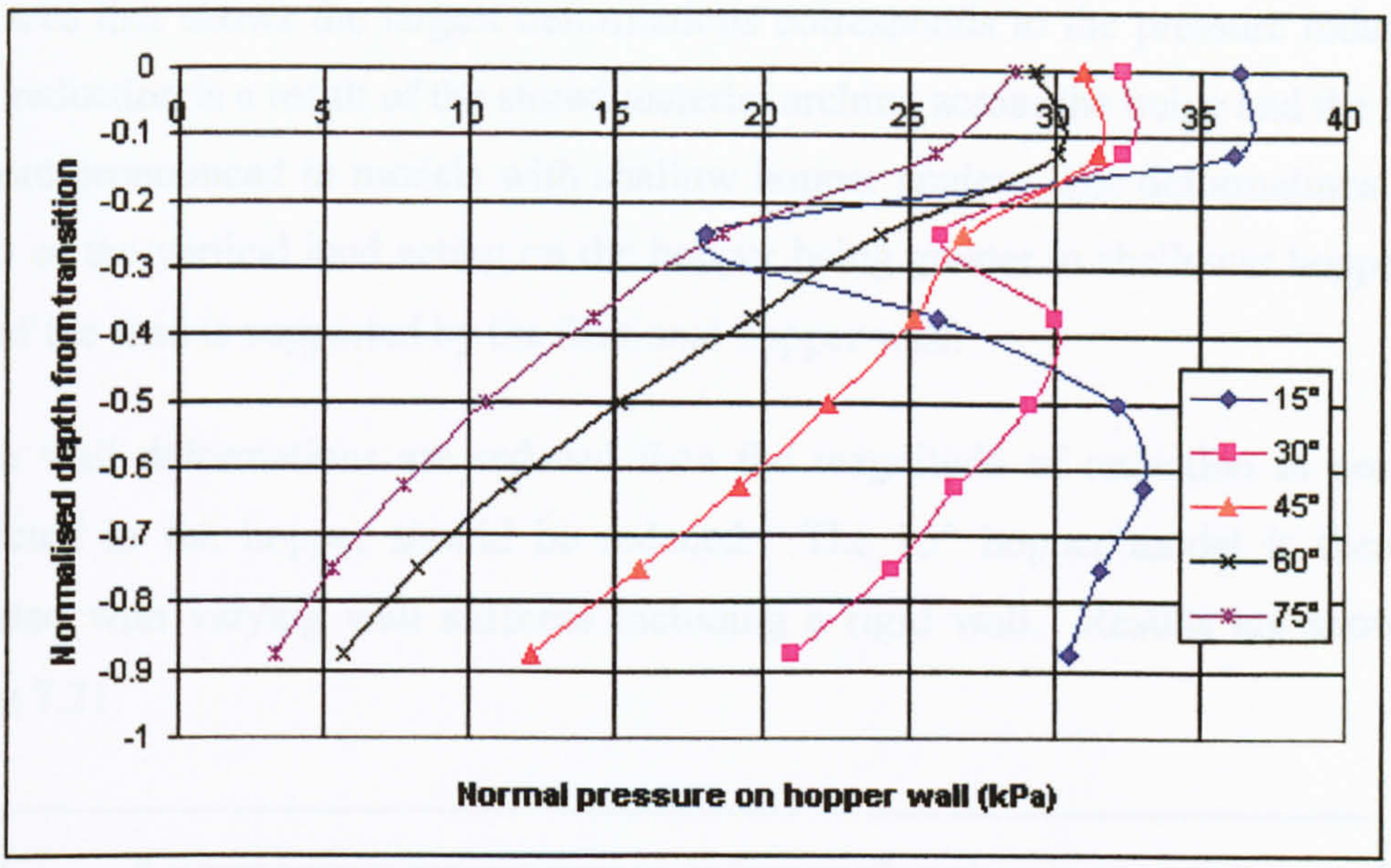

Figure 7.19 – Normal pressure in hoppers of varying angles

A pressure reduction just below the transition can be seen in the results for hoppers of shallow angles. Inspection of the deformed shape of the hopper wall shows that there is a deformation of the hopper wall away from the stored bulk solid in this area resulting in the observed lower pressure predictions. Figure 7.20 shows a much magnified plot of the wall deformations in the 15° hopper model.

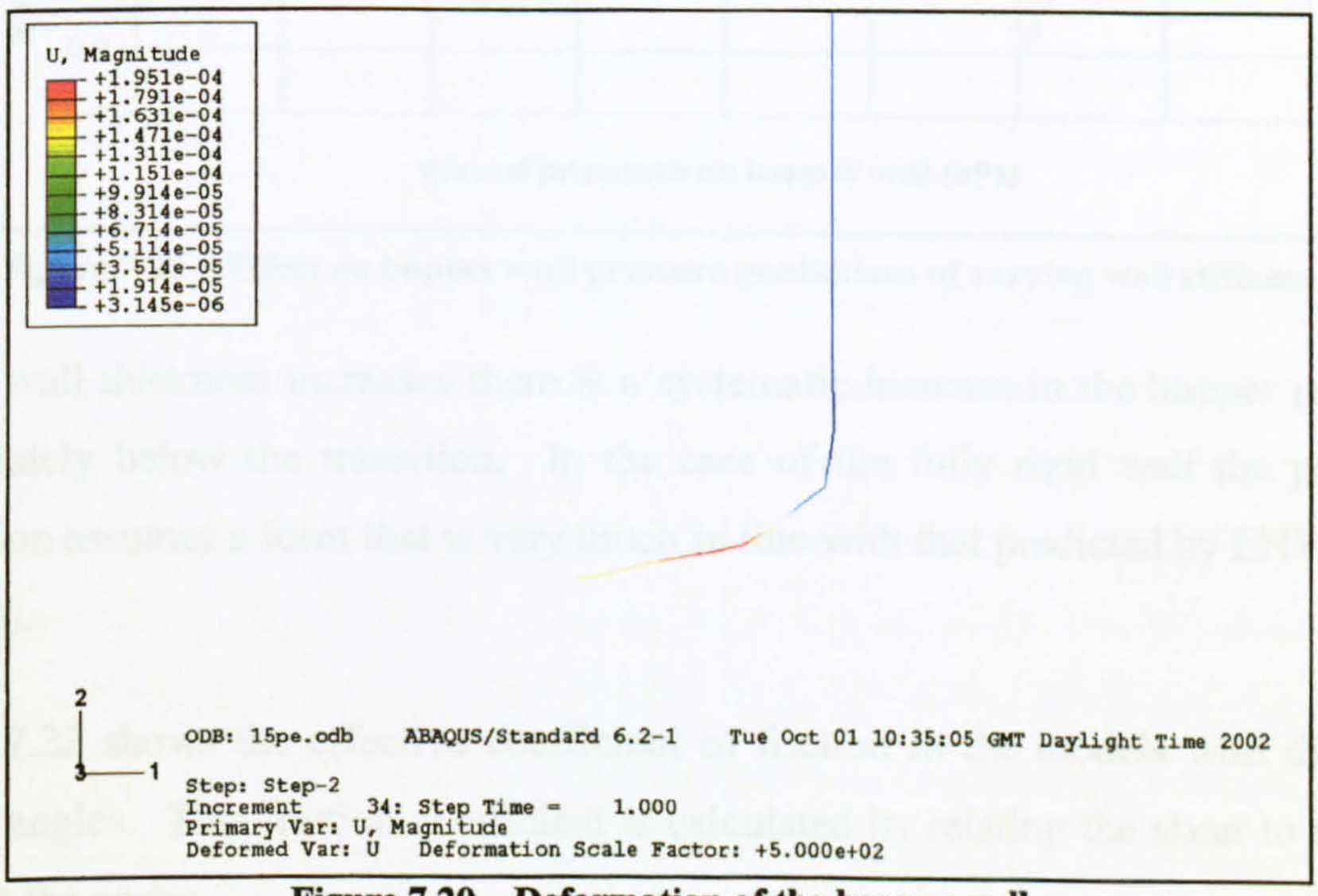

Figure 7.20 – Deformation of the hopper wall

The area that shows the largest deformations corresponds to the pressure reduction. This reduction is a result of the stored material arching across the bulge and the effect is more pronounced in models with shallow hopper angles. The deformations are a result of the vertical load acting on the hopper being greater in shallower hoppers as less of the load is supported by the frictional hopper wall.

If the wall deformations are reduced then the magnitude of reduction in pressure predicted in the hopper should be reduced. The 15° hopper model is therefore repeated with varying wall stiffness including a rigid wall. Results are shown in figure 7.21.

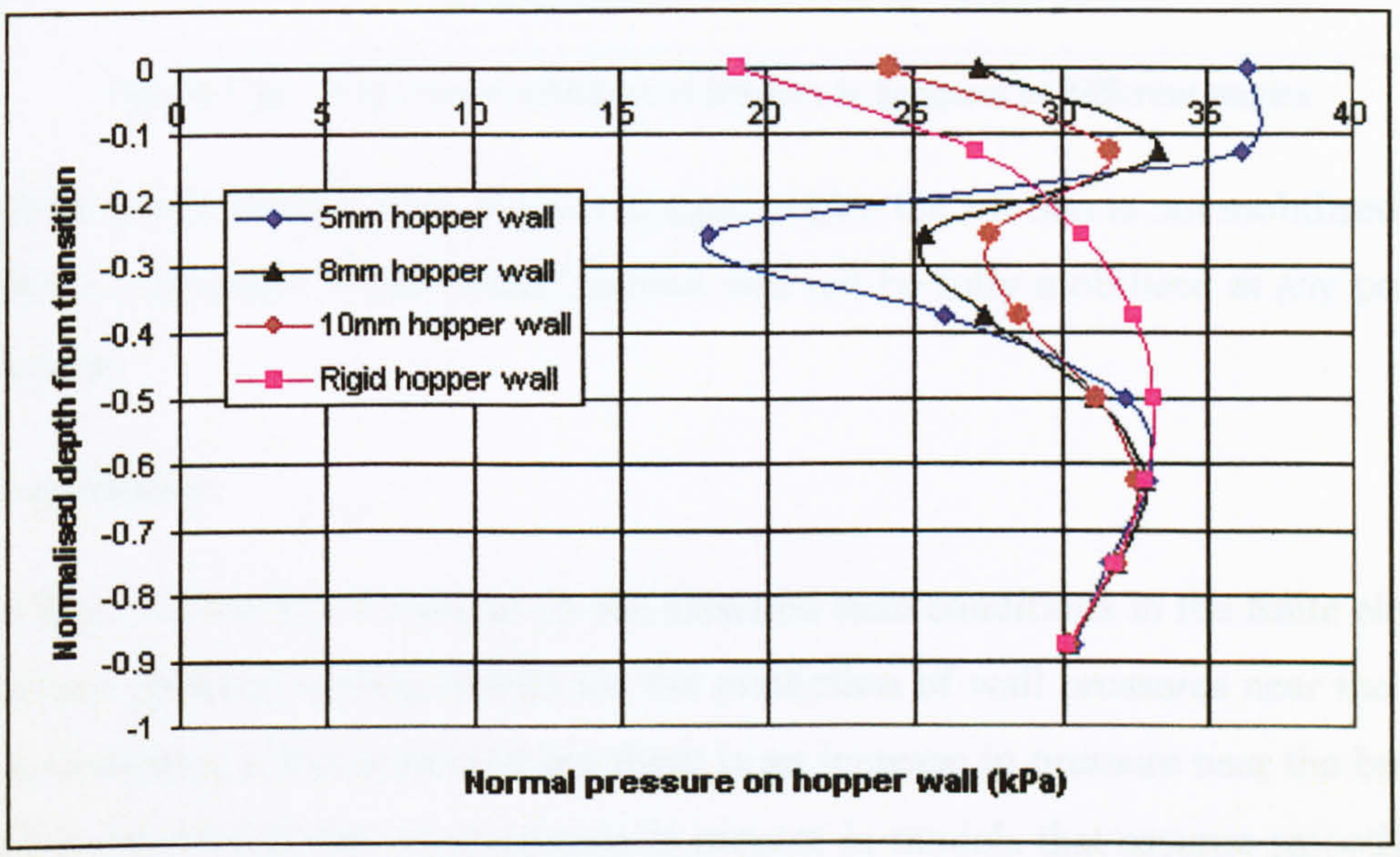

Figure 7.21 – Effect on hopper wall pressure predictions of varying wall stiffness

As the wall thickness increases there is a systematic increase in the hopper pressure immediately below the transition. In the case of the fully rigid wall the pressure prediction assumes a form that is very much in line with that predicted by ENV 1991-4 (1995).

Figure 7.22 shows the effective coefficient of friction in the models with different hopper angles. This friction coefficient is calculated by relating the shear to normal stress at the nodes.

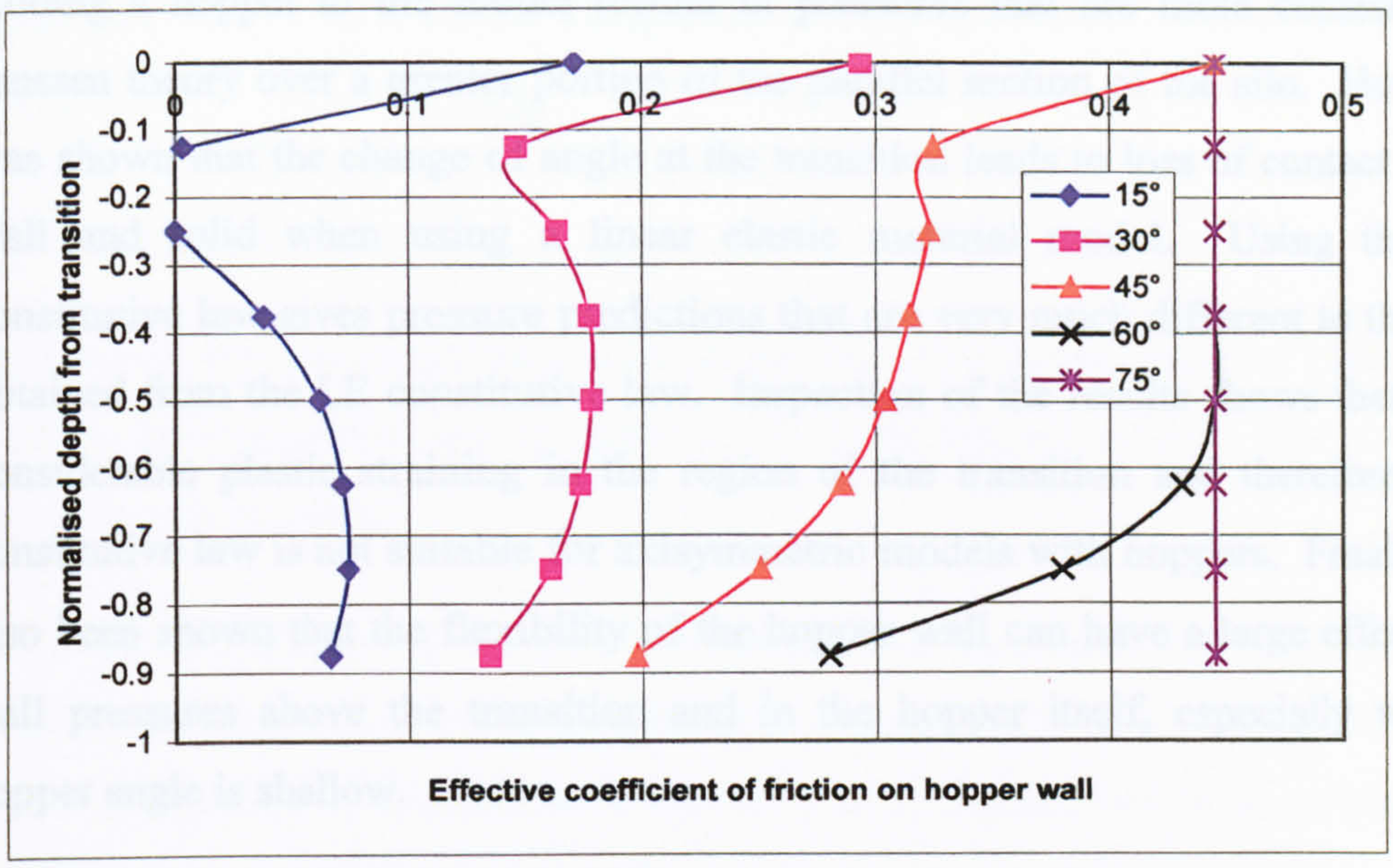

Figure 7.22 – Effective coefficient of friction in hoppers of different angles

It is clear that in models with shallow hopper angles the friction is not mobilised fully and there is an angle below which friction will not be fully mobilised at any point in the hopper.

7.6 Conclusion

It has been shown that variations in the assumed base conditions in the finite element model can produce varying results for the prediction of wall pressures near the base. When modelling a flat-bottomed bin there is an increase in pressure near the base. It has been shown that this phenomenon is present in models that assume smooth base conditions and frictional base conditions. A number of theoretical base conditions were also analysed in an attempt to determine a mechanism that explains the observed end effect. A suitable mechanism that accounts for the observed end-effects has been identified and with further testing appears sound. Based upon this mechanism it is proposed that a model with a reasonably flexible base and is supported at the edge could exhibit pressures very close to the Janssen prediction. As the load is applied the flexible base would deform reducing the effect that leads to the high vertical compressive strain at the centre of the bin. Such a model was attempted but elimination of the end-effect entirely was not possible.

Adding a hopper to the model results in pressures that are more consistent with Janssen theory over a greater portion of the parallel section of the silo. However, it was shown that the change of angle at the transition leads to loss of contact between wall and solid when using a linear elastic material model. Using the PEDP constitutive law gives pressure predictions that are very much different to the results obtained from the LE constitutive law. Inspection of the results shows that there is considerable plastic straining in the region of the transition and therefore the LE constitutive law is not suitable for axisymmetric models with hoppers. Finally, it has also been shown that the flexibility of the hopper wall can have a large effect on the wall pressures above the transition and in the hopper itself, especially when the hopper angle is shallow.

Chapter 8 - Further investigation of the geometry of Lahlouh *et al* (1995)

8.1 Introduction

In Chapter 6 some results for a small square silo using the geometry of Lahlouh *et al* (1995) were presented and compared to the finite element model. This comparison work is now extended.

As well as data giving the wall pressures in the bin, Lahlouh's work also gives detailed measurements of the stresses in the stored bulk solid. These values were used to investigate mechanisms of load transfer in the silo and to determine overall and local values of k for the materials.

Rotter *et al* (2002) analysed the data of Lahlouh *et al* (1995) and proposed an empirical rule to predict wall normal pressures in a square silo from two parameters. This proposed rule is now compared to the finite element results for various ensiled materials.

8.2 Patterns of vertical stress in the stored material

Chapter 6 presented some basic comparisons between experimental work (Lahlouh *et al*, 1995) and the finite element results. This showed that, for wall normal pressures, the finite element model and the experimental data showed a good level of agreement down and across the bin wall. From measurements made with free field cells the experimental work showed the horizontal and vertical stress levels in the stored solid to be non-uniform at a given level. In subsequent work Rotter *et al* (2002) proposed a mechanism to account for the observed internal stress patterns. These internal stresses lead to the wall pressures already discussed.

Based upon the experimental observations, Rotter *et al* (2002) proposed the arching mechanism (shown pictorially in figure 8.1) to explain the patterns of stress in the solid. This shows the stored granular bulk solid arching between the structurally stiff corners of the silo. The load caused by the weight of the material being transferred to

these structurally stiff areas results in higher stresses in the stored solid nearer the corner and lower internal stresses nearer the midside of the bin wall. Evidence of this load transferral is obtained from the observed wall pressure distributions and higher vertical stresses near the corners of the silo.

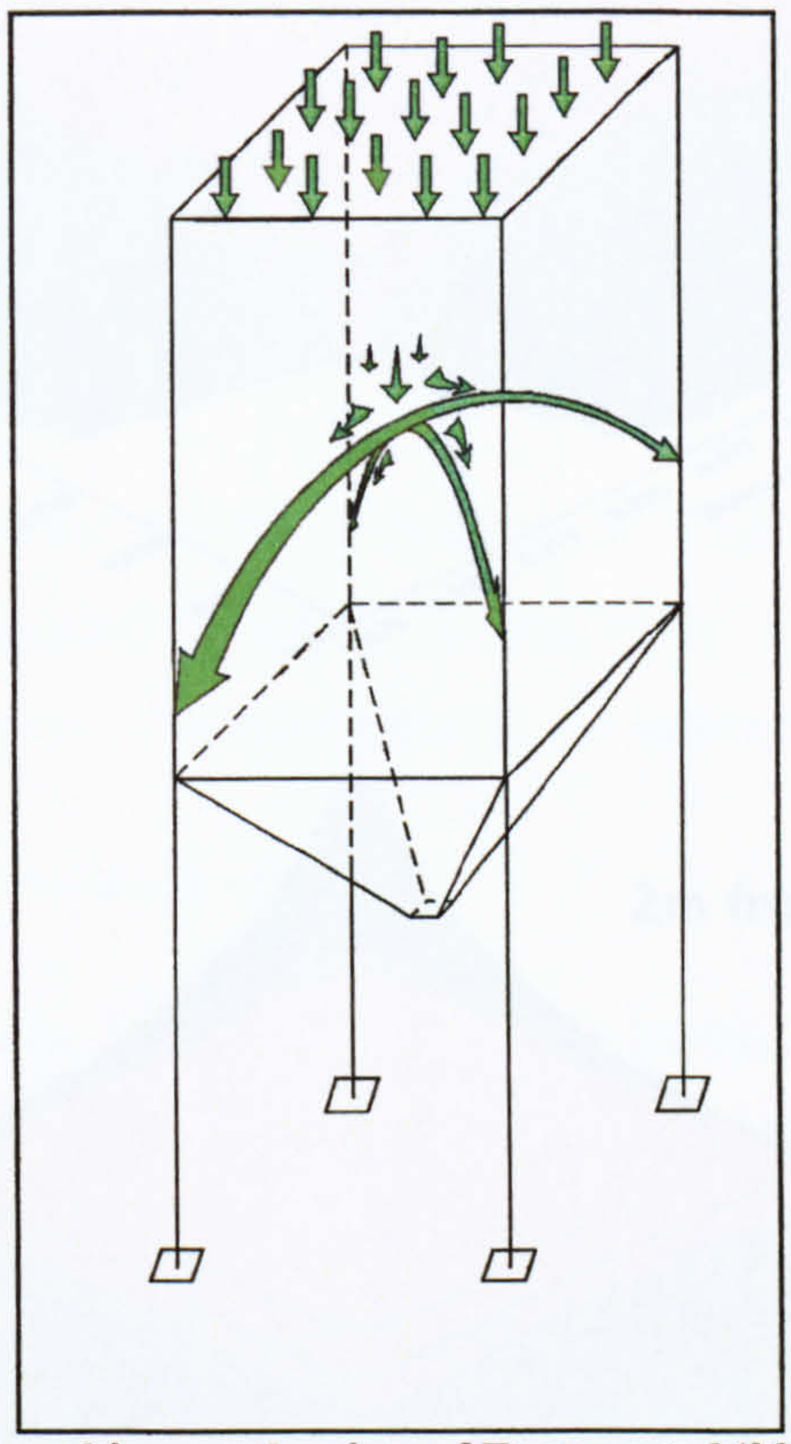

Figure 8.1 – Proposed arching mechanism of Rotter *et al* (2002) in rectangular silo

It is possible to compare the stress patterns in the granular bulk solid found in the work of Rotter *et al* (2002) with those produced by the finite element model. Figure 8.2 shows the vertical stress patterns in sand at two levels from the finite element model.

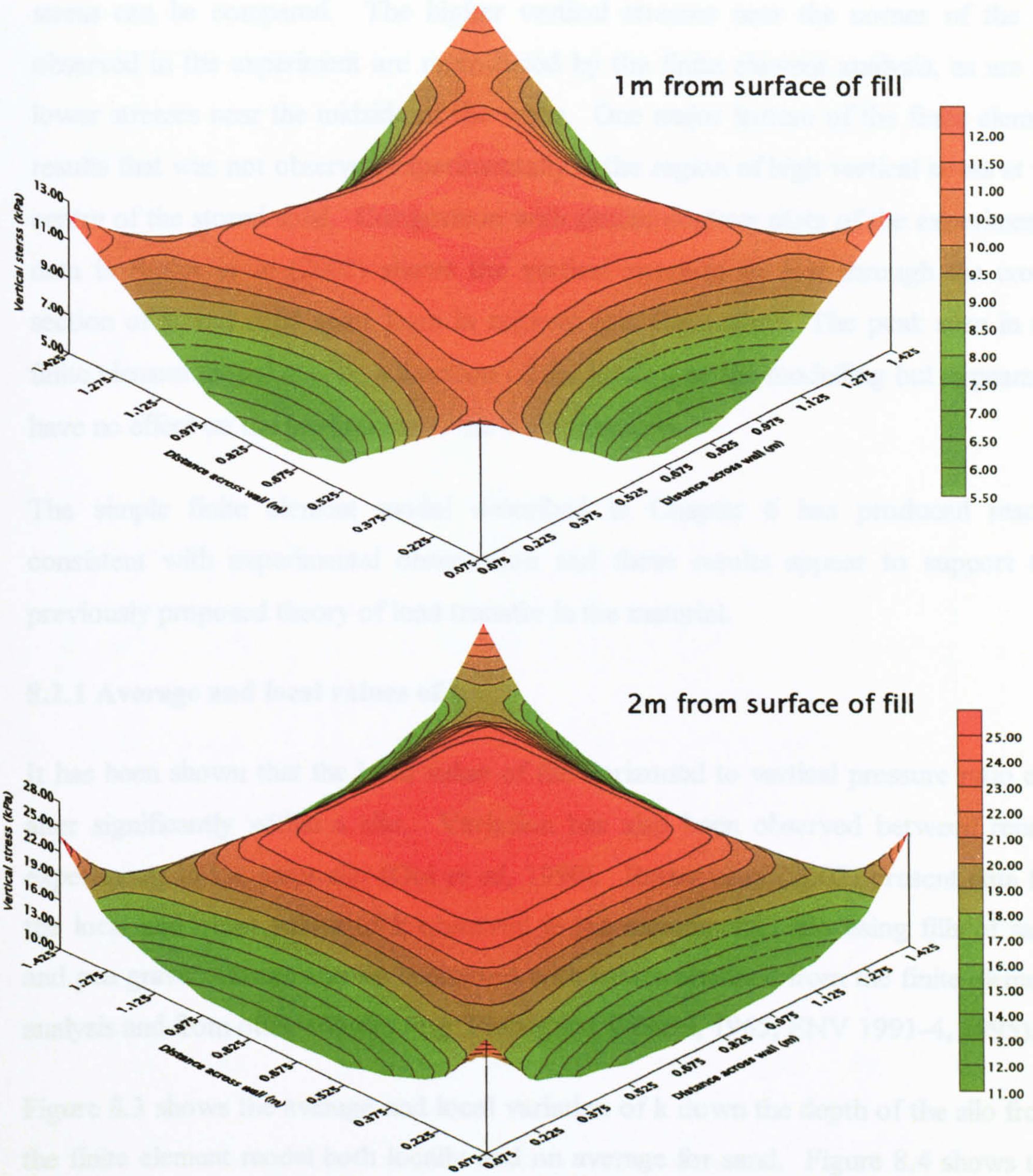

Figure 8.2 - Patterns of vertical stress at 1m and 2m below the surface of the solid

Direct comparison between the experimental and finite element results for these vertical stress readings is relatively meaningless. The fill method and nature of the stored material in the experiment means that repeatability is difficult to achieve no matter how carefully the experiment is performed. This random feature is difficult to recreate in the finite element analysis which will always produce the same results given the same materials, boundary conditions etc. However, the general patterns of

stress can be compared. The higher vertical stresses near the corner of the bin observed in the experiment are reproduced by the finite element analysis, as are the lower stresses near the midside of the walls. One major feature of the finite element results that was not observed experimentally is the region of high vertical stress at the centre of the stored solid. Comparison with similar contour plots of the experimental data in Rotter *et al* (2002) shows the vertical stress to be low through the cross-section of stored solid apart from in regions near the corner. The peak seen in the finite element model may be a function of the loading or the modelling but appears to have no effect on the predictions of the wall pressures.

The simple finite element model described in Chapter 6 has produced results consistent with experimental observation and these results appear to support the previously proposed theory of load transfer in the material.

8.2.1 Average and local values of k

It has been shown that the local value of the horizontal to vertical pressure ratio can alter significantly within a silo. Variation has also been observed between repeat experiments in the same silo (Ooi *et al*, 1990). Rotter *et al* (2002) present data for the local and mean values of k observed in the experimental silo using fills of sand and pea gravel. These may be compared with values obtained from the finite element analysis and from other sources (e.g. Pieper and Wenzel, 1965; ENV 1991-4, 1995).

Figure 8.3 shows the average and local variation of k down the depth of the silo from the finite element model both locally and on average for sand. Figure 8.4 shows the same for gravel. In both figures the Rankine active ratio of k is plotted as well as k from a current design code (ENV 1991-4, 1995).

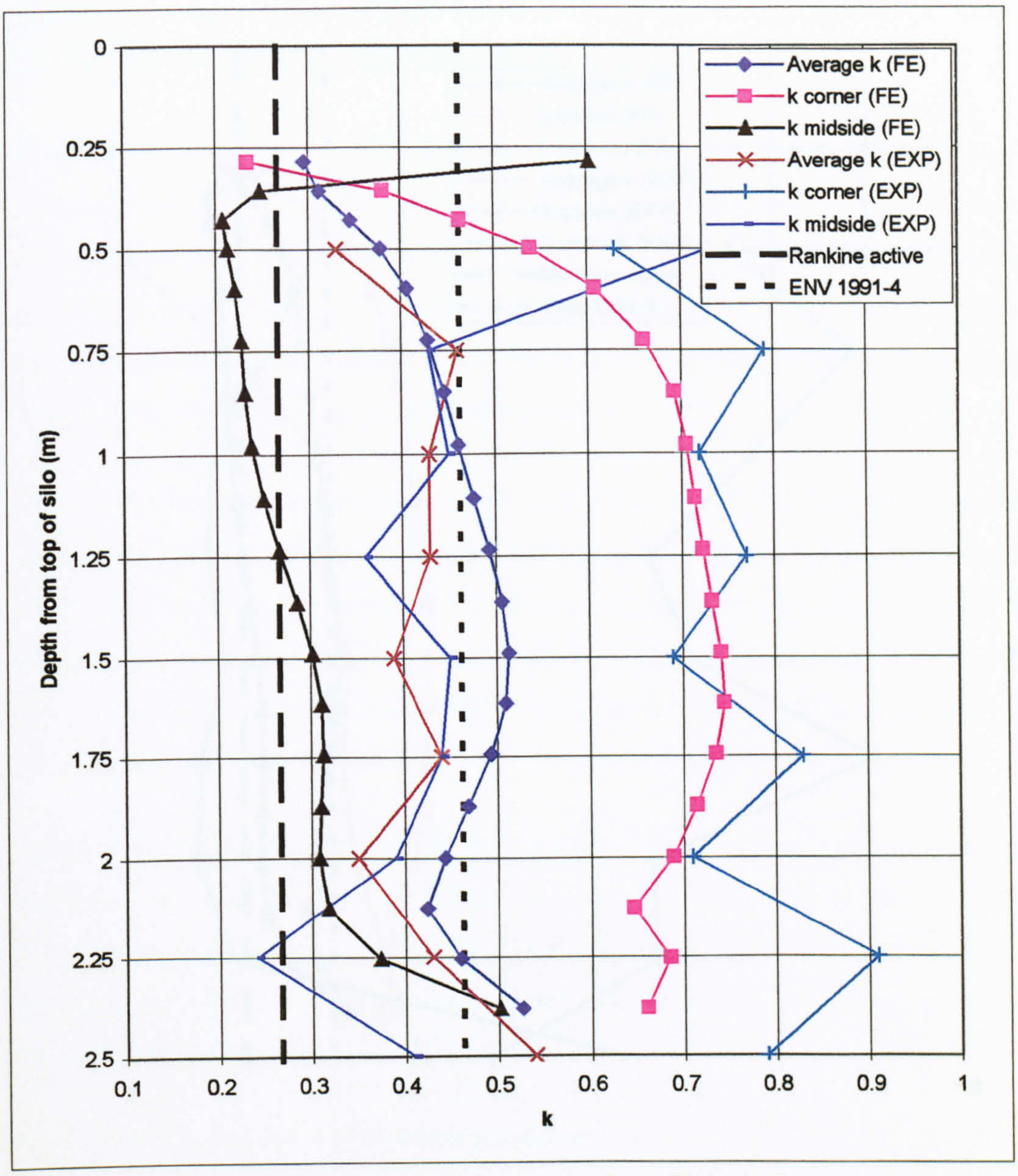

Figure 8.3 - Local and average values of k in sand

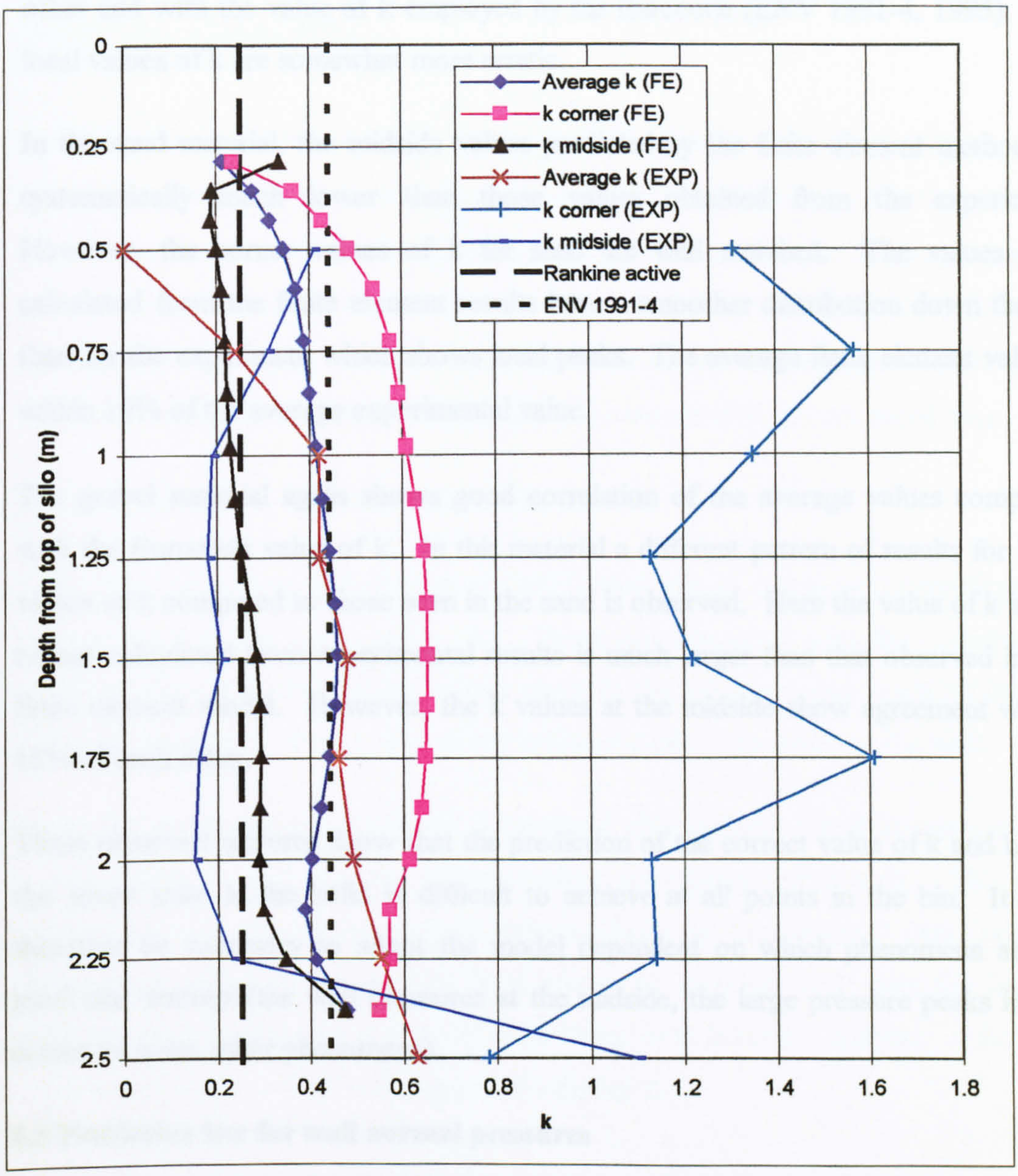

Figure 8.4 - Local and average values of k in gravel

It may first be noted that the value of k at the midside of the bin falls below the active Rankine value. This is a result of the Rankine active value being calculated from a Mohr-Coulomb value of internal friction whereas these predictions are from a Drucker-Prager model which does not match the Mohr-Coulomb at all points (figure 5.16).

The above graphs show that the average values of k determined from the finite element results and the experimental values show acceptable correlation with each

other and with the value of k employed by the Eurocode (ENV 1991-4, 1995). The local values of k are somewhat more erratic.

In the sand material, the midside values predicted by the finite element method are systematically much lower than those values obtained from the experiment. However, the corner values of k for sand are well matched. The values of k calculated from the finite element results have a smoother distribution down the bin than for the experiment which shows local peaks. The average finite element value is within 10% of the average experimental value.

The gravel material again shows good correlation of the average values compared with the Eurocode value of k. In this material a different pattern of results for local values of k compared to those seen in the sand is observed. Here the value of k in the corner calculated from experimental results is much larger than that observed in the finite element model. However, the k values at the midside show agreement within 15% of each other.

These observed patterns show that the prediction of the correct value of k and hence the stress state in the solid is difficult to achieve at all points in the bin. It may therefore be necessary to adapt the model dependent on which phenomena are of particular interest (the wall pressures at the midside, the large pressure peaks in the corner or some other phenomena).

8.3 Predictive law for wall normal pressures

Based upon the experimental measurements of Lahlouh *et al* (1995), Rotter *et al* (2002) proposed an empirical model to determine the pressure distribution across the wall in a square planform silo at a given level. This two parameter model was based upon a least squares fit to the experimental data and the resulting equation is a hyperbolic function based upon the mean pressure and some coefficient α. This coefficient α will be referred to as the redistribution parameter. The equation is given as 8.1 below.

$$p = p_m\left(\frac{\alpha}{\sinh\alpha}\right)\cosh\left(\frac{2\alpha x}{d}\right) \tag{8.1}$$

p_m is the mean wall pressure, x is the horizontal distance from the centreline of the silo and d is the width of the silo side. The ratio of the mid-side to corner pressure in the silo is given as cosh α. Rotter *et al* (2002) deduced that for the tests based on sand the value of α was about 2.5 and the value for gravel was about 2. This implies that sand shows a higher level of redistribution across the bin wall than gravel. Using these values, distributions can be calculated and compared to the measured data.

8.3.1 Comparison to experimental results in sand

From the values given by Rotter *et al* (2002) wall normal pressure distributions can be determined at any depth in the silo. These are compared with the experimental results to show that the guidance values given in the original paper could be used by structural designers to give an idea of the redistribution of pressure on the wall.

Figure 8.5 shows the experimentally determined distribution of wall normal pressure at two levels in sand and the corresponding calculated distribution. The mean pressure (p_m) is taken as the average pressure from the experimental data (given in Rotter *et al*, 2002) but as this has been shown to compare well with the Janssen value, this could be taken if the model were being used in design analysis. α for sand is taken as Rotter *et al*'s (2002) suggested value of 2.5.

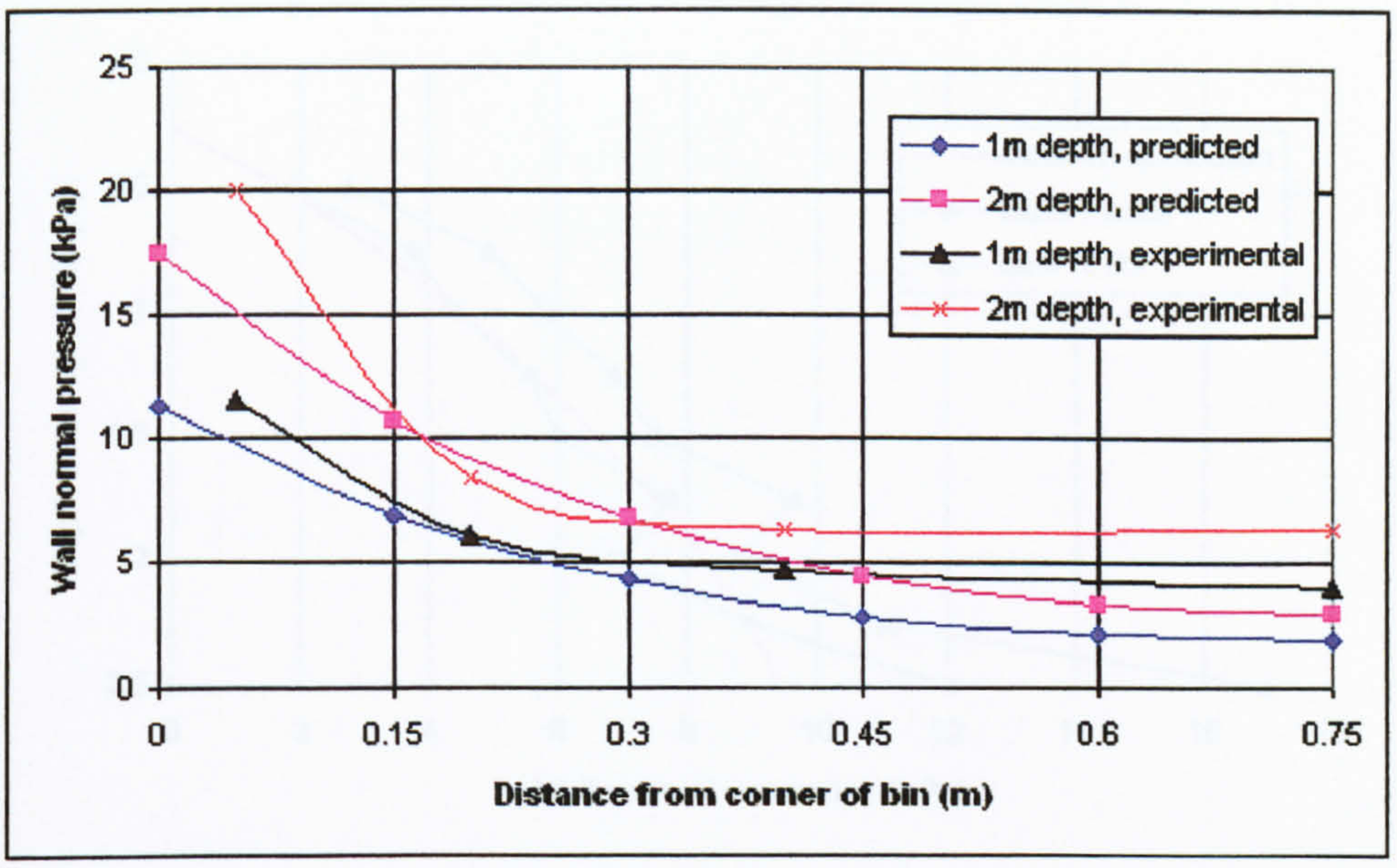

Figure 8.5 - Wall pressure distributions from sand experiments and predictive law

Figure 8.5 shows that the results from the predictive law (equation 8.1) are of a similar form to those observed in the experiment with a large pressure near the corner of the bin and lower pressures at the midside. The values of wall normal pressure at the centre of the bin are underestimated by the predictive law (similar to the observed trend in the initial finite element results) and using the suggested value of α also results in the corner pressure predictions being underestimated.

It must be noted that these distributions were generated using the suggested value of $\alpha = 2.5$. A better fit of the predictions to the experimental data could be achieved by varying α and p_m. A fitting exercise using the least squares method was performed between the experimental and predictive data for sand. Figure 8.6 shows the values of p_m produced by the least squares method compared to the Janssen distribution for sand. For comparison the integrated experimental data is also plotted on this graph (taken from Rotter *et al*, 2002). As before, the results are shown as a function of depth from the top of the silo as per the original paper (Rotter *et al*, 2002) rather than depth from surface of fill.

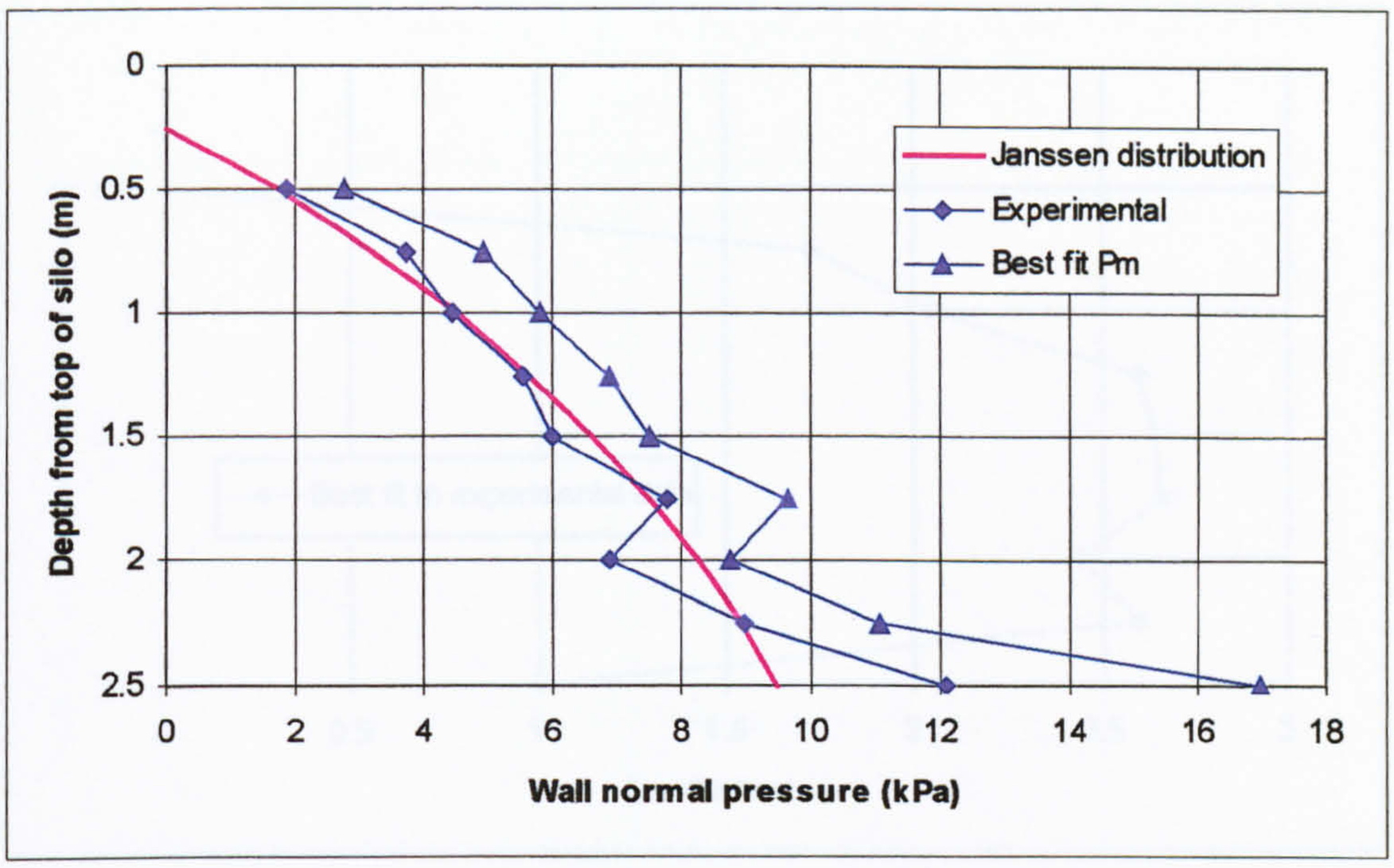

Figure 8.6 - Best fit mean pressures in sand

The values of p_m given by the best fit exercise are systematically around 20% higher than those determined from the original integration of the experimental data although the Janssen form of distribution remains. This may due to the experimental results not extending the full way across the wall (the first data point is not directly in the corner). In order to perform the integration in the paper Rotter *et al* (2002) assumed that the corner value was the same as that measured 0.05m from the wall. The predictive law gives a value of wall normal pressure in the very corner of the bin. This value will be higher than that assumed in the original integration leading to an increase in the area under the curve compared to the original data and hence a larger pressure.

Figure 8.7 shows the best fit distribution in sand of the redistribution parameter α down the depth of the bin.

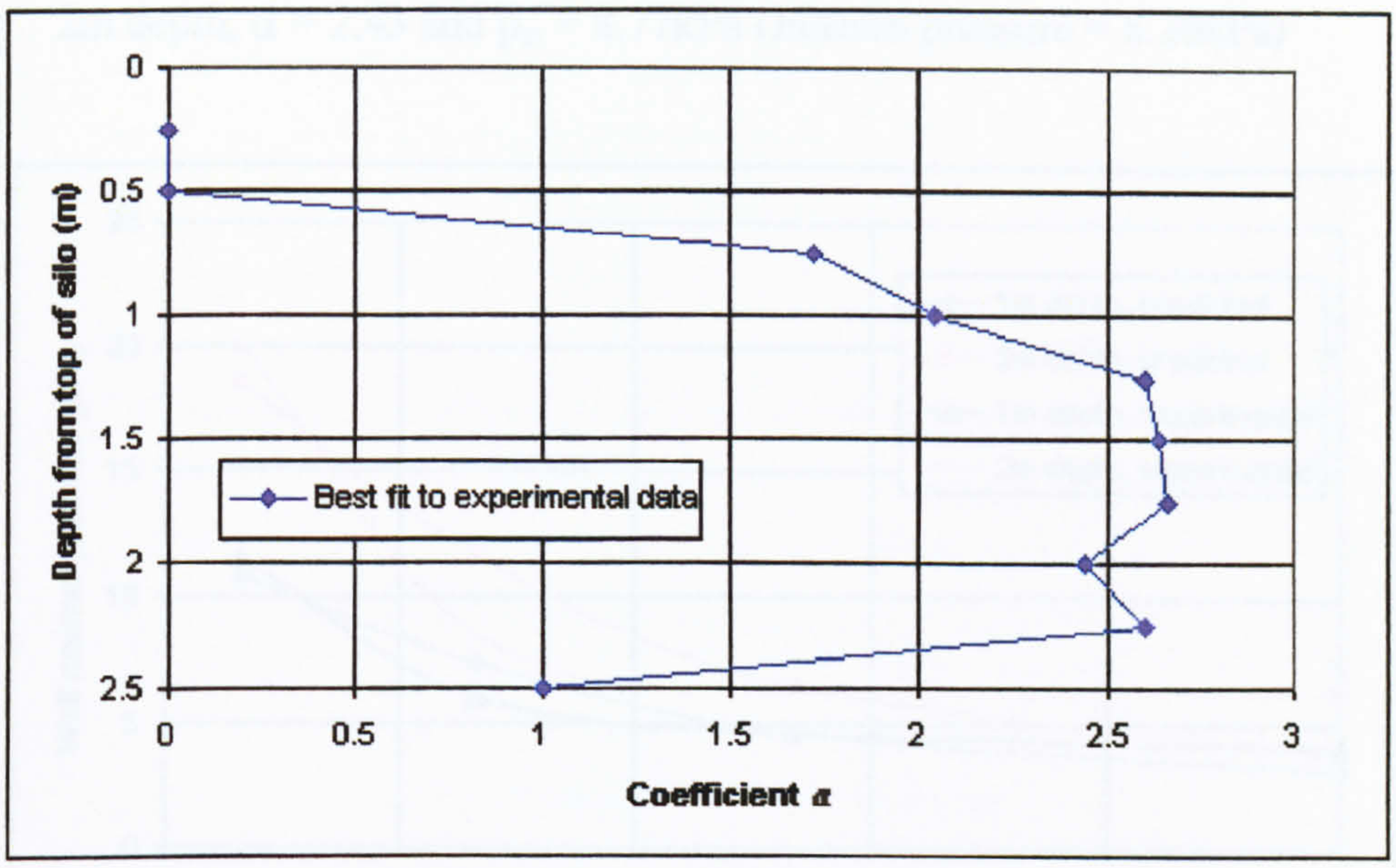

Figure 8.7 - The variation of the parameter α with depth in sand in the geometry of Lahlouh *et al* (1995)

Figure 8.7 clearly shows how the original recommendation of $\alpha = 2.5$ for sand was determined. α is close to 2.5 over a large percentage of the bin wall. It deviates away from this value nearer the surface and towards the transition. This deviation can be attributed to the end effects caused by these boundary conditions. It would be necessary to study a deeper silo in order to determine whether α remains stable for a larger portion of the bin (Chapter 9).

Using the values of α and p_m determined from the best fit exercise it is again possible to compare the predicted pressure distributions across the wall with the experimental values. Figure 8.8 shows this comparison at two different levels in the sand. The values of p_m and α as determined from the best fit exercise at these two levels are given below along with the appropriate Janssen wall normal pressure value for this depth for comparison.

- 1m depth; $\alpha = 2.05$ and $p_m = 5.81$kPa (Janssen pressure = 4.51kPa)

- 2m depth; $\alpha = 2.43$ and $p_m = 8.77$kPa (Janssen pressure = 8.26kPa)

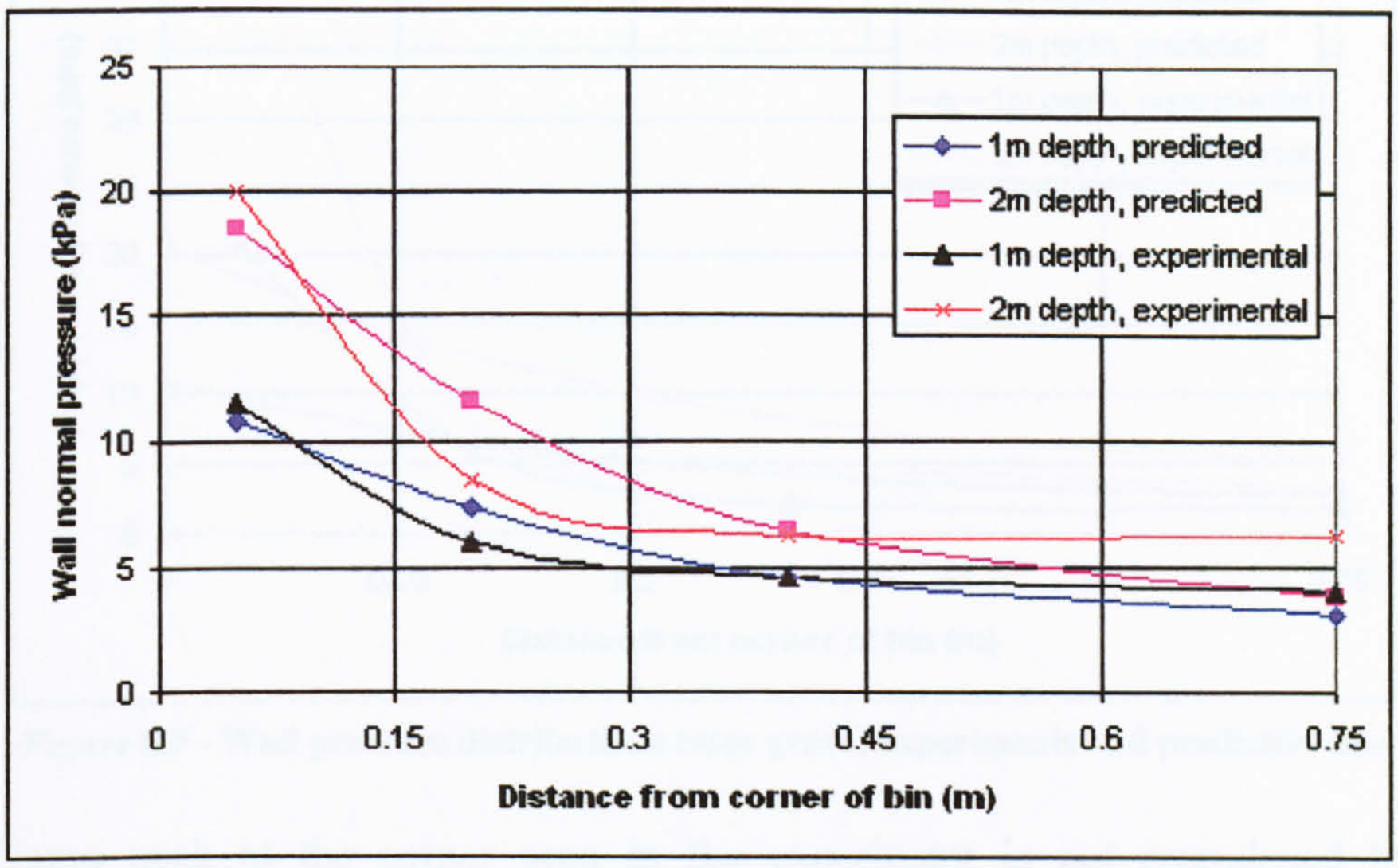

Figure 8.8 – Predicted distribution resulting from best fit value of α compared to original experimental data for sand (Lahlouh *et al*, 1995)

The predictive law now shows a value of pressure at the corner of the bin that is closer to the experimentally determined value. The form of the predictive law does not show as sharp a curve as the experimental data as the corner of the bin is approached. Again the pressures predicted at the midside are much lower than those shown in the experiment. The agreement between the results for 1m depth would appear visually better than those at 2m. This may be because of a possible end effect as the transition/hopper is approached. Due to the ring beam in the experimental rig the transition has a higher local stiffness than the rest of the bin which affects the distribution across the bin at this level.

8.3.2 Comparison to experimental results in gravel

A similar exercise to the one above was performed on the data for gravel. Rotter *et al* (2002) predicted a value of $\alpha = 2$ for this material. Figure 8.9 shows the experimental data compared to the predictive law for two depths using the value of $\alpha = 2$.

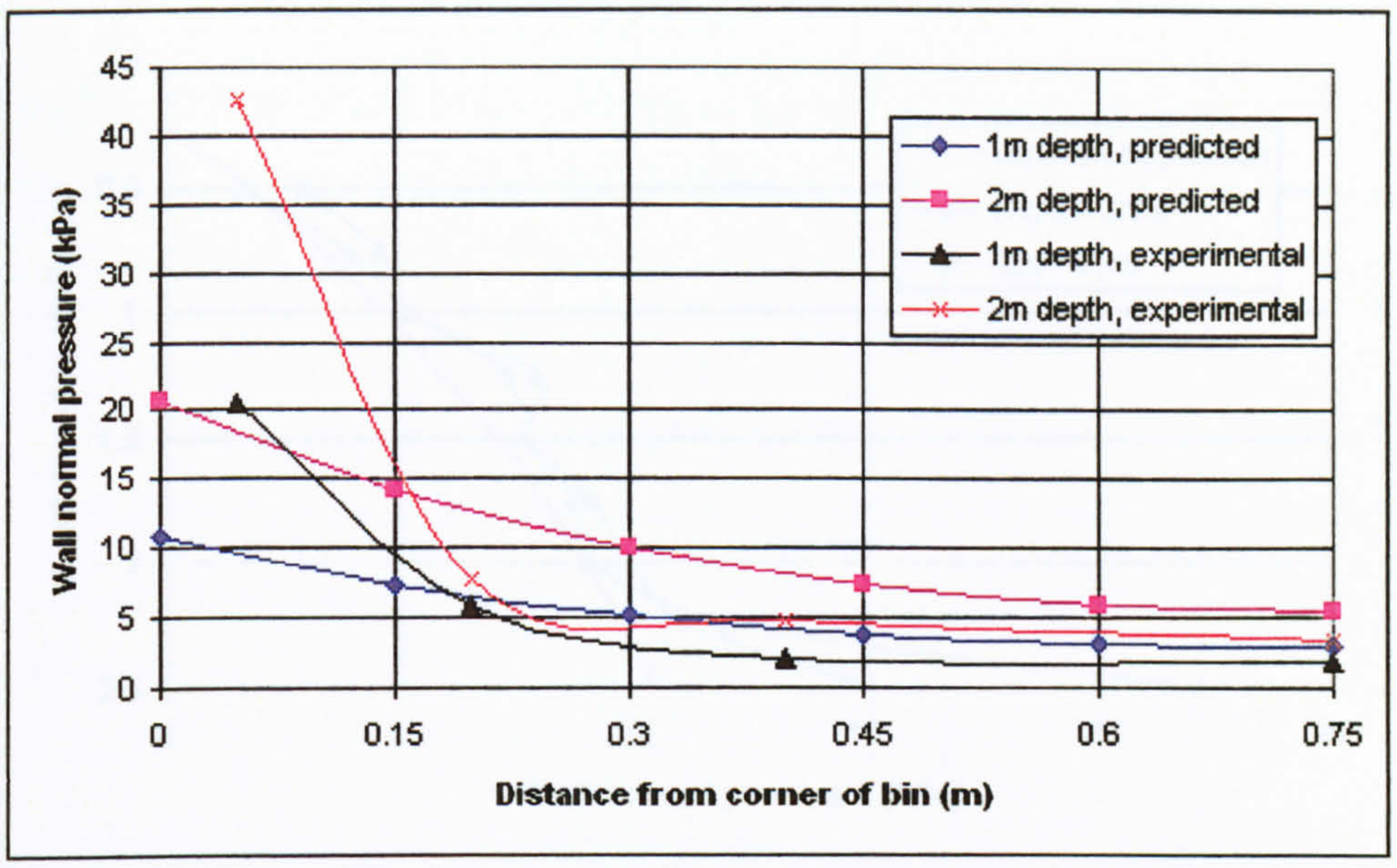

Figure 8.9 - Wall pressure distributions from gravel experiments and predictive law

The large peak at the corner seen in the experiment is not reproduced by the predictive law using the suggested value of α and the overall form of the prediction is not as curved as the experimental results. However, the predictive law does not underestimate the pressures at the midside as it did for the sand. This is advantageous from a design point of view for reasons already mentioned.

Figure 8.10 shows the best fit values of p_m against the Janssen distribution and the original integrated values for gravel.

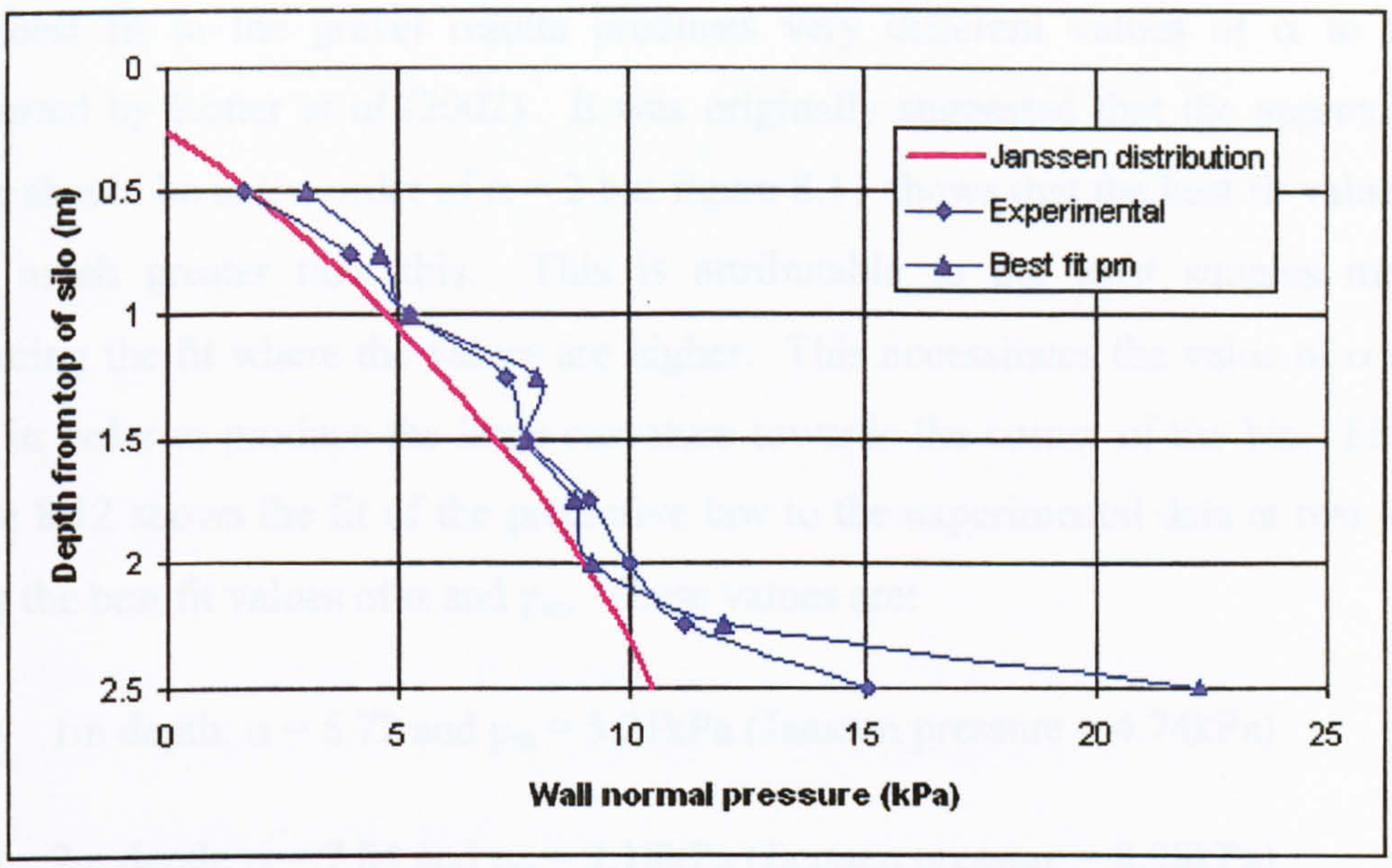

Figure 8.10 – Best fit values of p_m against experimental data and Janssen distribution

In this case the values of p_m produced by the best fit exercise do not produce the systematically higher results seen in the results for sand, the values are closer to the original experimental average but with some variation down the depth of the bin.

Figure 8.11 shows the corresponding best fit values of α.

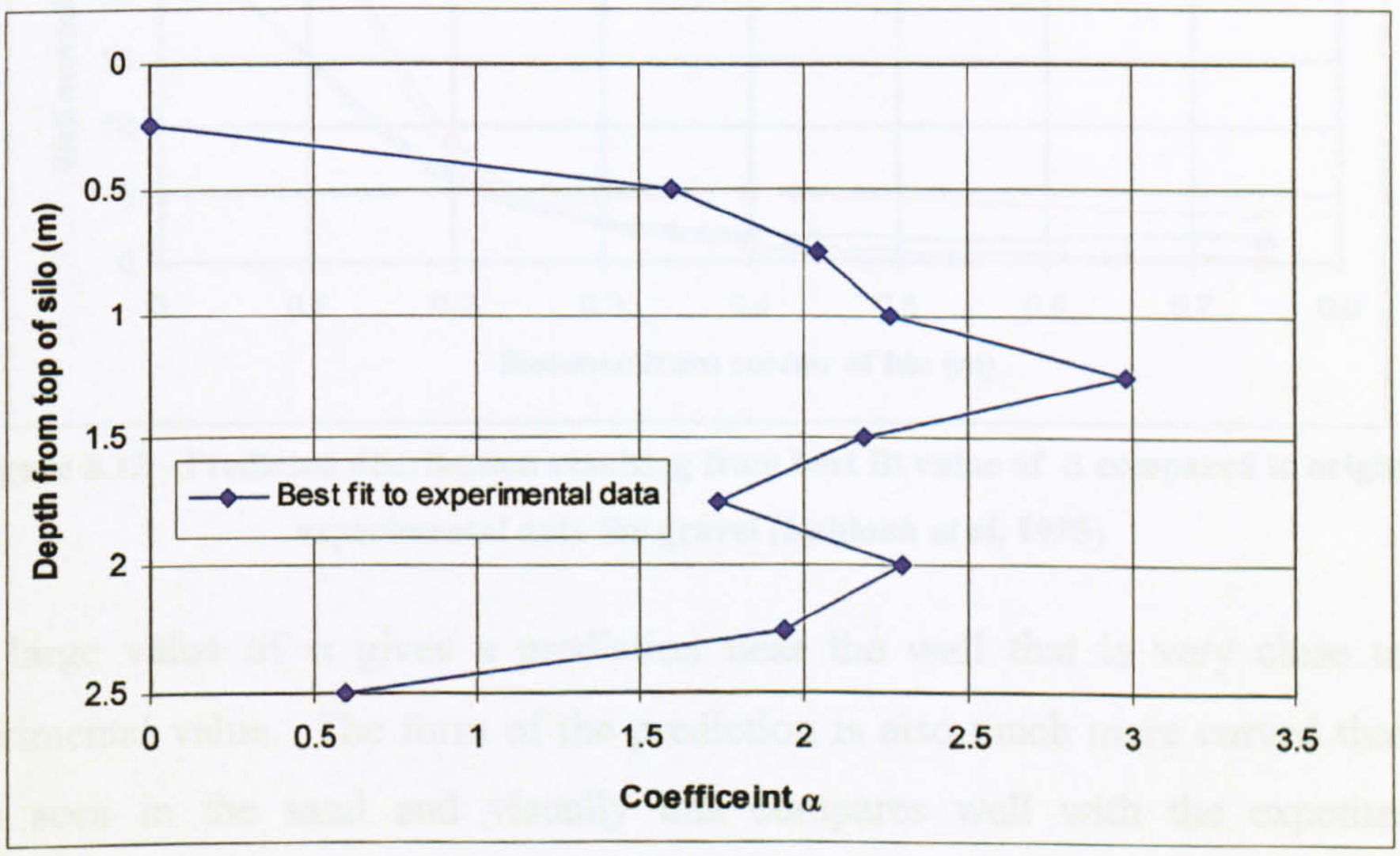

Figure 8.11 - The variation of the parameter α with depth in gravel in the geometry of Lahlouh *et al* (1995)

The best fit to the gravel results produces very different values of α to those suggested by Rotter *et al* (2002). It was originally suggested that the approximate value should be in the order of $\alpha = 2$ but figure 8.11 shows that the best fit values are very much greater than this. This is attributable to the least squares method favouring the fit where the values are higher. This necessitates the value of α to be high in order to produce the large curvature towards the corner of the bin. Finally, figure 8.12 shows the fit of the predictive law to the experimental data at two levels using the best fit values of α and p_m. These values are:

- 1m depth; $\alpha = 5.72$ and $p_m = 5.21$kPa (Janssen pressure = 4.74kPa)
- 2m depth; $\alpha = 7.84$ and $p_m = 9.18$kPa (Janssen pressure = 8.98kPa)

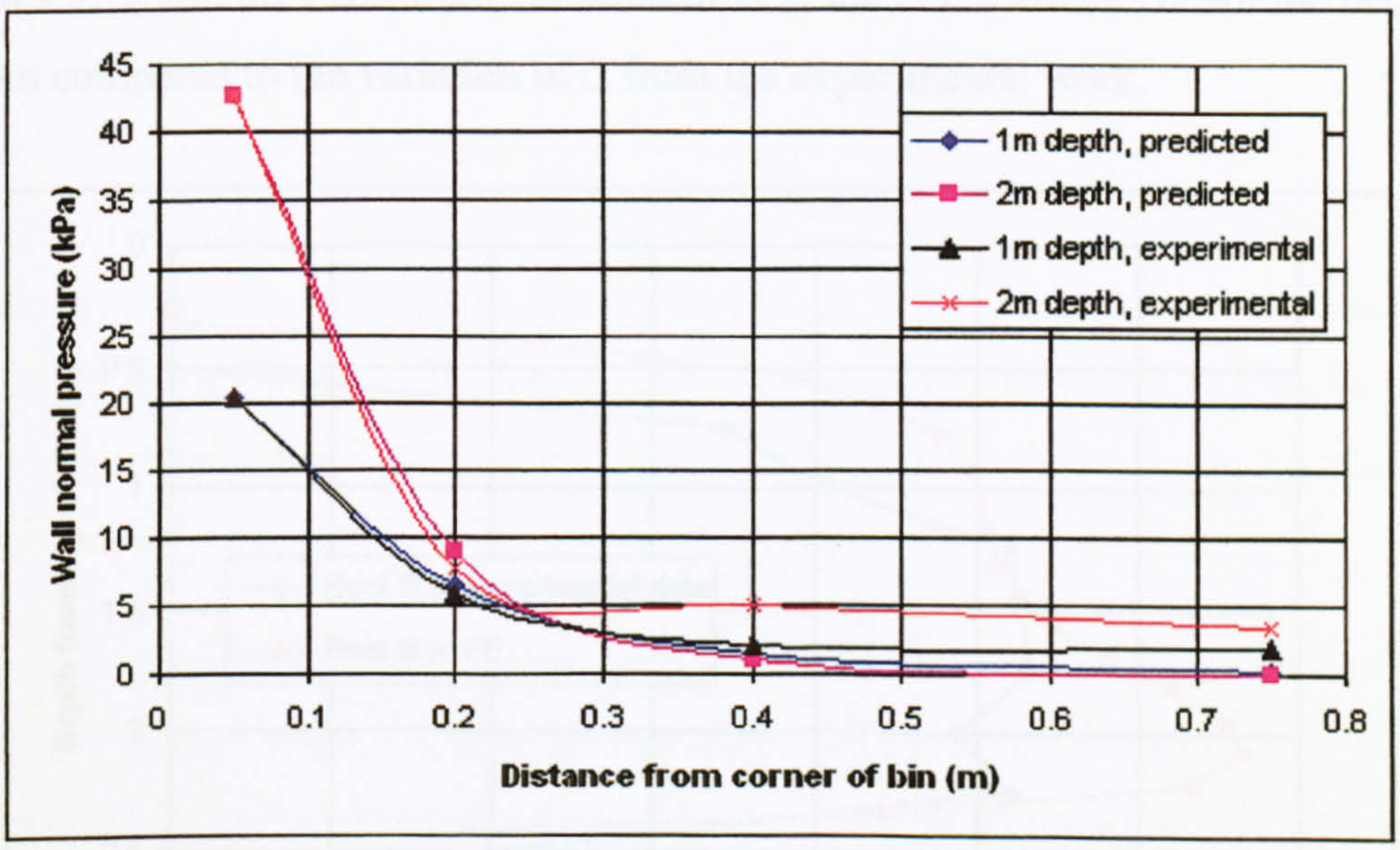

Figure 8.12 - Predicted distribution resulting from best fit value of α compared to original experimental data for gravel (Lahlouh *et al*, 1995)

The large value of α gives a prediction near the wall that is very close to the experimental value. The form of the prediction is also much more curved than the form seen in the sand and visually this compares well with the experimental observations. The high value of α causes the values of pressure predicted at the centre of the bin to be substantially lower than those measured in the experiment.

8.4 Comparison with finite element results

Using the previously described finite element model of Lahlouh *et al*'s (1995) experimental work, predictions for the wall pressures have been produced using the two different ensiled materials. The pressure distribution across the wall compared to the experimental data has already been examined in section 6.6.3 for sand and 6.6.5 for gravel. Here, Rotter *et al*'s (2002) predictive law will be compared with the finite element results.

A similar least squares best fit exercise to the one above was performed to fit the predictive law to the finite element results. This gives values of α and p_m that may be compared with the experimental data.

Figures 8.13 and 8.14 show the variation of α in the two materials down the depth of the bin compared to the variation of α from the experimental work.

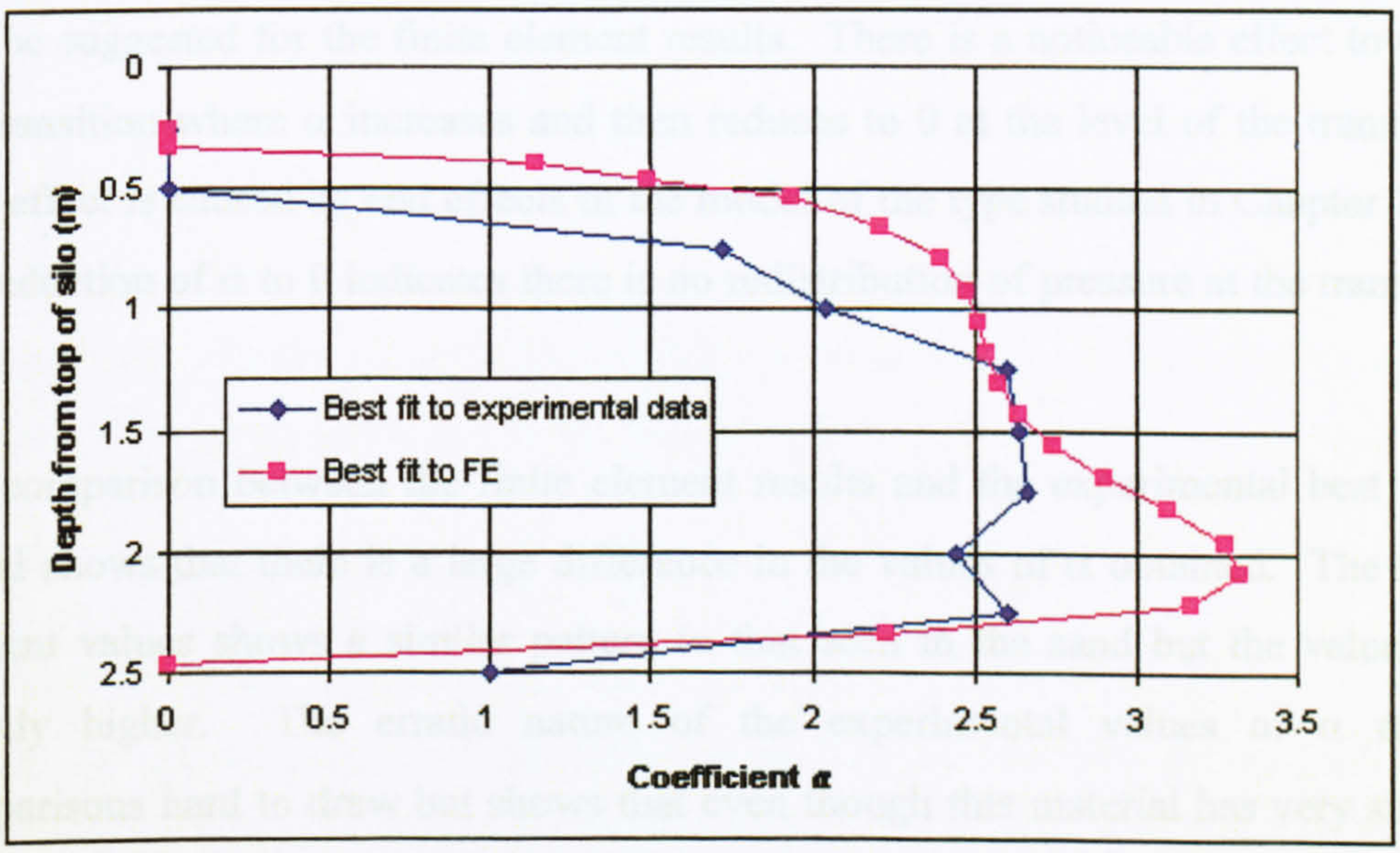

Figure 8.13 - Comparison of α determined from finite element method and experiment in sand

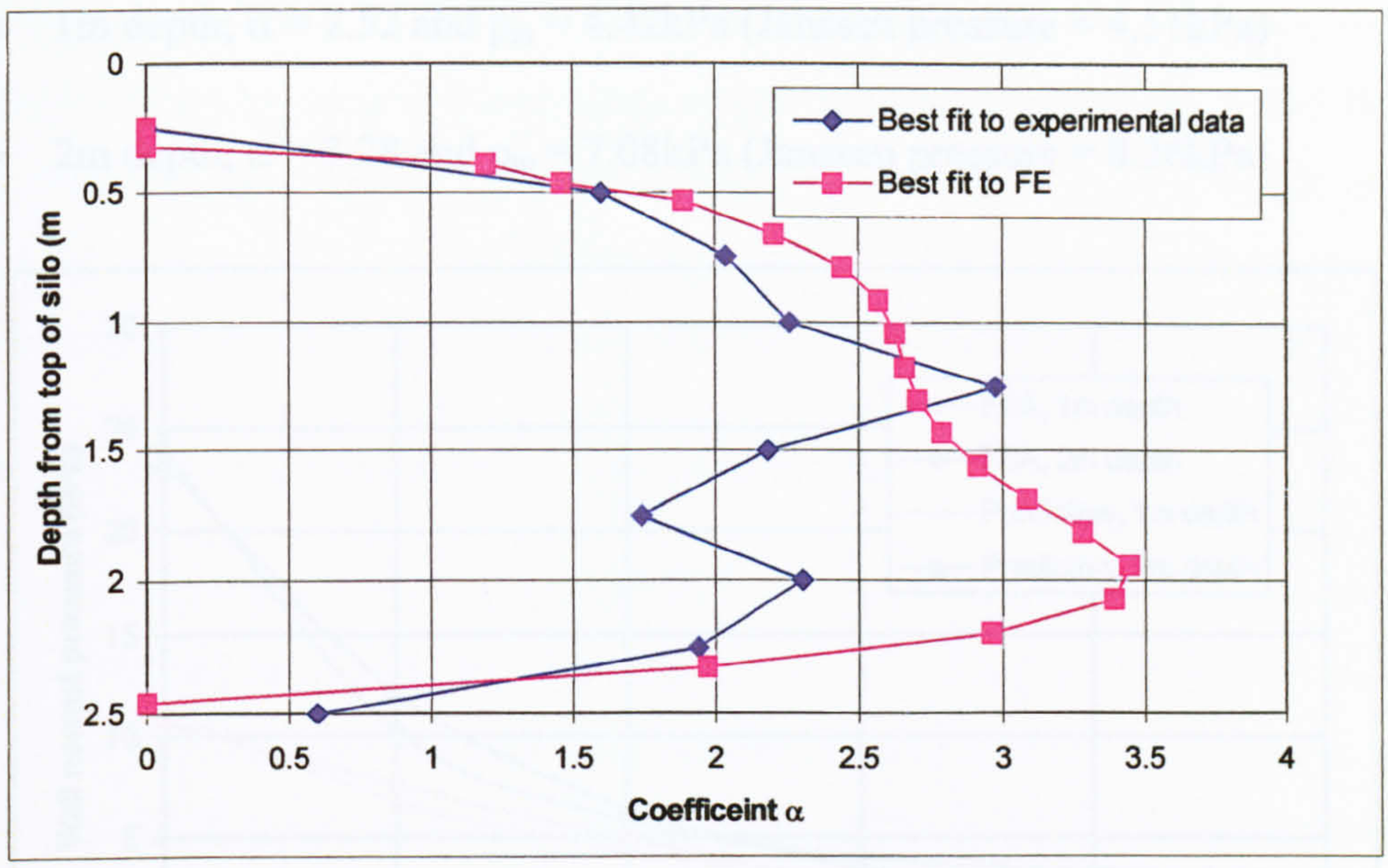

Figure 8.14 - Comparison of α determined from finite element method and experiment in gravel

For the sand material the maximum values obtained from the finite element model are in the same region as the experimental work. An overall value of $\alpha = 2.5$ might also be suggested for the finite element results. There is a noticeable effect towards the transition where α increases and then reduces to 0 at the level of the transition. This effect is caused by end effects in the model of the type studied in Chapter 7 and the reduction of α to 0 indicates there is no redistribution of pressure at the transition level.

The comparison between the finite element results and the experimental best fit in gravel shows that there is a large difference in the values of α obtained. The finite element values shows a similar pattern to that seen in the sand but the values are slightly higher. The erratic nature of the experimental values of α makes comparisons hard to draw but shows that even though this material has very similar properties to the studied sand, the measured pressures can be extremely variable.

Figure 8.15 shows the wall normal pressures in sand determined by finite element analysis at two levels in the bin. The best fit of the predictive law to these results is also shown. The values of α and p_m were:

- 1m depth; $\alpha = 2.52$ and $p_m = 4.42$kPa (Janssen pressure = 4.51kPa)
- 2m depth; $\alpha = 3.28$ and $p_m = 7.08$kPa (Janssen pressure = 8.26kPa)

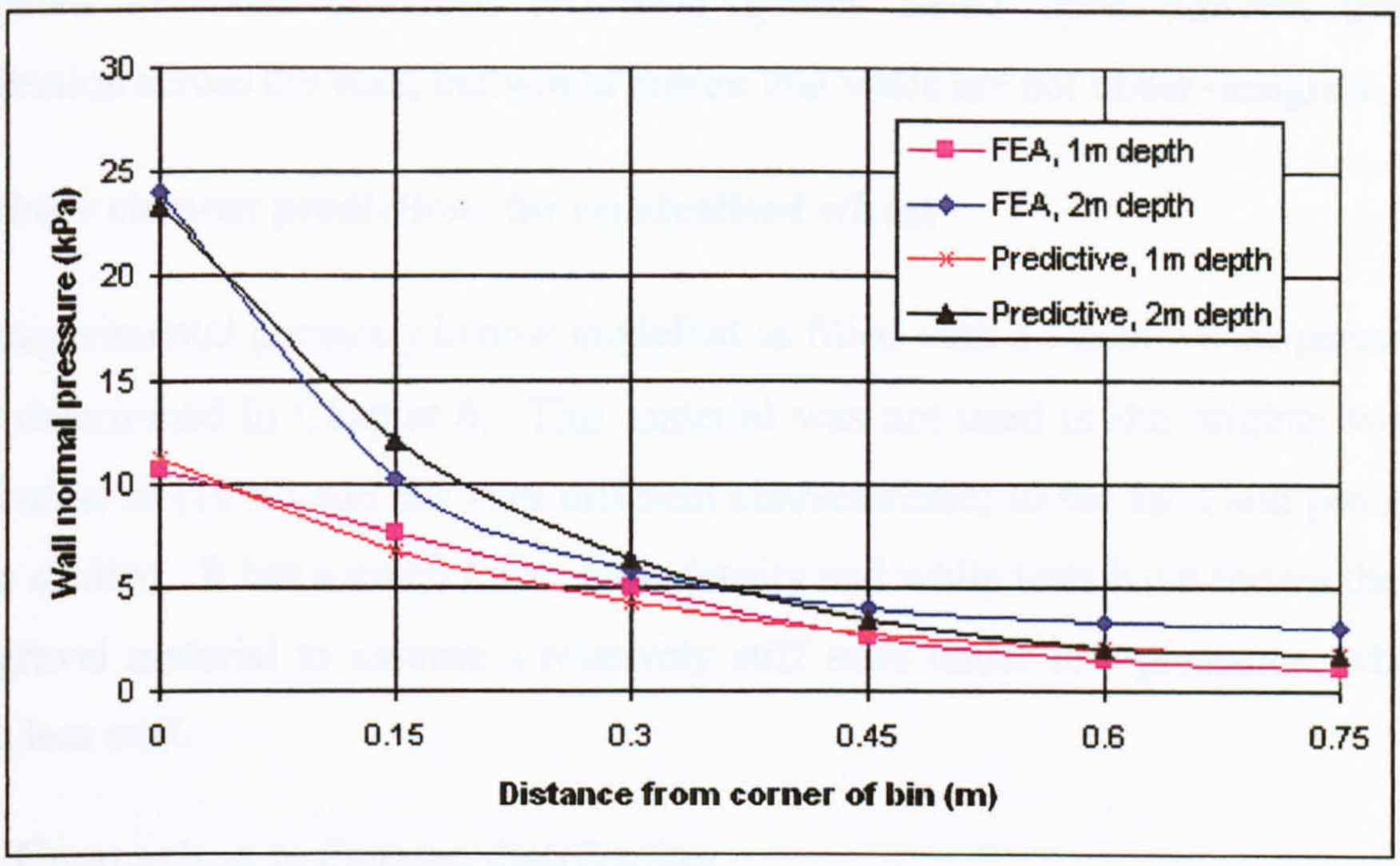

Figure 8.15 - Comparison between FEA results and predictive law of Rotter *et al* (2002)

The predictive law shows a very similar form of distribution to the finite element results. The values from the predictive law across the bin are within 5% of those given by the finite element model. At the 2m depth however, the experimental pressure rises rapidly towards the corner resulting in an underestimation of the pressure at the centre of the bin by the predictive law.

8.5 Summary

The work presented above revisits the work done by Rotter *et al* (2002). It shows that the predictive law proposed could be used as an effective design tool given values of α for different materials and geometries. It may be necessary to make some compromise on the choice of the value of α dependant on which feature in the bin is being studied. Most of the values of α that have been calculated from best fit exercises tend to underestimate the pressure at the centre while those determined from the experimental results underestimate the corner pressure. This is important for the calculation of the bending moments as under-estimation of the wall normal

pressure at the midside could lead to walls being designed with insufficient strength. Therefore it may be more useful to adopt a conservative value of approximately 2 for α as suggested by Rotter *et al* (2002). This would lead to more efficient designs compared to those produced following guides based upon uniform pressure distribution across the wall, but would ensure that walls are not under-designed.

8.6 Finite element predictions for an idealised wheat

The experimental geometry is now modelled as filled with a wheat whose parameters were determined in Chapter 6. This material was not used in the original work of Lahlouh *et al* (1995) and has very different characteristics to the sand and pea gravel so far studied. It has a much lower bulk density and while tests have shown the sand and gravel material to assume a relatively stiff state under low pressures, wheat is much less stiff.

8.6.1 Comparison to Janssen distribution

Figure 8.16 shows the average wall normal pressure down the depth of the silo as well as the appropriate Janssen distribution. Also shown are the best fit values of p_m.

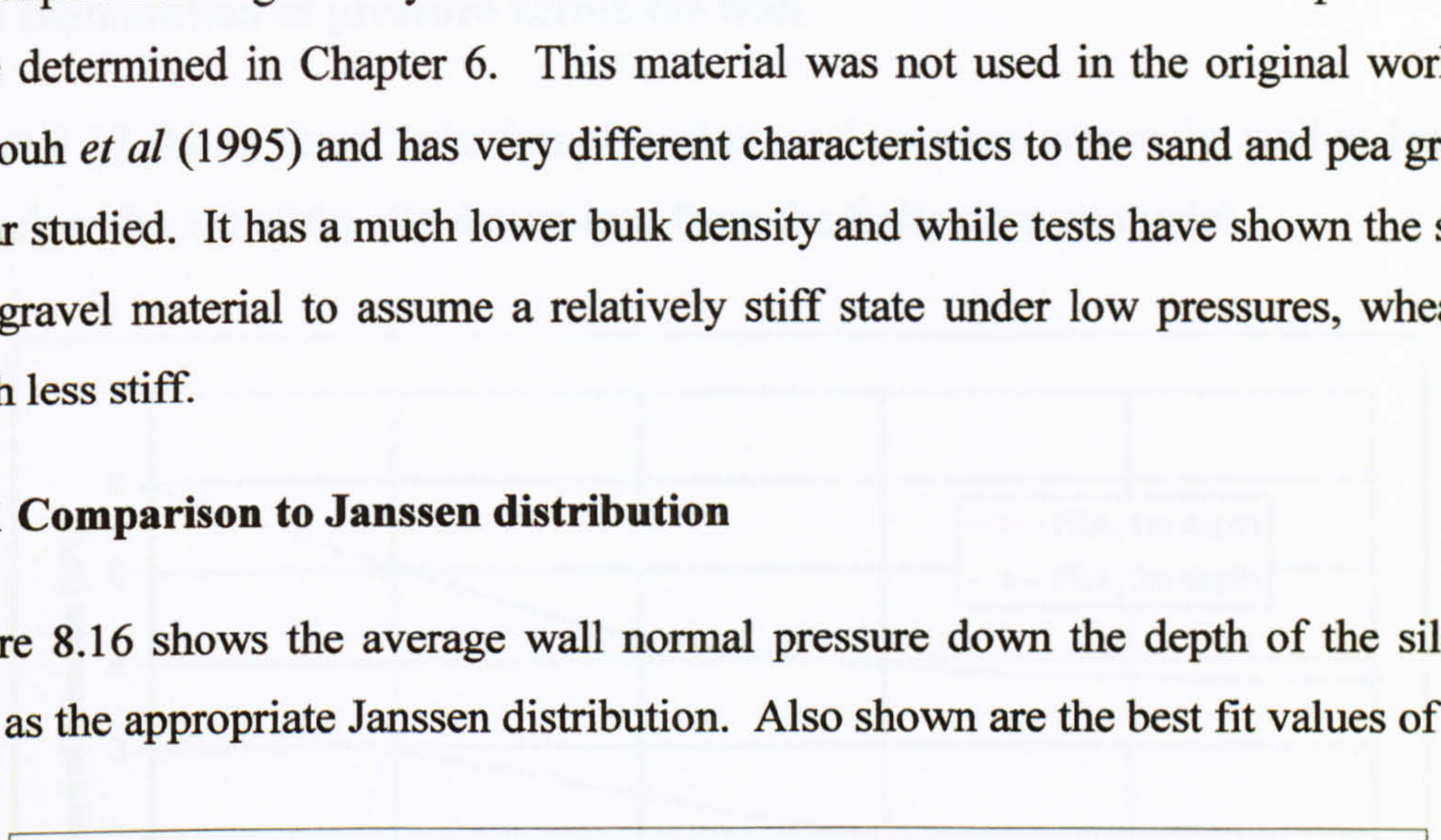

Figure 8.16 - Comparison to Janssen distribution in wheat

In this material the finite element predictions systematically underestimate the wall normal pressures by approximately 0.5kPa. The finite element predictions would appear to be tending towards an asymptote but due to the nature of the wheat material the depth required to develop this is much greater than the depth of bin studied here (see Chapter 9 for deeper silos). The best fit values of p_m are very close to the integrated values from the finite element model. The previously observed end effects are also much reduced in this model due to the softer nature of the stored material.

8.6.2 Distribution of pressure across the wall

Figure 8.17 shows the distribution of wall normal pressure across the wall at 1m and 2m below the top of the silo determined from the finite element model.

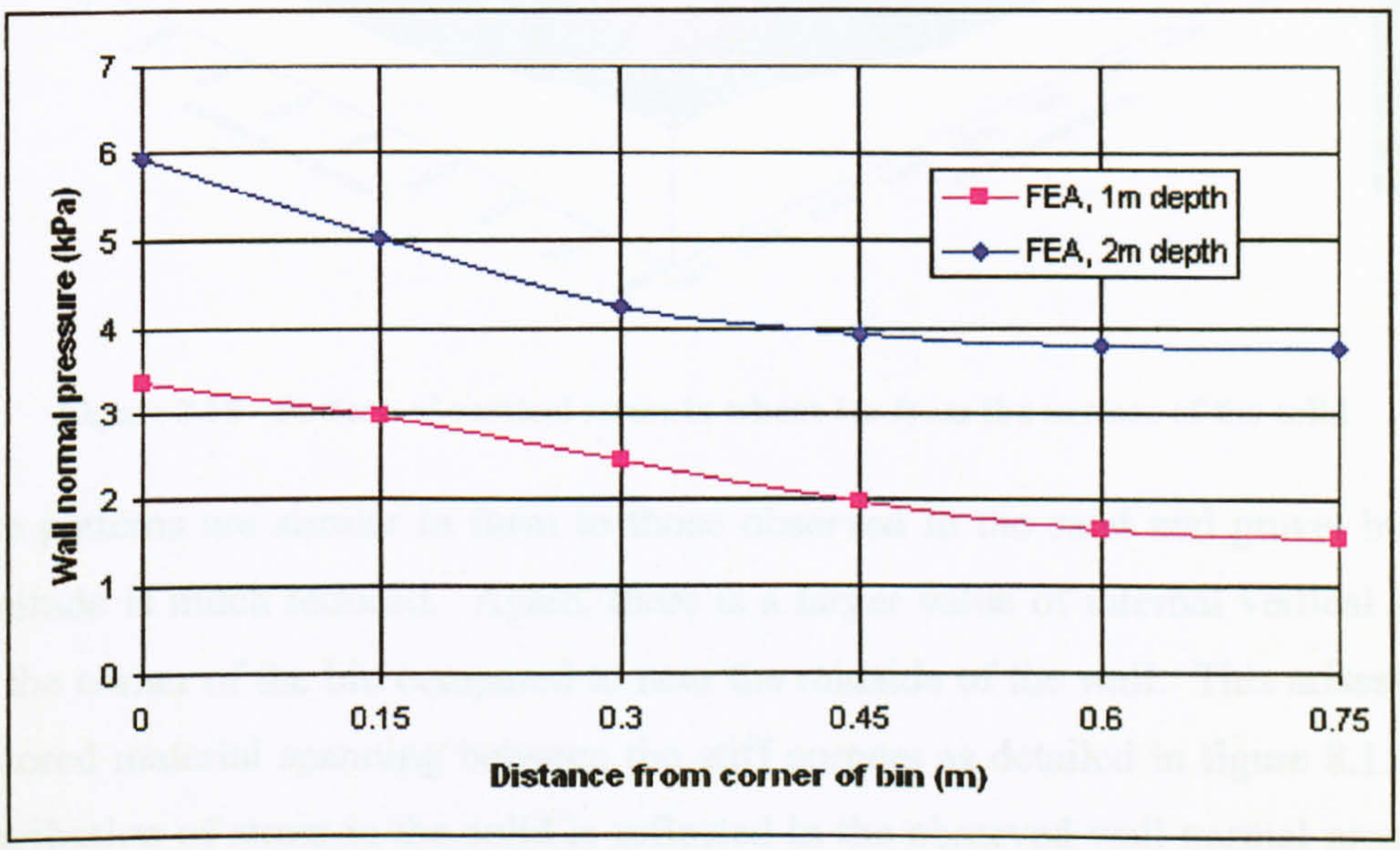

Figure 8.17 - Wall normal pressure distribution across the wall in wheat

With this softer material the amount of redistribution across the wall is less than that shown by the sand or gravel as would be expected due to the relative stiffness between the wall and the solid being much reduced. The results still show some redistribution with a pressure peak near the corner of the bin which reduces to a minimum at the midside position.

8.6.3 Patterns of vertical stress in the solid

Figure 8.18 shows the patterns of vertical stress in the ensiled material.

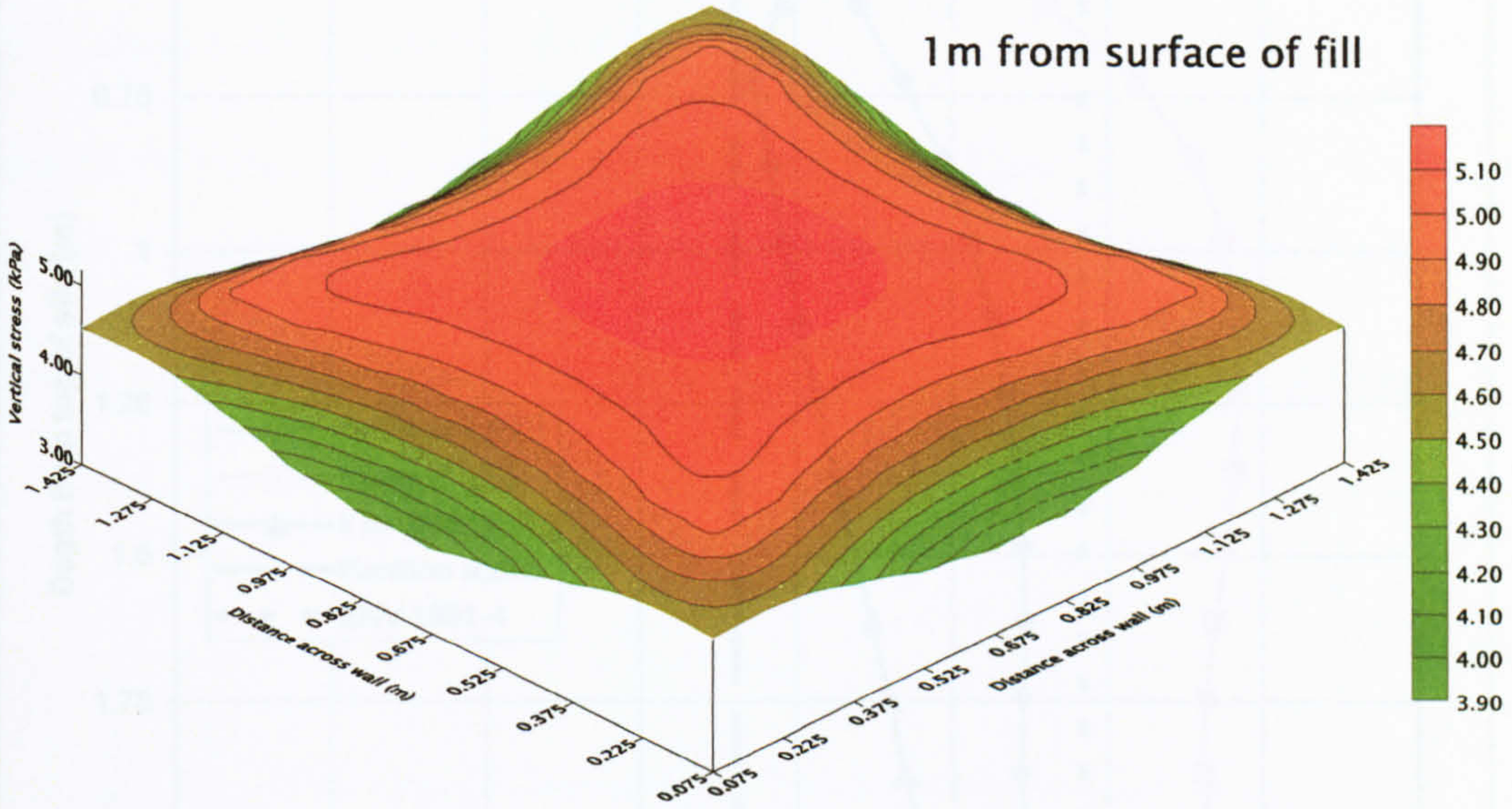

Figure 8.18 - Pattern of vertical stress in wheat 1m from the surface of the solid

These patterns are similar in form to those observed in the sand and gravel but the magnitude is much reduced. Again, there is a larger value of internal vertical stress near the corner of the bin compared to near the midside of the wall. This arises from the stored material spanning between the stiff corners as detailed in figure 8.1. The redistribution of stress in the solid is reflected in the observed wall normal pressures (figure 8.17).

8.6.4 Average and local values of k in the solid

Figure 8.19 shows the average and local values of k calculated from the finite element model.

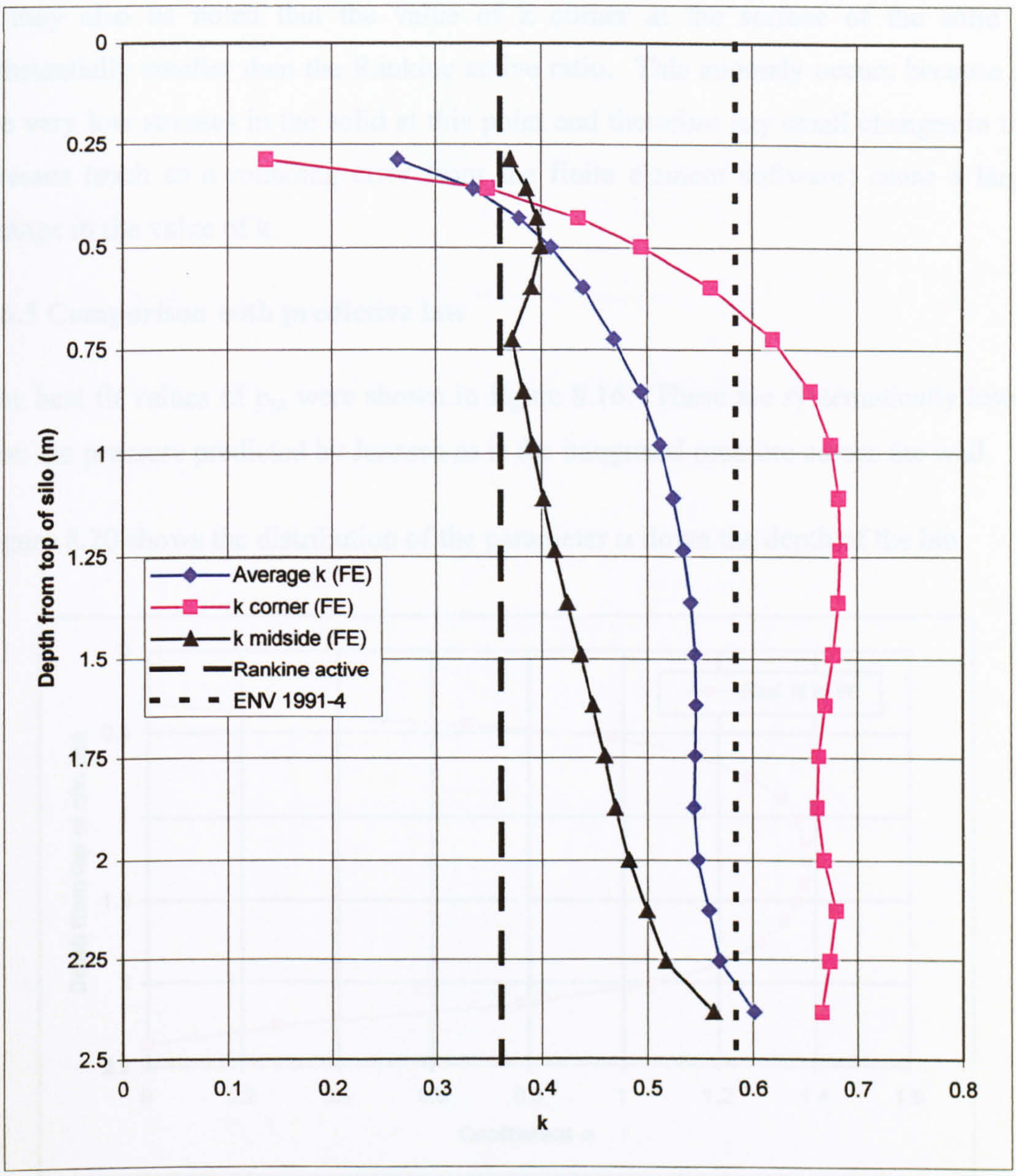

Figure 8.19 - Local and average values of k in wheat

The wheat material shows similar trends to the sand and gravel models. The average value of k compared with the Eurocode value is about 10% lower. This compares favourably with the values found in the previous materials. As would be expected the value of k at the midside is lower than the average value and at the corner, higher. This is because the material at the midside is failing where the wall deforms outwards and material near the corner is confined by the stiff structural elements.

It may also be noted that the value of k corner at the surface of the solid is substantially smaller than the Rankine active ratio. This anomaly occurs because of the very low stresses in the solid at this point and therefore any small changes in the stresses (such as a rounding error from the finite element software) cause a large change in the value of k.

8.6.5 Comparison with predictive law

The best fit values of p_m were shown in figure 8.16. These are systematically lower than the pressure predicted by Janssen as is the integrated pressure across the wall.

Figure 8.20 shows the distribution of the parameter α down the depth of the bin.

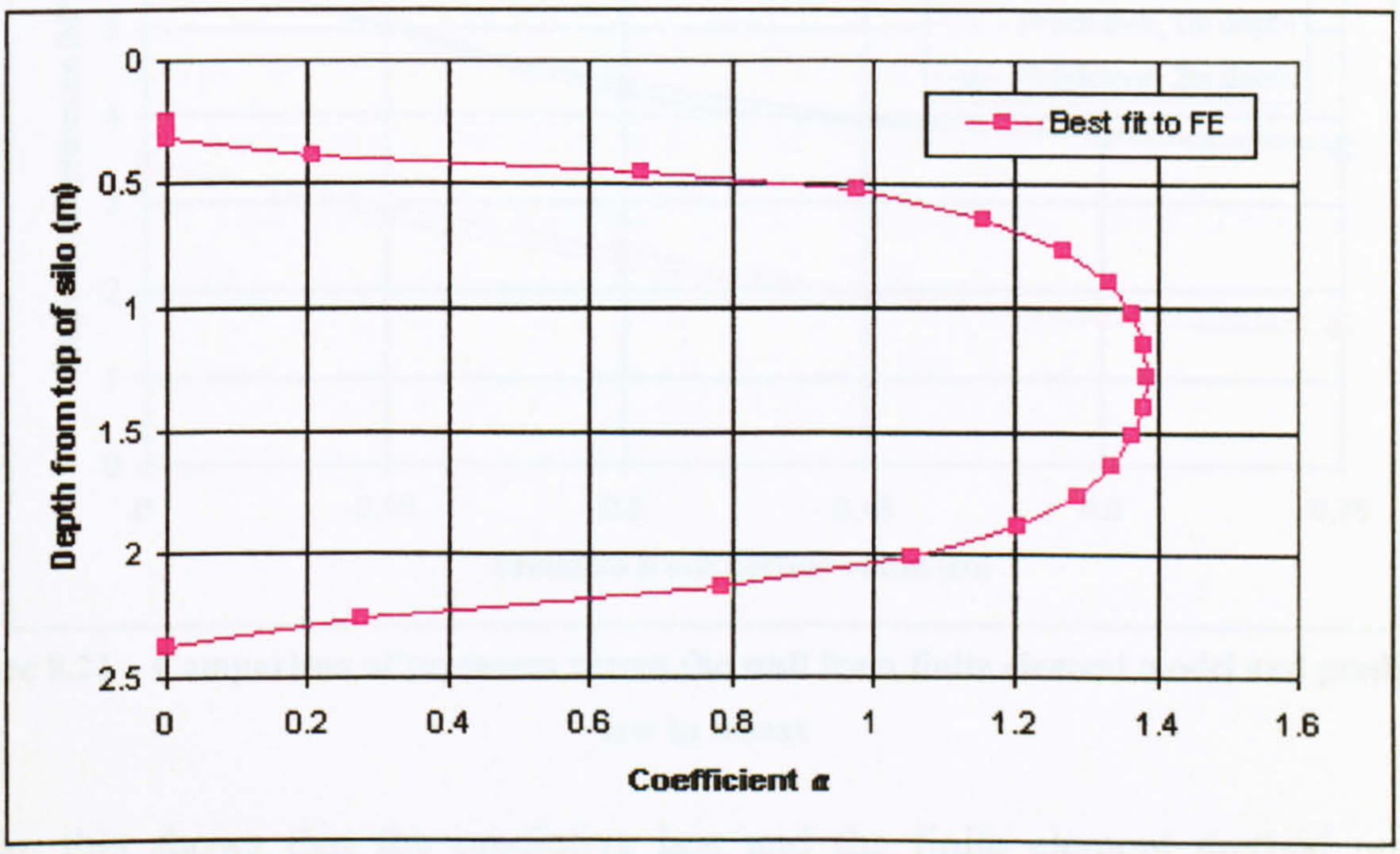

Figure 8.20 - α determined from finite element method in wheat

The value of α is lower for this soft material than it is for the stiffer sand and gravel. This indicates that there is less redistribution of the pressure in this case. The redistribution is affected by the deformation of the wall and therefore this softer, lighter material exhibiting smaller values of α compared to the sand (or gravel) is not unexpected. The observed form of distribution of α down the bin differs from that exhibited by the sand and gravel in that there is no increase in α towards the transition. This is due to the relative stiffness between the material and the wall

being much lower and therefore any extra stiffening effect at the transition has no measurable effect on the value of α.

Finally, the results from the finite element model are compared to the predictive law at two levels. The values of p_m and α determined from the best fit exercise were:

- 1m depth; $\alpha = 1.37$ and $p_m = 2.26$kPa (Janssen pressure = 2.72kPa)
- 2m depth; $\alpha = 1.05$ and $p_m = 4.36$kPa (Janssen pressure = 4.73kPa)

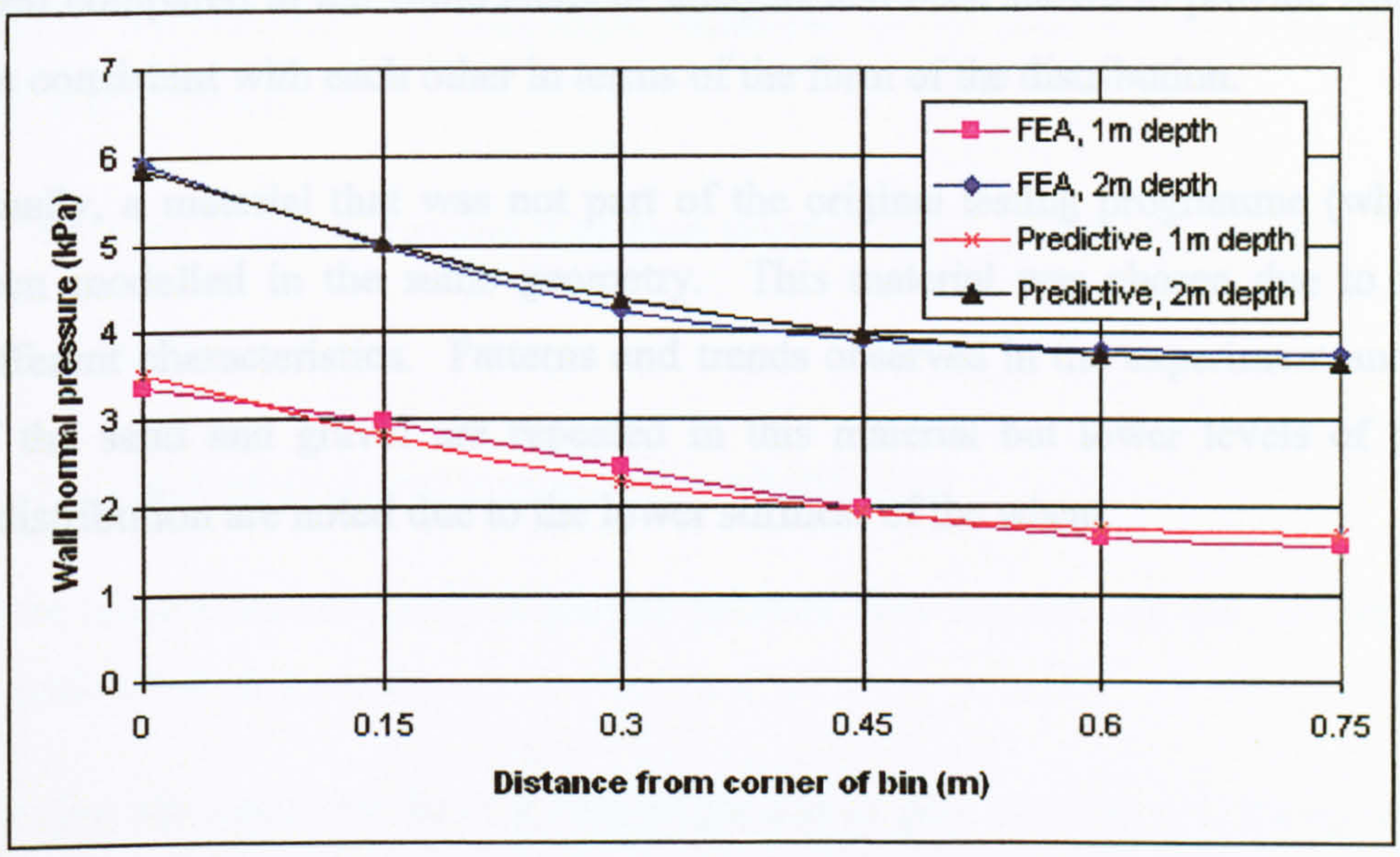

Figure 8.21 – Comparison of pressures across the wall from finite element model and predictive law in wheat

Again, this shows that the predictive law and the finite element method provide comparable results with agreement being within 5% across the bin. It may however be noted that this comparison merely shows that the predictive law can reproduce the distribution determined from the finite element analysis. It gives no indication about the form obtained from an experimental study.

8.7 Summary

The experimental geometry of Lahlouh *et al* (1995) has been modelled with the finite element method. Results have been obtained for the two materials that were used in

the experiment and comparisons drawn. The finite element analysis has shown comparable distributions of internal stress in the solid, k values and wall normal pressures. The finite element method cannot however reproduce the random features in the stored solid caused by filling (for example). These features have been shown to be important in their effect on the wall normal pressures (Ooi *et al*, 1990).

The predictive law of Rotter *et al* (2002) has been introduced and the work from the paper revisited and extended in order to show that the predictive law can reproduce the pressure distributions shown in experimental work. The predictive law has also been compared to the finite element analysis and been shown to provide results that are consistent with each other in terms of the form of the distribution.

Finally, a material that was not part of the original testing programme (wheat) has been modelled in the same geometry. This material was chosen due to its very different characteristics. Patterns and trends observed in the experiment and model of the sand and gravel are repeated in this material but lower levels of pressure redistribution are noted due to the lower stiffness of the wheat.

Chapter 9 - Parametric study of a square planform silo

9.1 Introduction

This section of the thesis aims to use the finite element model described above (Chapter 6) to study the effect of several factors on the wall pressure distribution in a square planform silo. The results are compared to Janssen distributions and also to Rotter *et al*'s (2002) predictive law described in Chapter 8 to determine whether this law can be used for more general predictive work in silo design.

Results are presented for parametric variations of the square silo. The parameters that will be varied are:

- Type of stored material (Leighton Buzzard sand, pea gravel, wheat)
- Planform size
- Wall thickness (and by extension wall stiffness)

These parameters are varied to predict pressure distributions and the factors that are critical to their assessment.

The first silo model will be of a 10m height and of plan dimension 1.5m square. This height is chosen in order to make the silo sufficiently deep to allow the Janssen asymptotic pressure to develop when the wall length is 1.5m. The base is modelled as having a concentric hopper of approximately 45° wall angle (consistent with the definition of hopper angle given in Chapter 7). The use of this boundary condition aims to reduce any effects of the type discussed in Chapter 7.

This study aims to determine the effect that these parameters have upon the redistribution parameter α. It is predicted that α is related to the relative stiffness between the silo wall and the stored solid. Ooi and Rotter (1990) showed that the relative stiffness between the wall and stored solid could have an effect on the observed pressures in a cylindrical silo. A parameter was proposed for this relationship given by equation 9.1.

$$\alpha = \frac{E_s R}{E_w t} \tag{9.1}$$

In the cylindrical silo however the wall needs to be thin and the stored solid rather stiff in order for the flexibility to have an effect.

A similar expression may exist for the rectangular silo although rather than using the parameter R/t to characterise the shell rigidity, it would be more likely that some form of the plate flexural rigidity, $(L/t)^3$, would be incorporated. The plate flexural rigidity is given by equation 9.2.

$$D = \frac{Et^3}{12(1-\nu^2)} \tag{9.2}$$

Any relationship derived is likely to be of a higher order than the relationship given for the cylindrical bin.

9.2 Type of stored material

The three granular materials that were investigated in Chapter 6 are now modelled in a 10m deep bin of the same planform as used previously (1.5m square). The thickness of the wall however, is increased to 20mm. Initial investigation of this geometry showed that a thin wall (such as the 6mm used previously) leads to very large deflections in the wall. Further investigation showed that when deformations approach what may be defined as large (as a rule of thumb, as $w \Rightarrow t$) it becomes difficult to predict the behaviour of the stored solid and hence values of α that are determined also become difficult to predict. Further investigation of this is given in section 9.5.1 but the work presented below is, for now, limited to cases where the wall deformation is small.

Figure 9.1 shows the average wall normal pressures in this bin using the three stored granular materials. The average wall normal pressure plotted is the value of p_m obtained by fitting the predictive law of Rotter *et al* (2002) to the finite element results (equation 9.3).

$$p = p_m\left(\frac{\alpha}{\sinh\alpha}\right)\cosh\left(\frac{2\alpha x}{d}\right) \tag{9.3}$$

The value of p_m is used as the curved distribution of the predictive law provides a better approximation of the integrated value (assuming the function is a good fit to the data) whereas Simpson's rule assumes the points to be joined by straight lines which can lead to numerical inaccuracy when applied to relatively coarse data such as this. The appropriate Janssen pressure distributions have also been plotted.

The mesh density of these models is chosen in a similar manner to the method described previously for the smaller bins in order to provide the most accurate results but minimise the computational time required.

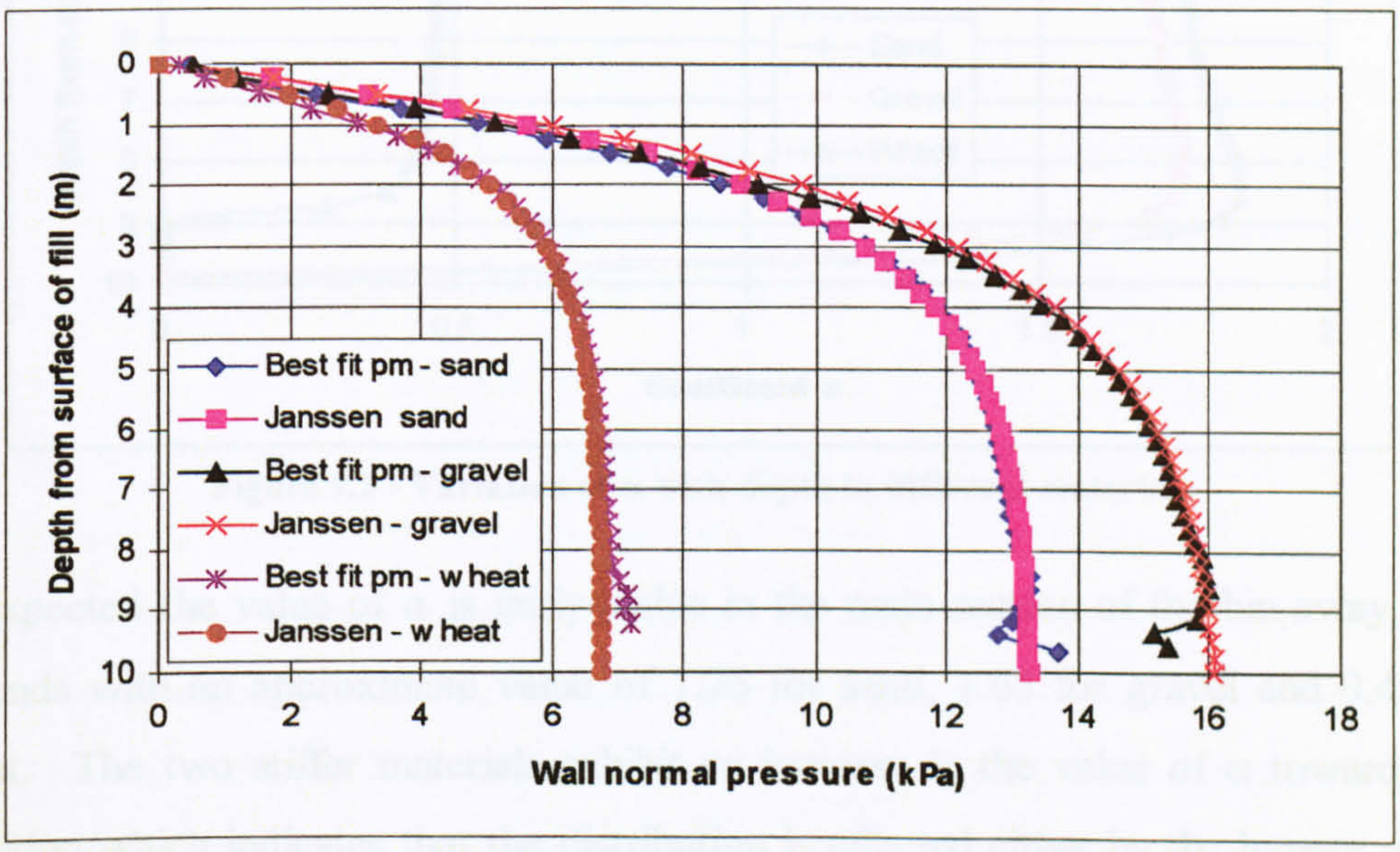

Figure 9.1 - Wall normal pressures in deep square planform bin

In this deep bin it is easy to see that at a depth the Janssen distribution tends towards an asymptotic (constant) value and the finite element results follow this trend. The finite element predictions down the bin agree with the Janssen values within the bounds of experimental error. There are noticeable end effects and these are most pronounced in the silos filled with the two stiffer solids (sand and gravel). As noted previously the end node has been disregarded because the pressure recorded is the result of the node moving into the hopper.

These results have been fitted to the predictive law (Rotter *et al*, 2002) and therefore values of α have been determined. In section 8.3.1 it was shown that the value of α for sand was fairly stable away from the surface and the transition. A deep bin should demonstrate whether a stable value of α exists in regions away from the boundary conditions (surface and hopper). Figure 9.2 shows the value of α down the bin for the three materials as determined from the best fit to the finite element results.

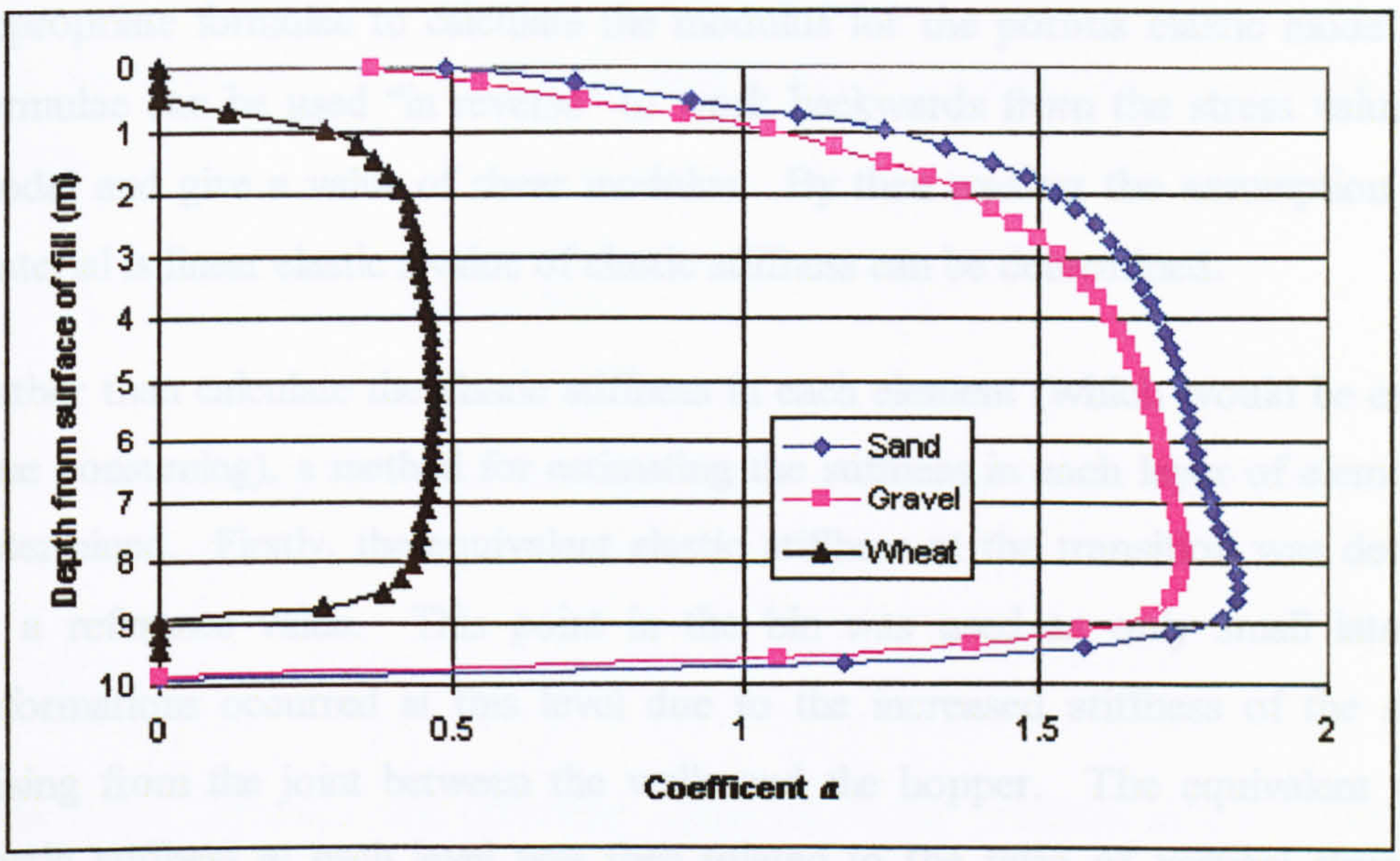

Figure 9.2 - Variation of α with depth in different materials

As expected the value of α is fairly stable in the main section of the bin away from the ends with an approximate value of 1.75 for sand, 1.65 for gravel and 0.45 for wheat. The two stiffer materials exhibit an increase in the value of α towards the transition which indicates that the distribution is affected either by the hopper or the increased wall stiffness where the hopper and walls meet.

9.2.1 Relative stiffness between wall and stored solid

In each of the three materials above, different values of α occur at a given depth. This describes the varying degrees of redistribution in each of the granular solids. It is expected that this phenomenon is attributable to the relative stiffness between the wall and the solid. Since the wall material and geometry (and hence stiffness) is the

same in the above three models the observed differences must be due to the stored solids having different equivalent elastic stiffness'. The constitutive model used in the finite element analysis does not explicitly define a stiffness, nor can it be readily determined because the constitutive law exhibits barotropy i.e. the stiffness is related to the stress level. Therefore the results from the finite element analysis are interpreted to give a value of equivalent elastic stiffness that can be related to the elastic stiffness of the wall. The ABAQUS theory manual (2001) gives the appropriate formulae to calculate the modulus for the porous elastic model. These formulae can be used "in reverse" to work backwards from the stress values in the model and give a value of shear modulus. By then making the assumption that the material is linear elastic a value of elastic stiffness can be determined.

Rather than calculate the elastic stiffness in each element (which would be extremely time consuming), a method for estimating the stiffness in each layer of elements was determined. Firstly, the equivalent elastic stiffness at the transition was determined as a reference value. This point in the bin was used as only small lateral wall deformations occurred at this level due to the increased stiffness of the structure arising from the joint between the walls and the hopper. The equivalent value of elastic stiffness at each level was then related to the ratio of vertical stress at the transition to the vertical stress at the point under consideration. It was found that using a Janssen vertical stress distribution for this was sufficiently accurate. As a check, calculations were performed at each level using the value of vertical stress determined from the finite element model. It was found that the results obtained from this method and the method using the Janssen predicted value of vertical stress were very close and therefore this simplified approach was used for the remainder of the calculations.

The calculation firstly requires the determination of the elastic volume change in the material. This is related to the stress level in the material and various material constants and is given by equation 9.4.

$$J^{el} = \frac{\lambda}{(1+e_0)} \ln\left(\frac{p_0 + p_t^{el}}{p + p_t^{el}}\right) + 1 \tag{9.4}$$

The value of p (which is called the average pressure stress in the ABAQUS manual) is given as the mean of the three directional stresses.

$$p = -\frac{1}{3}(\sigma_{11} + \sigma_{22} + \sigma_{33}) \tag{9.5}$$

It is then possible to directly determine the instantaneous shear modulus using equation 9.6.

$$G = \frac{3(1-2\nu)(1+e_0)}{2(1+\nu)\lambda}(p + p_t^{el})(J^{el}) \tag{9.6}$$

If the assumption of a linear isotropic material is made then it is possible to directly convert this value to an elastic stiffness using equation 9.7.

$$E = 2G(1+\nu) \tag{9.7}$$

Using these formulae the reference value of elastic stiffness at the transition was calculated for each of the three materials. The results are presented in table 9.1.

Stored material	**Sand**	**Gravel**	**Wheat**
Reference value of elastic stiffness (MPa)	18.10	15.15	0.73

Table 9.1 - Equivalent elastic stiffness of the three materials

Figure 9.2 showed that the material exhibiting the largest variation of pressure across the wall is the Leighton Buzzard sand (characterised by the higher values of α). This material also exhibits the highest equivalent elastic stiffness at the transition and therefore it may be deduced that α may be closely related to solid and wall stiffness. Further investigation was therefore carried out to attempt to identify a more general relationship.

9.2.2 Deformations in the wall

The analysis performed thus far has been a large deformation analysis. This does not necessarily mean that large deformations are occurring in either the solid or the wall but as was shown in section 3.10 the behaviour of plates can be affected even when the deformations are only approaching what may be defined as large (Ugural, 1981). As a check, the deformations down the centreline of the silo wall were inspected to determine whether large deflections were occurring. There could also be a significant effect on the value of α. The opposite could be said if the deformation is small. Figure 9.3 shows the normal deformations of the wall down the centreline of the silo described above when filled with the three materials.

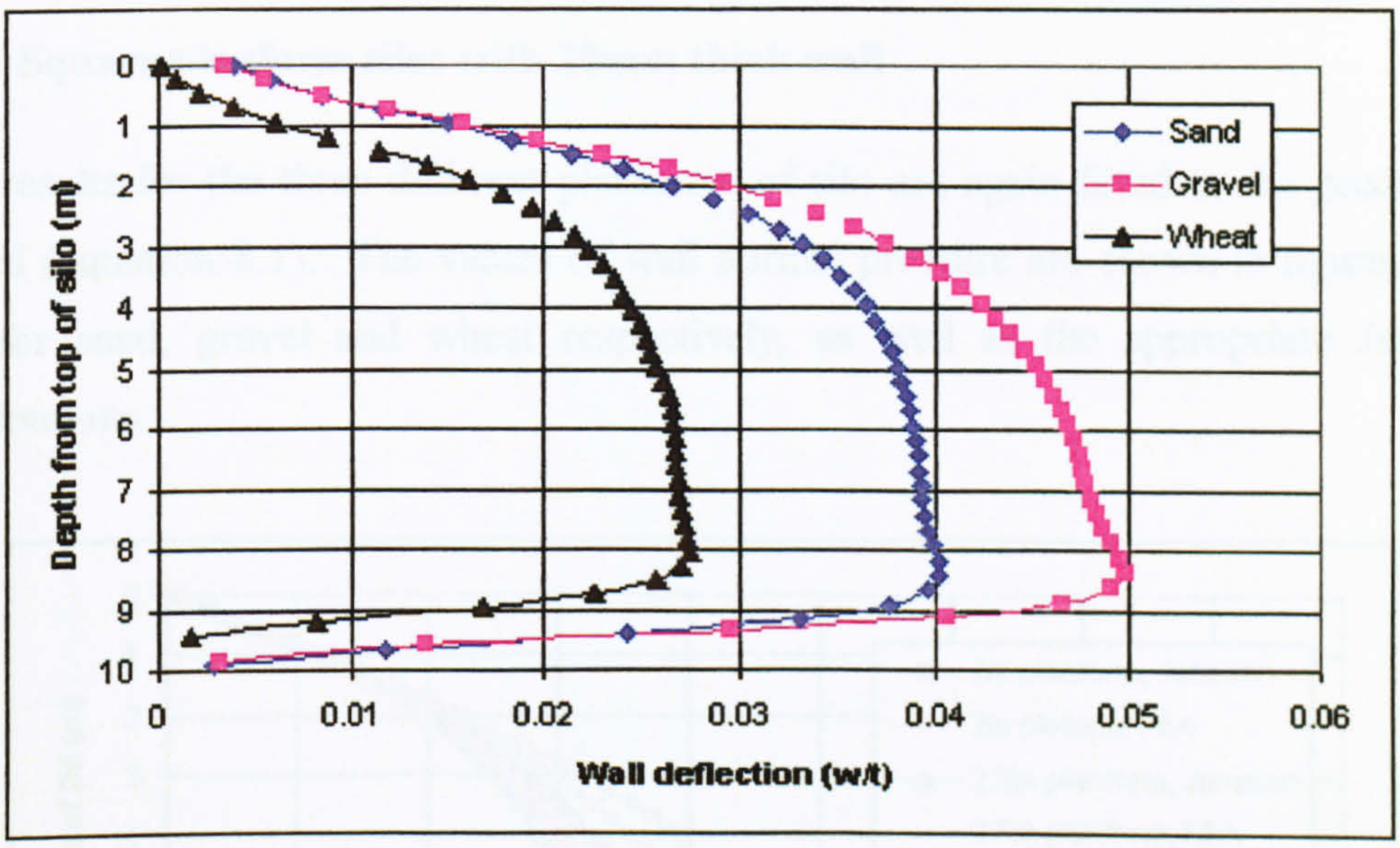

Figure 9.3 – Normal deformations (w/t) down the centreline of the bin wall

The predicted deflections in the model are small compared to the thickness of the plate. In order to fully take advantage of structural savings in this type of silo then the wall thickness would need to lower in order to induce some membrane tension into the plate.

9.3 Planform

In the previous sections the silo studied was square with a width of 1.5m. This silo will now be increased in planform but will still be maintained square. The choice of planform sizes are 2m square, 2.5m square and 3m square. The initial wall thickness is chosen as 20mm. This is an arbitrary choice based upon the observed pressures and deformations above. An unstiffened silo wall of 20mm wall thickness will allow an observable level of redistribution of the wall normal pressure but still be thick enough to avoid excessive deflections in the wall.

The mesh density of the finite element model is kept the same as for the previous study.

9.3.1 Square planform silos with 20mm thick wall

The results for the three different planforms of silo are again fitted to the predictive model (equation 8.1). The values of wall normal pressure are shown in figures 9.4-9.6 for sand, gravel and wheat respectively, as well as the appropriate Janssen distributions.

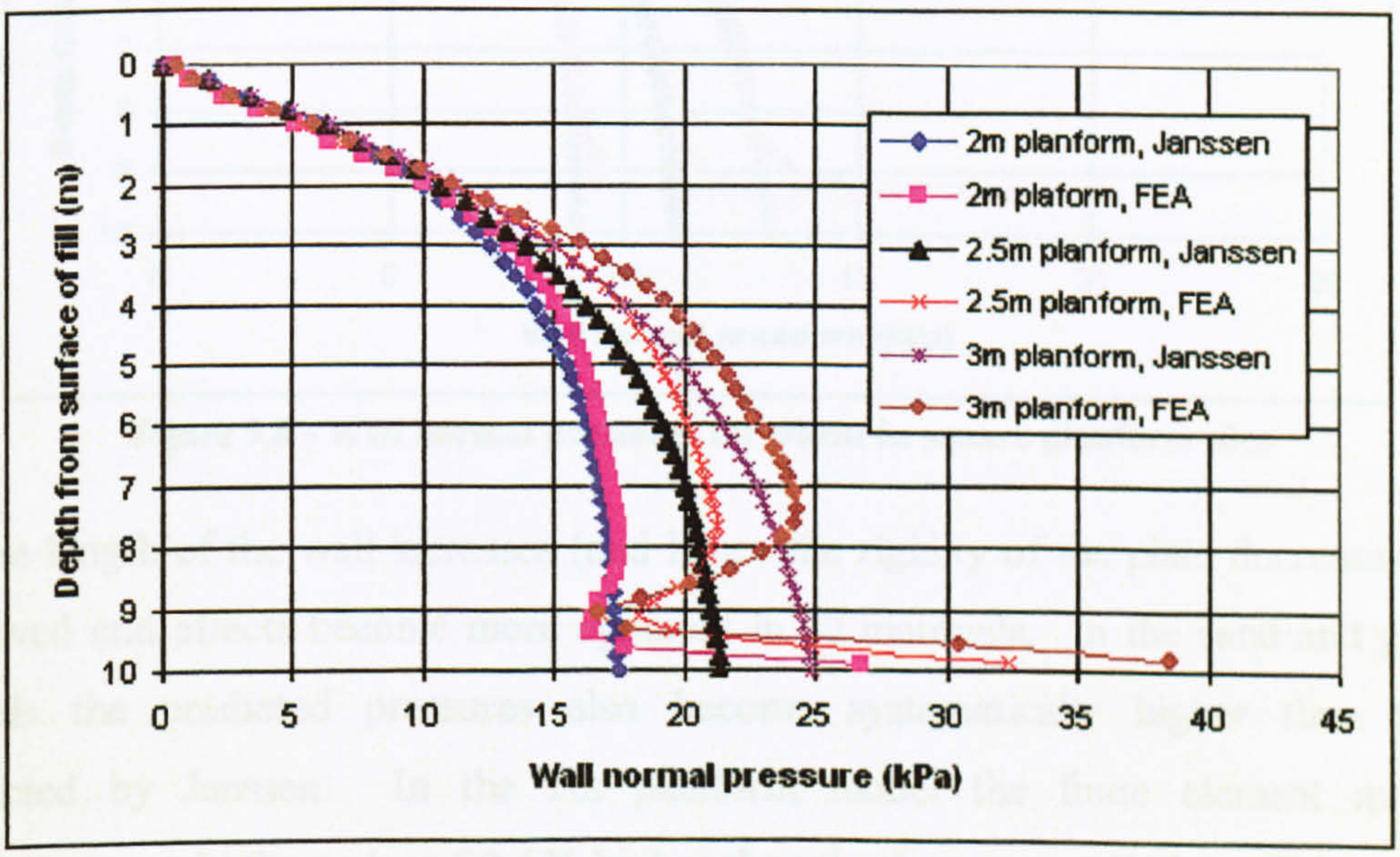

Figure 9.4 - Wall normal pressures for sand in square planform silos

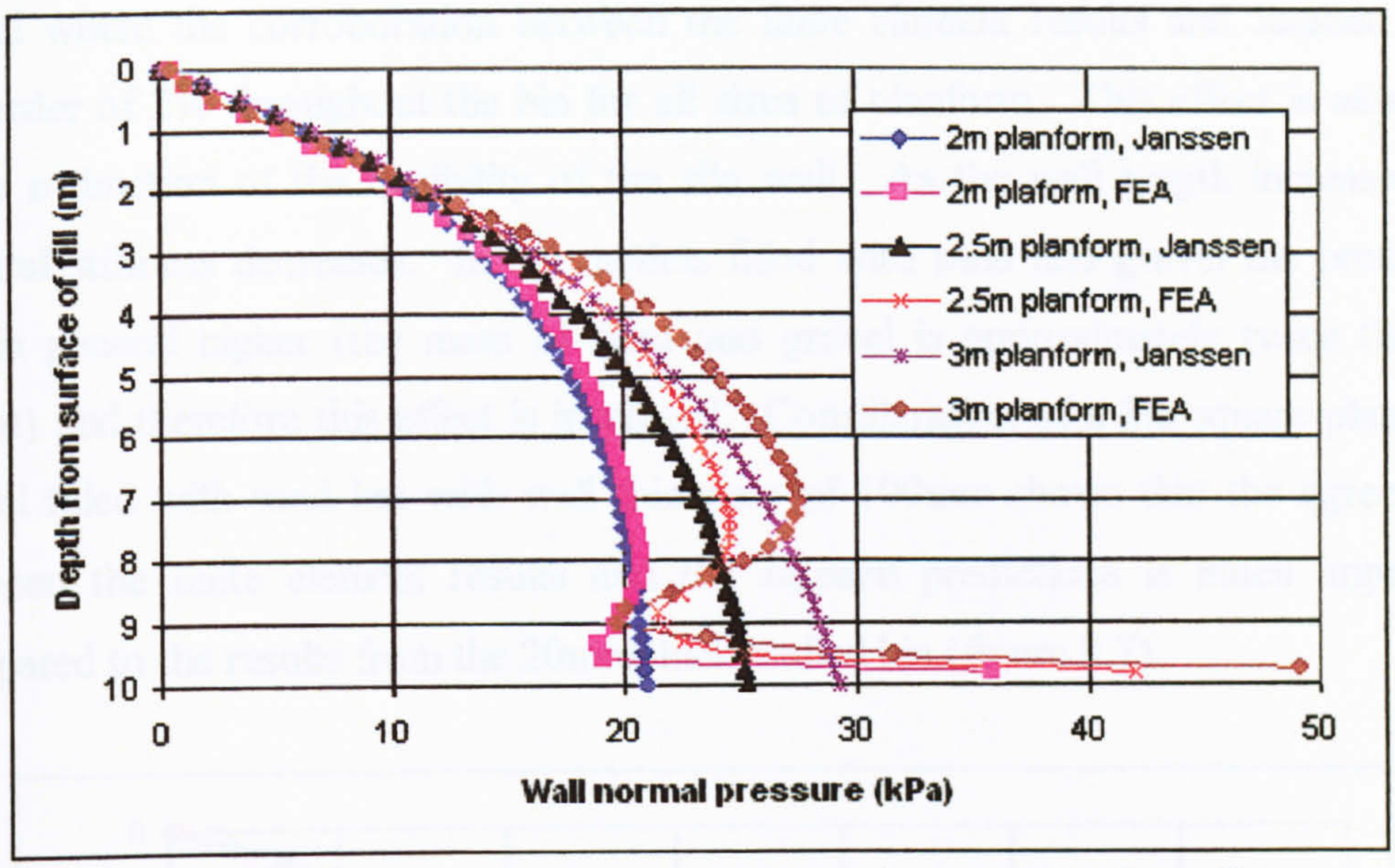

Figure 9.5 - Wall normal pressures for gravel in square planform silos

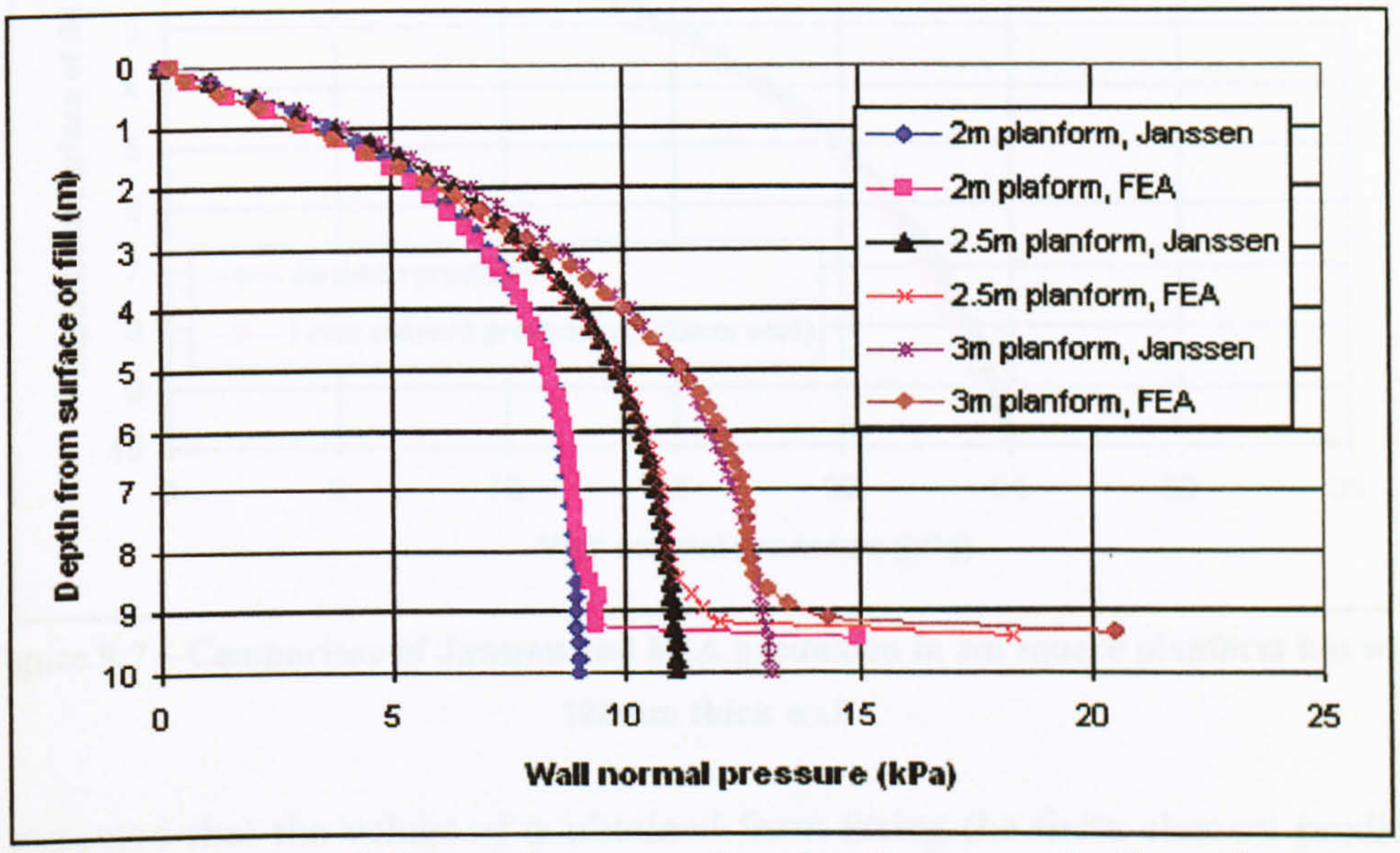

Figure 9.6 - Wall normal pressures for wheat in square planform silos

As the length of the wall increases (and hence the rigidity of the plate decreases) the observed end effects become more apparent in all materials. In the sand and gravel models the predicted pressures also become systematically higher than those predicted by Janssen. In the 2m planform model the finite element method predictions are in the order of 3-5% higher than the Janssen prediction. This rises to 5-7% higher in the 3m planform model. This same pattern is not seen in the wheat

model where the corroboration between the finite element results and Janssen is in the order of 2% throughout the bin for all sizes of planform. This effect is assumed to be a function of the flexibility of the silo wall. As the wall length increases the flexural stiffness decreases. In the models filled with sand and gravel the pressures are in general higher (the mass of sand and gravel is approximately twice that of wheat) and therefore this effect is increased. Consideration of a 3m square planform model filled with sand but with wall thickness of 100mm shows that the agreement between the finite element results and the Janssen predictions is much improved compared to the results from the 20mm thick walled bin (figure 9.7).

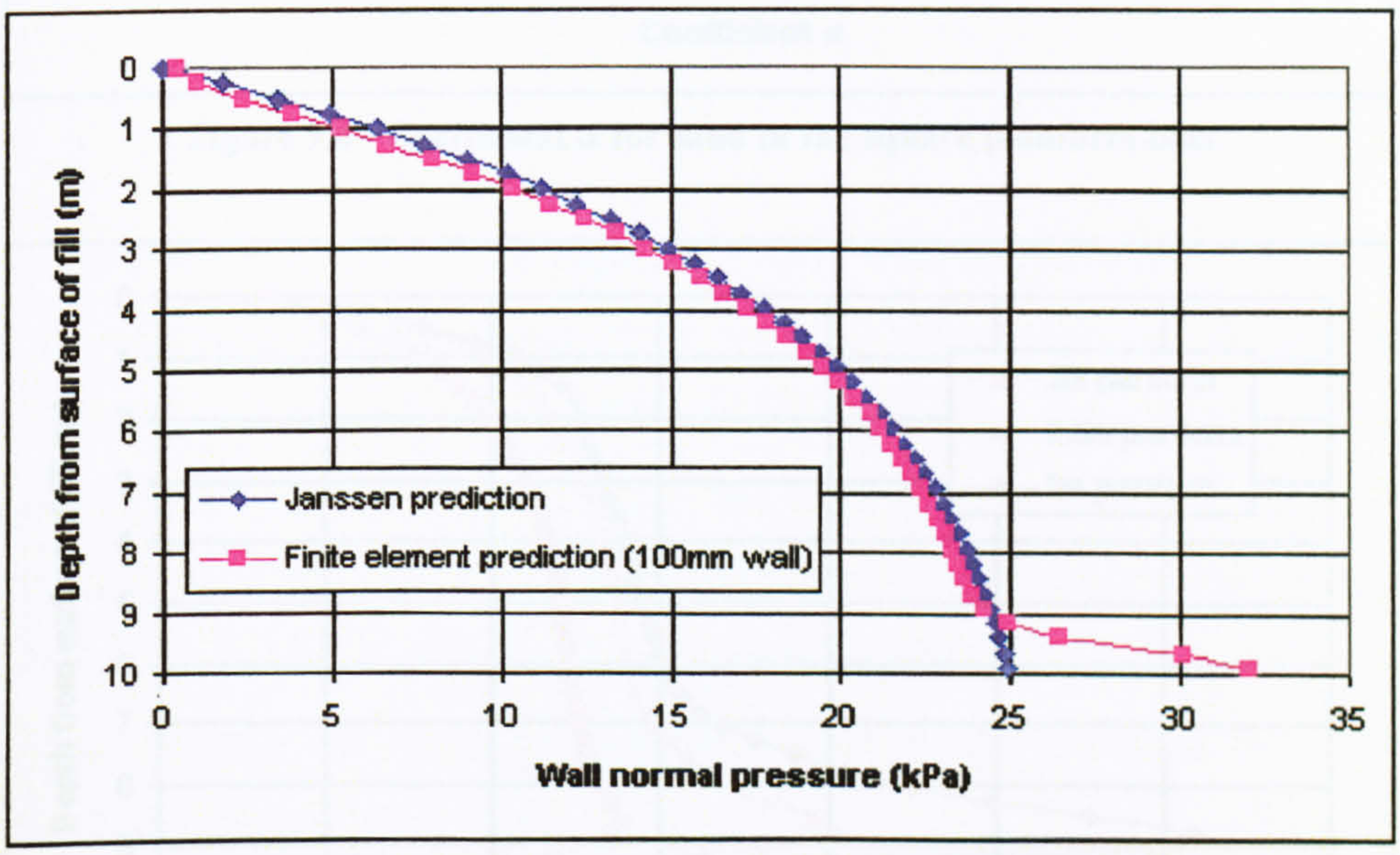

Figure 9.7 – Comparison of Janssen and FEA prediction in 3m square planform bin with 100mm thick wall

It is expected that the values of α obtained from fitting the finite element predictions to the predictive law (equation 9.3) will be higher for those silos with a larger side length. This is due to the decreased rigidity of the plate and since the ensiled material is the same (and should therefore assume a similar stiffness) the relative stiffness between wall and material should be reduced. Figures 9.8-9.10 show the values of α for the three silos above again for sand, gravel and wheat respectively.

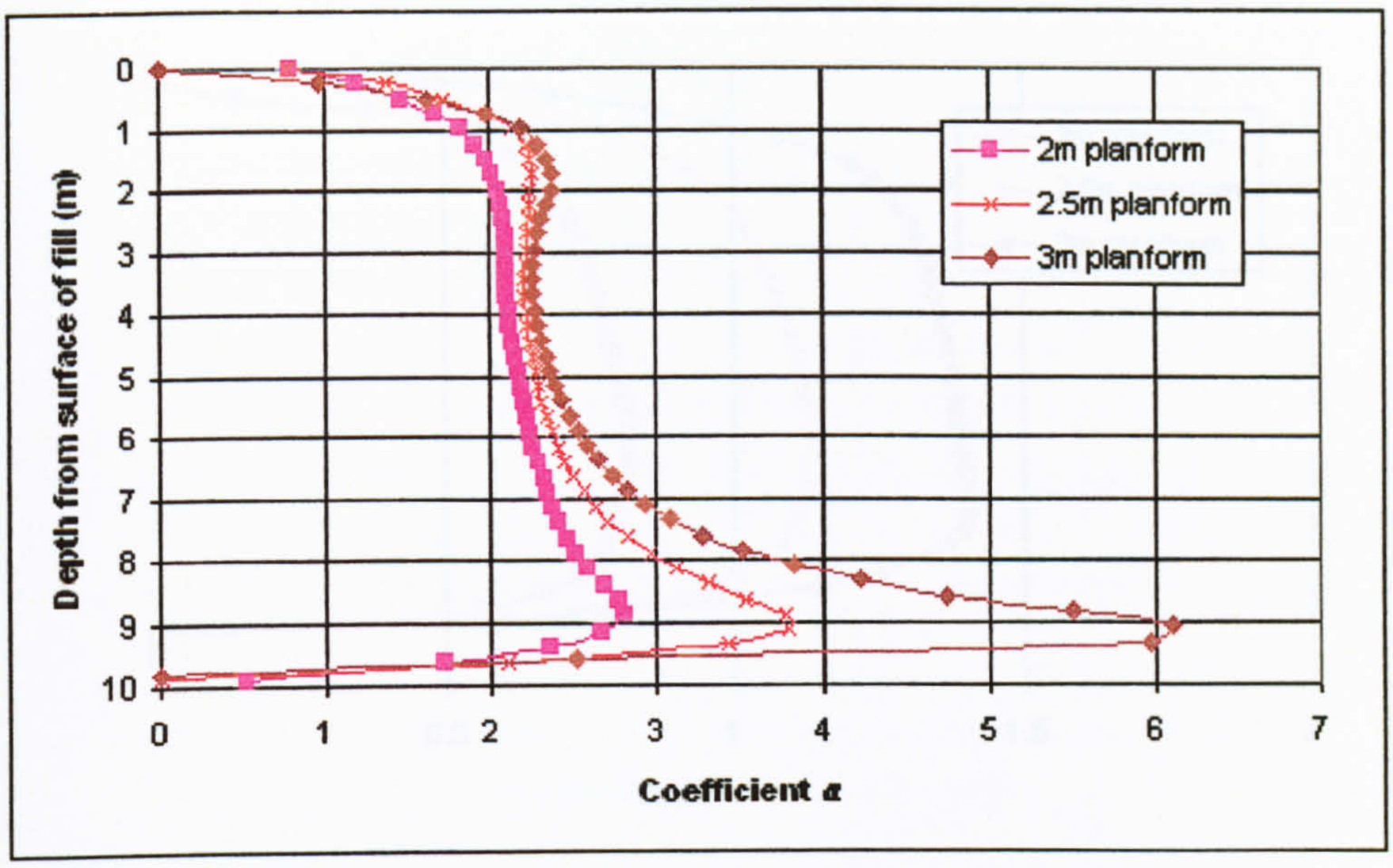

Figure 9.8 - Coefficient α for sand in the square planform bins

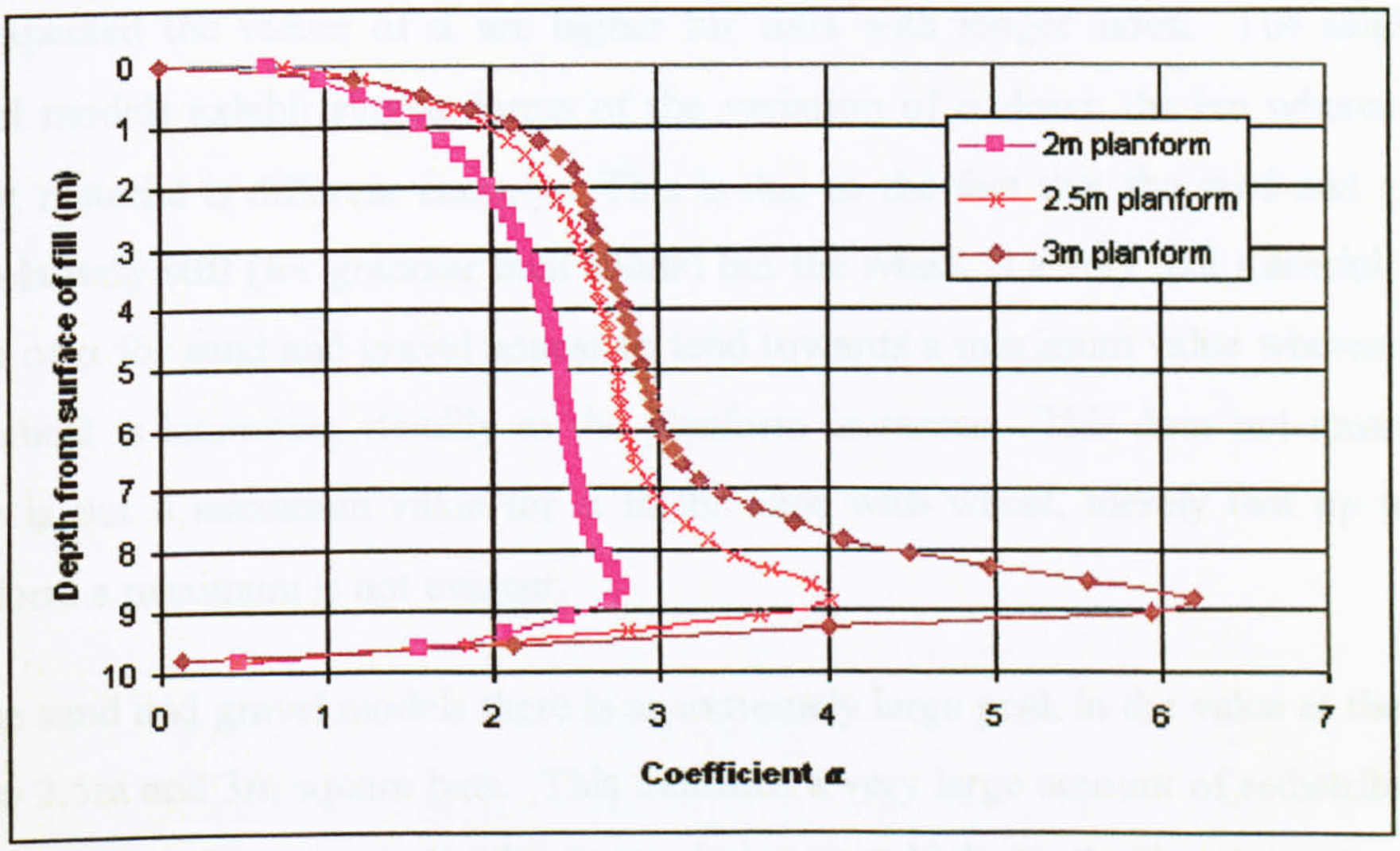

Figure 9.9 - Coefficient α for gravel in the square planform bins

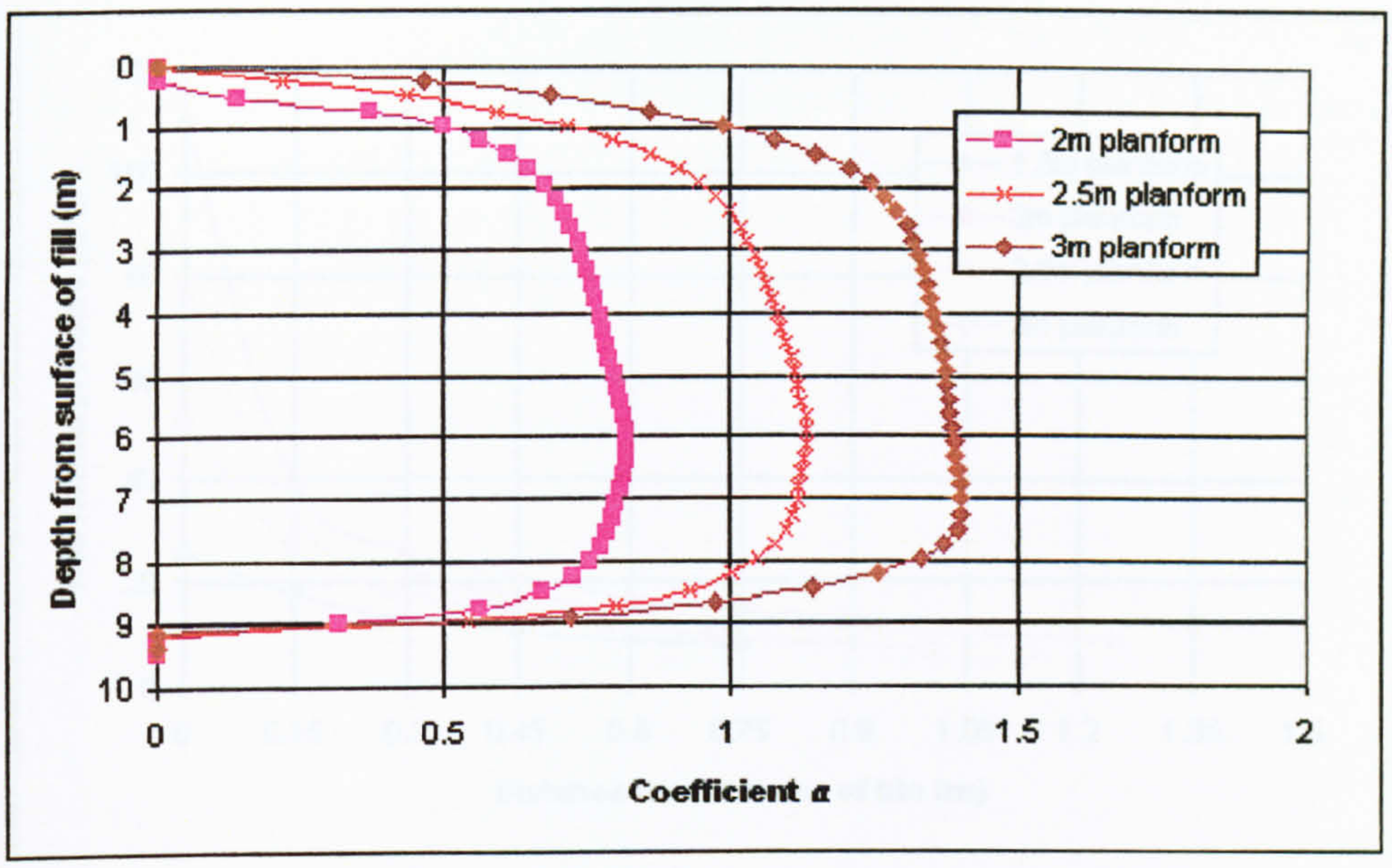

Figure 9.10 - Coefficient α for wheat in the square planform bins

As expected the values of α are higher for silos with longer sides. The sand and gravel models exhibit similar forms of the variation of α down the bin whereas the wheat material is different entirely. This is due to the fact that the sand and gravel are relatively stiff (for granular bulk solids) but the wheat is a very soft material. The value of α for sand and gravel appear to tend towards a maximum value whereas α in the wheat is increasing steadily as the planform increases. This does not mean that there is not a maximum value for α in the silos with wheat, merely that up to 3m planform a maximum is not evident.

In the sand and gravel models there is an extremely large peak in the value at the base in the 2.5m and 3m square bins. This indicates a very large amount of redistribution. This is due to the pressure in the corner being very high due to the presence of the stiff structural area where the walls meet the hopper. This leads to the observed large values of α.

Figure 9.11 shows the horizontal distribution of wall pressure in sand just above the level where the bin meets the hopper for 20mm thick bins of varying planform.

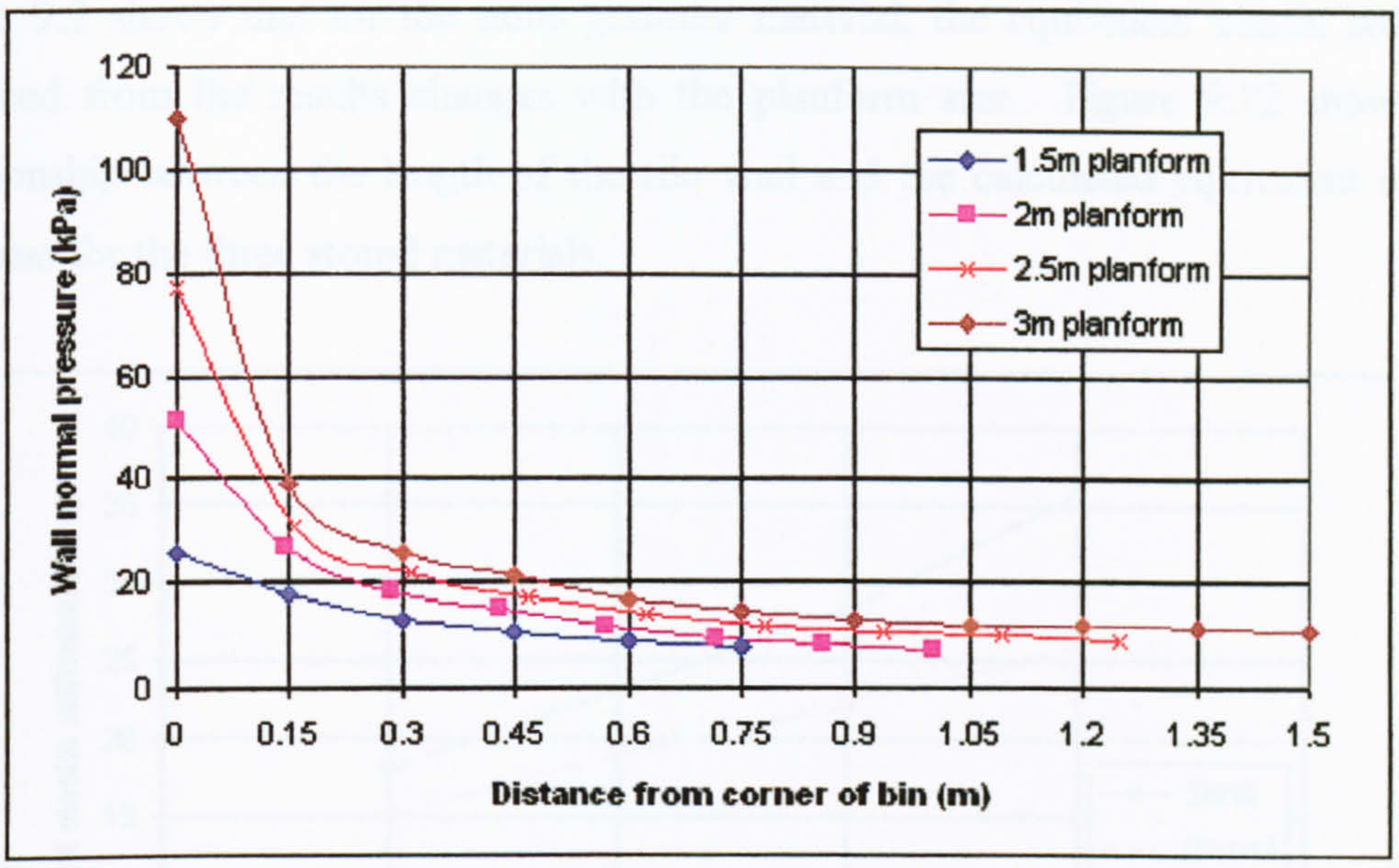

Figure 9.11 - Distribution of pressure above the transition

This figure clearly indicates that the larger models experience much higher peak pressures near the corner of the bin leading in turn to very large values of α. A large percentage of the load is carried by the corners as the wall length increases because the hopper/wall junction becomes less stiff at the midpoint. This leads to arching of the stored material between the structurally stiff corners producing the observed lower pressures at the midpoint.

9.3.2 Stiffness of ensiled material

The calculations detailed in equations 9.4 – 9.7 were again performed for the bins of varying planform with a 20mm wall thickness. The reference equivalent elastic modulus, E, of the three materials at the transition level are shown in table 9.2.

Planform size (m)	Reference equivalent elastic modulus, E (MPa)		
	Sand	Gravel	Wheat
1.5	18.10	15.15	0.73
2.0	23.10	19.03	1.18
2.5	28.27	22.21	1.47
3.0	37.74	26.05	1.70

Table 9.2 - Equivalent elastic stiffness in the square planform bins

Table 9.2 shows that for the same granular material, the equivalent elastic stiffness deduced from the results changes with the planform size. Figure 9.12 shows the relationship between the length of the silo wall and the calculated equivalent elastic stiffness for the three stored materials.

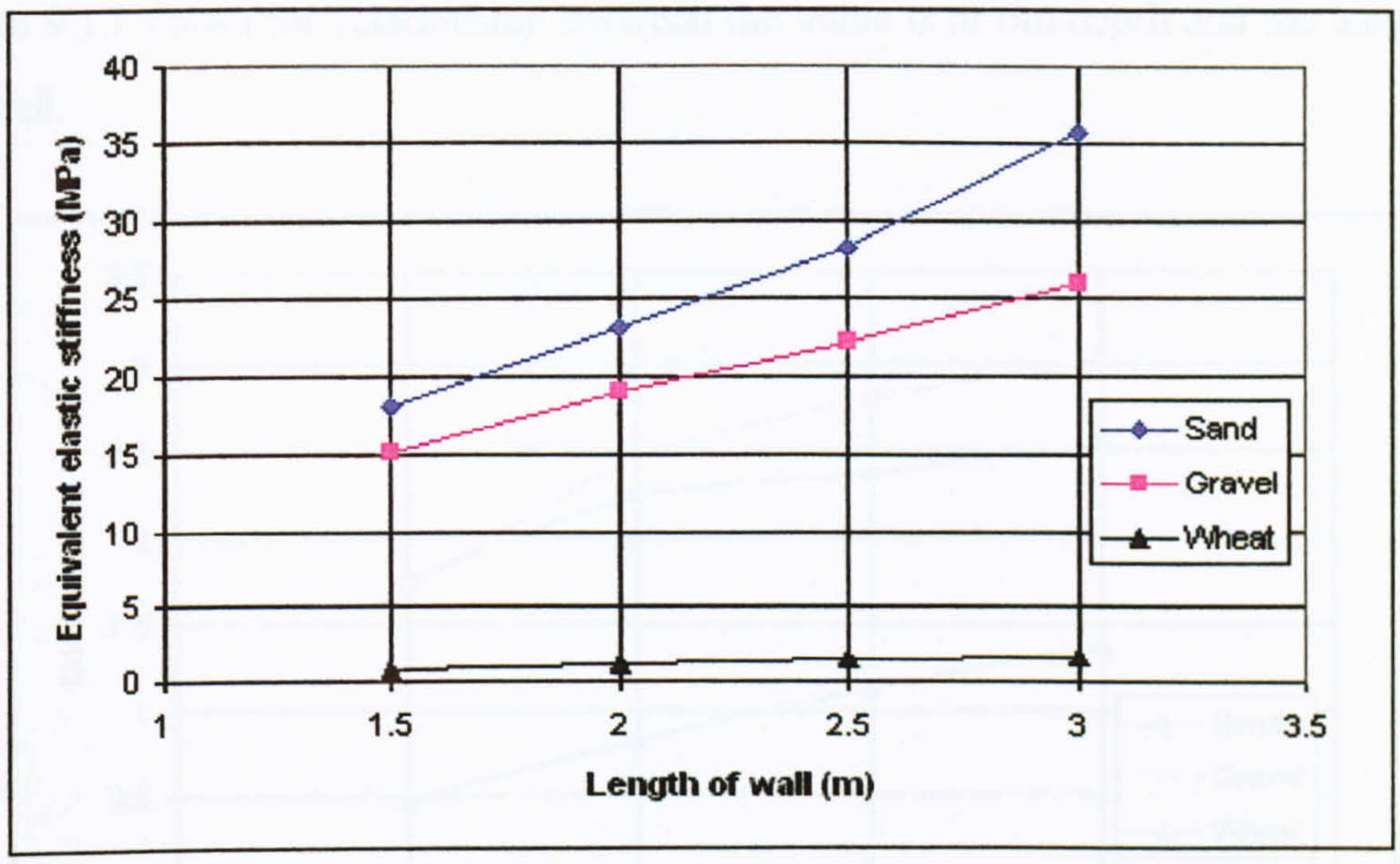

Figure 9.12 - Relationship between wall length and elastic stiffness of stored material

The relationships for all three materials are almost linear apart from the 3m wall length bin when filled with sand. Inspection of the wall deformations shows that the 3m bin experiences large deflections ($w>0.5t$) at this 20mm wall thickness (no matter what the ensiled material is modelled as) whereas the smaller bins do not. It may be that the relationship between the elastic stiffness and the wall length is linear until the bin experiences large deflections at which point the possible effect on equivalent elastic stiffness becomes difficult to predict. The conclusion might also be drawn that the equivalent elastic stiffness of the material is affected by the large deformation of the wall. This was assumed to be correct because it is known that the interaction between the wall and the solid has a direct effect on the observed wall pressures (Ooi and Rotter, 1990) and by extension, the stress state of the solid.

As noted earlier there is a large end effect present in some of these bins. Therefore in order to study the relationship between the wall length and the value of α it is

necessary to study some area of the bin that is away from these end effects. The level chosen is 6m depth. This depth is chosen because it is reached before the end effects become apparent but it is also deep enough in the silo to allow the Janssen equilibrium to be almost developed.

Figure 9.13 shows the relationship between the value α at 6m depth and the length of the wall.

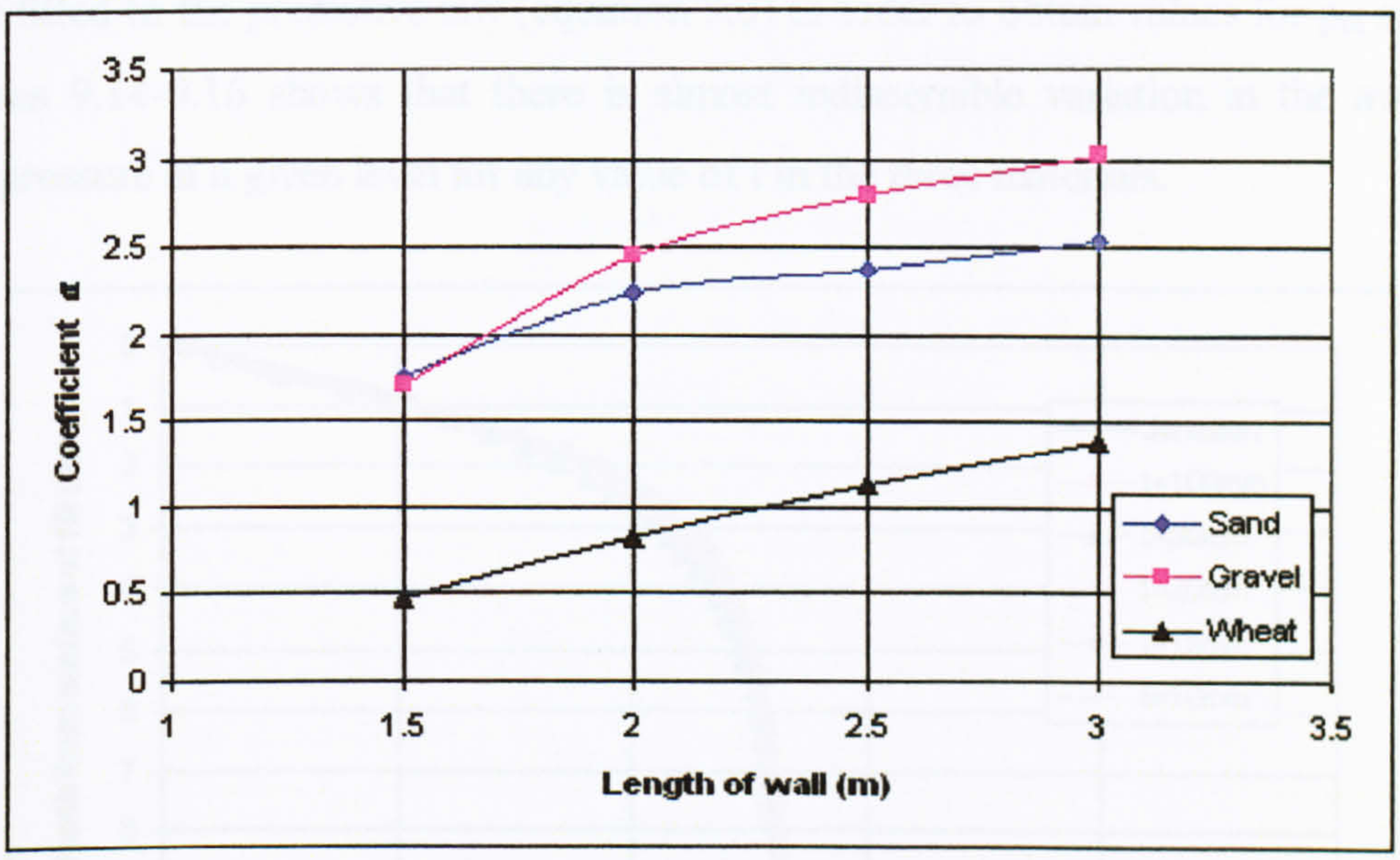

Figure 9.13 - Relationship between wall length and α

This figure appears to indicate that rather than exhibiting direct proportionality, the value of α may tend towards an asymptote. At this wall thickness (20mm) it is not possible to create larger models since large deflections will occur which appears to interfere with the trends noted so far. It would therefore be advantageous to incorporate a study into the relationship between t and α. The two studies could then be combined and enable many cases to be examined since a dimensionless measure of wall geometry could be formulated with which to compare the value of α.

9.4 Wall thickness

In order to investigate the effect of the wall thickness, a number of tests were performed using the small geometry as before (1.5m square planform) but with

increasing values of t. Section 9.3.2 showed that the relative stiffness between the wall and the solid had an effect on the level of redistribution across the silo wall but it was not possible to identify a direct relationship between these parameters. If the wall thickness is increased then the redistribution should decrease for a given solid and vice versa. The wall thickness used in section 9.2 for this model was 20mm and in this section results are present for wall thicknesses of 10, 15, 20, 30 and 100mm. The choice of wall thicknesses used is arbitrary. As before, the finite element results were fitted to the predictive law (equation 9.3) in order to obtain values for p_m and α. Figures 9.14-9.16 shows that there is almost indiscernible variation in the average wall pressure at a given level for any value of t in the three materials.

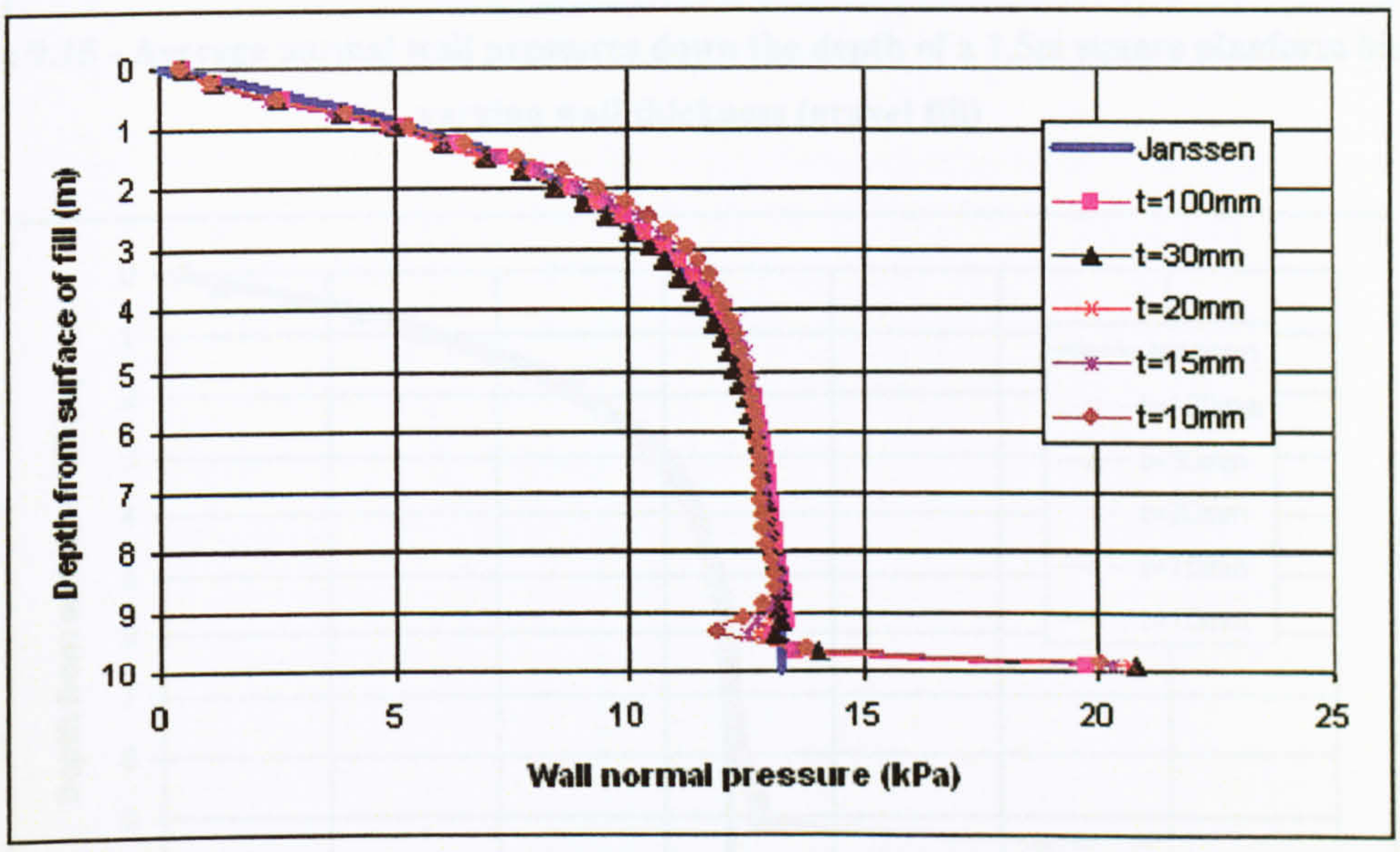

Figure 9.14 – Average normal wall pressures down the depth of a 1.5m square planform bin with varying wall thickness (sand fill)

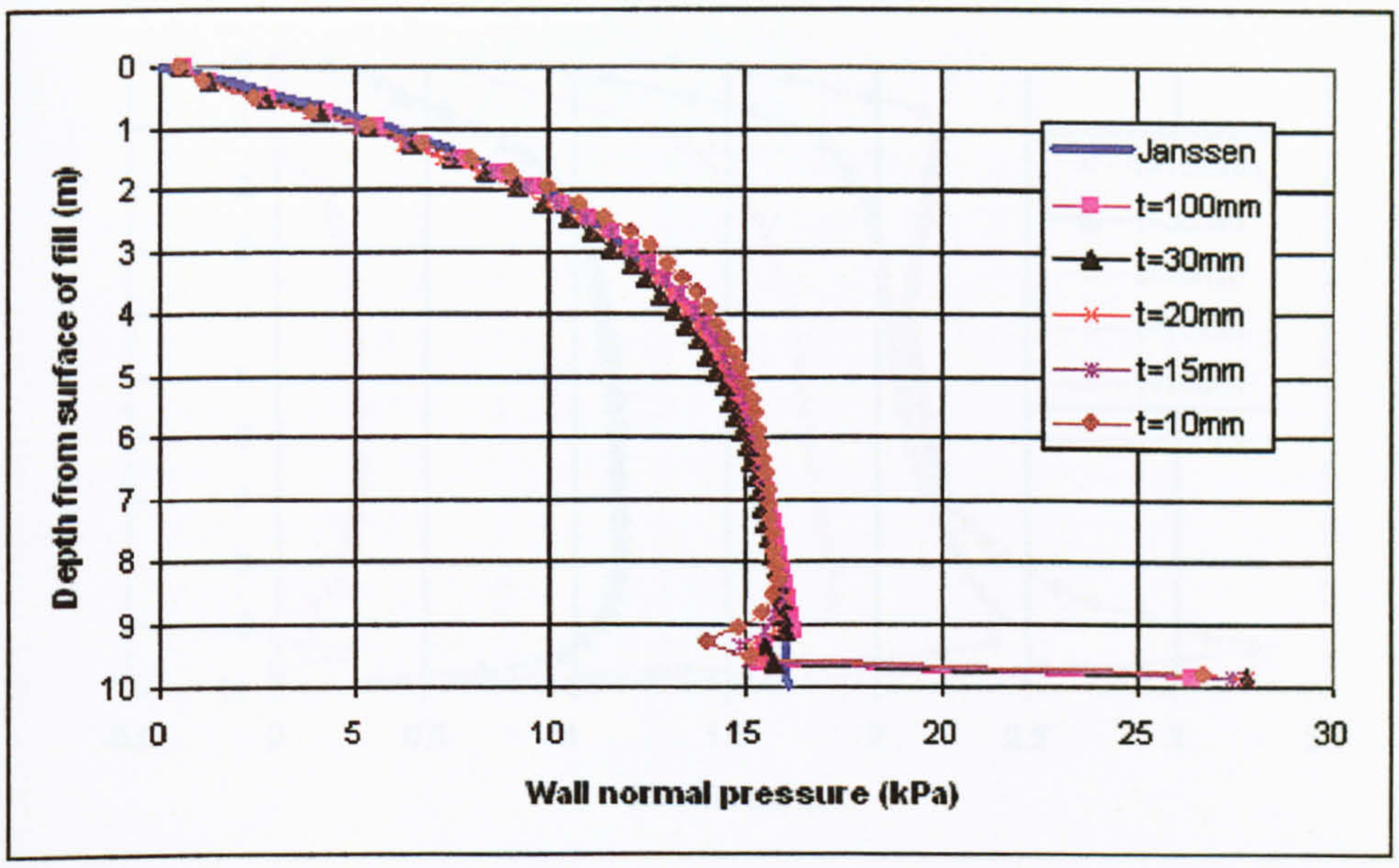

Figure 9.15 - Average normal wall pressures down the depth of a 1.5m square planform bin with varying wall thickness (gravel fill)

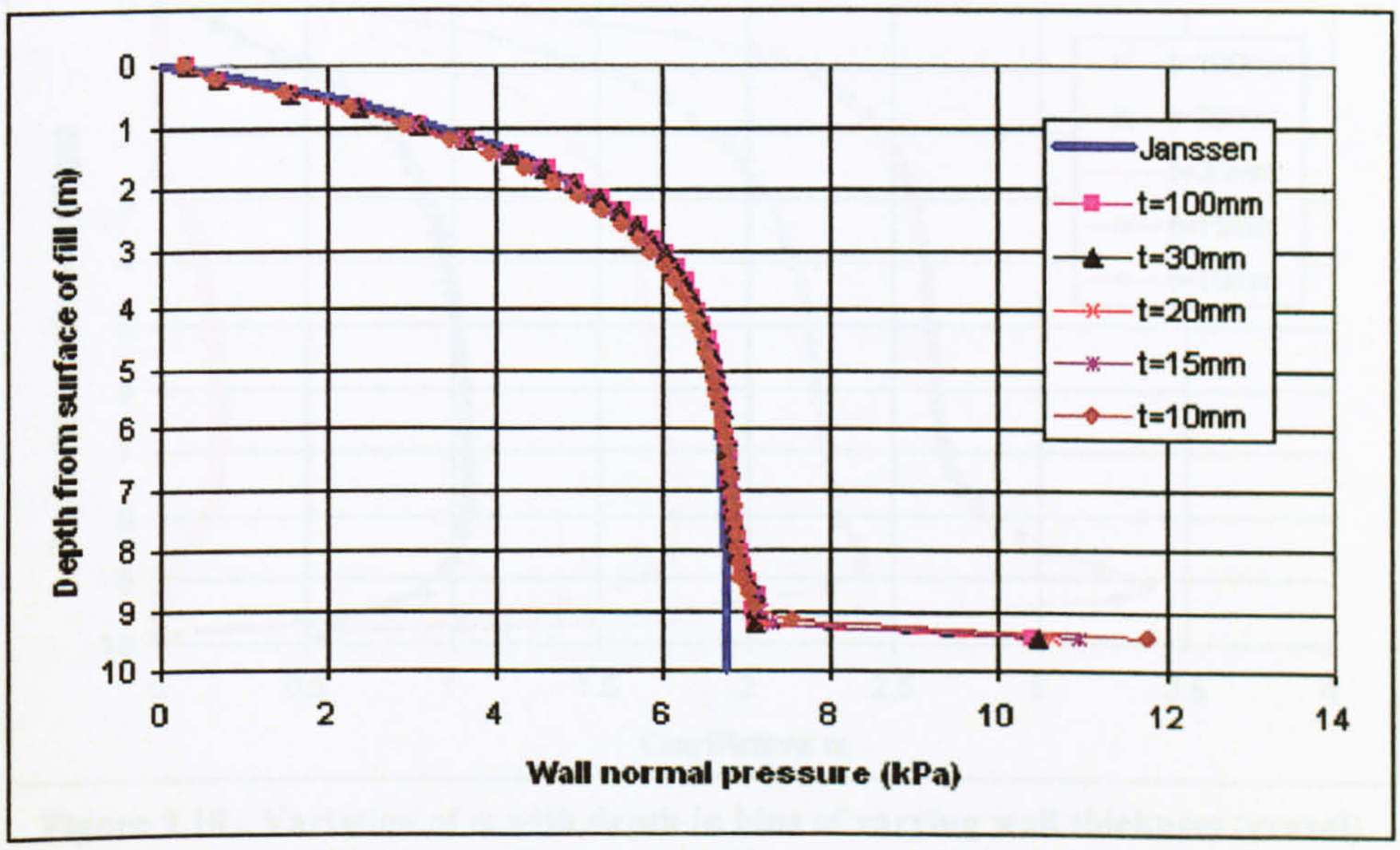

Figure 9.16 - Average normal wall pressures down the depth of a 1.5m square planform bin with varying wall thickness (wheat fill)

There are again some end effects as the transition of the bin is approached which are more pronounced when the bin wall is very thin. Fitting these results to the predictive law gives values of α at all points down the bin wall. Figures 9.17-9.19 show the distribution of α for all the wall thickness' in the three materials.

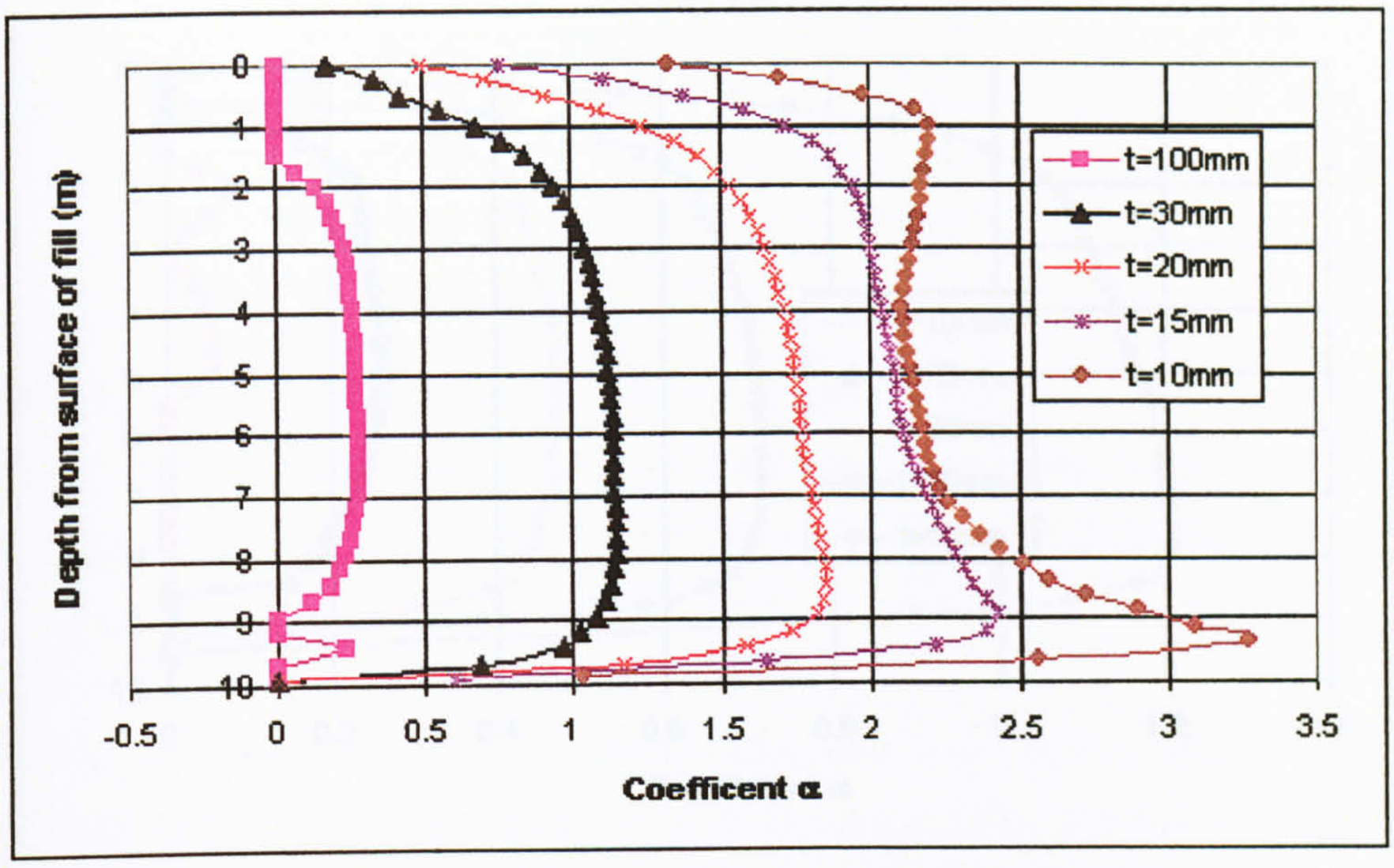

Figure 9.17 - Variation of α with depth in bins of varying wall thickness (sand)

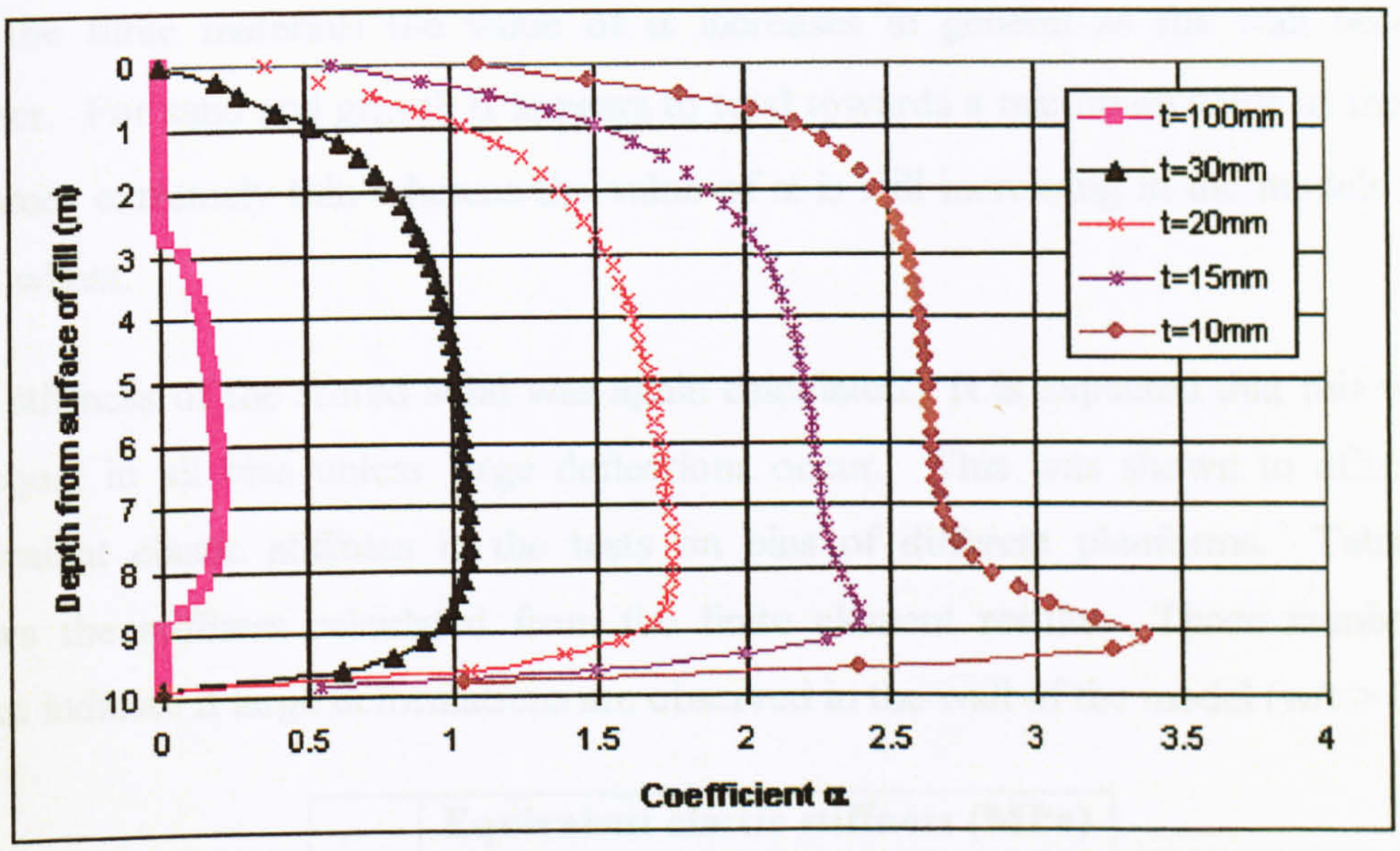

Figure 9.18 - Variation of α with depth in bins of varying wall thickness (gravel)

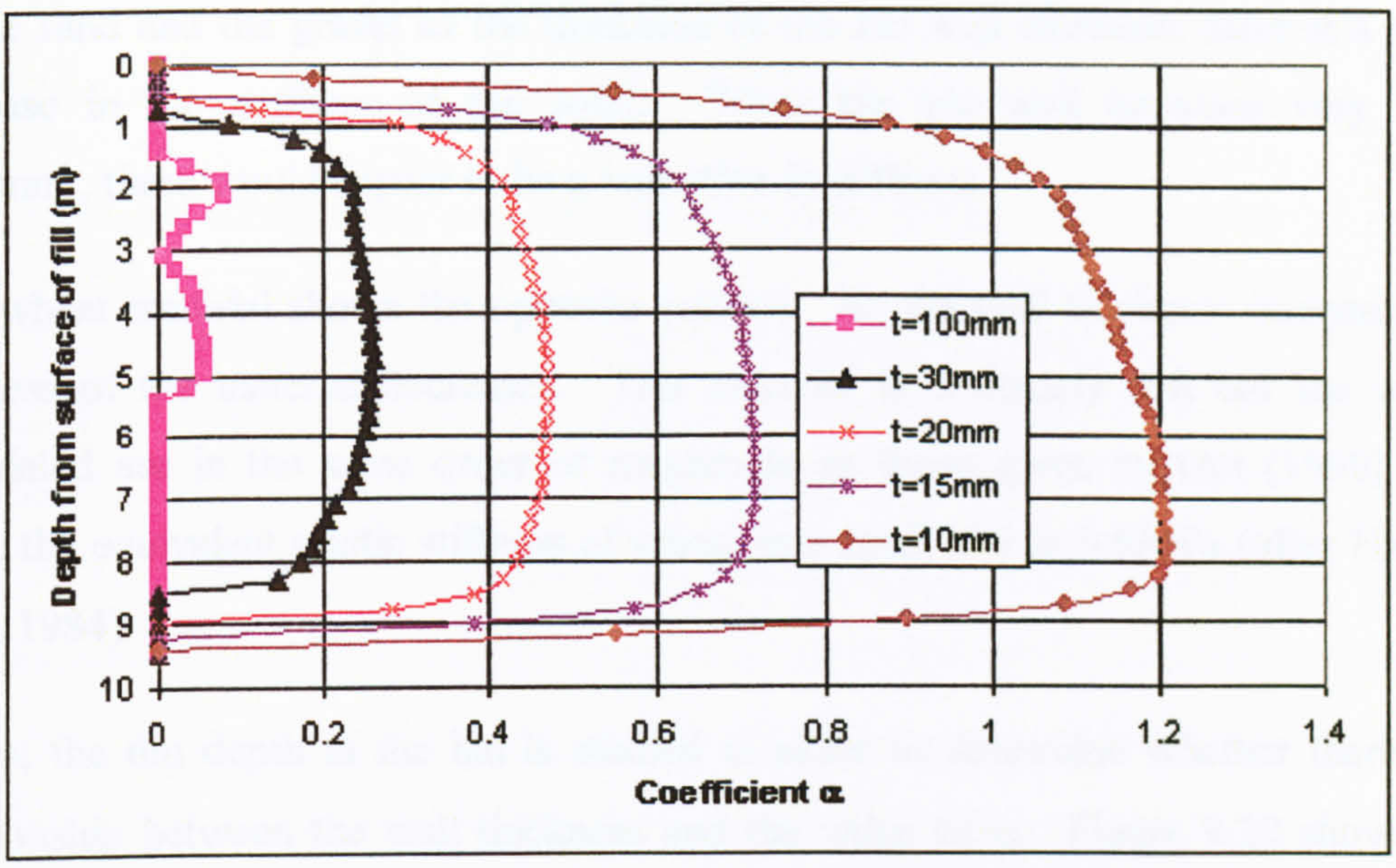

Figure 9.19 - Variation of α with depth in bins of varying wall thickness (wheat)

For the three materials the value of α increases in general as the wall becomes thinner. For sand and gravel, α appears to tend towards a maximum value as the wall becomes extremely thin whereas the value of α is still increasing in the models filled with wheat.

The stiffness of the stored solid was again calculated. It is expected that this would be equal in all bins unless large deflections occur. This was shown to affect the equivalent elastic stiffness in the tests on bins of different planforms. Table 9.3 shows the stiffness calculated from the finite element results. Those numbers in italics indicate if large deformations are observed in the wall of the model ($w/t > 0.5$).

	Equivalent elastic stiffness (MPa)		
t	**Sand**	**Gravel**	**Wheat**
10	***17.04***	***13.87***	0.95
15	17.48	14.65	0.89
20	18.10	15.15	0.73
30	18.55	15.42	0.72
100	17.57	14.69	0.72

Table 9.3 - Equivalent elastic stiffness with varying wall thickness

In the sand and the gravel as the thickness of the bin wall increases there is a slight increase in the stiffness of the solid. When the bin wall becomes very thick (100mm), there would appear to be a reduction in stiffness.

The wheat material shows the opposite pattern. As the wall thickness increases the stiffness of the material decreases. This material is extremely soft but the values calculated are in the same order of magnitude as those given by Ooi (1990) who gives the equivalent elastic stiffness of wheat in a small silo as 0.6MPa (after Hartlen *et al*, 1984)

Again, the 6m depth in the bin is studied in order to determine whether there is a relationship between the wall thickness and the value of α. Figure 9.20 shows the variation of α at 6m beneath the surface of the solid with the wall thickness.

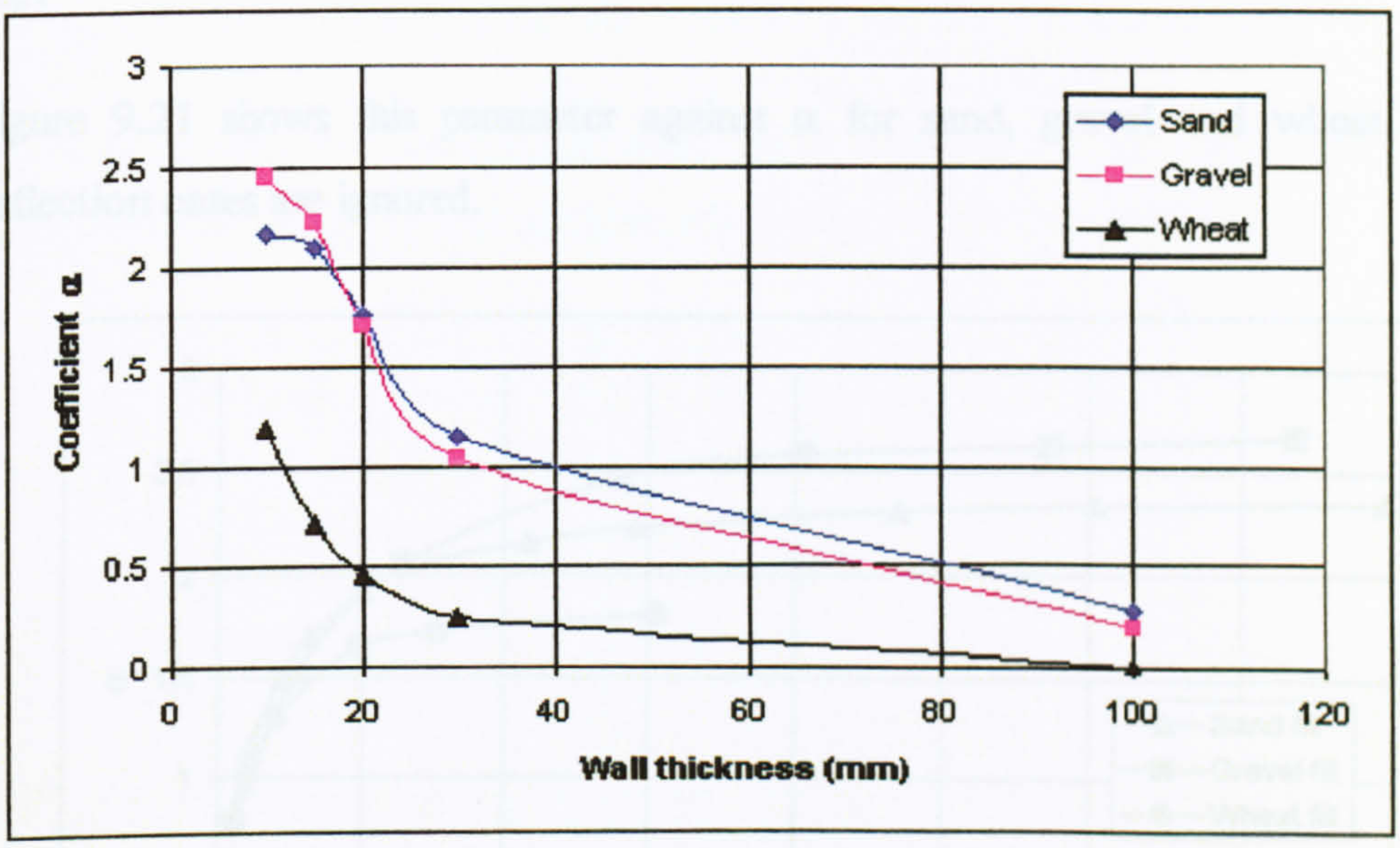

Figure 9.20 - Variation of α at 6m depth with wall thickness

In the sand and gravel materials the first point on the graph (t=10mm) might be ignored as there is the possibility that this result has been affected by the observed large deformation. As t increases the value of α rapidly decreases and at t=30mm the redistribution is greatly reduced. When t=100mm the value approaches zero and therefore implies that there is no redistribution. This figure shows that there is likely

to be a point where the advantage of decreasing the wall thickness reaches a limit as the maximum amount of redistribution is already reached.

9.5 Relative stiffness of silo wall and ensiled material

It was suggested in section 9.1 that in the same way that the ratio R/t had been identified as a measure of the stiffness of a cylindrical silo, a form of the ratio L/t could be the equivalent measure for flat plates. If the wall is considered to be made from strips of unit width then the stiffness of each strip is related to L^3/t^3. The results presented above show that the value of α is affected by the relative stiffness of the wall and the stored solid and therefore the proposed parameter for the relative stiffness between the silo wall and the contents may be estimated from equation 9.8.

$$\frac{E_s L^3}{E_w t^3} \tag{9.8}$$

Figure 9.21 shows this parameter against α for sand, gravel and wheat. Large deflection cases are ignored.

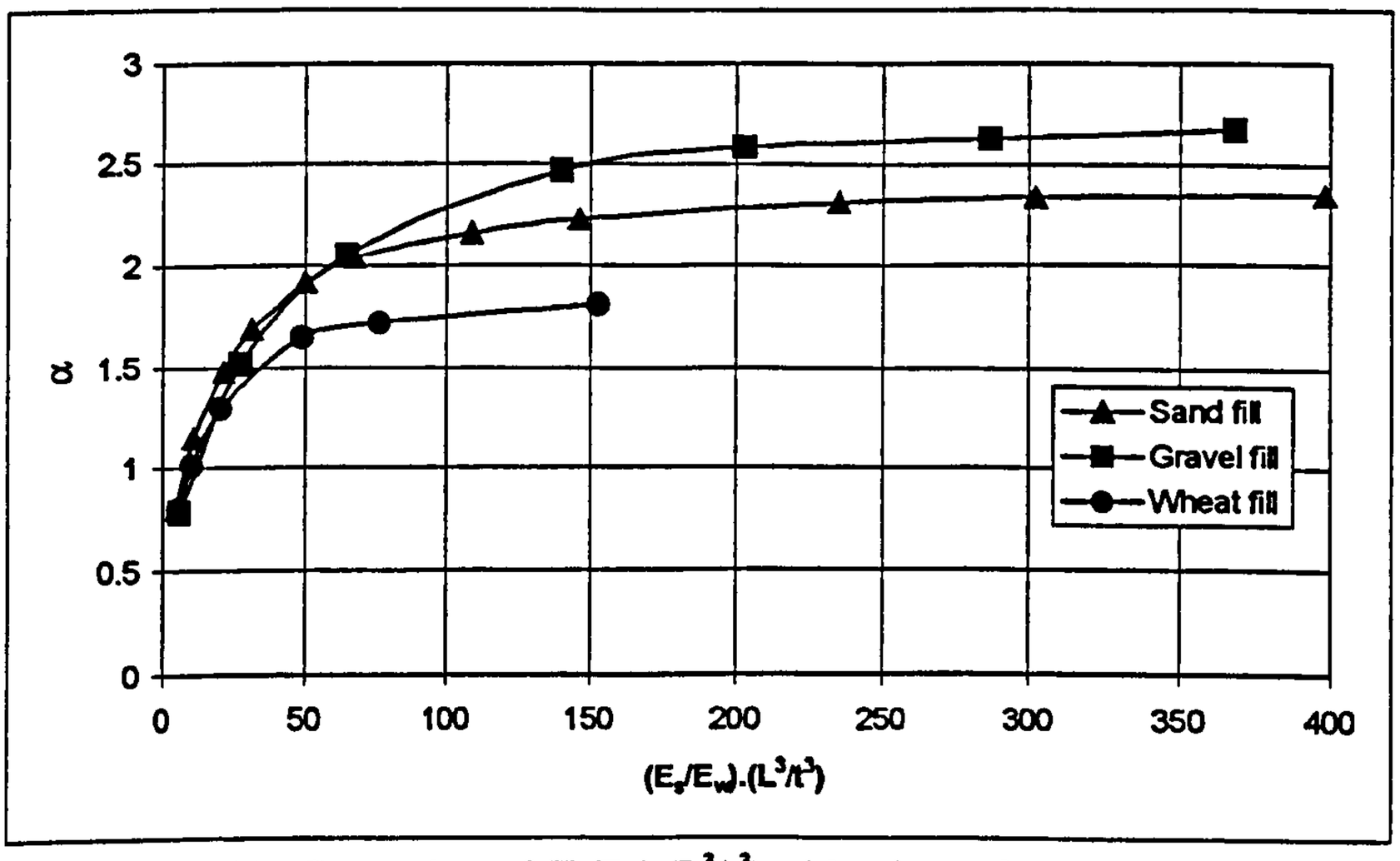

Figure 9.21 - Comparison of $(E_s/E_w).(L^3/t^3)$ with α in sand, gravel and wheat

It is not easy to create "small deflection" models that lead to high values (comparable with sand and gravel) of E_sL^3/E_wt^3 when using the wheat material because of the extremely low stiffness of the solid. Large L/t values lead to large delfections.

The figure shows that an asymptotic situation is approached as the value of the parameter E_sL^3/E_wt^3 increases. An increase in the value of this signifies an increase in the wall length, a decrease in wall thickness or a combination of both. The asymptotic value of α for the sand appears to be around 2.3, for gravel the value might be taken as 2.7 and for wheat about 1.8.

9.5.1 Effect of large deformations in the wall

The cases studied above have been concerned with those deformations that are classified as small (i.e. $w/t<0.5$). It has been shown that when a large deflection occurs there is a significant effect on the value of α and the stiffness of the solid.

Figure 9.22 shows the results for sand from figure 9.21 but with two large deformation cases added. These are indicated by the square data markers.

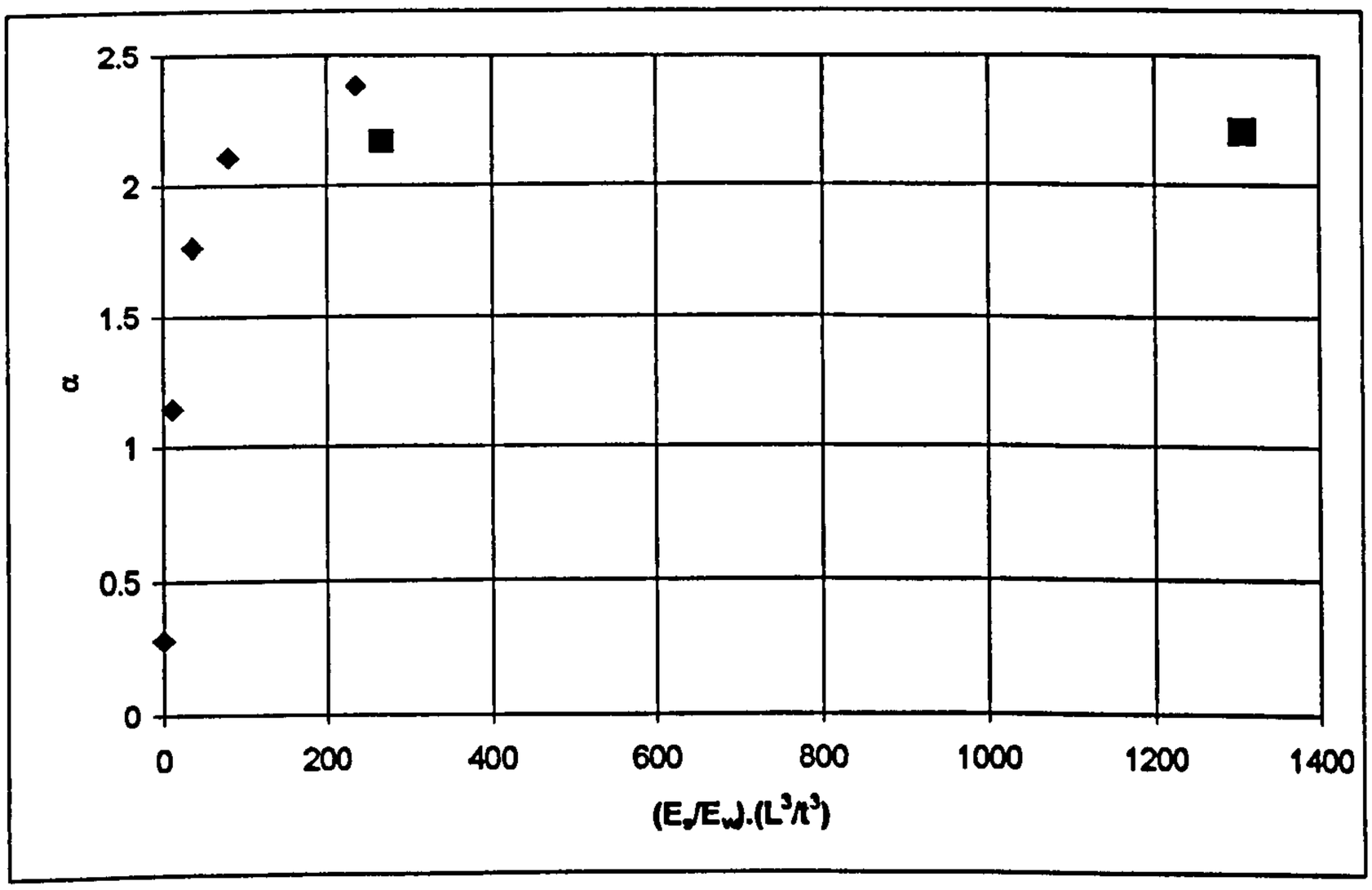

Figure 9.22 – Effect of large deformations on the value of α

The two cases that experience large deformations show a reduction in the value of α indicating that there is less redistribution of pressure when the deformation is large. However, due to the presence of large deformations, the value of the parameter E_sL^3/E_wt^3 is overestimated and therefore this graph is slightly misleading. If a measure of the relative stiffness of wall and solid that incorporated large deflections could be determined it is expected that all data points would sit on the same curve.

The results shown suggest that in the type of bin modelled above the level of redistribution does not increase significantly even though the value of the parameter E_sL^3/E_wt^3 has increased substantially. This indicates that the maximum value of α in large deformation cases may exhibit a lower maximum level than the cases presented earlier where α appeared to tend towards 2.25 for sand.

9.6 Variation of height of silo

All the silos modelled in this chapter thus far have had a height of 10m. Some of the same planforms and wall thicknesses are now modelled at 5m height in order to investigate whether these silos display similar trends to the deeper models. Figure 9.23 shows the comparison of wall normal pressures in a 1.5m planform silo. The 5m high silo is shown against results for the 10m high silo. Results are shown for a sand fill.

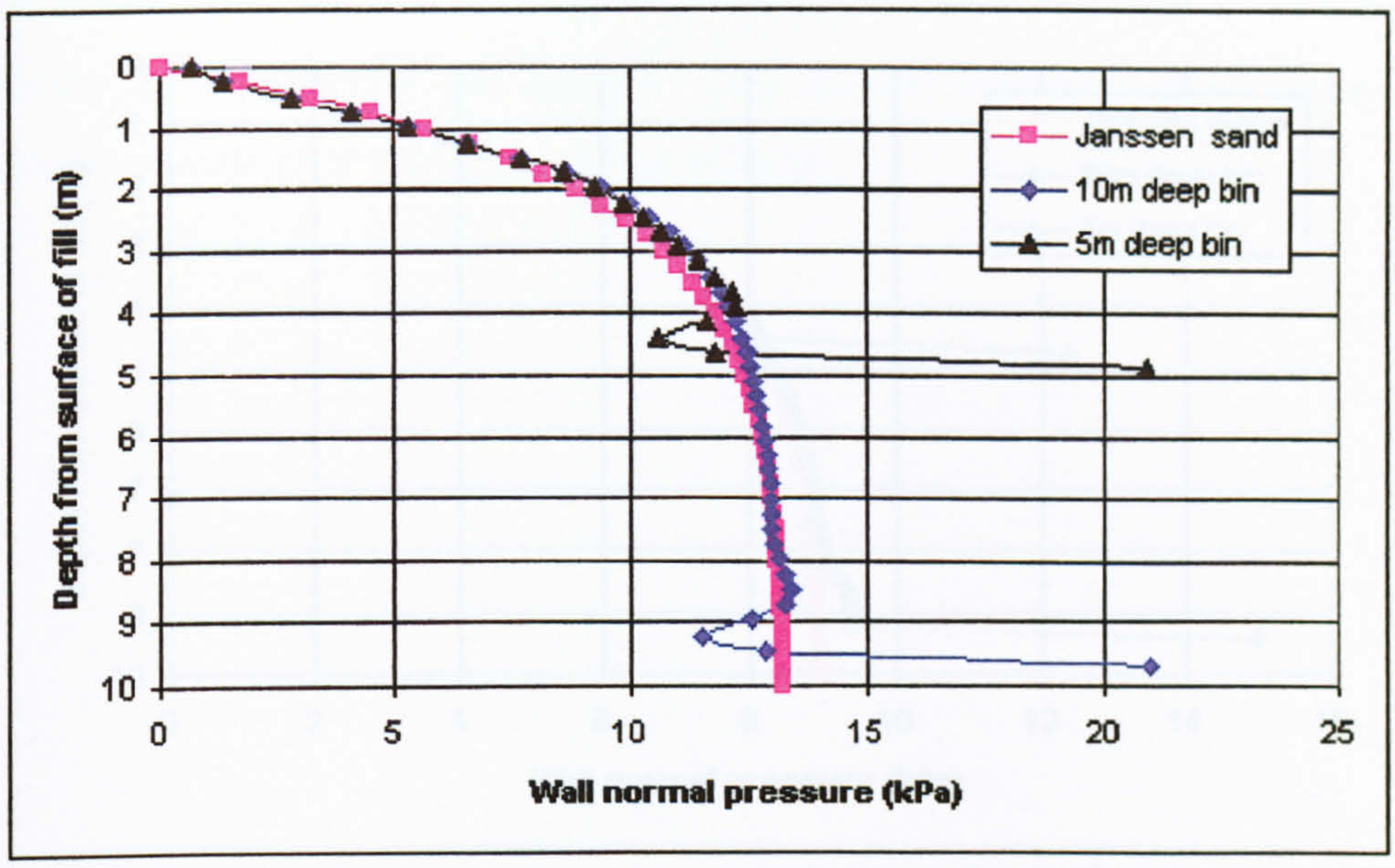

Figure 9.23 – Comparison of results obtained in a 10m deep bin and 5m deep bin (sand fill)

The pressures in the 5m deep bin are very close to those predicted in the 10m deep bin near the surface. Moving down the bin the pressure deviates away from that in the 10m deep bin as the transition is reached. This end effect is similar to that exhibited by the 10m deep bin.

This pattern is also evident in the bins of different wall thickness, planform and when they are modelled with different materials. Figure 9.24 shows results for 5m and 10m deep bins with 2m planform filled with wheat. The wall thickness is 20mm.

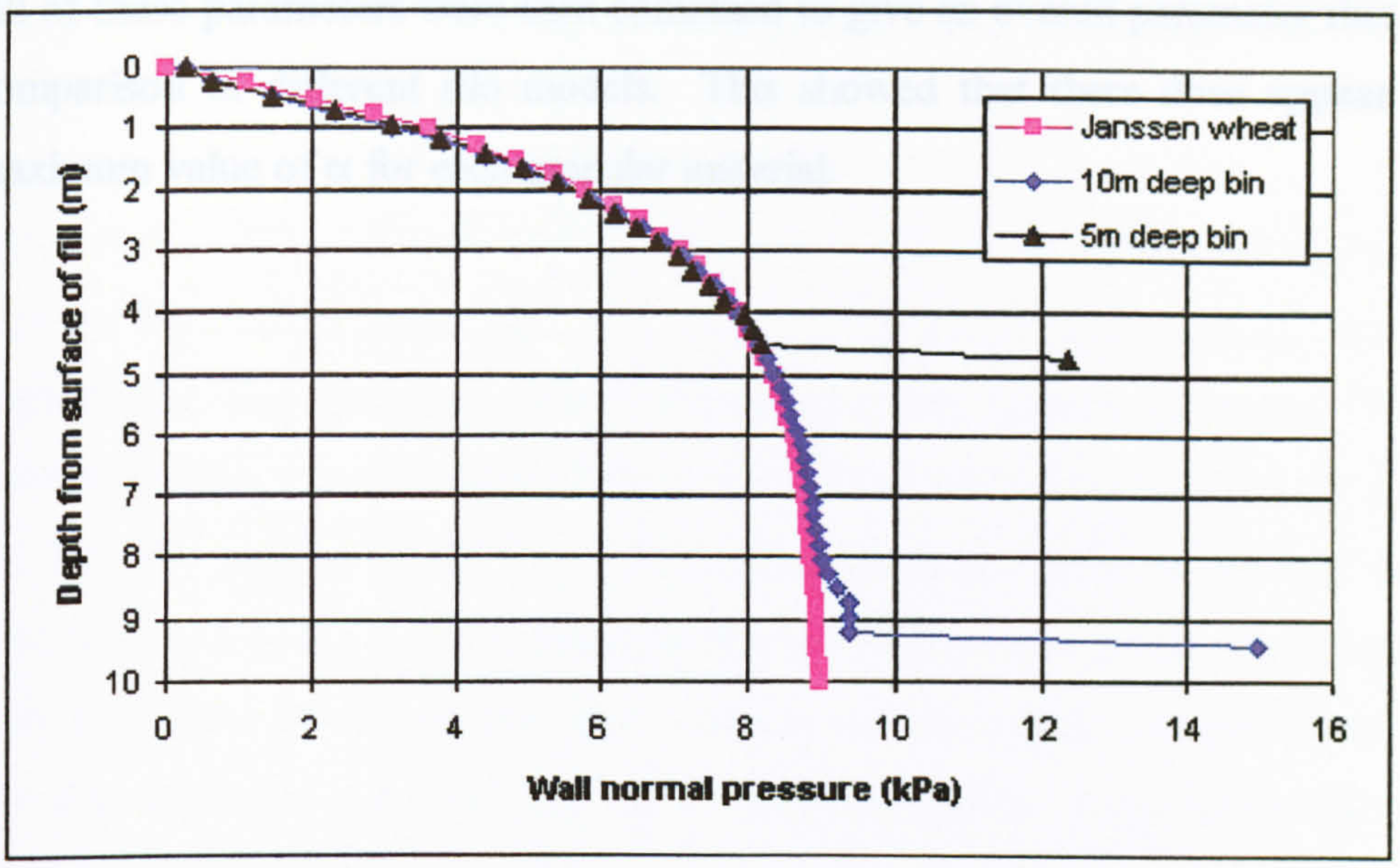

Figure 9.24 – Average wall pressures in a 2m square planform silo of different height (wheat fill)

Again, a similar pattern of results is observed.

9.7 Summary

The work presented above has investigated a number of variations in a square planform silo. The stored material modelled was first altered and this showed that different materials exhibit different levels of redistribution across the wall but on average compare well with the Janssen distribution for pressures down the bin wall. The equivalent elastic stiffness of the materials was calculated and it was shown that the stiffest material showed the highest level of redistribution.

The variation of the planform size was then investigated and it was again shown that the Janssen theory was a good predictor of the pressure down the wall. The equivalent elastic stiffness was calculated and found to be almost linearly proportional to the size of the planform no matter what the stored material was modelled as.

The wall thickness was then varied and it was found that there appeared to be a maximum value of α that was tended towards for each material as the wall got thinner.

All of these parameters were then combined to give an overall parameter that allowed comparison of different silo models. This showed that there does appear to be a maximum value of α for each granular material.

Chapter 10 - Experimental investigation of a very thin-walled square silo

Jarrett *et al* (1995), Lahlouh *et al* (1995) and Rotter *et al* (2002) have shown that the pressure distribution across the wall in a square silo is non-uniform. In previous chapters this fact has been corroborated by finite element analysis. The finite element analysis was then used to show that if the wall of the structure is made very thin then the membrane stiffness of the plate supports some of the load and large deflections can safely occur without permanent deformation of the silo structure. In order to further investigate this phenomenon an experiment was performed using a very thin walled model steel silo filled with pea gravel of the same type used by Lahlouh *et al* (1995).

10.1 Silo geometry and construction

The silo studied is a 1m square plan-form and is constructed with a flat base. The overall height of the silo is 1.5m and the wall thickness is 1.6mm. The silo is constructed from a 5mm thick steel angle section frame that supports flat wall panels that are joined to the frame using epoxy adhesive. This method was chosen as it was felt that other techniques would have a detrimental effect upon the quality of the internal walls. When using sheet metal that is of such a thin gauge, welding or mechanical fixing could cause local deformations near the corners. It has been shown by Ooi and She (1997) that silos are very sensitive to geometric defects and by using adhesive any effects of this type would be reduced whilst still retaining sufficient strength in the joints. Tests were performed on a range of adhesives in order to determine whether they were of suitable strength to support the walls. Figure 10.1 shows an overall view of the silo rig. There is some staining visible on the front face of wall as a result of the metal sheets getting damp during delivery. However, the sheets were mounted in such a way as to ensure the internal faces were free from this type of defect.

Figure 10.1 – Overall view of the experimental silo structure

Filling and emptying are by means of an aero-mechanical conveyer. This takes stored material and places it into a filler box. This box can be seen at the top of figure 10.1 and an internal view is shown in figure 10.2.

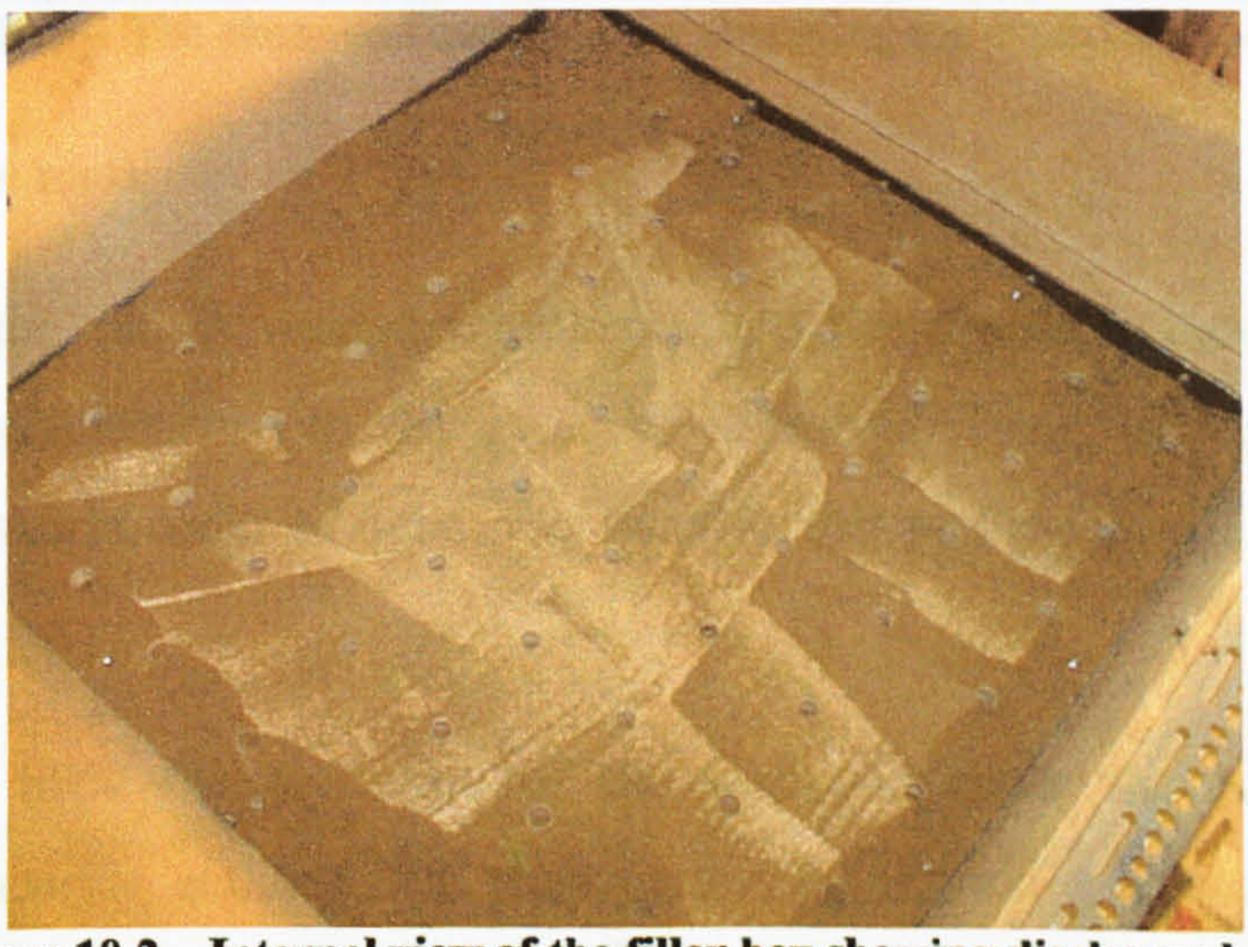

Figure 10.2 – Internal view of the filler box showing discharge holes

The purpose of this box is to produce as even and repeatable fill as possible in the silo. The holes may be shut off and then granular material placed in the box via the conveyor. This material is then allowed to discharge from the filler box into the silo. This process aims to give a level and evenly distributed fill. As the filler box is much shallower than the silo the process must be repeated several times until the silo is full. The silo is emptied by means of a large flap in the base of the silo. This experiment does not intend to measure emptying pressures and therefore the only consideration for this flap was that the silo could be emptied quickly in order to speed up the experimental process. Figure 10.3 shows the chute and conveyor that takes material away from the silo and back into the storage hopper.

Figure 10.3 – The chute and conveyor for emptying the experimental silo rig

10.1.1 Adhesive tests

The frame of the silo is welded together. Into this frame is mounted flat metal panels. These are attached to the frame by adhesive. Tests were carried out on a range of adhesives in order to determine whether this method would provide enough strength.

As the silo is filled the deflection of the wall will cause the adhesive joint to experience a shearing action. The tests performed therefore replicated this action. Samples were prepared by bonding two strips of mild steel with a joint surface area

of 625mm^2. These were then mounted in an Instron 8500 series machine and loaded until failure occurred. Table 10.1 shows the results of this series of tests.

Adhesive type	**Maximum load (kN)**
Araldite epoxy (type available in DIY shops)	5.848
Araldite rapid (type available in DIY shops)	3.137
Devcon 2 tonne epoxy	2.053
Loctite 4080 cynoacrylate	9.332
Araldite 2013	4.928
Araldite 2014	7.204

Table 10.1 - Results from shear tests of different adhesives

The Loctite brand cynoacrylate gives the strongest bond in these tests. However, the disadvantage to this is that it prohibitively expensive for the quantities required and it has a limited storage life. The Araldite 2014 however is available in large quantities, can be stored for a considerable time (it is a two part epoxy) and provides sufficient strength for the silo model. It was estimated that one wall (which is bonded along three sides) would have an adhesive contact surface area of approximately 0.1m^2 and by extrapolating the above results it was determined that the chosen epoxy would have sufficient reserves of strength to support the entire mass of ensiled solid with ease. As a safety measure the top of the frame is tied together with angle section. This section allows the walls to move but in the event of a failure will prevent the wall from coming away from the model completely.

10.2 Instrumentation

The current work is concerned with the measurement of wall normal pressures in silos because these can be used to determine bending moments and are therefore extremely important for the design of rectangular steel silos. In order to determine whether the pressure distribution in the experimental silo is as predicted by the finite element model it would be ideal if the wall pressures could be measured directly. However, this may not be possible for reasons discussed below and it may be

necessary to make other measurements in order to infer the pressure distribution behind the wall. Possible methods that could be used are discussed below.

10.2.1 Deflections of the wall

Normal deflections of the wall could be measured and these compared to the finite element model. Unfortunately this would give little information about the state of stress in the wall or the stored solid. Small changes in the wall deflections could result in large changes in the stress state of the stored solid (and hence the wall normal pressures) and it would therefore be difficult to deduce much information by studying this alone.

If the silo used by Lahlouh *et al* (1995) is considered it can be shown using finite element analysis that the deflected form is not too sensitive to the wall normal pressure. Figure 10.4 shows the deflections across the wall (at an arbitrary height) taken from the finite element analysis performed previously. It also shows the same silo geometry subjected to a hydrostatic pressure distribution. It can be seen that although the pressure distribution on the wall is now radically different there is little difference in the deflected form and hence it would be difficult to infer any information about the pressures on the wall and the stress state in the solid.

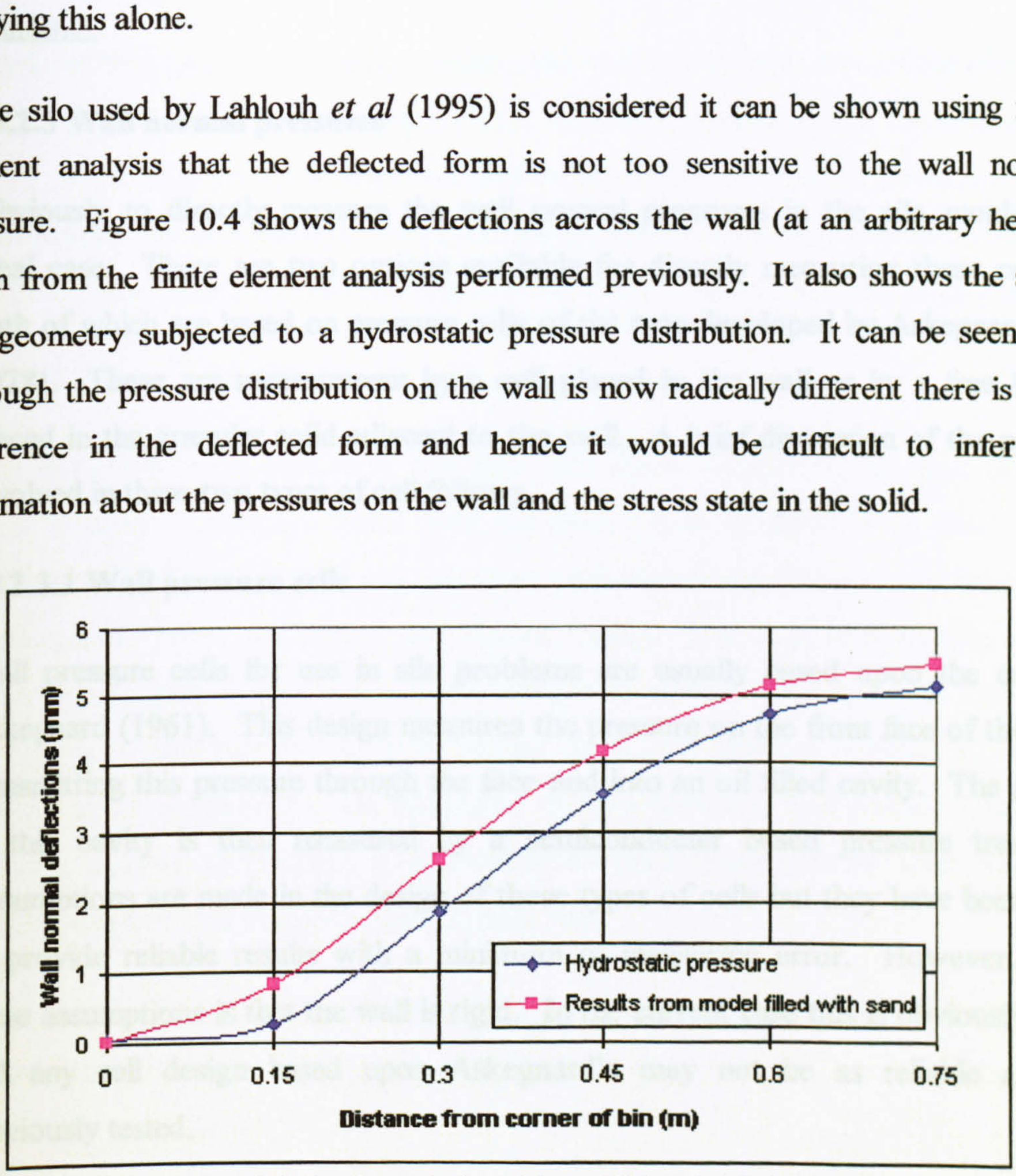

Figure 10.4 - Wall normal deflections calculated from FEA under different loading conditions

10.2.2 Strain in the wall

Some researchers (e.g. Chen *et al*, 1996) have suggested that it is possible to infer the pressure behind a wall from strain readings taken from gauges attached to the exterior of the wall. This method would make the instrumentation of the silo relatively simple and would not affect the pressure readings by disturbing the continuity of the wall inside the silo. However, this method makes a large number of assumptions which reduce the accuracy and has mostly been applied to circular silos which, being shells of revolution, are radically different to the plate type structure being studied here. The presence of large deformations would almost certainly render this method unusable.

10.2.3 Wall normal pressures

Obviously to directly measure the wall normal pressures in the silo would be the ideal case. There are two options available for directly measuring these pressures, both of which are based on pressure cells of the type developed by Askegaard (1961; 1978). These are measurement by a cell placed in the wall or by a free field cell placed in the granular solid adjacent to the wall. A brief discussion of the principles involved in these two types of cell follows.

10.2.3.1 Wall pressure cells

Wall pressure cells for use in silo problems are usually based upon the design of Askegaard (1961). This design measures the pressure on the front face of the cell by transmitting this pressure through the face and into an oil filled cavity. The pressure in this cavity is then measured by a semiconducter based pressure transducer. Assumptions are made in the design of these types of cells but they have been shown to provide reliable results with a minimum of measuring error. However, one of these assumptions is that the wall is rigid. In the current case this is obviously not so and any cell design based upon Askegaard's may not be as reliable as those previously tested.

Figure 10.5 shows the principles of operation of this type of cell.

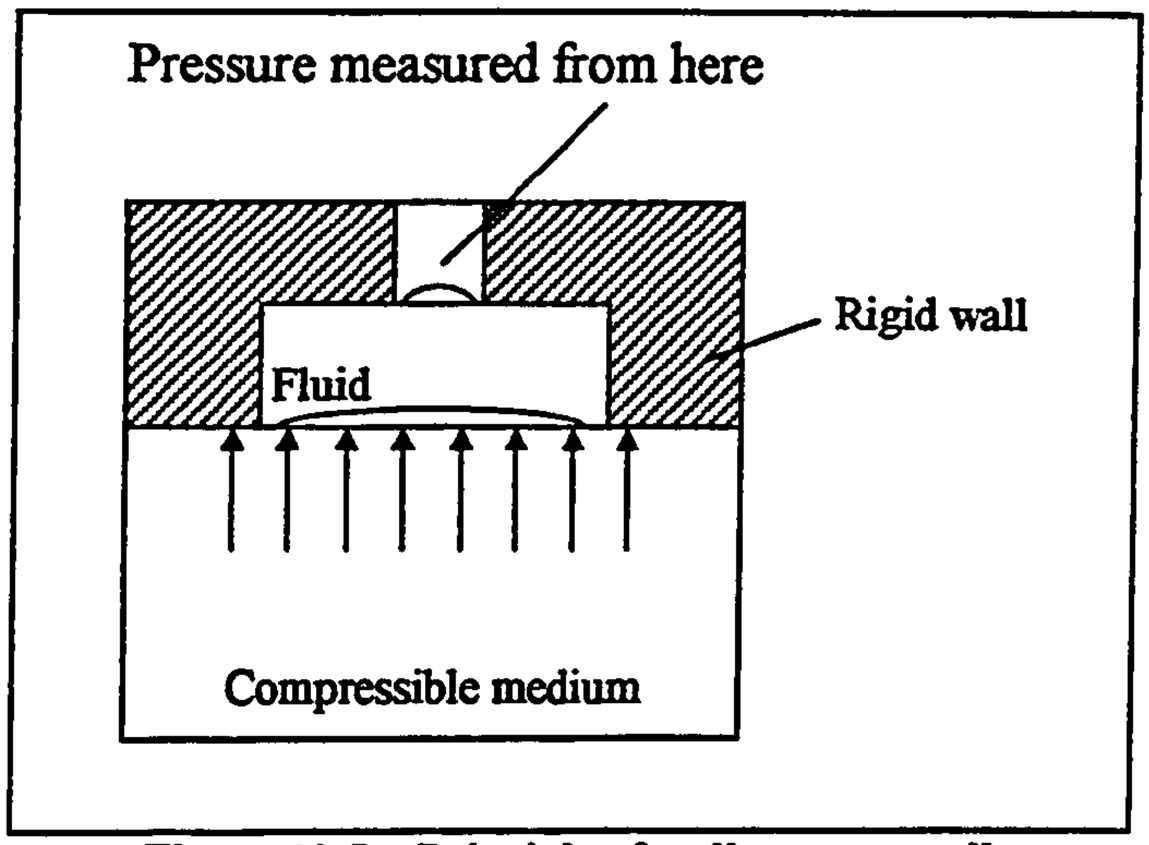

Figure 10.5 – Principle of wall pressure cell

Cells of this type are generally constructed by removing a section of the silo wall and machining the cell into the front of this. It is most important that the cell is made as stiff as possible to avoid any localised arching that may lead to erroneous pressure measurements (Askegaard, 1998). Investigation of some wall pressure cells of this type and the design of a cell for use in a thin-walled silo can be found in Appendix E.

10.2.3.2 Free field cells

As an alternative to wall cells, free field cells which measure the pressure in the solid can be used. These are based upon the theory of an inclusion in an elastic medium (Eshelby (1957)) and their use has been well documented (Munch-Anderson, 1982; Askegaard, 1995; Askegaard and Brown, 1995). Free field cells require a greater degree of "skill" when using them compared to wall cells because they can be sensitive to the way the material around them is in contact. Garnier *et al* (1999) investigated methods for the placement of free field cells and deduced that with a certain amount of practice it is possible to place these cells by hand and obtain consistent readings between experimental runs.

Free field cells of the type shown in figure 10.6 are available for this project and would seem to be the ideal solution.

Figure 10.6 – Free field cell of the type designed by Askegaard (1978)

Unlike the wall cell the bending of the wall will not induce an incorrect reading in the cell but there may be other problems associated with the large deflection expected in this experiment. As previously stated, this type of cell is sensitive to errors induced by the packing of the bulk solid around it. If a large normal deflection occurs at the midside of the wall then the solid behind that wall will undergo a large plastic deformation. This may adversely affect any cell that was placed in the bulk solid as the model silo was filled.

In short, although measuring the wall pressure would appear to be the only reliable way to demonstrate the non-linear patterns of wall pressure that may exist, there are problems associated with both types of pressure cell available. It may therefore be necessary to infer that the pressure distribution is non-linear by measuring pressures in the (relatively) stiff corner (where bending would have a minimum effect on wall pressure cells and deformations would be small reducing possible effects on free field cells) and then comparing with finite element results and the predictive law proposed by Rotter *et al* (2002). Free field cells could also be used near the midside of the silo wall but these results may be unreliable.

10.3 Finite element predictions of the experimental rig

The previously described finite element method is used to model the experimental rig. In order to model more accurately the corner of the walls (which will be stiffer due to the presence of the angle-section framework) the shell elements in this area are

assigned a larger thickness than those modelling the wall. The granular bulk solid used here is the pea gravel. Figure 10.7 shows the finite element predictions of the pressure down the wall compared with the Janssen prediction.

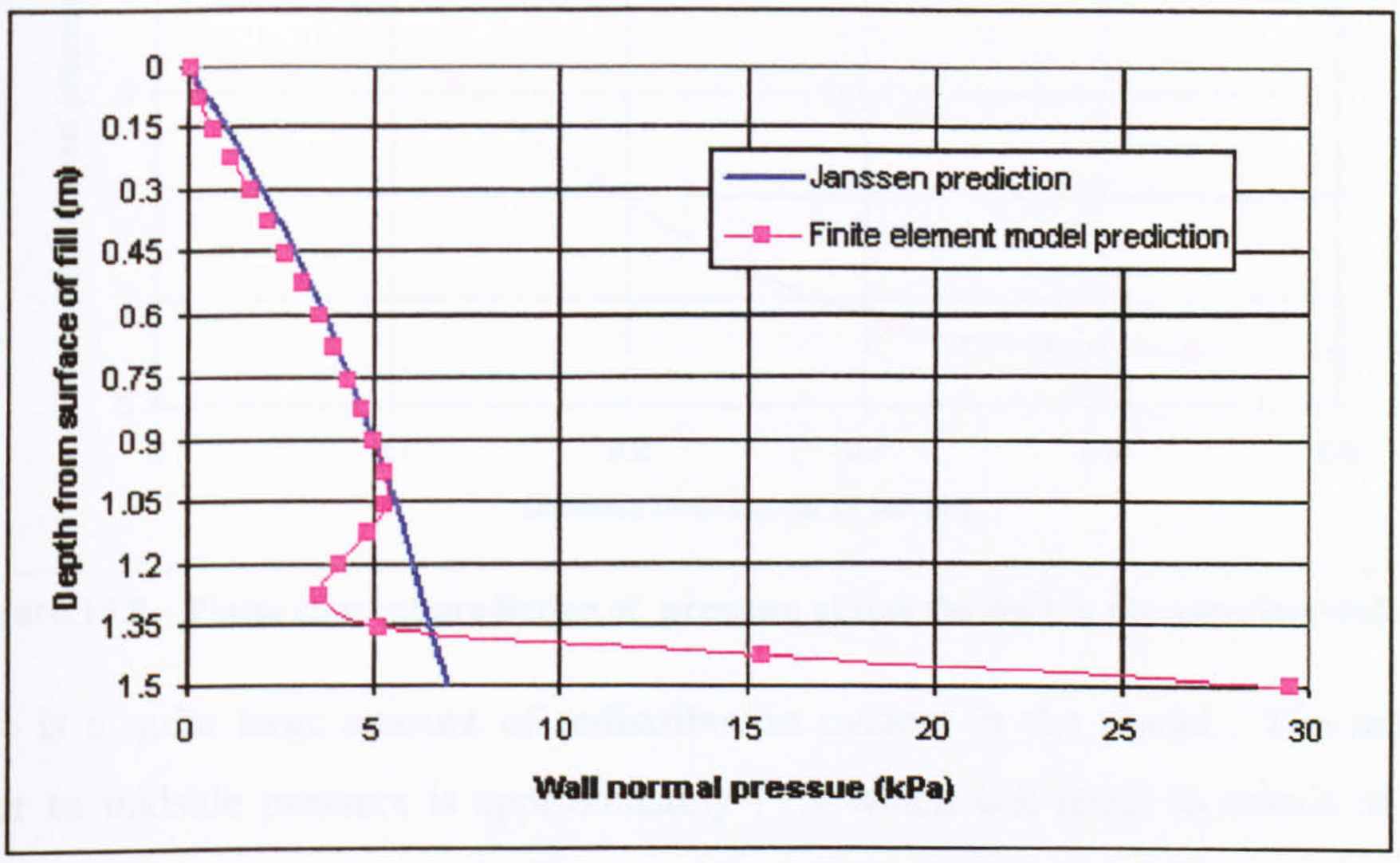

Figure 10.7 – Finite element and Janssen predictions of the mean pressure in the experimental rig

There is a large end effect associated with the finite element model. This is due to the flat-bottomed base condition and similar effects were seen in Chapter 7. Overall agreement between the Janssen theory and the finite element results is comparable to the agreement seen in previous models.

Figure 10.8 shows the distribution of pressure across the wall halfway down the bin (0.75m) from the finite element model.

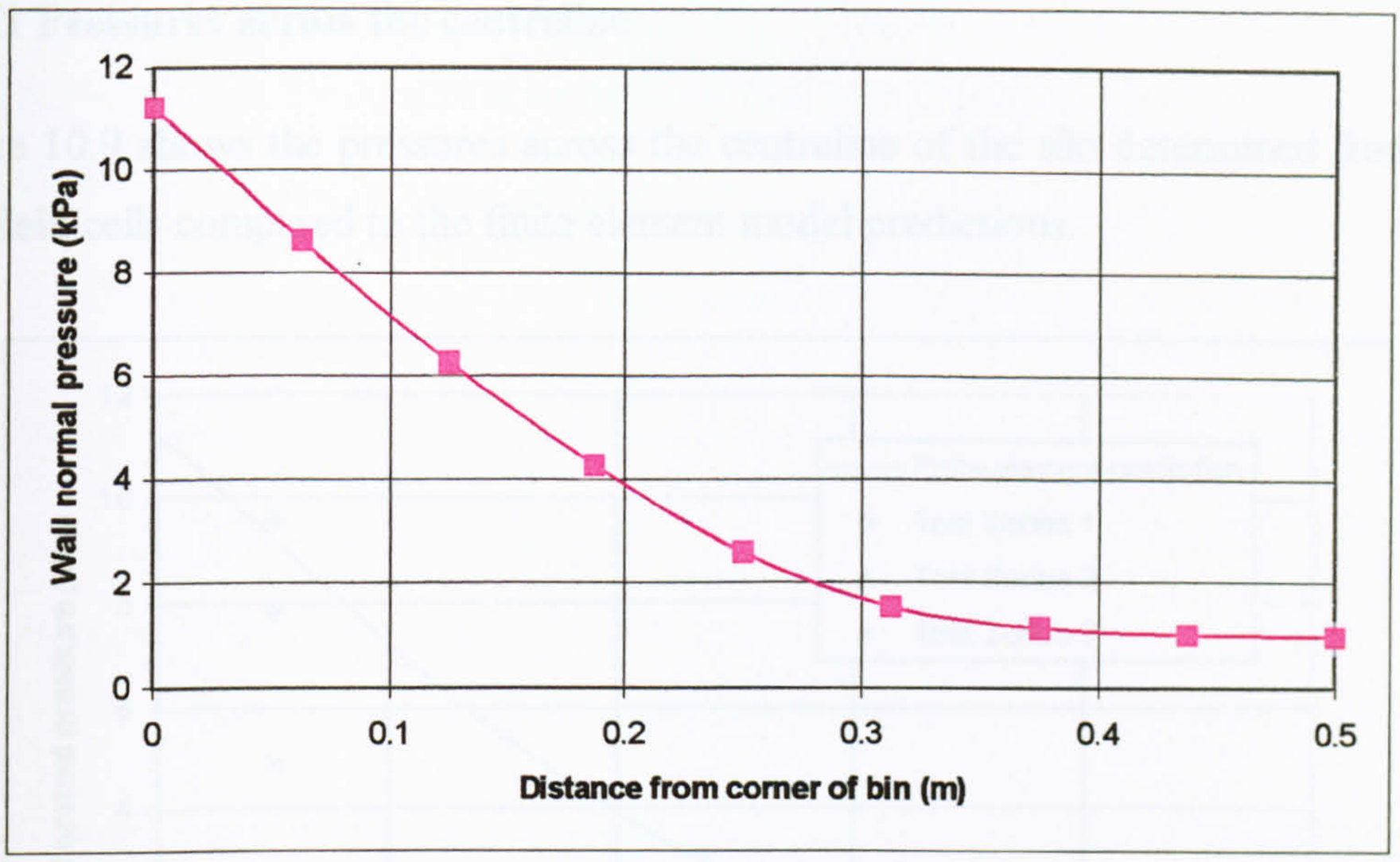

Figure 10.8 – Finite element prediction of pressure across the wall in the experimental rig

There is a quite large amount of redistribution evident in the model. The ratio of corner to midside pressure is approximately 11:1 which will result in values of α of around 3 and should be easily measurable in the experimental rig. Fitting the predictive law (equation 9.3) to these finite element results gives a value of α at this depth of 2.99.

Evaluation of the solid stiffness as outlined in Chapter 9 is also possible. This gives a value for the relative stiffness parameter (equation 9.8). The appropriate value of E_sL^3/E_wt^3 for this silo is therefore 9242 and referring to figure 9.21 shows that, since this is a very large value, the value of α predicted is going to be close to 3.

10.4 Experimental results

The experiment was performed a number of times. The strain gauges attached to the silo were zeroed and filling via the wooden filler box commenced. The silo was filled to the halfway point and then the pressure cells were placed in the gravel. Zero readings were taken for these cells. The silo was then filled to the top and readings taken from the pressure cells and strain gauges.

10.4.1 Pressures across the centreline

Figure 10.9 shows the pressures across the centreline of the silo determined from the free field cells compared to the finite element model predictions.

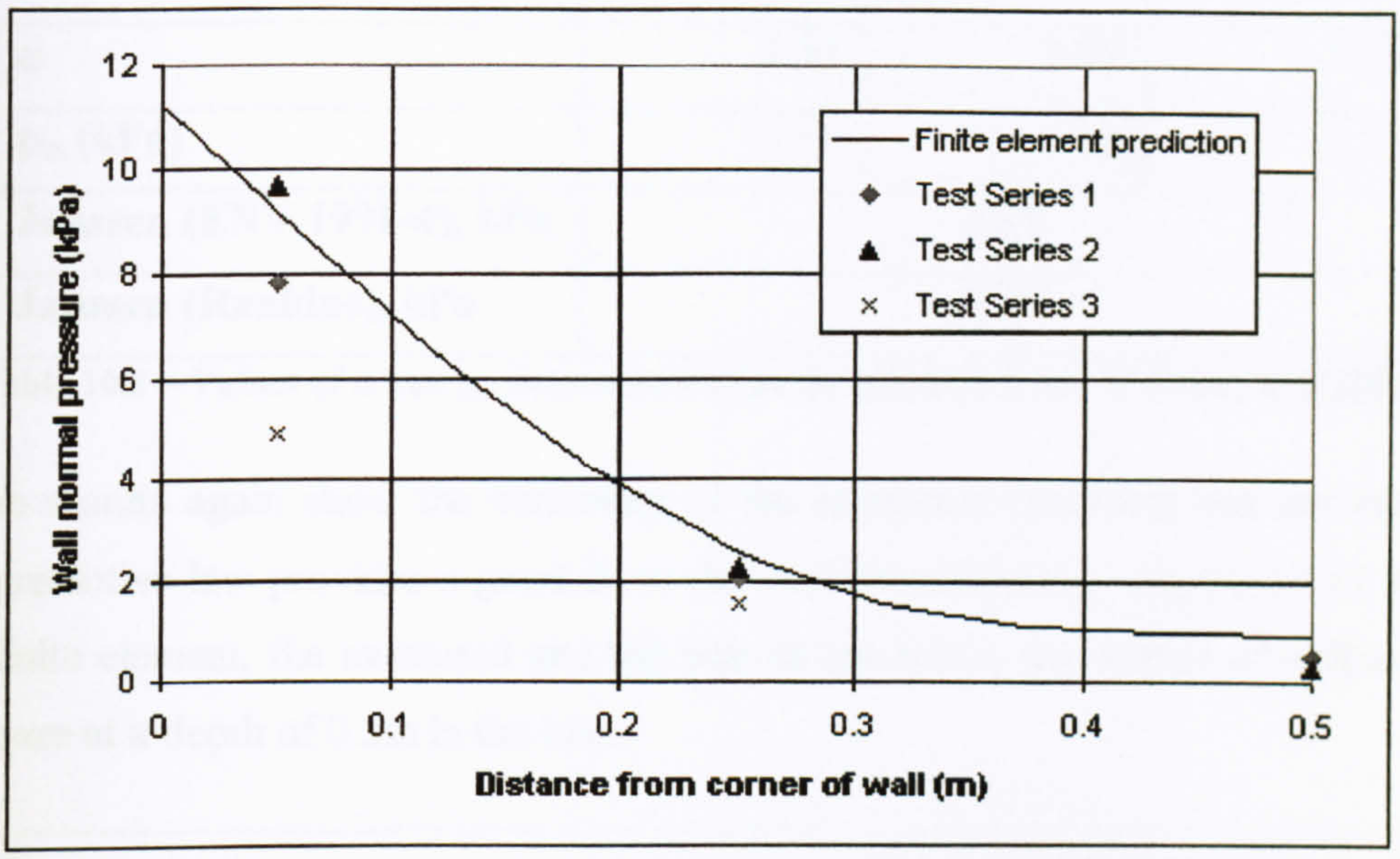

Figure 10.9 – Pressures in the model silo from free field cells and finite element model

A large variation in the predicted pressure is observed between different test runs. The pressures measured in the experimental silo show a distribution in agreement with the finite element model with a large pressure near the corner and very low pressures at the mid-point of the wall where the normal deformation is quite large.

The pressures measured show high degrees of variation between repeat experiments even with the use of the filler box to attempt to make the fill as even and repeatable as possible. This phenomenon has been noted by other researchers (Zhong *et al*, 2001).

10.4.2 Comparison with predictive law

The pressures measured across the centreline are fitted to the predictive law outlined previously. This gives values of p_m and α. Table 10.2 shows values determined from the three test series as well as the appropriate Janssen pressure predictions. The Janssen values shown are calculated using a k value as recommended by ENV 1991-

4 (1995) and using the Rankine active ratio. Using this ratio may be more suitable for this silo due to its squat nature and the fact that deformations that could lead to stored solid failure are expected.

	Test series 1	Test series 2	Test series 3
α	3.53	3.85	3.24
p_m (kPa)	3.14	3.68	2.11
Janssen (ENV 1991-4), kPa	4.38		
Janssen (Rankine), kPa	2.76		

Table 10.2 – Values of α and p_m determined from the predictive law of Rotter *et al* (2002)

These results again show the variability of the measured pressures but nevertheless the predictive law provides a good fit to the experimental data. Figure 10.10 shows the finite element, the measured and the best fit predictive law values of wall normal pressure at a depth of 0.5m in the bin.

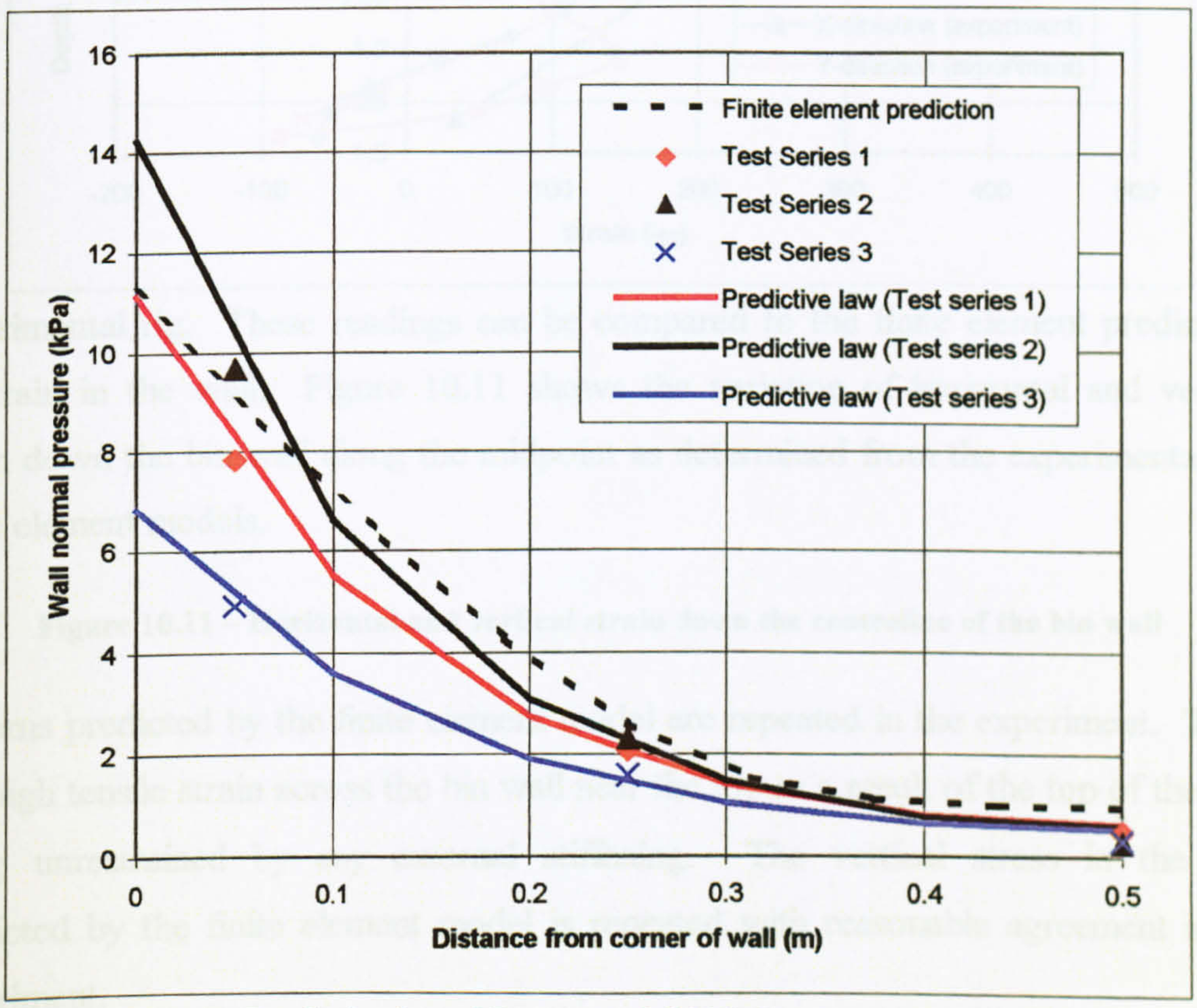

Figure 10.10 – Predictive law of Rotter *et al* (2002) fitted to experimental results

Of course, due to the variability of the test results there is a similar variation in the results from the best fit to the predictive law. However, the previously proposed predictive law of Rotter *et al* (2002) has again been shown to provide a good fit to experimental data.

10.4.3 Strain in the silo wall

As well as measuring pressures across the centreline of the silo wall a number of strain readings in the wall were taken from gauges attached to the exterior of the

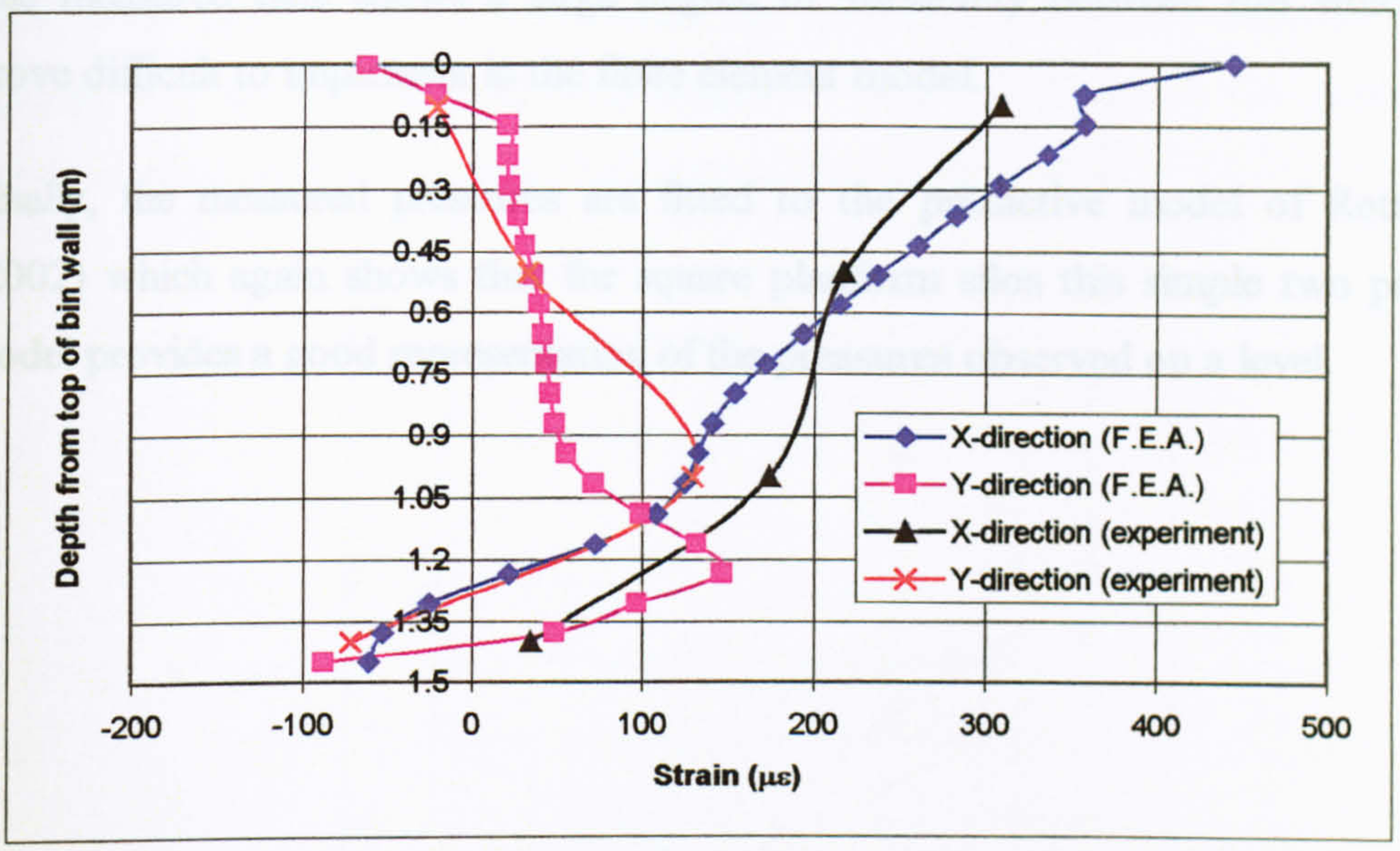

experimental rig. These readings can be compared to the finite element predictions of strain in the wall. Figure 10.11 shows the variation of horizontal and vertical strain down the bin wall along the midpoint as determined from the experimental and finite element models.

Figure 10.11 – Horizontal and vertical strain down the centreline of the bin wall

Patterns predicted by the finite element model are repeated in the experiment. There is a high tensile strain across the bin wall near the top as a result of the top of the wall being unrestrained by any external stiffening. The vertical stress in the wall predicted by the finite element model is repeated with reasonable agreement in the experiment.

10.5 Summary

A small square silo with a very thin wall was designed and this design modelled using the finite element model that has been developed. The finite element model showed that using a wall thickness of 1.6mm should lead to large variations of normal pressure across the wall. From measurements taken using free field cells this has been shown to be correct and the pressures predicted by the finite element model agree reasonably with the measured data.

The measured data shows a large degree of variability between fills which would prove difficult to implement in the finite element model.

Finally, the measured pressures are fitted to the predictive model of Rotter *et al* (2002) which again shows that for square planform silos this simple two parameter model provides a good representation of the pressures observed on a level.

Chapter 11 – Rectangular planform silos

The work presented so far has concerned silos of a square planform. Therefore, due to symmetry of the finite element model only pressures on one wall have been considered. Although factors such as eccentric discharge and loading will affect the distribution of wall pressure, most codes are not specific about how these pressures will be dealt with.

Attention is now turned to silos that are rectangular and non-square in planform. Here both walls must be considered, as they may experience different pressure regimes due to the different wall lengths. Figure 11.1 shows the notation and conventions used below to describe rectangular planform silos.

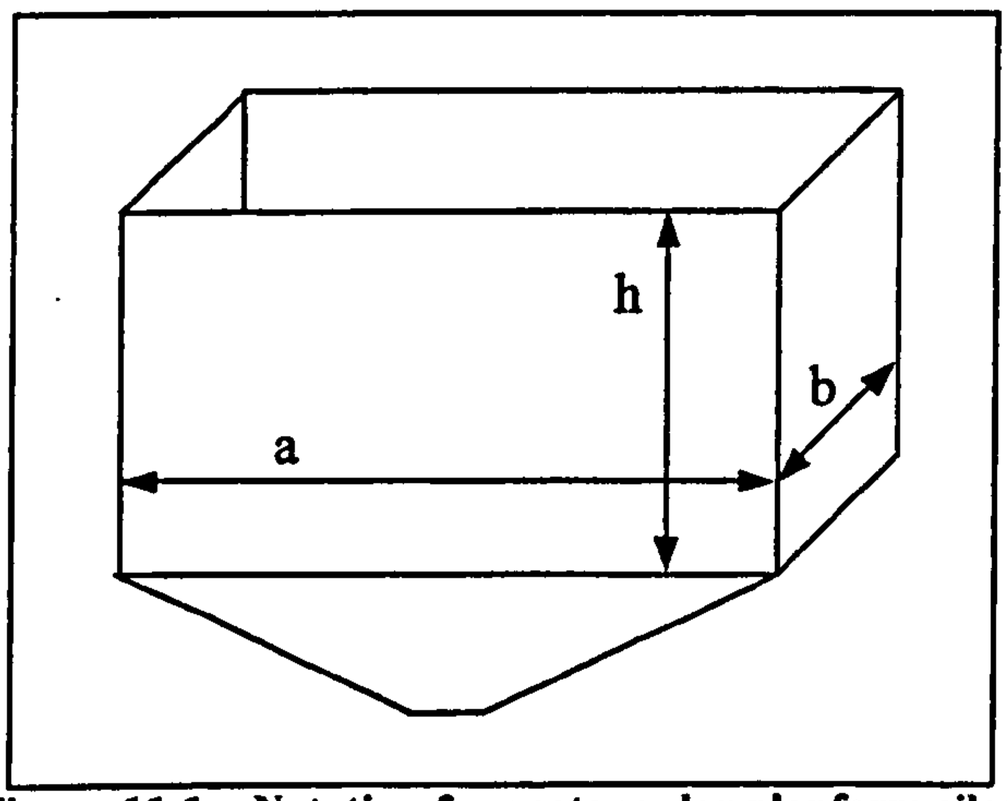

Figure 11.1 – Notation for rectangular planform silos

11.1 Limitations to this study

This study will investigate the pressures in rectangular silos that are close to square (2:1 is the largest ratio of a/b that will be considered), and that are either at the upper extreme of shallow or tall. Ratios less than 1.0 for h/a are relatively squat (defined as shallow or squat in EN 1991-4), but would be covered in most silo codes. Silos that are shallow and/or long will generally be treated as bunkers, and plane strain analyses may be valid for pressure predictions on the longer wall. This provides a known bound for the stress conditions.

Definition	h/d_c
Squat	Less than 0.4
Shallow	Between 0.4 and 1.0
Intermediate	Between 1.0 and 2.0
Slender	Greater than 2.0

Table 11.1 – Definitions according to EN1991-4 (Note: d_c=b for rectangular silos)

11.2 Current guidance available

A number of other authors have dealt with rectangular silos, and it is probably helpful to outline the approaches of Reimbert and Reimbert (1976) and Gaylord and Gaylord (1983). The former report their results for model-scale tests, and their deductions from measurements of pressure at the base of silos; with some assumptions these measurements enable an estimate of wall pressures to be made.

Reimbert and Reimbert base their theory upon the equilibrium of a slice (as Janssen), assuming that, at some depth in the silo, the wall friction equilibrates the downward force of the slice. They assume (and refer to experiments) that the pressure on the small wall is that which would act on a square silo of plan b * b. Hence a deduction about the pressure on the longer walls is made, and the "mean" thrust derived on both walls based on a hydraulic radius, R. These are calculated from equations 11.1 and 11.2 where subscripts S and L refer to the shorter and longer walls respectively.

Short wall $$R_S = \left(\frac{b}{4}\right) \tag{11.1}$$

Long wall $$R_L = \left(\frac{b}{4}\right)\left(2 - \frac{b}{a}\right) \qquad (a > b) \tag{11.2}$$

This asymptotic value can only be reached if the silo is sufficiently deep, and again implies a constant value of lateral pressure ratio – although it should be noted that Reimbert and Reimbert report the mean pressure.

As side length a becomes much greater than b, then the pressure on the longer wall tends to a limiting value that is twice the pressure on the shorter wall. This is shown in the relationship in Figure 11.2 The ratio of the side lengths directly determines the pressure ratio.

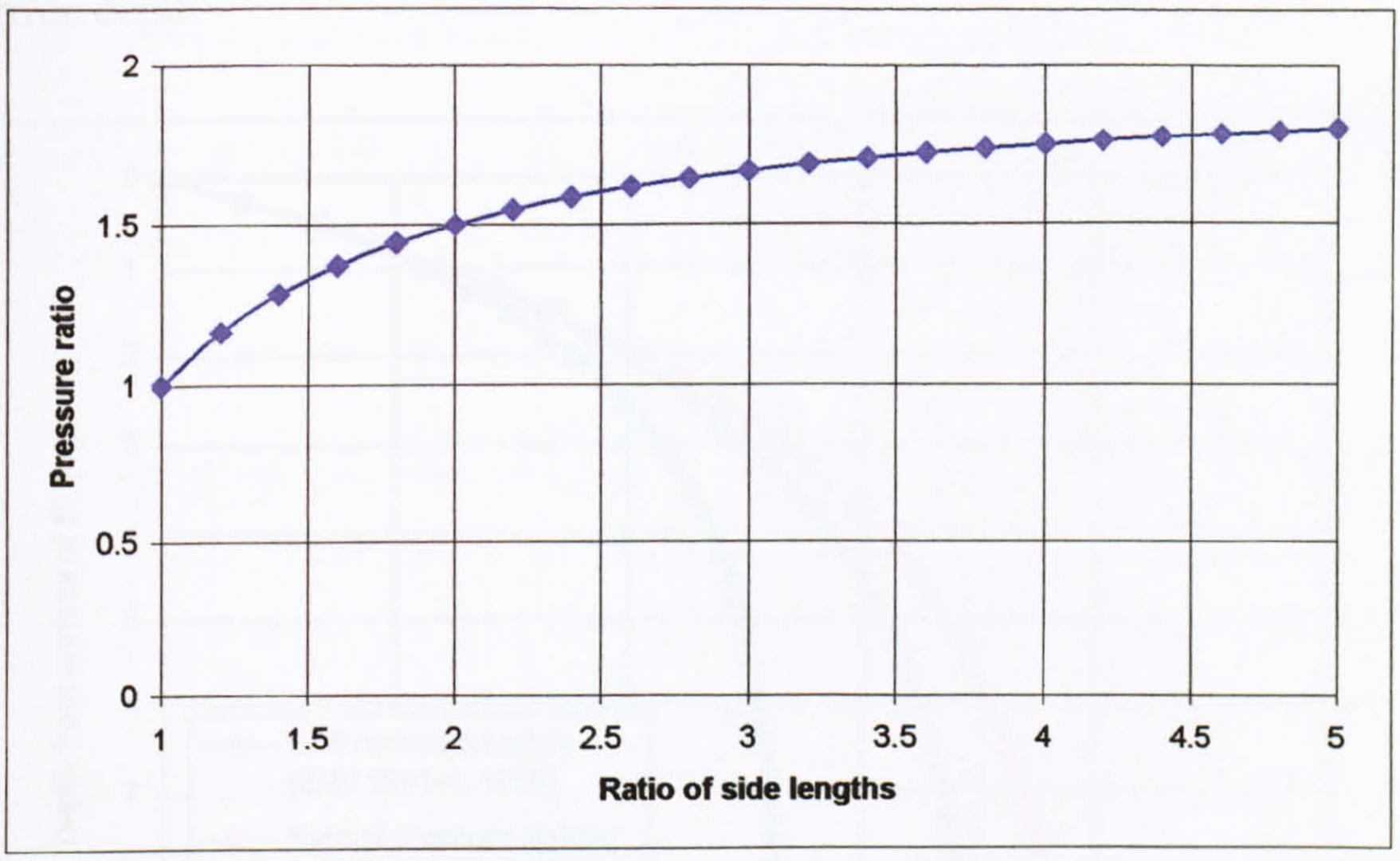

Figure 11.2 – Ratio of pressures on long side to short side (after Reimbert)

Gaylord and Gaylord also report this same derivation using different notation, but somewhat confusingly conclude that the pressure on the longer side is lower than that on the shorter side, in spite of the formulae presented. It is probable that this may be an error, and their intention is to suggest the pressure on the longer side is the larger.

Lightfoot and Michael (1966) conducted full scale and model tests on squat coal bunkers. Some design rules are given in this work for these types of structures but these are not extended to deeper silos.

Figure 11.3 shows the wall normal pressure predictions in a bin of planform ratio 2:1 as calculated from ENV 1991-4 (1995) and formulae 11.1 and 11.2. In the latest draft of EN1991, the hydraulic radius is still used in the Janssen calculations:

$$\frac{A}{U} = \left(\frac{b}{2}\right)\left(1 + \frac{b}{a}\right) \tag{11.3}$$

This leads to different pressure regimes, as shown in Figure 11.3. The main thing to note is that it implies the Janssen assumptions of constant lateral pressure ratio, k, at any given depth.

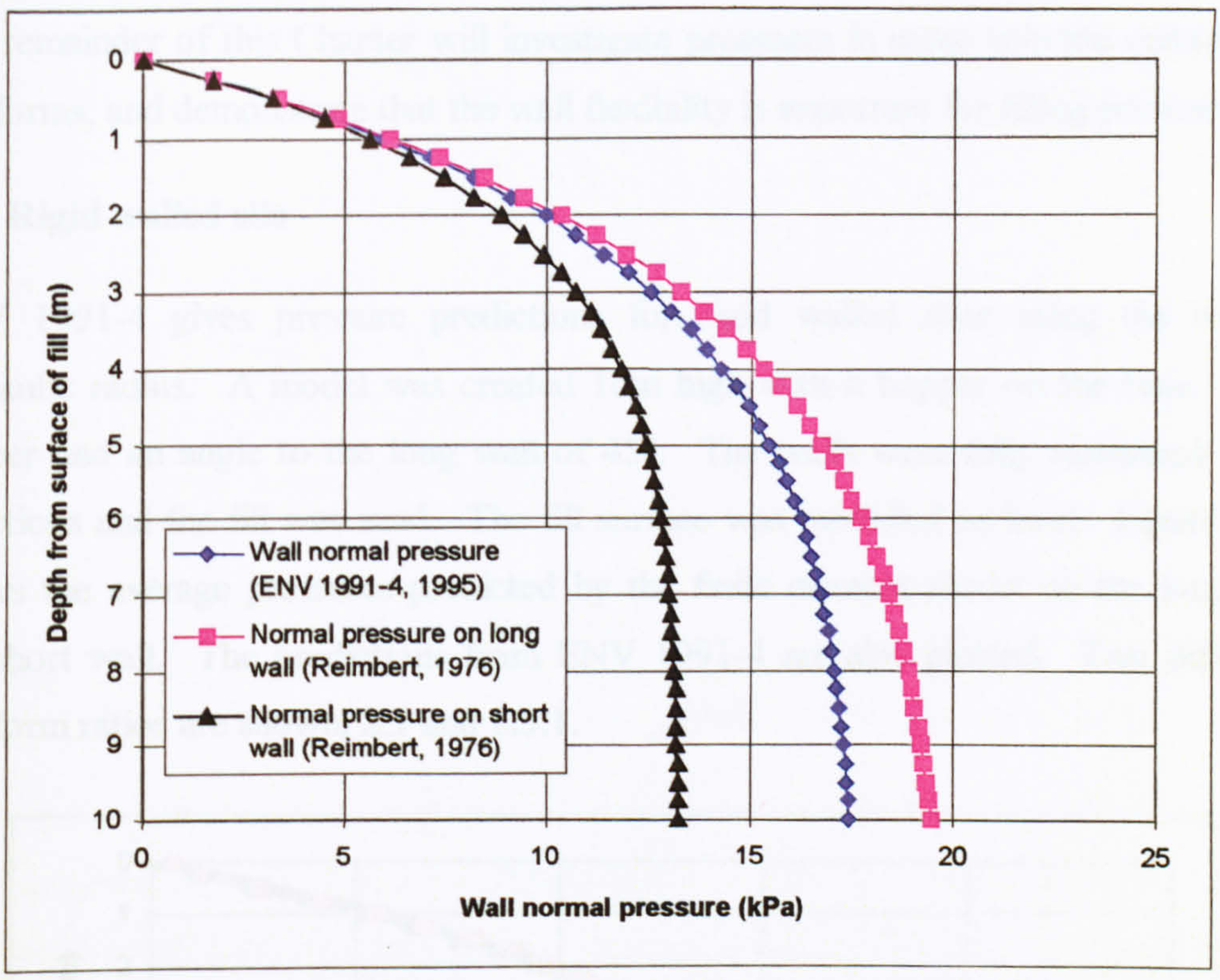

Figure 11.3 – Wall normal pressure predictions in a rectangular planform silo

The consequence is that the designer has different sources of information giving at least two pressure regimes. Both of them imply that the wall of the silo is rigid and that the lateral pressure ratio is constant throughout. This may be perfectly acceptable for concrete silos, but for flexible walled silos the pressure regimes predicted on filling may be inappropriate.

It is also noted that for silos that have very large planform ratios the pressure predicted by the Eurocode and the pressure on the long wall as predicted by Reimbert and Reimbert converge to a value determined from a hydraulic radius twice that of the short wall (i.e. R = b/2).

The structural design will be based on the wall pressures, but will also have implications for continuity at the corners, and the wall pressures that are developed. If the longer wall moves outwards away from the stored material, then if there is structural continuity at the corners (i.e. identical wall rotations about a vertical axis through the corner will be continuous) the shorter wall must move inwards – towards the stored material, and *vice versa*.

The remainder of this Chapter will investigate pressures in some selected rectangular silo forms, and demonstrate that the wall flexibility is important for filling pressures.

11.3 Rigid walled silo

ENV 1991-4 gives pressure predictions for rigid walled silos using the overall hydraulic radius. A model was created 10m high with a hopper on the base. This hopper had an angle to the long wall of 45°. The walls were fully restrained in all directions and the fill was sand. The fill surface was modelled as level. Figure 11.4 shows the average pressures predicted by the finite element model on the long and the short wall. The predictions from ENV 1991-4 are also plotted. Two different planform ratios are shown, 2:1 and 1.5:1.

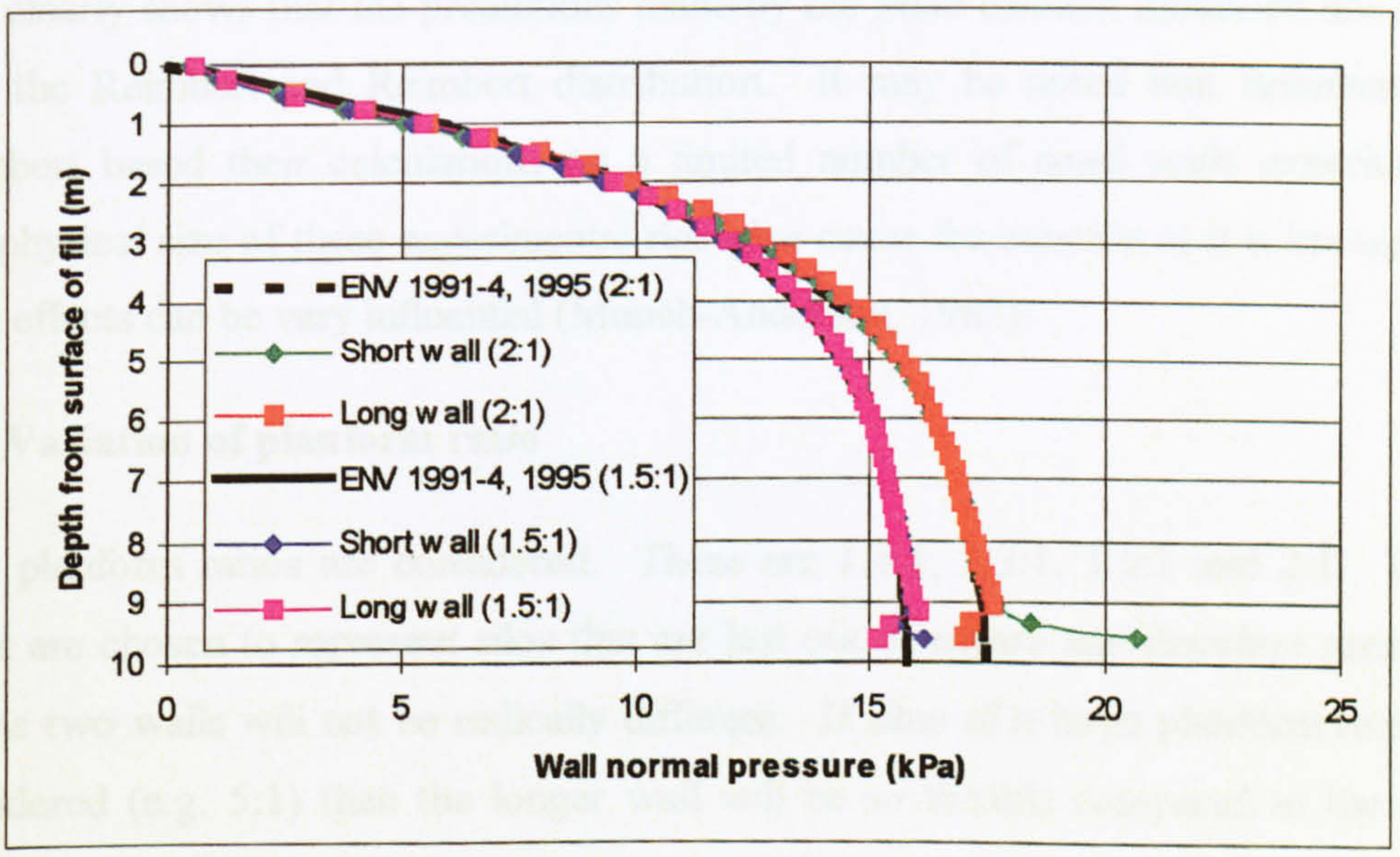

Figure 11.4 – Long and short wall pressures in a 2:1 planform ratio bin compared to predictions from ENV 1991-4 (1995)

This shows that for rigid walls the internal pressures are well predicted by ENV 1991-4 (1995).

Figure 11.5 shows the 2:1 planform ratio rigid-walled bin compared to the predictions based upon equations 11.1 and 11.2 of Reimbert and Reimbert (1976).

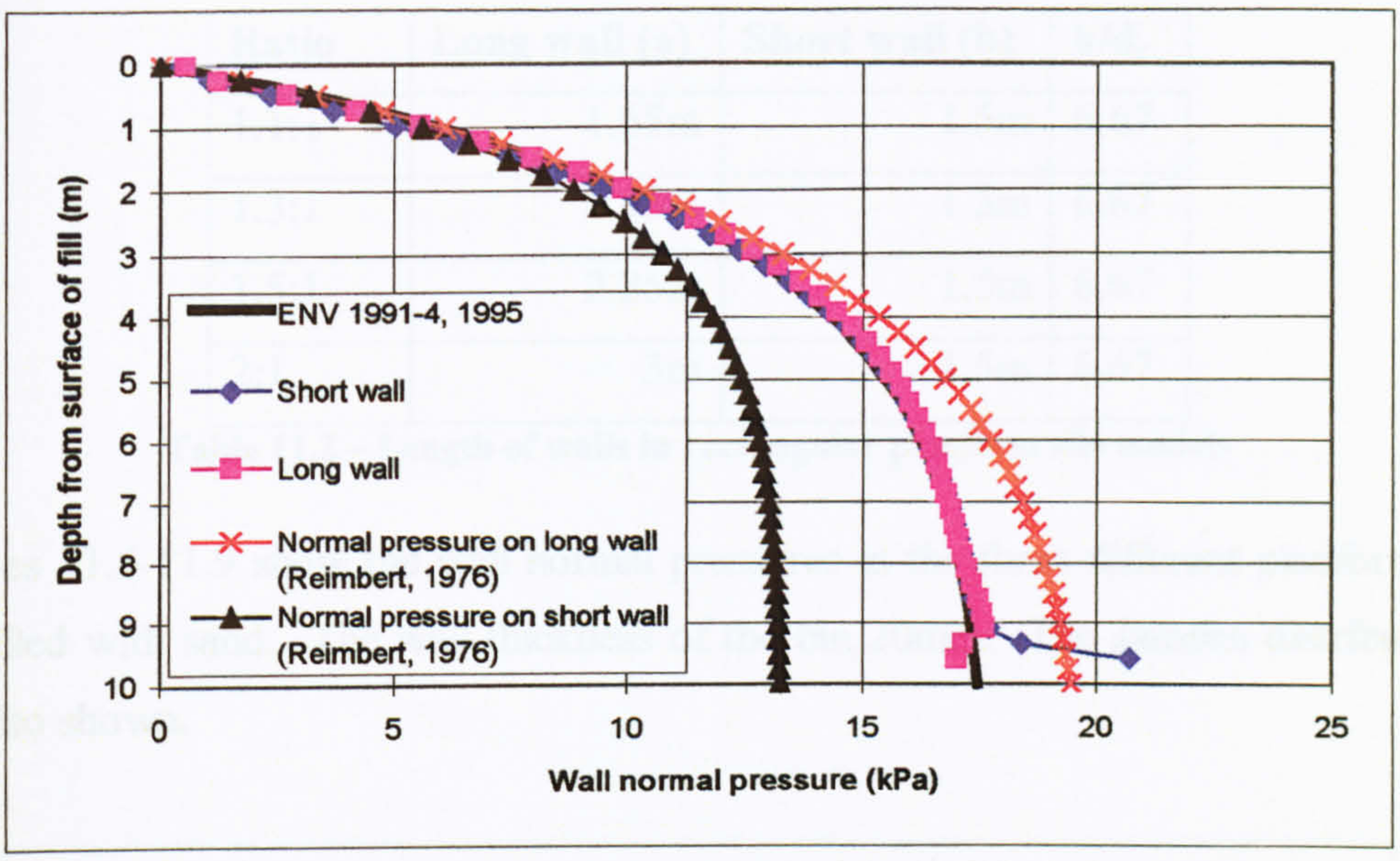

Figure 11.5 – FEA predictions compared to the predictions of Reimbert and Reimbert (1976)

This clearly shows that the predictions made by the finite element model do not agree with the Reimbert and Reimbert distribution. It may be noted that Reimbert and Reimbert based their calculations on a limited number of small scale experiments. The physical size of these experimental rigs give cause for concern as it is known that scale effects can be very influential (Munch-Anderson, 1983).

11.4 Variation of planform ratio

Four planform ratios are considered. These are 1.1:1, 1.3:1, 1.5:1 and 2:1. These ratios are chosen to represent silos that are just out of square and therefore pressures on the two walls will not be radically different. If silos of a large planform ratio are considered (e.g. 5:1) then the longer wall will be so flexible compared to the short wall that its behaviour will dominate the silo response and comparisons between the two walls will be difficult to draw.

Results from the finite element model are compared to wall pressures predictions which are calculated from the Janssen formula using the value of hydraulic radius given ENV 1991-4 (1995). The actual sizes of the bins modelled are given in table 11.2. The boundary condition at the base is modelled as for the rigid walled model. The mesh density is kept the same as was used in the study of the square silo.

Ratio	Long wall (a)	Short wall (b)	h/d_c
1.1:1	1.65m	1.5m	6.67
1.3:1	1.95m	1.5m	6.67
1.5:1	2.25m	1.5m	6.67
2:1	3m	1.5m	6.67

Table 11.2 – Length of walls in rectangular planform silo models

Figures 11.6-11.9 show the wall normal pressures in the three different planforms of bin filled with sand. The wall thickness of the bin 20mm. The Janssen distributions are also shown.

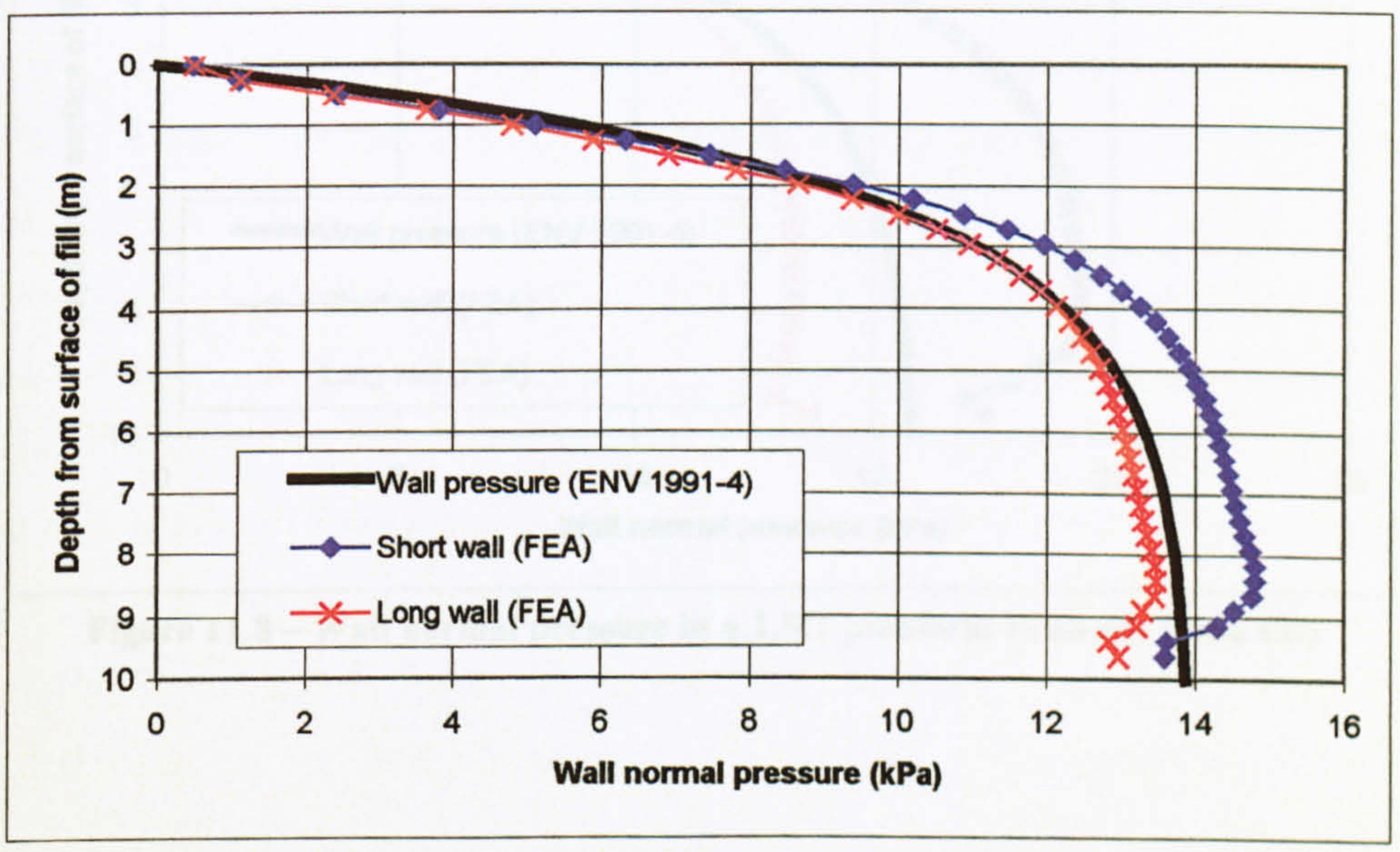

Figure 11.6 – Wall normal pressure in a 1.1:1 planform ratio silo (sand fill)

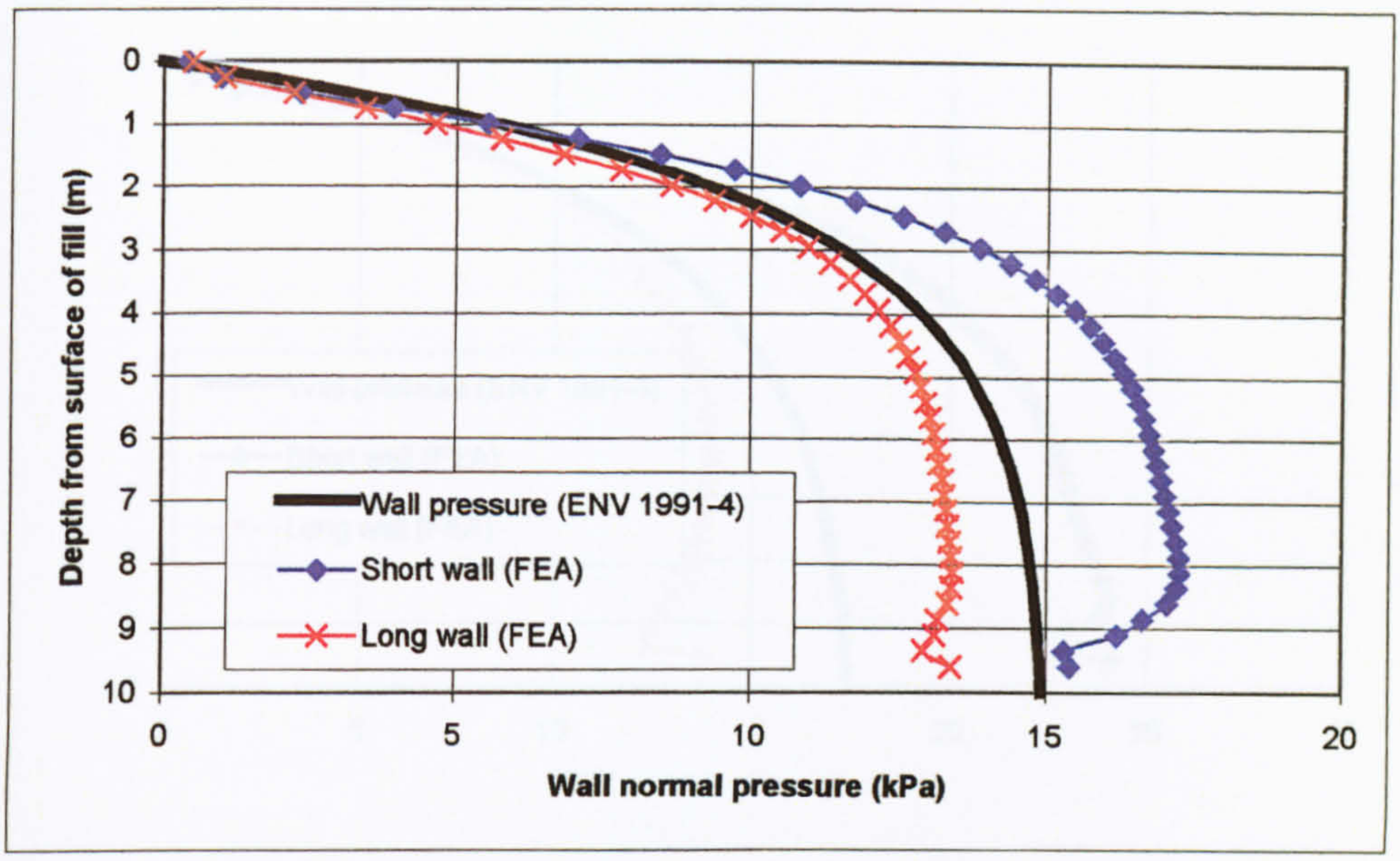

Figure 11.7 – Wall normal pressure in a 1.3:1 planform ratio silo (sand fill)

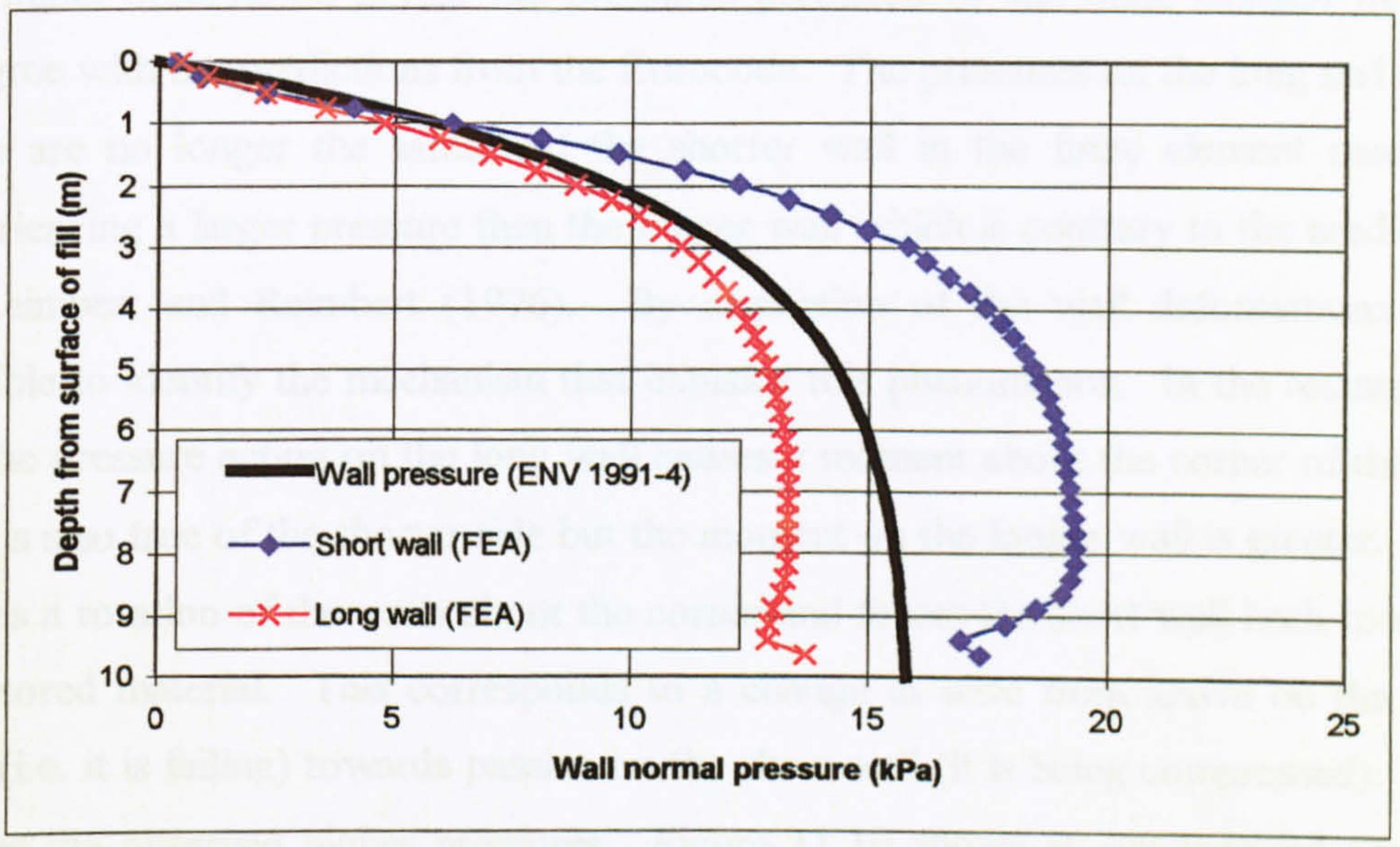

Figure 11.8 – Wall normal pressure in a 1.5:1 planform ratio silo (sand fill)

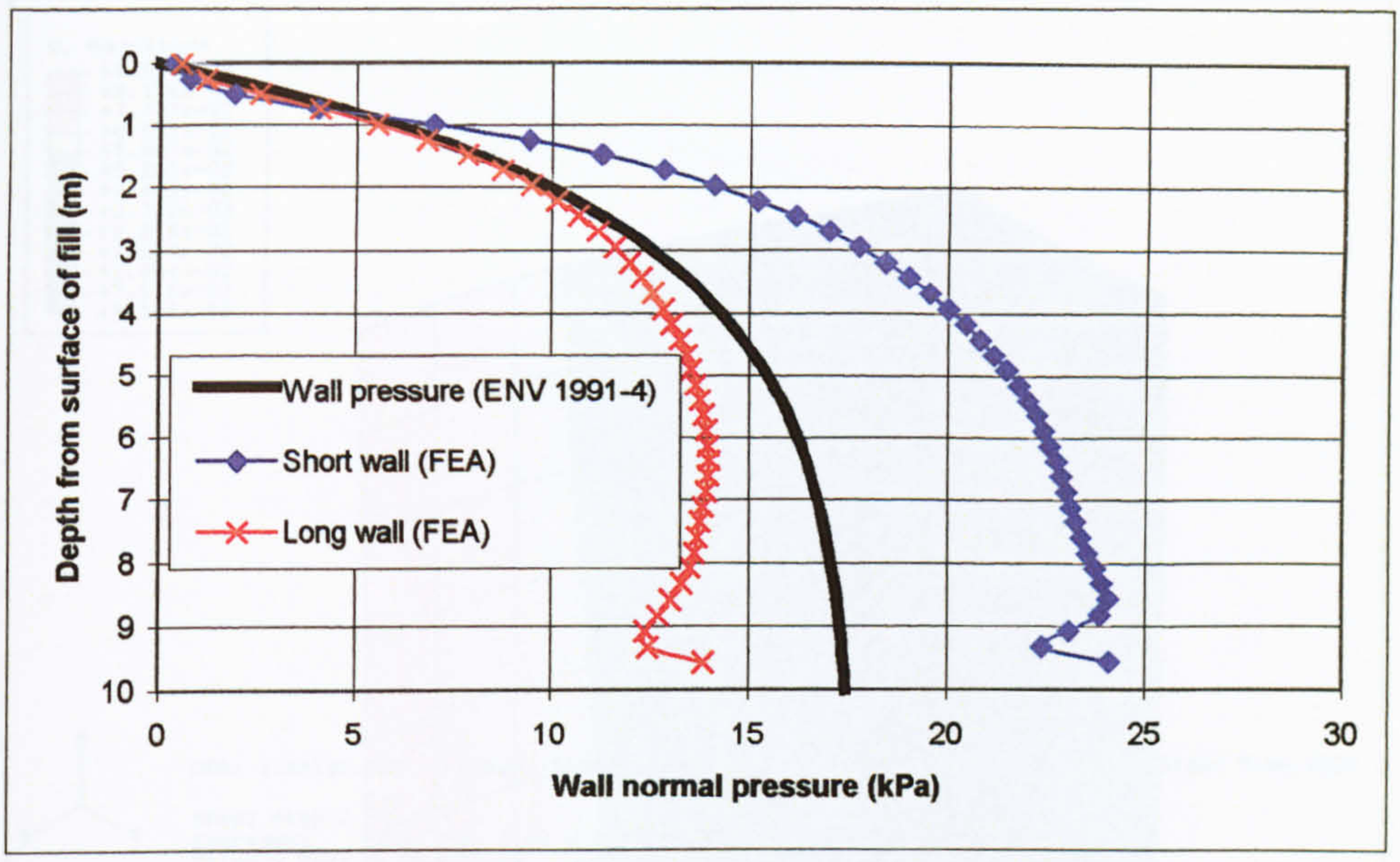

Figure 11.9 – Wall normal pressure in a 2:1 planform ratio silo (sand fill)

The initial observation is that the pressures predicted by the finite element method disagree with the predictions from the Eurocode. The pressures on the long and short walls are no longer the same and the shorter wall in the finite element model is experiencing a larger pressure than the longer wall which is contrary to the prediction of Reimbert and Reimbert (1976). By inspection of the wall deformations it is possible to identify the mechanism that explains this phenomenon. In the rectangular bin the pressure acting on the long wall causes a moment about the corner of the bin. This is also true of the shorter side but the moment on the longer wall is greater. This causes a rotation of the walls about the corner and forces the short wall back towards the stored material. This corresponds to a change in state from active on the long wall (i.e. it is failing) towards passive on the short wall (it is being compressed). This causes the observed higher pressures. Figure 11.10 shows an exaggerated contour plot of the top of the silo walls. The magnitude of the deformation is shown. This plot clearly shows the longer wall deforming outwards (i.e. away from the stored material) and the shorter wall deforming inwards (i.e. towards the stored material).

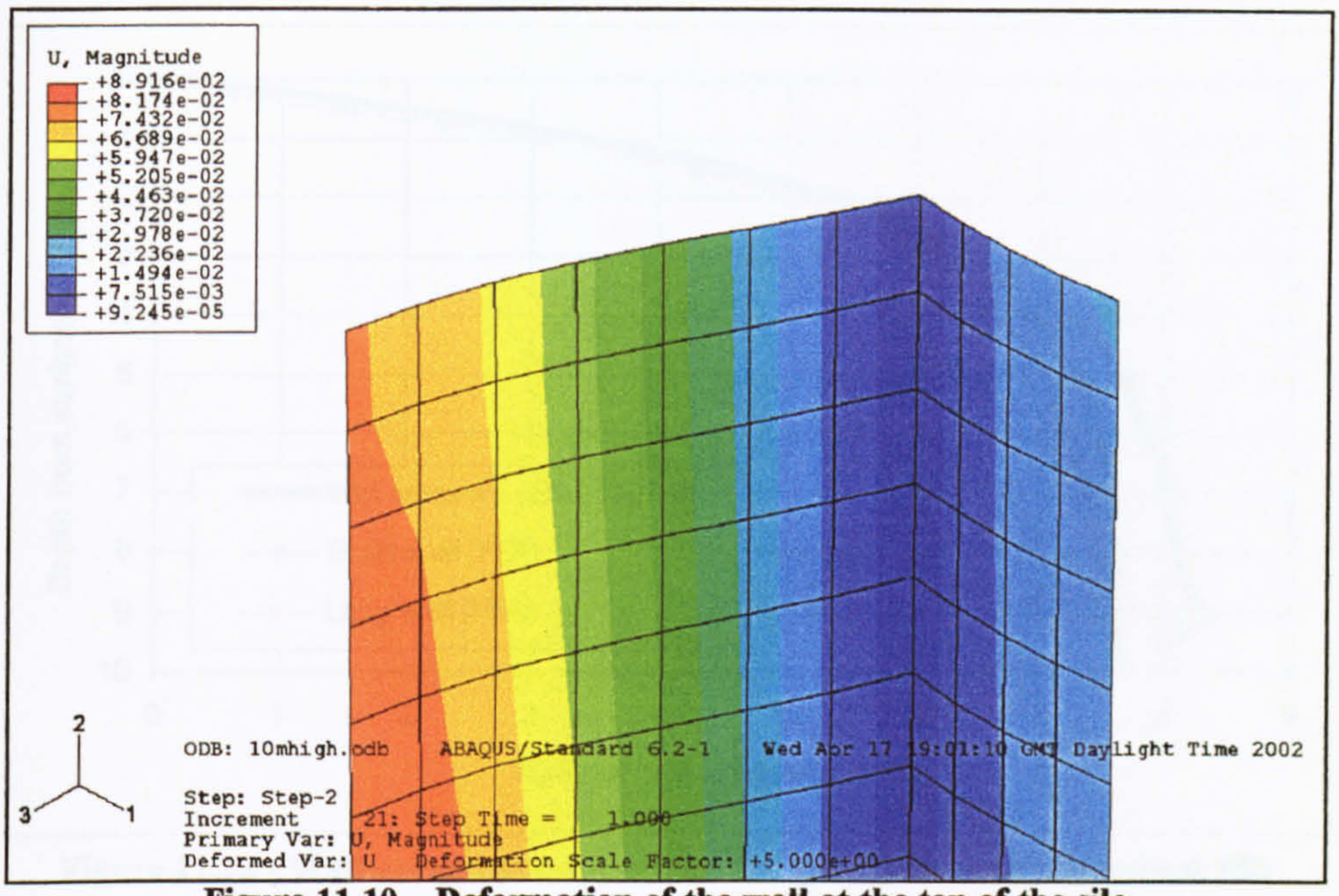

Figure 11.10 – Deformation of the wall at the top of the silo

Clearly, for flexible rectangular bins there are shortcomings in the current theory. In this unstiffened case the observed pressures, whilst still conforming to a Janssen form of distribution, are poorly predicted by the theory.

Figures 11.11-11.14 show the same three bins but filled with wheat material.

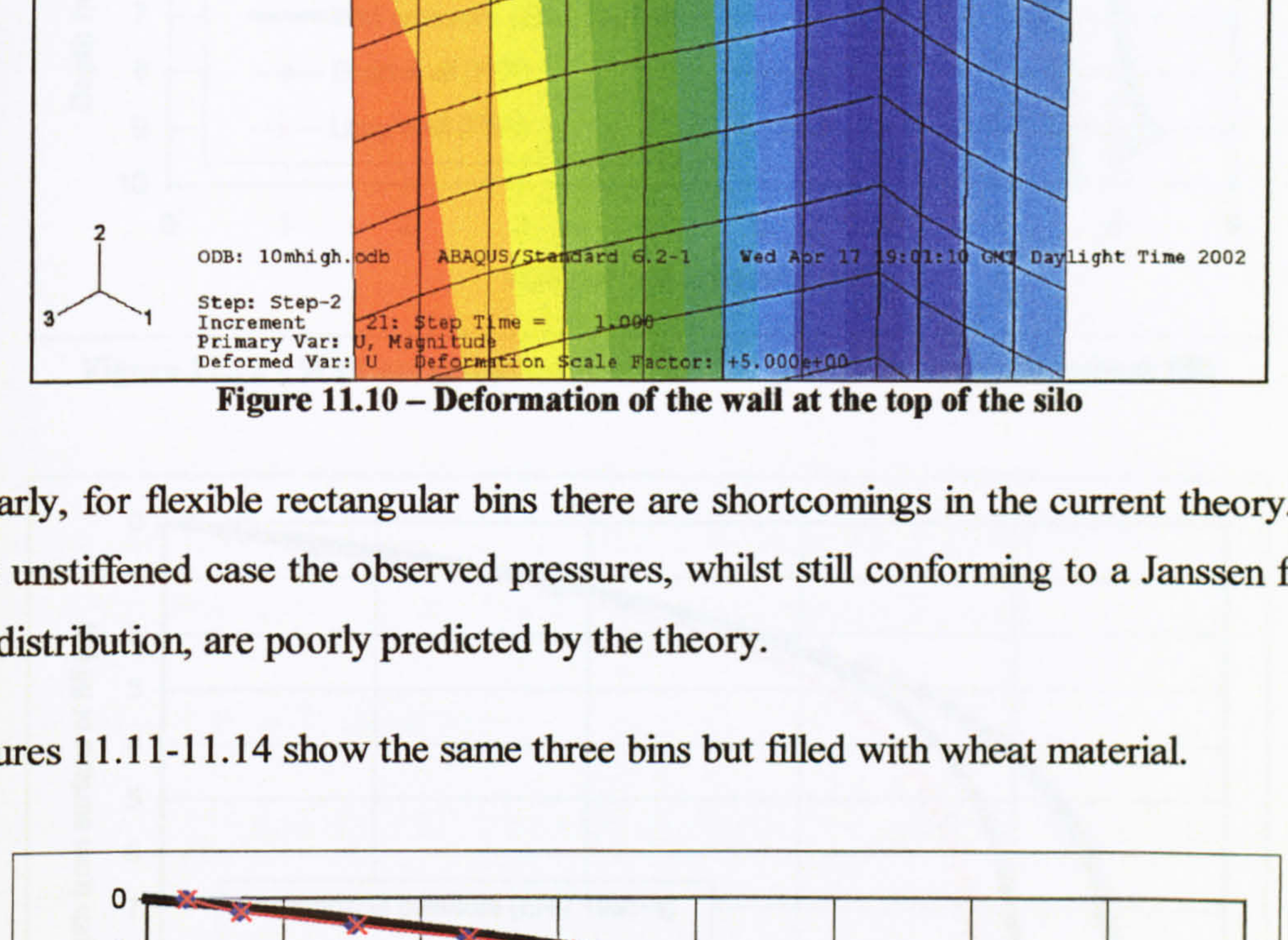

Figure 11.11 - Wall normal pressure in a 1.1:1 planform ratio silo (wheat fill)

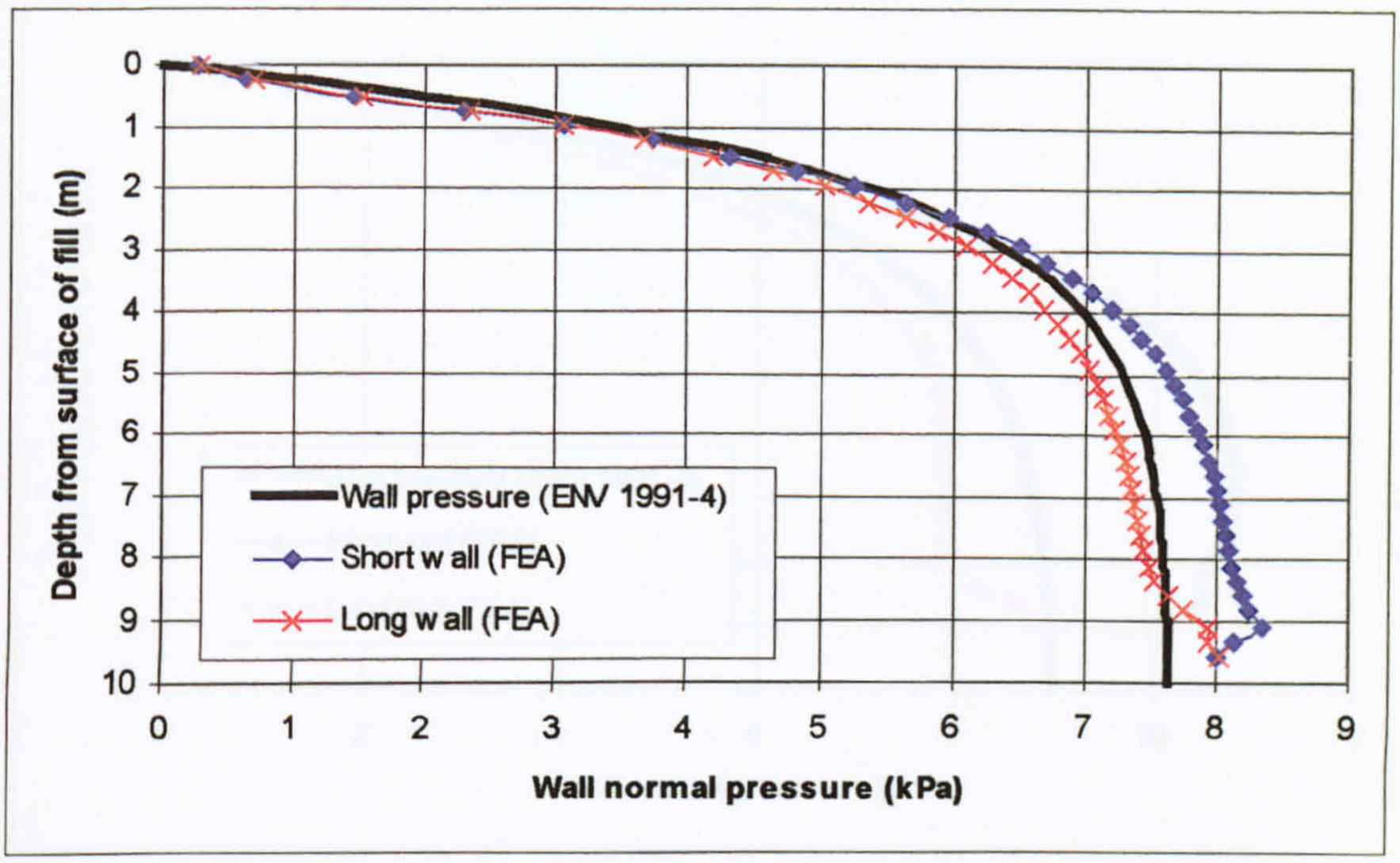

Figure 11.12 - Wall normal pressure in a 1.3:1 planform ratio silo (wheat fill)

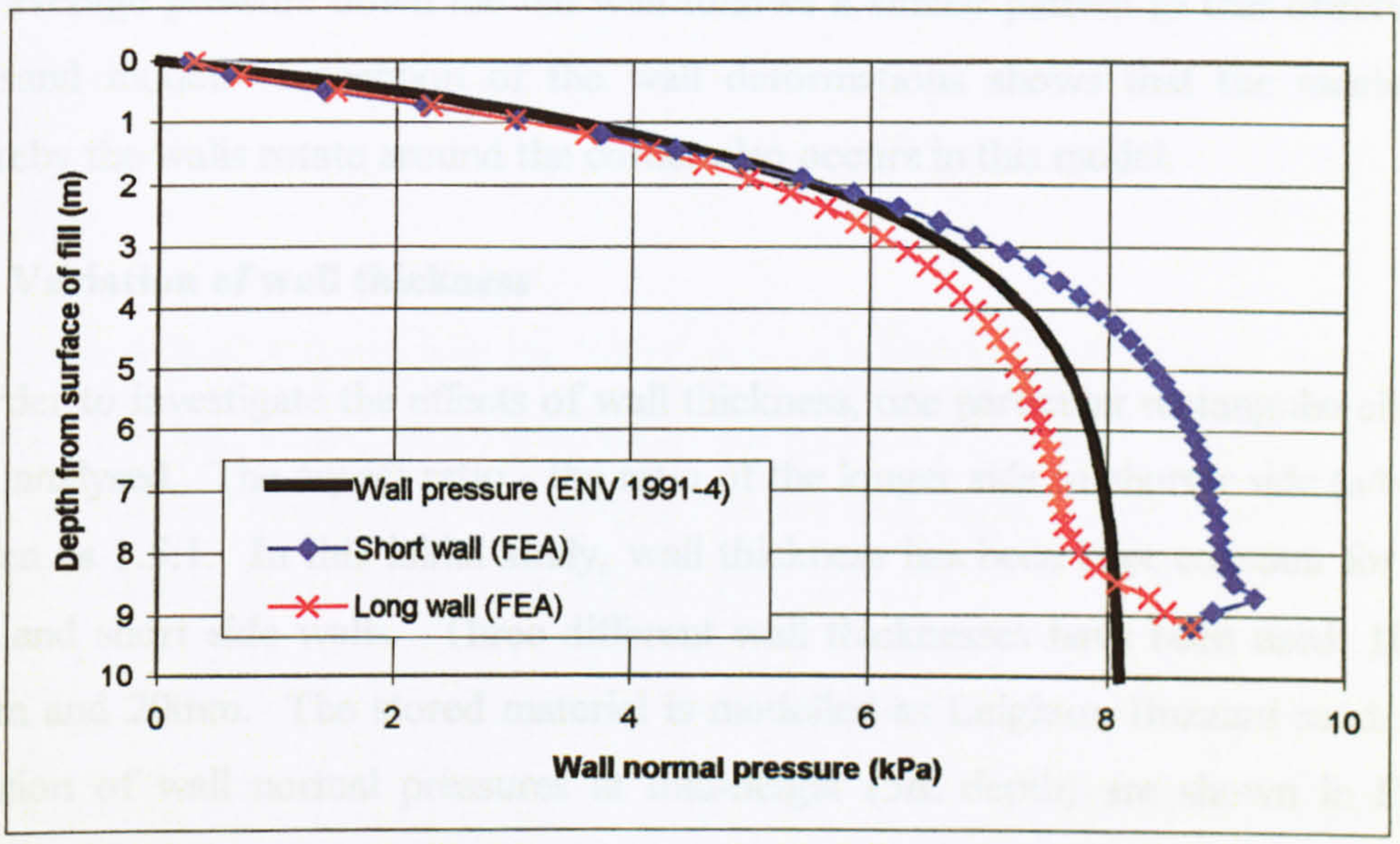

Figure 11.13 - Wall normal pressure in a 1.5:1 planform ratio silo (wheat fill)

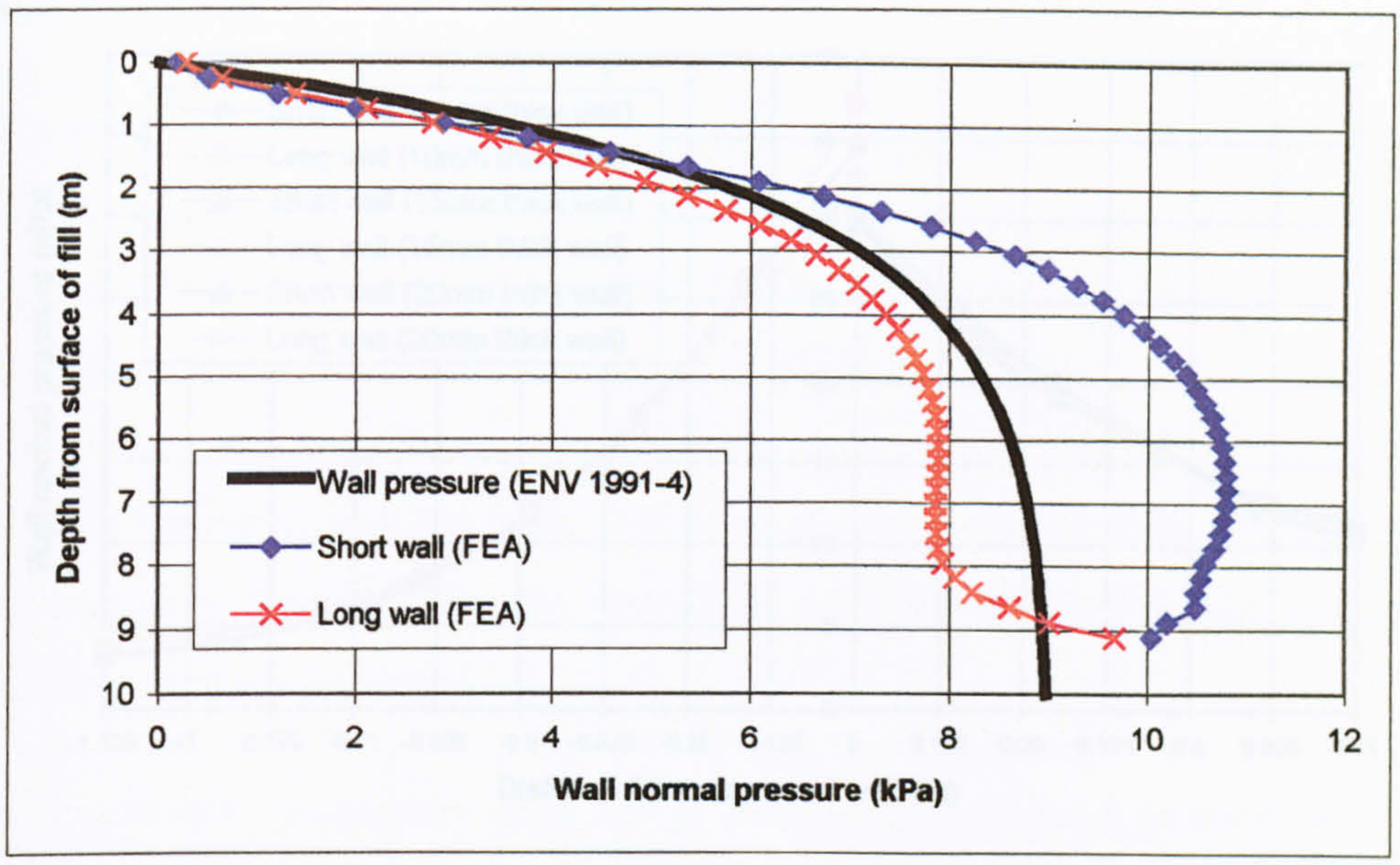

Figure 11.14 - Wall normal pressure in a 2:1 planform ratio silo (wheat fill)

The average pressure down the bin wall follows a similar pattern to that observed in the sand model. Inspection of the wall deformations shows that the mechanism whereby the walls rotate around the corner also occurs in this model.

11.5 Variation of wall thickness

In order to investigate the effects of wall thickness, one particular rectangular silo has been analysed. The aspect ratio - the ratio of the longer side to shorter side (a/b) – is chosen as 1.5:1. In this initial study, wall thickness has been kept constant for both long and short side walls. Three different wall thicknesses have been used: 10mm, 15mm and 20mm. The stored material is modelled as Leighton Buzzard sand. The variation of wall normal pressures at mid-height (5m depth) are shown in Figure 11.15.

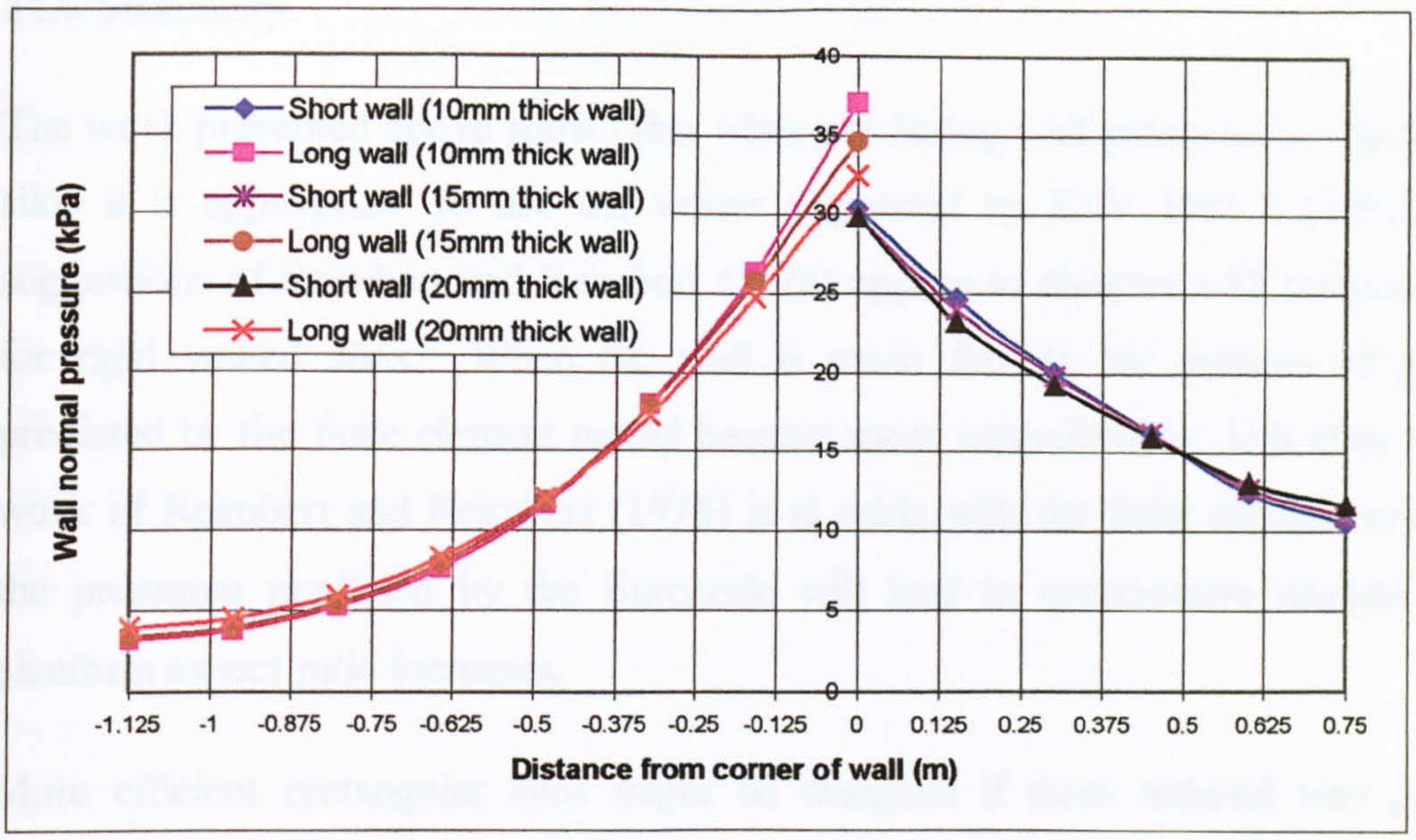

Figure 11.15 – Redistribution of wall normal stress in a rectangular bin of planform ratio 1.5:1

The long wall shows a much lower pressure at the midpoint compared to the short wall. This can be attributed to the decreased flexural stiffness of the wall. The higher values seen on the short wall can be attributed to the rotational effect observed.

For all three wall thicknesses, the previously reported normal pressure variation is present. For the thinner walls the ratio of corner to midside pressure is higher. The graph also shows that the average pressure on the short wall is higher than that of the long wall (due to the previously described rotations).

Figure 11.15 shows the redistribution of wall normal stress across the wall for three different wall thicknesses. The section is chosen – somewhat arbitrarily – as the mid-height of the bin section (i.e. at a depths of 5m). At the corner of the bin the orthogonal stresses differ. Assuming the major principal stress is vertical, the implication is that the principal direction on a horizontal plane is not at 45° to the wall. The results are consistent with an arching mechanism between corners.

11.6 Summary

The work presented above shows that when predicting wall pressures for rigid walled silos it is appropriate to use the values suggested by ENV 1991-4 (1995). The suggestions of Reimbert and Reimbert (1976) appear to disagree with the predictions for rigid walled silos. When the wall is made flexible the patterns of pressure predicted by the finite element model become more unpredictable. It is clear that the work of Reimbert and Reimbert (1976) is at odds with the finite element model but the pressures predicted by the Eurocode will lead to conservative designs as the planform aspect ratio increases.

More efficient rectangular silos might be designed if these reduced wall pressure phenomena are exploited, with sufficient ductility in the vertical corner joints. If designs are enabled that allow reduced midside wall pressures to be used, a thinner wall section can be used. Structural efficiency becomes important in several applications, but knowledge of the pressure patterns is also essential to understand the relationship between internal pressures and flow patterns in the stored solid

Chapter 12 – Conclusions and further work

The work presented here has investigated several aspects of silo problems.

Firstly, the general problem of describing a discrete, granular material using a continuum method was considered. Previous finite element work has either used laws based on a linear elastic assumption or based upon parameters (such as the internal angle of friction) regularly used to describe granular materials. It has been shown that these parameters alone may not lead to constitutive laws that are suitably robust for the prediction of silo wall pressures. In particular the use of a parameter (in this work, the logarithmic bulk modulus) that relates the stiffness of the stored bulk solid to the stress level is especially important. Chapter 6 showed that two granular materials whose properties are very similar when described in terms of "standard" bulk solids parameters could produce pressure distributions across the wall of a square planform silo that were markedly different. This replicated observations that had been made in experimental work (Lahlouh *et al*, 1995).

Chapter 7 investigated some observed end-effects in an axisymmetric model. Wall pressures increase above the Janssen predicted pressures near the base of the silo, and confirm previously reported results. A mechanism was proposed that explains the observed pressures. In axisymmetric models with hoppers, it was noted that, even though these models were relatively thick-walled, small deformations of the hopper were shown to have very large effects on the wall pressures both above and below the transition.

A parametric survey was carried out on a square planform silo and investigated the effect of varying the stored solid, the wall thickness and the planform size. A parameter was formulated that characterised the relative stiffness between stored bulk solid and silo wall. Further investigation showed that there appears to be a maximum level of redistribution of pressure across the wall and therefore there is a limit to the structural savings to be made by further reducing the wall thickness.

An experimental silo with a very thin wall (1.6mm) showed patterns of wall pressure that agreed with the finite element model and the redistribution law of Rotter *et al* (2002).

Rectangular planform silos were investigated and the finite element results showed that patterns of pressure on the long and the short wall disagree with existing knowledge. It had been suggested that the long wall would experience a larger pressure than the shorter wall but in the modelled flexible walled silos this was shown to be untrue. A mechanism was identified whereby there is rotation about the corner of the silo resulting in the observed pressure distributions.

12.1 Summary of main conclusions

In summary the main findings of the work are:

- Constitutive laws for granular materials in silo models must (in all but the most simple axisymmetric cases) account for plastic deformations. This is especially true in thin-walled silos.

- Common parameters used to classify bulk solids (such as ϕ) may not be sufficient to accurately model their behaviour in silo problems. It is necessary to have some parameter comparable to the logarithmic bulk modulus in order to account for volumetric change. Use of the porous elastic law in ABAQUS means that the material stiffens as the overall stress increases. This feature must be incorporated in any constitutive model for non-circular silos.

- End-effects observed in finite element modelling of silos are a real phenomenon as a result of the stiffness of the base and the friction between the wall and the stored bulk solid.

- In axisymmetric silo problems the flexibility of the hopper has a large effect on the pressures both above the transition and in the hopper. Even when the hopper is modelled with thick walls, small deformations that occur can have a radical effect on the pressure regimes.

- Simple one-dimensional consolidation tests on granular bulk solids were shown to provide material parameters that resulted in finite element predictions which agreed well with experimental data.

- Analysis of three-dimensional square silos shows that the value of k is not constant at a given depth. This is one of the major assumptions in the Janssen equations and therefore the use of this theory in relation to square silos must be questioned. It was however shown that the Janssen distribution was a good predictor of the mean pressure.

- The predictive law of Rotter *et al* (2002) gives a good representation of finite element results for pressures across the wall. A material not used in the original paper was modelled (wheat) and the patterns seen previously were predicted.

- Following a previous study, a parameter α to characterise pressure disrtibutions has been postulated. This work shows that it relies on the relative stiffness between silo wall and stored material. There is an asymptotic value of α for a given material and therefore there is a theoretical limit to the amount of stress redistribution. It was also shown that if large deformations occurred the value of α was hard to predict based upon the proposed relative stiffness parameter.

- An experiment using a very thin-walled silo was conducted and the showed that the finite element predictions were a good comparison. The results obtained fitted the predictive law very well and the values of α agreed with the patterns predicted by the relative stiffness parameter. Large deflections did not occur.

- Current methods for the prediction of the pressures on the long and the short wall in a rectangular silo are inadequate, when the silo wall is flexible. Reimbert and Reimbert (1976) suggest a larger pressure on the long wall and lower on the short wall. The finite element results suggest that this is not the case It was also shown that ENV 1991-4 (1995) was only applicable to silos that featured rigid walls and this would appear to be a shortcoming.

12.2 Further work

During the course of this research a number of avenues of exploration have been identified.

- Fill method; the work presented here used an incremental gravity fill method but other researchers have used a layered fill method. It would be of interest to investigate whether results would be affected dependent on which method was used, and which is more appropriate.

- Hopper pressures; there are a number of theories for the prediction of pressures in hoppers. Hopper pressures are only discussed briefly here but the finite element model could be used to investigate the effect on filling pressures of different hoppers (e.g. mass flow, funnel flow, eccentric etc).

- Stiffened silos; it was noted that rectangular silos are often stiffened. The finite element model could be used to investigate the effect of these stiffeners on pressure distributions.

- Rectangular silos; chapter 11 identified some general trends in rectangular silos but further work is needed to formulate an accurate method for the prediction of pressures in rectangular silos, especially those with very flexible walls.

- Discharge pressures; this work has been solely interested in pressures exerted on the walls of a full silo. The natural extension to this work would be to move towards a model that could predict the pressures during discharge.

References

ABAQUS users manual (2001), Version 6.2, Hibbitt, Karlson & Sorensen Inc.

Airy, W. (1897), "The pressure of grain", Minutes of Proc. Inst. Civ. Eng., London, Vol. 131, pp. 347-358.

Atkinson, J.H. and Bransby, P.L. (1978), The Mechanics of Soils, McGraw-Hill.

Aribert, J.M. and Ragneau, E. (1990), "Stress calculations in silos by finite element method using different behaviour laws for the ensiled material", 10th Int. Congr. Of Chem. Eng, Chem. Equipment Design and Automation, Praha, Czechoslovakia.

Arnold, P.C., McLean, A.G. and Roberts, A.W. (1980), Bulk Solids: Storage, Flow and Handling, Tunra Bulk Solids Handling Research Associates, 2nd edn., University of Newcastle, Australia.

Askegaard, V. (1961), "Measurement of pressure between a rigid wall and a compressible medium by means of pressure cells", Bulletin No. 14, Structural Research Laboratory, Technical University of Denmark, Kobenhavn.

Askegaard, V. (1978), "Stress and strain measurements in solid materials", Report No. 92, Structural Research Laboratory, Technical University of Denmark, Kobenhavn.

Askegaard, V. (1989), "Three component pressure cells for steel model silo", Report S.8817, Dept. Struct. Engng., Tech. Univ. of Denmark.

Askegaard, V. (1995), "Applicability of normal and shear stress cells embedded in cohesionless materials", Experimental Mechanics, Vol. 35, No. 4, pp. 315-321.

Askegaard, V. (1998), "Normal and shear stress on a silo wall, and stress and strain state in a silo medium", Silos, Fundamentals of Theory and Design, Brown, C.J. and Nielsen, J., E & FN Spon.

Askegaard, V., Bergholdt, M. and Nielsen, J. (1971), "Problems in connection with pressure cell measurement in silos", Byggningsstatiske Meddelelser, pp. 33-73, Copenhagen.

Askegaard, V. and Brown, C.J. (1995), "Influence of Personal Factor on Cell Response when Mounting Embedded Pressure Cells", Bulk Solids Handling, vol. 15, no.25, pp. 221-224.

Barés, R. (1979), Tables for the Analysis of Plates, Slabs and Diaphragms Based on the Elastic Theory, 3rd ed., Bauverlag GmbH (English translation by Carel van Amerogen), Macdonald and Evans Ltd.

Been, K., Jefferies, M.G. and Hachey, J. (1991), "The critical state of sands", Géotechnique 41, No.3, pp. 365-381.

Bishop, A.W. and Henkel, D.J. (1957), The Measurement of Soil Properties in the Triaxial Test, Arnold.

Boyce, H.R. (1980), "A non-linear model for the elastic behaviour of granular materials under repeated loading", Microstructural Science, vol. 1, pp. 285-294.

Brown, C.J. (1998), "Rectangular silo structures", Silos, Fundamentals of Theory and Design, Brown, C.J. and Nielsen, J., E & FN Spon.

Chen, J.F., Ooi, J.Y. and Rotter, J.M. (1996), "A rigorous statistical technique for inferring circular silo wall pressures from wall strain measurements", Engineering Structures, Vol. 18, No. 4, pp. 321-331.

Chen, J.F., Rotter, J.M. and Ooi, J.Y. (1999), "A review of numerical prediction methods for silo wall pressures", Advances in Structural Engineering, Vol. 2, No. 2, pp. 119-135.

Chen, J.F., Yu, S.K., Ooi, J.Y. and Rotter, J.M. (2000), "Finite element prediction of filling pressures in a ring stiffened imperfect full-scale silo", Proc. 14th Eng. Mech. Conf., ASCE, Austin, Texas.

Chen, W.F. (1994), Constitutive Equations for Engineering Materials – Vol. 2 Plasticity and Modelling, Elsevier Science.

Coulomb, C.A. (1776), "Essai sur une application des regles de maximis et minimis a quelques problemes de statique, relatifs a l'architecture", Memoires de Mathematique de l'Acadamie Royale des Sciences, pp. 343-382.

DIN 1055 (1987), "Design loads for buildings: loads in silo bins", DIN 1055 Part 6, Deutsches Institut für Normung, Berlin.

Drucker, D.C. and Prager, W. (1952), "Soil mechanics and plastic analysis or limit design", Quarterly of Applied Mathematics, vol. 10, pp. 157-165.

Eibl, J. (1998), Assorted papers in Silos, Fundamentals of Theory and Design, Brown, C.J. and Nielsen, J., E & FN Spon.

Emanuel, J.H., Mahmoud, M.H., Best, J. and Hasanain, G.S. (1983), "Parametric study of silo-material interaction", Powder Technology, 36, pp. 223-233.

ENV 1991-4 (1995) Eurocode 1: Basis of design and actions on structures, Part 4 – Silos and tanks, CEN, Brussels.

ENV 1998-4 (1999) Eurocode 8: Design provisions for earthquake resistance of structures, Part 4 – Steel silos, tanks and pipelines, CEN, Brussels.

Eshelby, J.D. (1957), "The determination of the elastic field of an ellipsoidal inclusion and related problems", Proc. Royal Society Series A, vol. 241, no. 1226, pp. 376-396.

Feise, H.J. and Daiß, A. (2001), "Building a numerical model for bulk solid materials from standard shear test data", 7th Int. Conf. Bulk Materials Storage, Handling and Transportation, Newcastle, Australia.

Feise, H.J. and Schwedes, J. (1998), "Constitutive laws for granular materials", Silos, Fundamentals of Theory and Design, Brown, C.J. and Nielsen, J., E & FN Spon.

Fischer, W. (1966), "Silos und Bunker in Stahlbeton", Veb Verlag Für Bauwesen, Berlin.

Garnier, J., Ternet, O., Cottineau, L.-M. and Brown, C.J. (1999), "Placement of embedded pressure cells", Géotechnique 49, No. 3, pp. 405-414.

Gaylord, E.H. and Gaylord, C.N. (1984), Design of Steel Bins for Storage of Bulk Solids, Prentice-Hall International, New Jersey.

Goodey, R.J., Brown, C.J. and Rotter, J.M. (2001), "Finite element predictions of filling pressures in rectangular steel silos", 7th Int. Conf. Bulk Materials Storage, Handling and Transportation, Newcastle, Australia.

Guines, D., Ragneau, E. and Kerour, B., "3D finite element simulation of the wall flexibilty in a square silo during filling and discharge," 14th Engineering Mechanics Conf., University of Texas, Austin, Texas, May 2000.

Hartlen, J., Nielsen, J., Ljunggren, L., Martensson, G. and Wigram, S. (1984), "The wall pressure in large grain silos", Document D2:1984, Swedish Council for Building Research, Stockholm.

Holst, J.M.F.G., Ooi, J.Y. and Rotter, J.M. (1996), "Filling and discharge stages by finite element analysis", CA-SILO Collaborative Action WG4, Internal report for the European Working Group, Rennes.

Hooke, R. (1678), De Potentia Restitutiva, London.

Hujeux, J.C. (1979), Calcul Numérique de Problèmes de Consolidation Elastoplastique, Thèse de Docteur-Ingénieur, Ecole Centrale de Paris.

Ibrahim, A.G. and Dickenson, R.P. (1983), "Analysis of silo-material interaction for powdered coal", 2nd Int. Conf., Design of Silos for Strength and Flow, Stratford upon Avon, England.

Jaky, J. (1948), "Pressures in silos", Proc. 2nd Int. Conf. On Soil Mechanics and Foundation Engineering, Rotterdam.

Janssen, H.A. (1895), "Verusche über Getreidedruck in Silozellen", Zeitschrift VDI, vol. 39, no. 35, pp. 1045-1049.

Jarrett, N.D. (1991), "A study on the influence of wall flexibility on pressure in rectangular silos", PhD Thesis, Brunel University.

Jarrett, N.D., Brown, C.J. and Moore, D.B. (1995), "Pressure measurements in a rectangular silo", Geotechnique, vol. 45, no. 1, pp. 95-104.

Jenike, A.W. (1964), "Storage and flow of solids", Bull. No. 123, Utah Engineering Experiment Station, University of Utah, Salt Lake City.

Jenike, A.W. and Johnson, J.R. (1968), "Bin loads", Journal of the Structural Division, ASCE, Vol. 94, No. ST4, April, pp. 1011-1041.

Jenike, A.W., Johnson, J.R. and Carson, J.W. (1973), "Bin loads – Part 3: Mass flow bins", Jnl. Engng. Industry, Trans ASME, 95, pp. 6-12.

Jenkyn, R.T. and Goodwill, D.J. (1987), "Silo failures: lessons to be learned", Engineering Digest (Toronto), vol. 33, no. 8.

Jofriet, J.C., LeLievre, B. and Fwa, T.F. (1977), "Friction model for the finite element analyses of silos", Trans. ASAE, 2C(4), pp 735-744.

Khelil, A. (1998), "Internal structures (ties and internals)", in Silos, Fundamentals of Theory and Design, Brown, C.J. and Nielsen, J., E & FN Spon.

Kolymbas, D. (1988), Veröffentl. Inst. Bodenmech. Felsmech. Univ. Karlsruhe, Heft 109.

Lahlouh, E.H., Brown, C.J. and Rotter, J.M. (1995), "Loads on rectangular plan-form steel silos", Research Report R95-027, University of Edinburgh.

Lee, K.L. (1970), "Comparison of plane strain and triaxial tests on sands", Proc. of ASCE, Vol. 96, No. SM3, pp. 901-923.

Levy, S. (1942), "Square plate with clamped edges under normal pressure producing large deflections", National Advisory Committee for Aeronautics, Tech. Note 847.

Lévy, M. (1899), "Sur l'équlibre élastique d'une plaque rectangulaire", C. R. Acad. Sci., 129, pp. 535-539.

Lightfoot, E. and Michael, D. (1966), "Prismatic coal bunkers in structural steelwork", The Structural Engineer, Vol. 44, No. 2, pp. 55-62.

Link, R.A. and Elwi, A.E. (1987), "Incipient flow in silo-hopper configurations", Journal of Engineering Mechanics, Vol. 116, No. 1, pp. 172-188.

Mahmoud, A.A. and Abdel-Sayed, G. (1981), "Loading on shallow cylindrical flexible grain bins", Jnl. Powder Bulk Solids Tech., 5(3), pp. 12-19.

Martínez. M.A., Alfaro, I. and Doblaré, M. (2002), "Simulation of axisymmetric discharging in metallic silos. Analysis of the induced pressure distribution and comparison with different standards", Engineering Structures, 24, pp. 1561-1574.

Mayniel, K. (1808), "Traité expérimental, analytique et practique de la poussée des terres et des murs de revêtement", Paris.

Müller-Breslau, H. (1906), Erddruck auf Stutzmauern, Alfred Kroner, Stuttgart.

Munch-Andersen, J. (1983), "Scale errors in model silos tests", Second International Conference on Design of Silos for Strength and Flow, Stratford-upon-Avon, UK, November.

Munch-Andersen, J., Askegaard, V. and Brink, A. (1992), Silo model tests with sand, SBI Bulletin 91, Danish Building Research Institute.

Nanninga, N. (1956), "Does the conventional method of calculating bin pressures give correct results?" (In Dutch), Ingenieur, 44 pp. 190-194.

Nedderman, R.M. (1992), Statics and Kinematics of Granular Materials, Cambridge University Press.

Nielsen, J. (1979), "Opmaling af silo i Karpalund", Report No. 4, Department of Structural Engineering, Technical University of Denmark, Lyngby.

Nielsen, J. (1983), "Load distribution in silos influenced by anisotropic grain behaviour", International conference on Bulk Materials Storage, Handling and Transportation, Institution of Engineers, Newcastle, Australia.

Nielsen, J. (1998), "Pressures from flowing", Phil. Trans. R. Soc. Lond., 356, pp. 2667-2684.

Nielsen, J. and Andersen, E.Y. (1982), "Loads in grain silos", Bygningsstatiske Meddelelser, Vol. 53, No. 4, pp. 123-135.

Nielsen, J. and Weidner, J. (1998), "The choice of constitutive laws for silo media", in Silos, Fundamentals of Theory and Design, Brown, C.J. and Nielsen, J., E & FN Spon.

Ooi, J.Y. (1990), The Mechanical Behaviour of Bulk Solids and the Prediction of Wall Pressures, Ph.D. Thesis, University of Sydney.

Ooi, J.Y., Pham, L., and Rotter, J.M. (1990), "Systematic and random features of measured pressures on full-scale silo walls", Engineering Structures, 12 (2), 73-87.

Ooi, J.Y. and J.M. Rotter (1990), "Wall pressures in squat steel silos from simple finite element analysis", Computers and Structures, vol. 37, no. 4, pp. 361-374.

Ooi, J.Y. and She, K.M. (1997), "Finite element analysis of wall pressure in imperfect silos", Int. J. Solids and Structures, Vol. 34, No. 16, pp. 2061-2072.

Ooi, J.Y., Chen, J.F., Lohnes, R.A. and Rotter, J.M. (1996), "Prediction of static wall pressures in coal silos", Construction and Building Materials, Vol. 10, No. 2, pp. 109-116.

Pieper, K. and Wenzel, F. (1965), "Pressure conditions in silos", Concrete and Constructional Engineering, vol. 60, no. 4.

Ragneau, E. and Aribert, J.M. (1993), "Prediction of loads in silos during filling and emptying stages by a finite element method", 2nd Int. Conf. On Micromechanics of Granular Media.

Ragneau, E., Aribert, J.M. and Sanad, A.M. (1994), "Modélisation numérique par élément fini tridimensionnel pour le calcul des actions aux parois des silos (remplissage et vindange)", Construction Métallique, No. 2.

Ragneau, E, Ooi, J.Y. and Rotter, J.M. (1998), "Finite element models for specific applications", Silos, Fundamentals of Theory and Design, Brown, C.J. and Nielsen, J., E & FN Spon.

Rankine, W.J.M. (1857), "On the stability of loose earth", Phil. Trans., Royal Society of London, Vol 147.

Reimbert, M. and Reimbert, A. (1976), Silos: Theory and practice, Trans Tech Publications, Revised 1987.

Roark, R.J. and Young, W.C. (1975), Formulas for Stress and Strain, McGraw-Hill Kogakusha, Tokyo.

Roberts, I. (1882), "Pressures of stored grain", Engineering, Vol. 34, p399.

Roberts, I. (1884), "Determination of the vertical and lateral pressures of granular substances", Proc. R. Soc. London, Vol. 36, pp. 225-240.

Roscoe, K.H., Schofield, A.N. and Thurairajah, A. (1965), Correspondence on "Yielding of clays in states wetter than critical", Géotechnique, 15, pp 127-120.

Rotter, J.M. (1985a), "Membrane theory of shells for bins and silos", Design of Steel Bins for the Storage of Bulk Solids, School of Mining and Civil Engineering, University of Sydney.

Rotter, J.M. (1985b), "Bending theory of shells for bins and silos", Design of Steel Bins for the Storage of Bulk Solids, School of Mining and Civil Engineering, University of Sydney.

Rotter, J.M. (1986), "The analysis of steel bins subject to eccentric discharge", Proc. Int. Conf. On Bulk Materials Storage, Handling and Transportation, Institution of Engineers, Wollongong, Australia.

Rotter, J.M. (2001), Guide for the Economic Design of Circular Metal Silos, Spon Press.

Rotter, J.M., Brown, C.J. and Lahlouh, E.H. (2002), "Patterns of wall pressure on filling a square planform steel silo", Engineering Structures, 24, pp. 135-150.

Rotter, J.M., Holst, J.M.F.G, Ooi, J.Y. and Sanad, A.M. (1998), "Silo pressure predictions using discrete-element and finite-element analyses", Phil. Trans. R. Soc. Lond., 356, pp. 2685-2712.

Rotter, J.M., Ooi, J.Y., Chen, J.F., Tiley, P.J., Mackintosh, I. and Bennett, F.R. (1995), Flow Pattern Measurement in Full Scale Silos, British Materials Handling Board publication, Ascot, UK, 230pp.

Runesson, K. and Nilsson, L. (1986), "Finite element modelling of the gravitational flow of a granular material", Bulk Solids Handling, Vol. 6, No. 5, pp. 877-884.

Schofield, A. and Wroth, P. (1968), Critical State Soil Mechanics, McGraw-Hill.

Schumaker, L.L. (1981), Spline Functions: Basic Theory, John Wiley and Sons.

Terzaghi, K. (1943), Theoretical Soil Mechanics, J. Wiley and Sons.

Timoshenko, S.P. and Woinowsky-Krieger, S. (1959), Theory of Plates and Shells, McGraw-Hill.

Trahair, N.S. (1985), "Characteristics of structural form", Design of Steel Bins for the Storage of Bulk Solids, School of Mining and Civil Engineering, University of Sydney.

Tresca, H. (1864), "Sur l'ecoulement des corps solids soumis a de fortes pression", Compt. Rend., Vol. 59.

Troitsky, M.S. (1980), "On the structural analysis of rectangular steel bins", Jnl. of Powder and Bulk Solids Tech., 4(4), pp. 19-25.

Ugural. A.C. (1981), Stresses in Plates and Shells, Mc-Graw Hill.

Von Kármán, T. (1910), "Festigkeitsprobleme im Muschinenbau", Encyklopaedie der Mathematischen Wissenschaften, Vol. 4, p349.

Von Mises, R. (1913), "Mechanik der festen koerper in plastisch deformablem zustand", Goettinger Nachr. Math. Phys., pp. 582-592.

Walker, D.M. (1966), "An approximate theory for pressures and arching in hoppers", Chemical Engineering Science, vol. 21, pp. 975-997.

Walters, J.K. (1973a), "A theoretical analysis of stresses in silos with vertical walls," Chem. Eng. Sci., Vol. 28, No. 1, pp. 13-21.

Walters, J.K. (1973b), "A theoretical analysis of stresses in axially-symmetric hoppers and bunkers", Chem. Eng. Sci., Vol. 28, No. 3, pp. 779-789.

Wilde (1979), Principes mathématiques et physiques des modèles élastoplastiques des sols pulvérulents, Compte rendu du colloque Franco-Polonais de Paris, LCPC, France.

Wu, Y.H. and Schmidt, L.C. (1992), "A boundary element method for prediction of silo pressures", Computers and Structures, Vol. 45, No. 2, pp. 315-323.

Zhang, Q., Puri, V.M. and Manbeck, H.B. (1986), "Finite element modelling of thermally induced pressures in grain bins filled with cohesionless granular materials", Trans. ASAE, 29(1), pp. 248-256.

Zhang, Q., Puri, V.M. and Manbeck, H.B. (1986), "Finite element predicted static and thermally induced loads in grain bins", Trans. ASAE, 32(6), pp. 2131-2136.

Zhong, Z., Ooi, J.Y. and Rotter, J.M. (2001), "The sensitivity of silo flow and wall stresses to filling method", Engineering Structures, 23, pp. 756-767.

Zienkiewicz, O.C. and Taylor, R.L. (1989), The Finite Element Method (4th Edition), McGraw-Hill.

Publications

Goodey, R.J., Brown, C.J. and Rotter, J.M. (2001), "Finite element predictions of filling pressures in rectangular steel silos", 7th Int. Conf. Bulk Materials Storage, Handling and Transportation, Newcastle, Australia.

Appendix A – Derivation of the Janssen formula

The Janssen (1895) theory that is referred to in this work and in most current codes (ENV 1991-4, 1995; DIN 1055, 1987) is based upon the equilibrium of a horizontal slice of material in a deep silo. This equilibrium is shown in figure A.1.

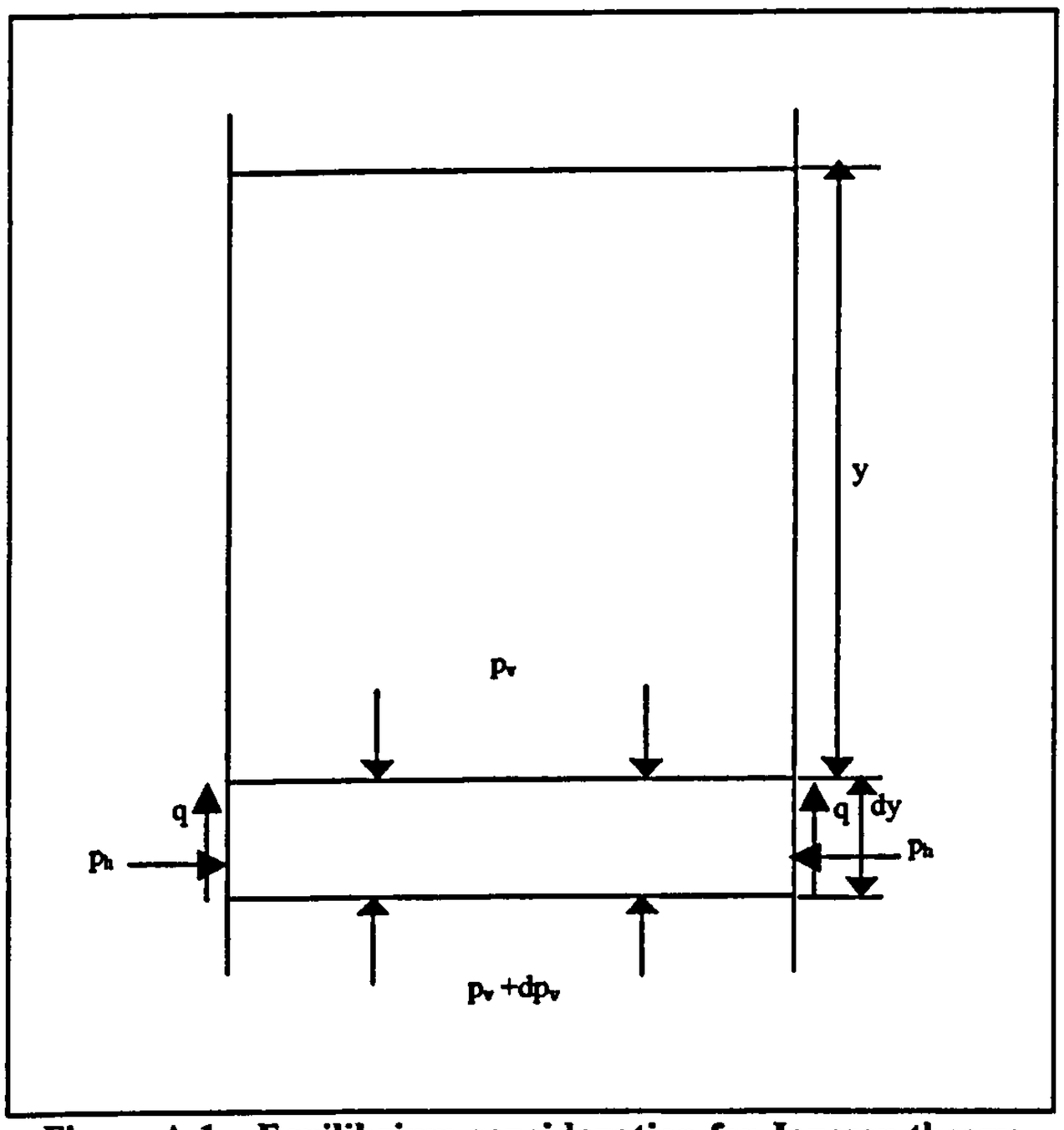

Figure A.1 – Equilibrium consideration for Janssen theory

Summation of the vertical forces gives equation A.1.

$$dp_v A - \gamma A dy + qC dy = 0 \qquad \text{(A.1)}$$

The relationship between the pressure on the wall and the friction coefficient is given by equation A.2.

$$q = \mu p_h \qquad \text{(A.2)}$$

The relationship between the horizontal and vertical pressure is taken as constant and defined by equation A.3.

$$p_h = kp_v \tag{A.3}$$

Substituting equations A.2 and A.3 into equation A.1 and integrating gives equations A.4 and A.5 for the vertical and horizontal pressure on the wall respectively.

$$P_v = \frac{\gamma R}{\mu k}\left(1 - e^{-\mu k\, y/R}\right) \tag{A.4}$$

$$P_h = \frac{\gamma R}{\mu}\left(1 - e^{-\mu k\, y/R}\right) \tag{A.5}$$

Appendix B – Convergence test on the three-dimensional model

In order to choose a mesh density for the three-dimensional model that provides accurate results with the minimum of computational time a convergence test was performed. The geometry of Lahlouh *et al* (1995) was meshed with increasingly larger numbers of elements and the horizontal displacement at the centre-top of the silo wall was monitored. This displacement will converge to a value It is expected that a very coarse mesh will poorly estimate this value, while a very fine mesh will provide an accurate result but at the expense of increased computational time. Five meshes were considered and table B.1 gives the total number of elements in each model. The distribution of elements is uniform along each edge. Distributions with a mesh density greater than those outlined below generate a large number of very small elements. When the contact pairs are created in such a model the position of some nodes is adjusted slightly to ensure the slave and master contact surfaces are correctly orientated. This can lead to the very small elements adjacent to the contact surface being defined incorrectly and having a negative volume or turning inside out. This type of error will cause the Abaqus solver to terminate the analysis.

	Coarse →→→→→→→→→→→→→→→→→ Fine				
	Mesh 1	**Mesh 2**	**Mesh 3**	**Mesh 4**	**Mesh 5**
Total no. of elements	297	527	1013	1711	2657

Table B.1 – Number of elements in each mesh

Figure B.1 gives a pictorial representation of the element distribution in the part of the model representing the stored solid in the parallel section of the bin.

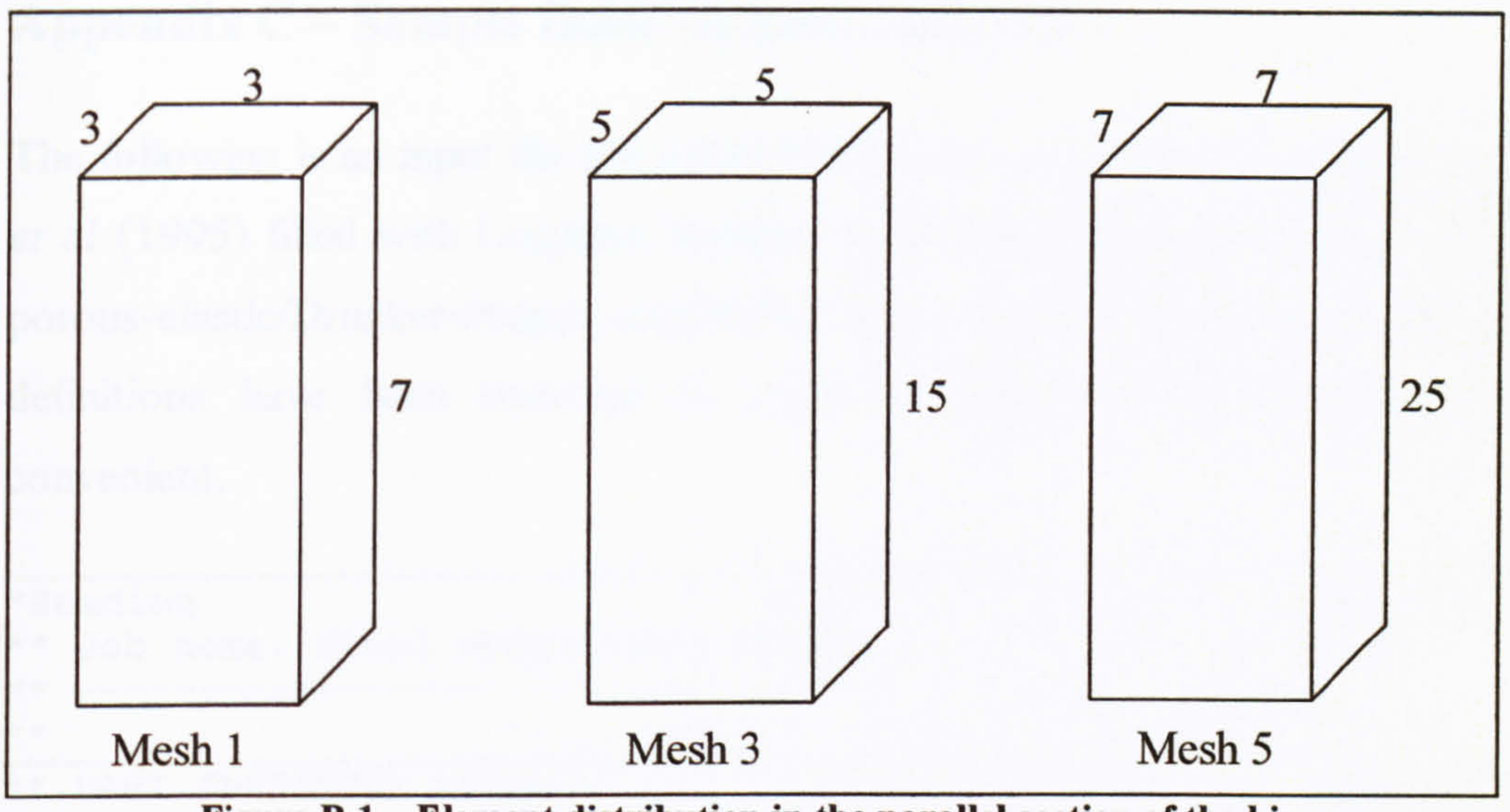

Figure B.1 – Element distribution in the parallel section of the bin

The choice to monitor the displacement of the bin is an arbitrary one. Any of the output variables could feasibly be monitored. Figure B.2 shows the displacement of this point as determined by the five different meshes.

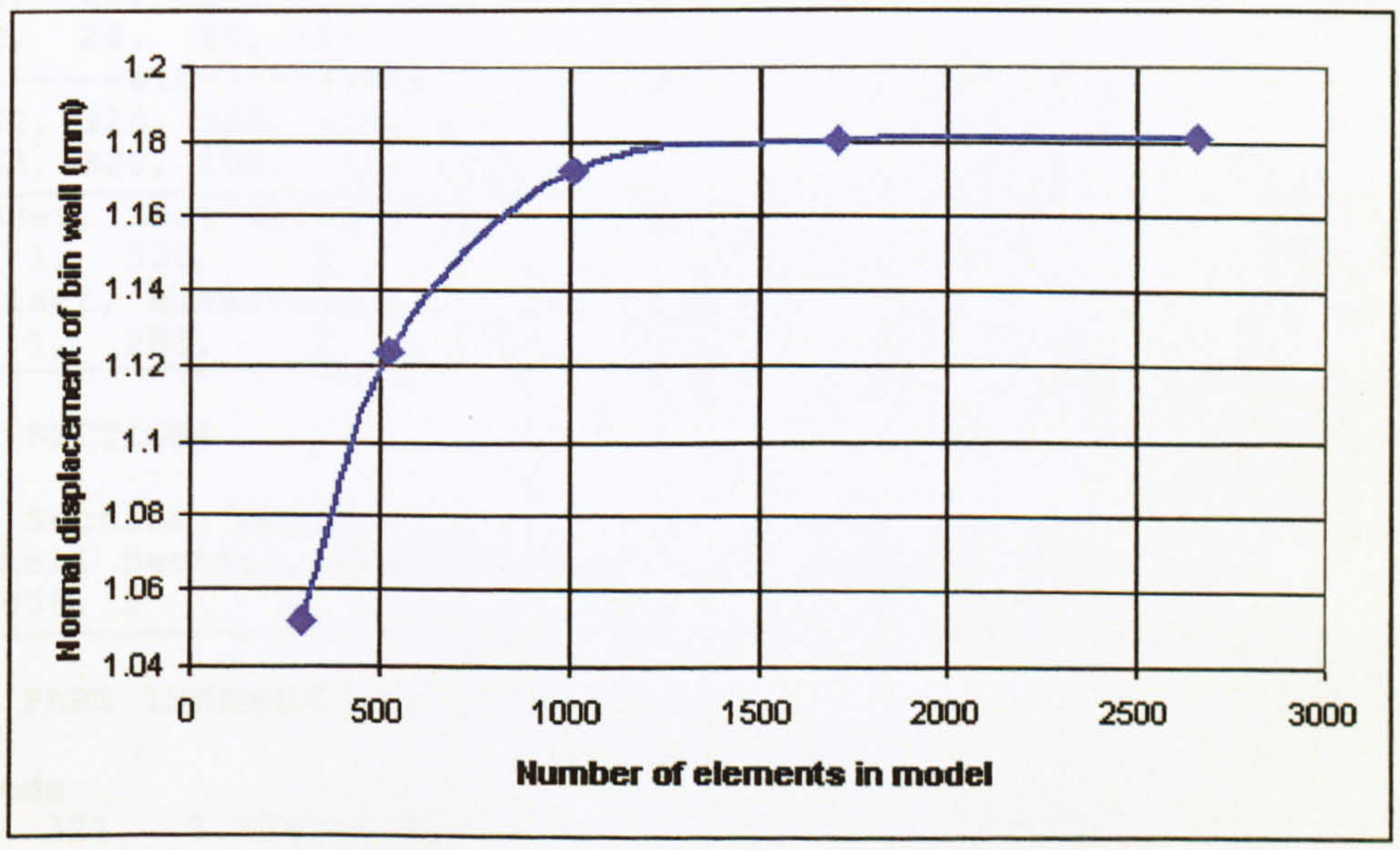

Figure B.2 – Wall normal deformation at the top mid-point of the bin

It shows clearly that the value of the displacement tends towards 1.18mm and that meshes 3, 4 and 5 give the most accurate results. This indicates that any mesh above the density of mesh 3 could be used and it would in fact be advantageous to use mesh density 3 as it is the quickest to solve.

Appendix C – Sample finite element input file

The following is an input file for ABAQUS 6.2 that models the geometry of Lahlouh *et al* (1995) filled with Leighton Buzzard sand whose behaviour is described by the porous-elastic/Drucker-Prager constitutive law. Sections of the node and element definitions have been removed in order to make the files presentation more convenient.

*Heading ** Job name: final Model name: Model-1 ** ---------- **	Define job title
** PART INSTANCE: walls-1 ** *Node 1, 0.75, -0.68, 0.71 2, 0.75, 0., 0. -------etc-------etc---------etc---------etc--------- 319, 0.45, 2.375, 0. 320, 0.6, 2.375, 0.	Define nodes for walls in X-Y-Z format
*Element, type=S4 1, 23, 24, 116, 113 2, 24, 25, 115, 116 -------etc-------etc---------etc---------etc--------- 282, 319, 320, 109, 110 283, 320, 108, 10, 109	Define shell elements for walls
*Nset, nset=walls-1._G16, generate 1, 320, 1 *Elset, elset=walls-1._G16, generate 1, 283, 1	Define wall node and element sets
** ** SECTIONS ** ** Section: walls *Shell Section, elset=walls-1._G16, material=steel 0.006, 5	Define shell behaviour, material and thickness
** ** PART INSTANCE: solid-1 ** *Node 321, 1.72456e-31, 0., 1.2326e-32 322, 0., 0., 0.75 -------etc-------etc---------etc---------etc--------- 1219, 0.3, 2.1775, 0.6 1220, 0.15, 2.1775, 0.6	Define nodes for solid in X-Y-Z format

*Element, type=C3D8 284, 376, 549, 885, 517, 321, 337, 485, 352 285, 549, 550, 886, 885, 337, 338, 486, 485 -------etc-------etc---------etc---------etc--------- 882, 1219, 1220, 884, 883, 835, 836, 465, 466 883, 1220, 860, 481, 884, 836, 464, 335, 465	Define solid elements for ensiled material
*Nset, nset=solid-1._G7, generate 321, 1220, 1 *Elset, elset=solid-1._G7, generate 284, 883, 1	Define wall node and element sets
** ** SECTIONS ** ** Section: ensiled *Solid Section, elset=solid-1._G7, material=sand 1.,	Define solid behaviour and material
*System *Nset, nset=_G12 1, 2, 7, 10, 11, 12, 13, 14, 15, 44, 45, 46, 47, 90, 91, 92 93, 94, 95, 96, 97, 98, 99, 100, 101, 102, 103, 104, 105, 106, 107, 108 477, 478, 565, 566, 567, 568, 569, 570, 571, 572, 573, 574, 575, 576, 577, 578 579, 580, 597, 598, 599, 600, 601, 602, 603, 604, 605, 606, 607, 608, 609, 610 611, 612, 613, 614, 615, 616, 617, 618, 619, 620, 621, 622, 623, 624, 625, 626 627, 628, 629, 630, 631, 632, 633, 634, 635, 636, 637, 638, 639, 640, 641, 642 643, 644, 645, 646, 647, 648, 649, 650, 651, 652, 837, 838, 839, 840, 841, 842 843, 844, 845, 846, 847, 848 *Elset, elset=_G12 4, 5, 6, 7, 8, 9, 59, 64, 69, 74, 79, 188, 193, 198, 203, 208 213, 218, 223, 228, 233, 238, 243, 248, 253, 258, 263, 268, 273, 278, 283, 304 305, 306, 307, 308, 329, 330, 331, 332, 333, 354, 355, 356, 357, 358, 379, 380 381, 382, 383, 404, 405, 406, 407, 408, 409, 414, 419, 424, 429, 434, 439, 444 449, 454, 459, 464, 469, 474, 479, 484, 489, 494, 499, 504, 509, 514, 519, 524 529, 534, 539, 544, 549, 554, 559, 564, 569, 574, 579, 584, 589, 594, 599, 604 609, 614, 619, 624, 629, 634, 639, 644, 649, 654, 659, 664, 669, 674, 679, 684 689, 694, 699, 704, 709, 714, 719, 724, 729, 734, 739, 744, 749, 754, 759, 764 769, 774, 779, 784, 789, 794, 799, 804, 809, 814, 819, 824, 829, 834, 839, 844 849, 854, 859, 864, 869, 874, 879	Define internal node and element sets for boundary conditions, output etc

```
*Nset, nset=_G13
   5,   6,   7,   8,  27,  28,  29,  30,  31,  40,
41,  42,  43,  71,  72,  73
  74,  75,  76,  77,  78,  79,  80,  81,  82,  83,
84,  85,  86,  87,  88,  89
 322, 323, 325, 326, 331, 332, 335, 336, 341, 342,
343, 344, 357, 358, 359, 360
 377, 378, 379, 380, 381, 382, 383, 384, 393, 394,
395, 396, 401, 402, 403, 404
 405, 406, 407, 408, 409, 410, 411, 412, 413, 414,
429, 430, 431, 432, 433, 434
 435, 436, 437, 438, 439, 440, 441, 442, 465, 466,
467, 468, 473, 474, 475, 479
 480, 481, 533, 534, 535, 536, 537, 538, 539, 540,
541, 542, 543, 544, 545, 546
 547, 548, 765, 766, 767, 768, 769, 770, 771, 772,
773, 774, 775, 776, 777, 778
 779, 780, 781, 782, 783, 784, 785, 786, 787, 788,
789, 790, 791, 792, 793, 794
 795, 796, 797, 798, 799, 800, 801, 802, 803, 804,
805, 806, 807, 808, 809, 810
 811, 812, 813, 814, 815, 816, 817, 818, 819, 820,
873, 874, 875, 876, 877, 878
 879, 880, 881, 882, 883, 884
*Elset, elset=_G13
  33,  34,  35,  36,  37,  38,  59,  60,  61,  62,
63,  84,  89,  94,  99, 104
 109, 114, 119, 124, 129, 134, 139, 144, 149, 154,
159, 164, 169, 174, 179, 288
 293, 298, 303, 308, 313, 318, 323, 328, 333, 338,
343, 348, 353, 358, 363, 368
 373, 378, 383, 388, 393, 398, 403, 408, 429, 430,
431, 432, 433, 454, 455, 456
 457, 458, 479, 480, 481, 482, 483, 504, 505, 506,
507, 508, 529, 530, 531, 532
 533, 554, 555, 556, 557, 558, 579, 580, 581, 582,
583, 604, 605, 606, 607, 608
 629, 630, 631, 632, 633, 654, 655, 656, 657, 658,
679, 680, 681, 682, 683, 704
 705, 706, 707, 708, 729, 730, 731, 732, 733, 754,
755, 756, 757, 758, 779, 780
 781, 782, 783, 804, 805, 806, 807, 808, 829, 830,
831, 832, 833, 854, 855, 856
 857, 858, 879, 880, 881, 882, 883
*Nset, nset=_G14
 3,
*Nset, nset=_G15, generate
    1,  1220,      1
*Elset, elset=_G15, generate
   1,  883,    1
*Nset, nset=_G46, generate
    1,  1220,      1
*Elset, elset=_G46, generate
   1,  883,    1
```

Define internal node and element sets for boundary conditions, output etc

*Nset, nset=w 321, 322, 330, 331, 334, 335, 337, 338, 339, 340, 389, 390, 391, 392, 429, 430 431, 432, 433, 434, 435, 436, 437, 438, 439, 440, 441, 442, 443, 444, 445, 446 447, 448, 449, 450, 451, 452, 453, 454, 455, 456, 461, 462, 463, 464, 479, 480 481, 482, 483, 484, 653, 654, 655, 656, 657, 658, 659, 660, 661, 662, 663, 664 665, 666, 667, 668, 669, 670, 671, 672, 673, 674, 675, 676, 677, 678, 679, 680 681, 682, 683, 684, 685, 686, 687, 688, 689, 690, 691, 692, 693, 694, 695, 696 697, 698, 699, 700, 701, 702, 703, 704, 705, 706, 707, 708, 849, 850, 851, 852 853, 854, 855, 856, 857, 858, 859, 860 *Elset, elset=w, generate 413, 883, 5	Define internal node and element sets for boundary conditions, output etc
** ** MATERIALS ** *Material, name=sand *Density 1587, *Drucker Prager 45.1,1.,0. *Drucker Prager Hardening 250,0. *Porous Elastic 0.002, 0.3164, 0.	Define sand constitutive law
*Material, name=steel *Density 7500., *Elastic 2.1e+11, 0.3	Define steel constitutive law
** ** INTERACTION PROPERTIES ** *Surface Interaction, name=_wall1-Property 1. *Surface Interaction, name=_wall2-Property 1. *Surface Interaction, name=frictional 1. *Friction 0.445, *Surface Interaction, name=smooth 1.	Define friction properties

** ** BOUNDARY CONDITIONS ** ** BC: fixed Type: Displacement *Boundary _G14, 2, 2 ** BC: symx Type: Typed *Boundary _G12, XSYMM ** BC: symz Type: Typed *Boundary _G13, ZSYMM	Define fixed and symmetry boundary conditions
*Elset, elset=__G6_SNEG, generate 59, 83, 1 *Surface Definition, name=_G6 __G6_SNEG, SNEG *Elset, elset=__G7_S1, generate 384, 408, 1 *Surface Definition, name=_G7 __G7_S1, S1 *Elset, elset=__G8_SNEG 30, 31, 32, 33, 34, 35, 36, 37, 38, 39, 40, 41, 42, 43, 44, 45 46, 47, 48, 49, 50, 51, 52, 53, 54, 55, 56, 57, 58, 84, 85, 86 87, 88, 89, 90, 91, 92, 93, 94, 95, 96, 97, 98, 99, 100, 101, 102 103, 104, 105, 106, 107, 108, 109, 110, 111, 112, 113, 114, 115, 116, 117, 118 119, 120, 121, 122, 123, 124, 125, 126, 127, 128, 129, 130, 131, 132, 133, 134 135, 136, 137, 138, 139, 140, 141, 142, 143, 144, 145, 146, 147, 148, 149, 150 151, 152, 153, 154, 155, 156, 157, 158, 159, 160, 161, 162, 163, 164, 165, 166 167, 168, 169, 170, 171, 172, 173, 174, 175, 176, 177, 178, 179, 180, 181, 182 183, *Surface Definition, name=_G8 __G8_SNEG, SNEG *Elset, elset=__G9_S4, generate 413, 883, 5 *Elset, elset=__G9_S3 284, 285, 286, 287, 288, 309, 310, 311, 312, 313, 334, 335, 336, 337, 338, 359 360, 361, 362, 363, 384, 385, 386, 387, 388 *Surface Definition, name=_G9 __G9_S4, S4 __G9_S3, S3	Define contact surfaces

*Elset, elset=__G10_SPOS 1, 2, 3, 4, 5, 6, 7, 8, 9, 10, 11, 12, 13, 14, 15, 16 17, 18, 19, 20, 21, 22, 23, 24, 25, 26, 27, 28, 29, 184, 185, 186 187, 188, 189, 190, 191, 192, 193, 194, 195, 196, 197, 198, 199, 200, 201, 202 203, 204, 205, 206, 207, 208, 209, 210, 211, 212, 213, 214, 215, 216, 217, 218 219, 220, 221, 222, 223, 224, 225, 226, 227, 228, 229, 230, 231, 232, 233, 234 235, 236, 237, 238, 239, 240, 241, 242, 243, 244, 245, 246, 247, 248, 249, 250 251, 252, 253, 254, 255, 256, 257, 258, 259, 260, 261, 262, 263, 264, 265, 266 267, 268, 269, 270, 271, 272, 273, 274, 275, 276, 277, 278, 279, 280, 281, 282 283, *Surface Definition, name=_G10 __G10_SPOS, SPOS *Elset, elset=__G11_S3 409, 410, 411, 412, 413, 434, 435, 436, 437, 438, 459, 460, 461, 462, 463, 484 485, 486, 487, 488, 509, 510, 511, 512, 513, 534, 535, 536, 537, 538, 559, 560 561, 562, 563, 584, 585, 586, 587, 588, 609, 610, 611, 612, 613, 634, 635, 636 637, 638, 659, 660, 661, 662, 663, 684, 685, 686, 687, 688, 709, 710, 711, 712 713, 734, 735, 736, 737, 738, 759, 760, 761, 762, 763, 784, 785, 786, 787, 788 809, 810, 811, 812, 813, 834, 835, 836, 837, 838, 859, 860, 861, 862, 863 *Elset, elset=__G11_S6, generate 284, 404, 5 *Surface Definition, name=_G11 __G11_S3, S3 __G11_S6, S6 *Elset, elset=__G45_S2, generate 859, 883, 1 *Surface Definition, name=_G45 __G45_S2, S2	Define contact surfaces
** Interaction: base *Contact Pair, interaction=smooth _G7, _G6 ** Interaction: wall1 *Contact Pair, interaction=_wall1-Property _G9, _G8 ** Interaction: wall2 *Contact Pair, interaction=_wall2-Property _G11, _G10	Define contact interactions
** *initial conditions, type=ratio solid-1._G7,0.67 *initial conditions, type=stress, geostatic solid-1._G7,-10,-0.68,-10,2.25,1	Define voids ratio and stress in stored solid

** ** STEP: equil ** *Step, nlgeom, unsymm=YES	Start non-linear analysis step
*Geostatic	Geostatic analyis
** ** LOADS ** ** Load: pressure *Dsload _G45, P, 10.	Apply load to balance initial stress
** ** OUTPUT REQUESTS ** *Restart, write, overlay *Output, field, op=NEW, frequency=99999 *Node Output U, RF, CF, POR *Element Output S, E, VOIDR, SAT *Contact Output CSTRESS, CDISP *Output, history, op=NEW, frequency=99999 *Energy Output ALLAE, ALLCD, ALLFD, ALLIE, ALLKE, ALLPD, ALLSE, ALLVD, ALLWK, ETOTAL *El Print, freq=999999 *Node Print, freq=999999	Request output
*End Step	End of step
** ** STEP: loading ** *Step, inc=1000, unsymm=YES	Start next analysis step
*Static 0.00125, 1., 1e-05, 1.	Static step
** ** BOUNDARY CONDITIONS ** ** BC: gravity Type: Velocity *dload, op=new _G46,grav,9.8,0,-1,0	Apply gravity load to ensiled material
** ** LOADS ** ** Load: pressure *Dsload, op=NEW	Remove load that was balancing initial stress

** Interaction: wall1 *Change Friction, interaction=_wall1-Property *Friction 0.445, ** Interaction: wall2 *Change Friction, interaction=_wall2-Property *Friction 0.445, **	Change friction coefficient on the walls from frictionless to μ=0.445
** OUTPUT REQUESTS ** *Restart, write, overlay *Output, field, op=NEW, frequency=99999 *Node Output U, RF, CF *Element Output S, E, PE, PEEQ, PEMAG *Contact Output CSTRESS, CDISP *Output, history, op=NEW, frequency=99999 *Energy Output ALLAE, ALLCD, ALLFD, ALLIE, ALLKE, ALLPD, ALLSE, ALLVD, ALLWK, ETOTAL *El Print, freq=999999 *Node Print, freq=999999 *contact file, freq=999999 *el file, elset=solid-1._g7, freq=999999 PE	Request output
*End Step	End analysis

Appendix D – Example contour plots from ABAQUS

The following plots show some example output from the finite element model in the form of contour plots. The model is that described in the input file in Appendix C.

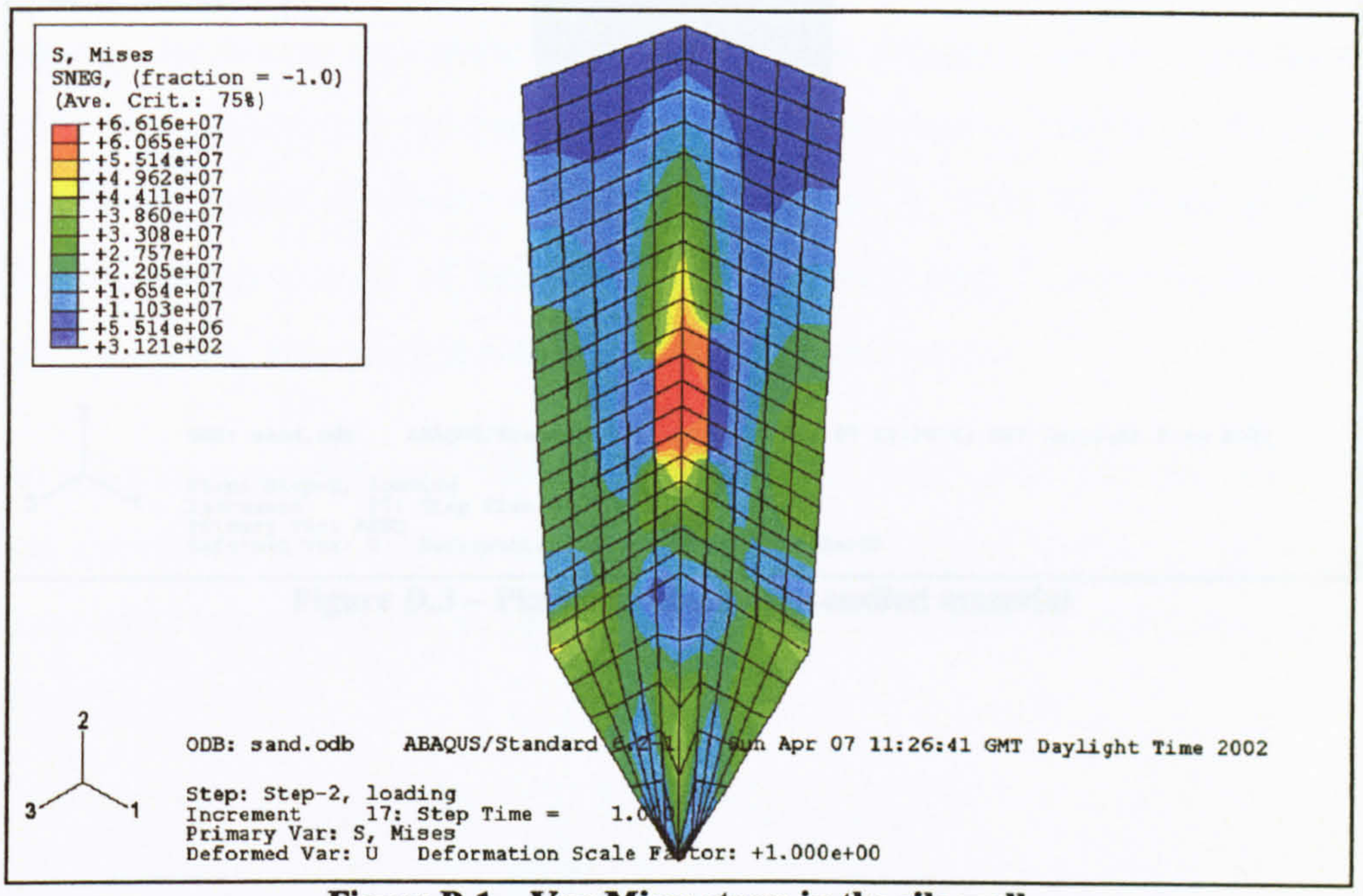

Figure D.1 – Von Mises stress in the silo wall

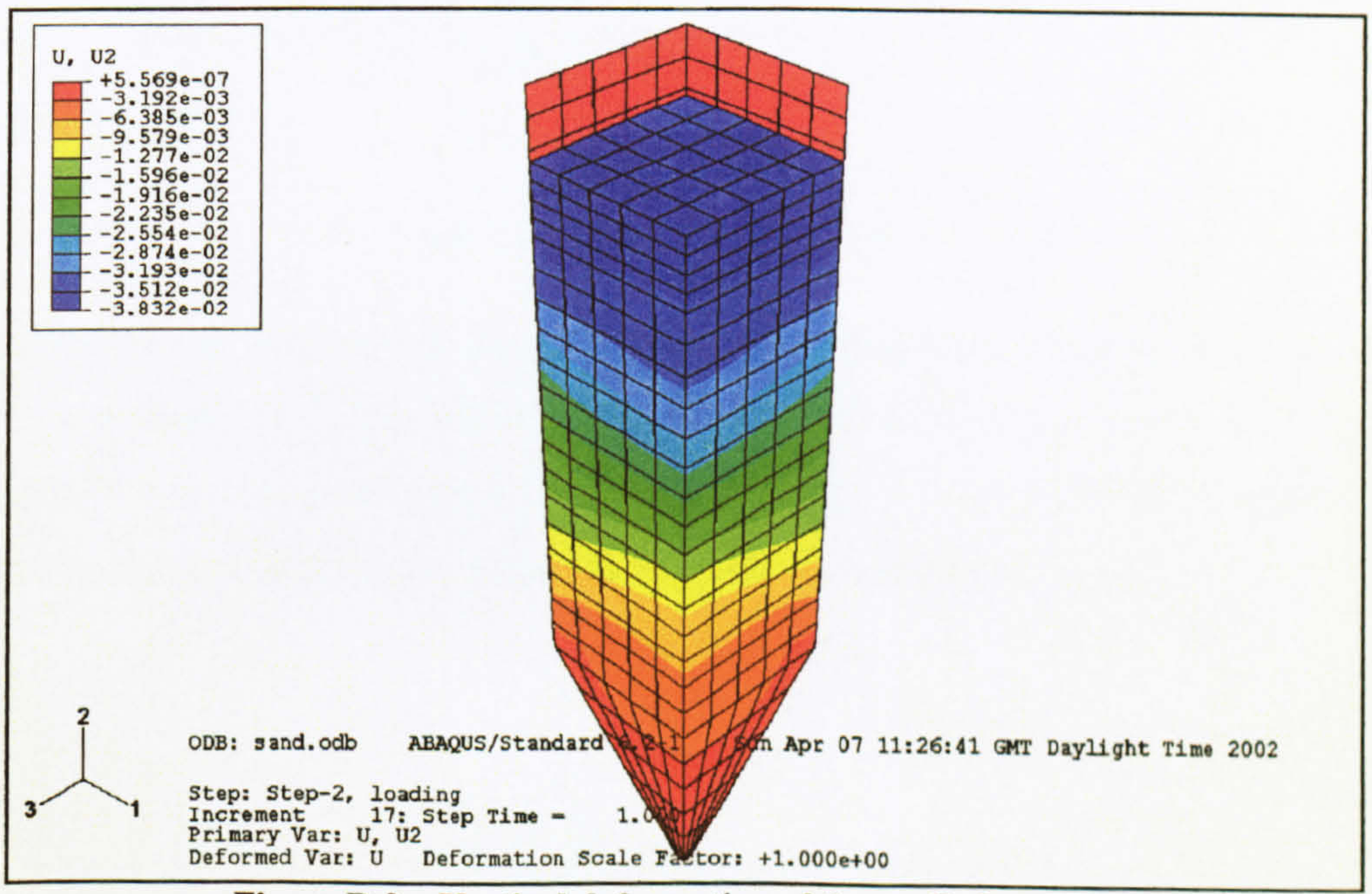

Figure D.2 – Vertical deformation of the ensiled material

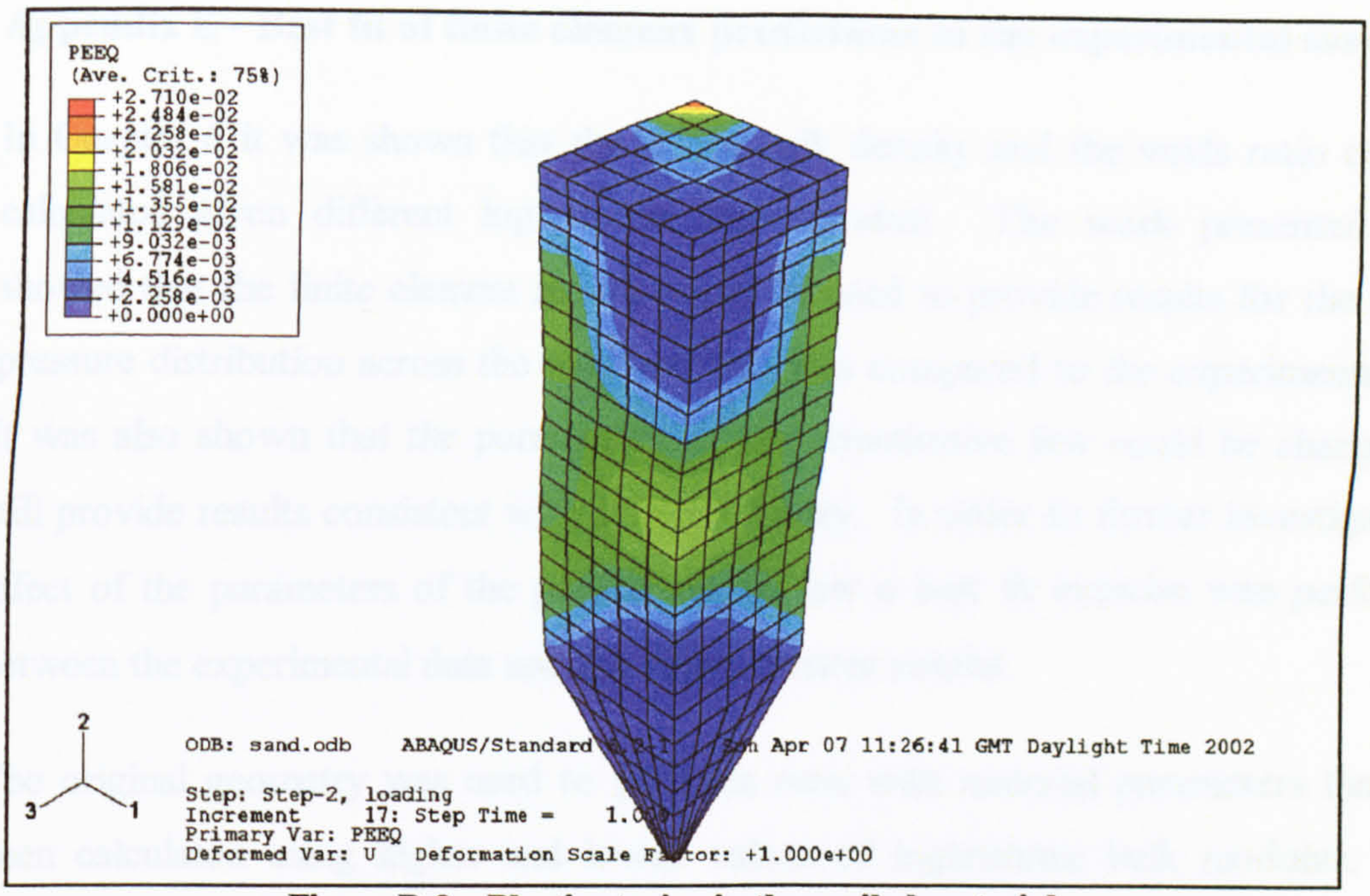

Figure D.3 – Plastic strains in the ensiled material

Appendix E - Best fit of finite element predictions to the experimental sand data

In Chapter 6 it was shown that the initial bulk density and the voids ratio could be calculated given different logarithmic bulk moduli. The work presented above showed that the finite element model could be used to provide results for the normal pressure distribution across the wall and this was compared to the experimental data. It was also shown that the parameters of the constitutive law could be changed yet still provide results consistent with Janssen theory. In order to further investigate the effect of the parameters of the porous elastic law a best fit exercise was performed between the experimental data and the finite element results.

The original geometry was used to perform runs with material parameters that had been calculated using higher and lower values of logarithmic bulk modulus. The values used are presented in table E.1 below (the values in italics are the original values for reference).

λ	e_0	$\gamma_{initial}$ (kg/m^3)
0.0005	0.65	1606
0.0020	0.66	1595
0.0044	*0.68*	*1576*
0.0080	0.71	1550

Table E.1 - Values used for best fit exercise

Results for the four models compared to the experimental results are shown in figure E.1 at a depth of 1.25m below the surface of the fill. This depth, being the mid-height of the bin, is chosen to illustrate the form of the distribution and show the relative effect of altering the parameters of the finite element model.

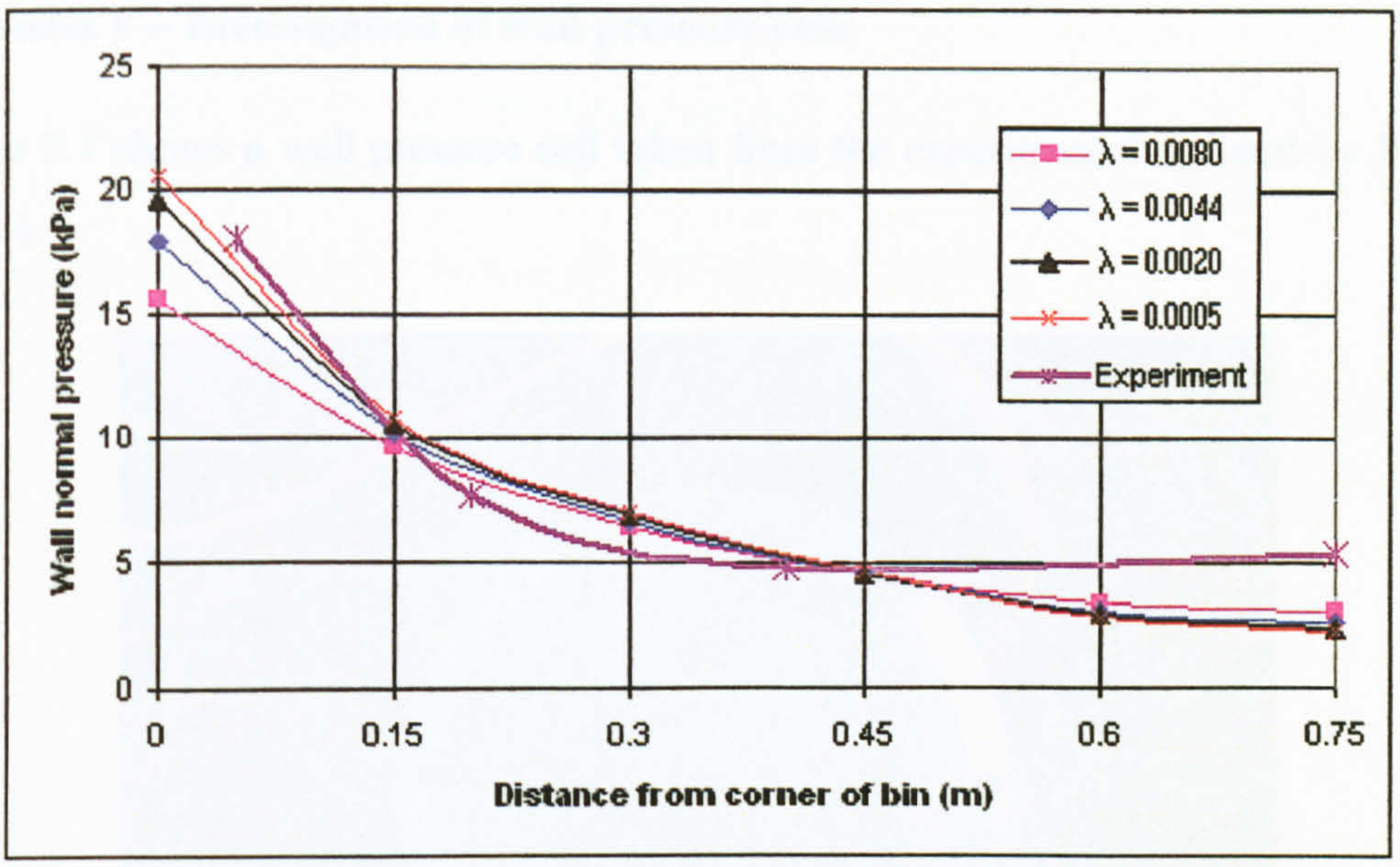

Figure E.1 - Wall normal pressures across the wall from FEA and experiment at 1.25m depth

Results are available for other levels and a least squares mathematical fit has been performed on the data. In order to do this the finite element results must be interpolated so that corresponding values for wall pressure can be obtained at the points where experimental data is available. Firstly, this was performed by using a linear interpolation technique and secondly a cubic spline technique (Schumaker, 1981). Linear interpolation assumes the data to be connected via straight lines and provides values based on this assumption. The cubic spline interpolation fits a function between each point to produce a smooth curve. This function is then used to provide values at the appropriate points.

Both of these best fit techniques fail to point to a conclusive value of λ for sand. They merely show that the value must be small in order to obtain the best fit. This is because the least squares method tends to minimise the difference where the numbers are large (in this case, in the corner). In order to reduce the sum of the least squares there must be a good fit in this area and therefore the value of $\lambda = 0.0005$ provides the mathematically best fit. However, it can be seen from figure E.1 that none of the models provide accurate results for the pressure in the middle of the wall. The need for a good prediction in the middle if this method were to be used for design was discussed in Chapter 6.

Appendix F – Investigation of wall pressure cells

Figure F.1 shows a wall pressure cell taken from the experimental rig used by Jarrett (1995).

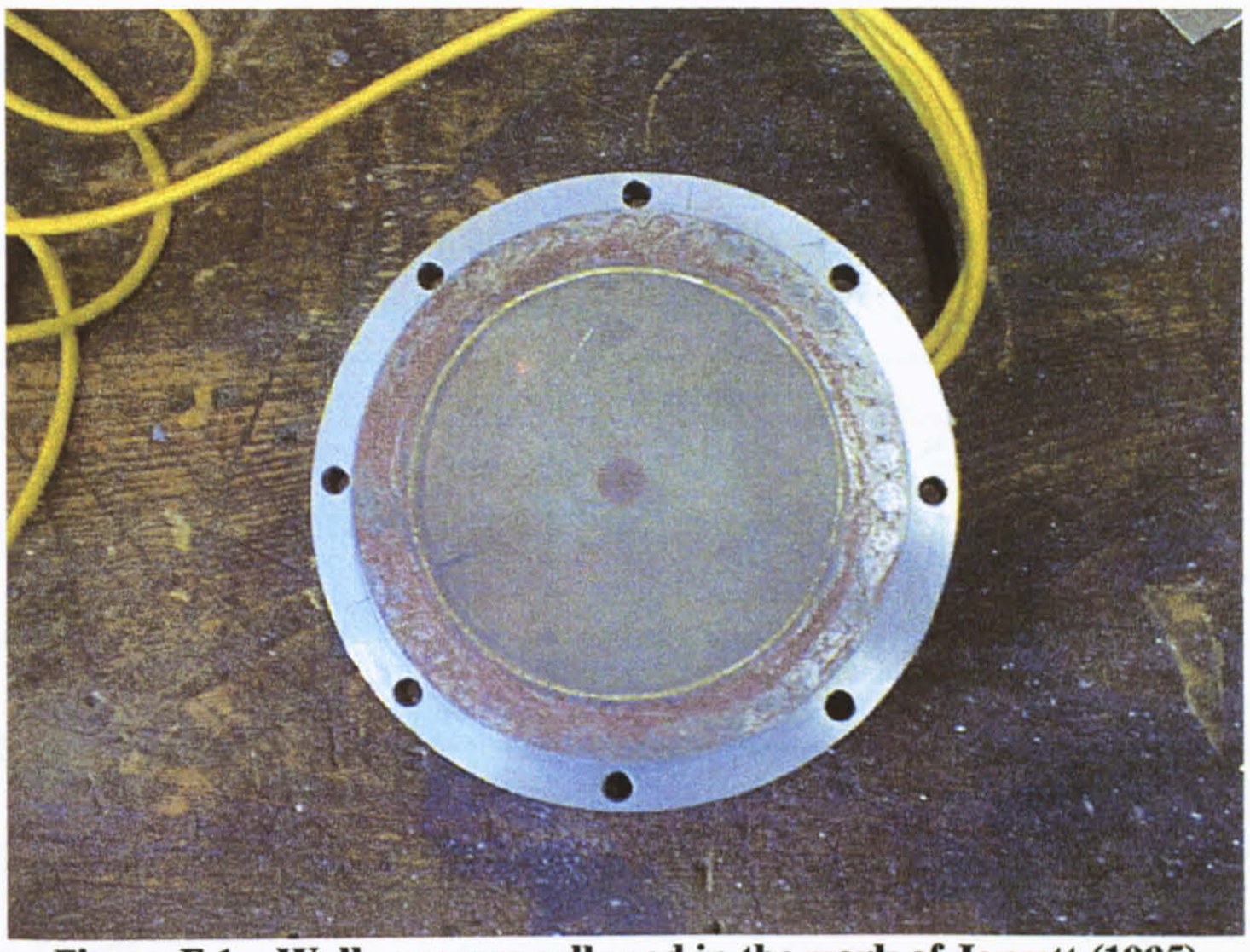

Figure F.1 – Wall pressure cell used in the work of Jarrett (1995)

This cell was manufactured by Askegaard along with 3 others for use in the aforementioned work. Sections of the wall of the bin were removed and the workings of the cell built into them. These sections were then replaced in the bin wall. This technique aims to reduce any effect on the continuity of the wall caused by the installation of pressure cells.

Each cell is constructed from a 10mm thick piece of the bin wall. A 0.5mm thick piece of mild steel forms the front face of the cell and this is placed into a 0.7mm by 100mm diameter recess machined into the wall section. The cell face is welded to the centre of the recess and sealed at the edge by a rubber membrane. The resulting 0.2mm gap between face and wall section is charged with a silicone oil. This transmits the pressure on the face to a semiconductor pressure gauge. The front face of the cell remains very stiff with the deflection being measured at less than 1 micron per 100kPa.

These cells are filled with silicone oil via an aperture in the back of the cell. The oil gap is evacuated using a vacuum pump and fresh oil is drawn into the cell when the pump is turned off. The presence of any air (which is highly compressible) in the cell will lead to non-linear behaviour of the cell making it useless.

The cells were charged with oil and then calibrated using air pressure. The pressure transducer is wired in a full bridge configuration and the excitation voltage is set to 10V. Figure F.2 shows the calibration of one of these types of cell.

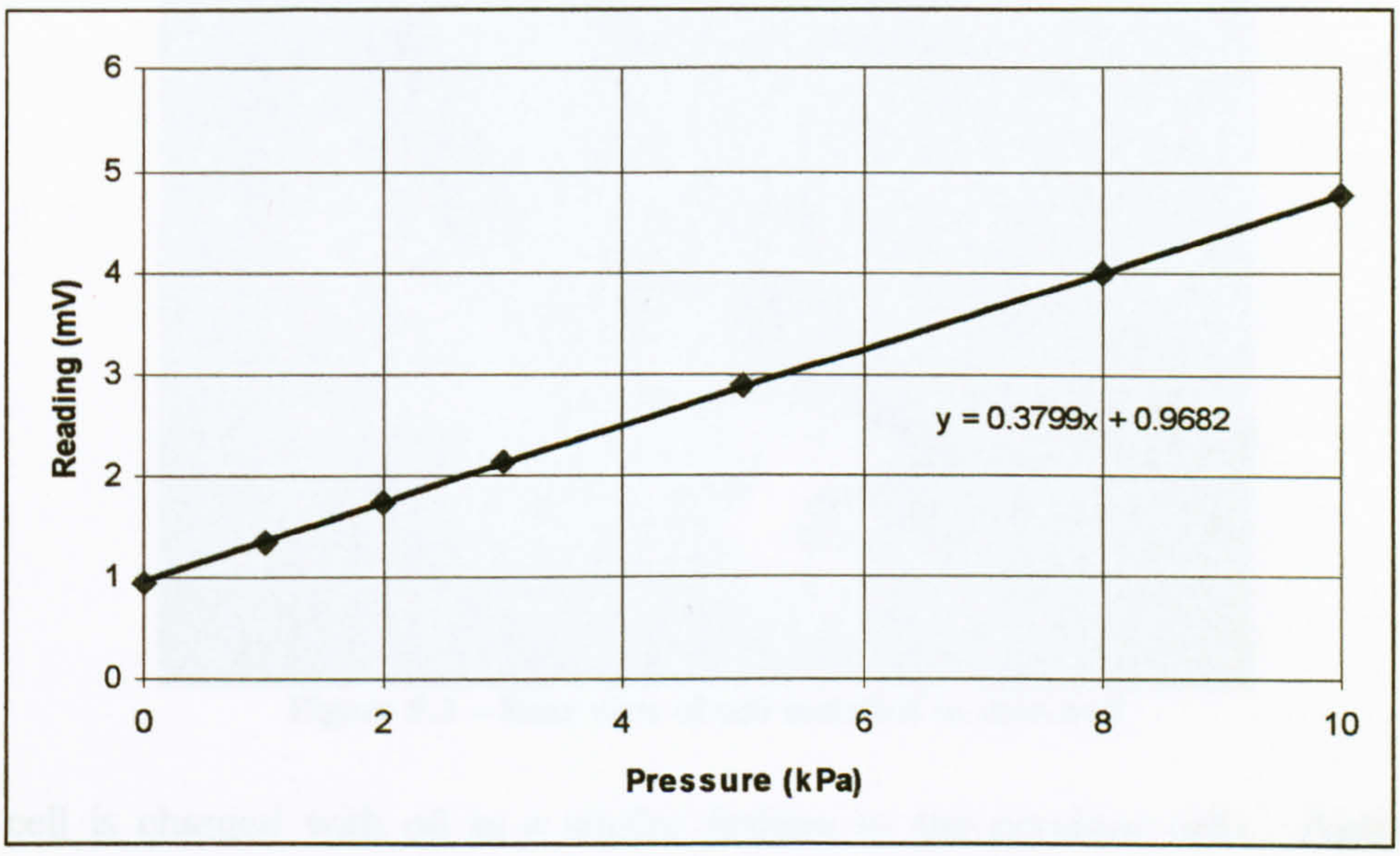

Figure F.2 – Calibration of a wall pressure cell

The best fit straight line to the readings gives a value of 37.99 μV per volt excitation per kPa. This figure agrees with the original specification supplied with the cells.

These cells are not suitable for use in a thin-walled silo model. Installation in the thin wall would lead to erroneous results due to the drastically increased local stiffness in the region of the cell. In order to use cells of this type in a thin-wall a new design is required.

Pervious work has shown that wall cells must be installed flush with the wall in order that the results they provide are as accurate as possible (ref). With this in mind it was proposed that the workings of a cell be machined into the back of the wall. This

would preserve the smooth continuity of the wall inside the bin. A circular recess 1.1mm deep and 50mm diameter was machined into a plate of overall thickness 1.6mm. A step of 0.3mm was left around the circumference. This allows another piece of plate to be installed in the back leaving a gap for the oil. A point to allow the oil into the cell and a pressure transducer were mounted onto the backing plate and the whole piece glued into the recess. Figure F.3 shows the back of the cell.

Figure F.3 – Rear view of cell installed in thin-wall

The cell is charged with oil in a similar fashion to the previous cells. Again, the pressure transducer is wired in a full bridge configuration and the calibration is performed using air pressure.

Unfortunately this cell was unable to provide any useful results. The overall bending of the plate was shown to induce a large reading into the cell and when pressurised the readings obtained were non-linear. There was also a large amount of hysteresis in the system and therefore once the load was removed the readings could not be induced to return to zero.

More research in this area could lead to a viable method for directly determining the wall pressures in a thin-walled silo but this is outside the scope of this project. Therefore, the use of the free field cells was deemed most suitable.